MECHANICAL AND WATER SORPTION PROPERTIES OF NAFION AND COMPOSITE NAFION/TITANIUM DIOXIDE MEMBRANES FOR POLYMER ELECTROLYTE MEMBRANE FUEL CELLS

May Barclay Satterfield

A DISSERTATION

PRESENTED TO THE FACULTY

OF PRINCETON UNIVERSITY

IN CANDIDACY FOR THE DEGREE

OF DOCTOR OF PHILOSOPHY

RECOMMENDED FOR ACCEPTANCE

BY THE DEPARTMENT OF

CHEMICAL ENGINEERING

Advisor: Jay Benziger

November, 2007

© Copyright by May Barclay Satterfield, 2007.

All rights reserved.

Abstract

The mechanical properties of the membranes used in polymer electrolyte membrane fuel cells are important to the performance and longevity of the cell. The speed and extent of membrane water uptake depend on the membrane's viscoelastic mechanical properties, which are themselves dependent on membrane hydration, and increased hydration improves membrane proton conductivity and fuel cell performance. Membrane mechanical properties also affect durability and cell longevity, preventing membrane failure from stresses induced by changing temperature and water content during operational cycling. Further, membrane creep and stress-relaxation can change the extent of membrane/electrode contact, also changing cell behavior. New composite membrane materials have exhibited superior performance in fuel cells, and it is suspected that improved mechanical properties are responsible.

Studies of polymer electrolyte membrane (PEM) fuel cell dynamics using Nafion membranes have demonstrated the importance of membrane mechanical properties, swelling and water-absorption behavior to cell performance. Nonlinear and delayed dynamic responses to changing operating parameters were unexpected, but reminiscent of polymer viscoelastic behavior and water sorption dynamics, illustrating the need to better understand membrane properties to design and operate fuel cells. Further, Nafion/TiO_2 composite membranes developed by the Princeton Chemistry Department improve fuel cell performance, which may be due to changes in membrane microstructure and enhanced mechanical properties.

Mechanical properties, stress-relaxation behavior, water sorption and desorption rates and pressures exerted during hydration by a confined membrane have been

measured for Nafion and for Nafion/TiO_2 composite membranes. Mechanical properties, including the Young's modulus and limits of elastic deformation are dependent on temperature and membrane water content. The Young's modulus decreases with increasing water content and temperature, is less temperature-dependent in hydrated membranes than dry membranes and is slightly higher in the composite membranes. Stress-relaxation also follows two distinct behaviors depending on its temperature, humidity and degree of strain. The water sorption and desorption dynamics are not controlled by diffusion rates but by interfacial mass transport resistance and, during sorption, by the kinetics of swelling and stress-relaxation. Pressure exerted by a swelling membrane scales with membrane thickness, is slightly higher for the composite membranes and is relevant to fuel cell design.

Acknowledgements

I have tried to confine this list to just a page, which was a difficult task after five years of working with astonishingly top-notch people, all of whom have helped me along the way and, by their examples, inspired me both professionally and personally. In particular, my heartfelt thanks go to:

My advisor, Prof. Jay Benziger, for his inexhaustible patience, generosity and guidance throughout my time here and his tremendous help in assembling this document.

My parents, June and Joe Satterfield, for being a better support team than I could have ever wished for.

My group members, James Nehlsen for his uncanny ability to help with nearly everything, Paul Majstrik for being a fun and insightful research partner, and Erin Kimball, Warren Hogarth, Joanne Chia, May Jean Cheah, Claire Woo, Jonathan Mann, Brent Kirby, Hitoshi Ota, Shannon Klaus and Sharonmoyee Goswami for teaching and befriending me in equal measure.

The Woodrow Wilson School and Princeton Environmental Institute's Science, Technology and Environmental Policy program, which was an excellent experience, and particularly Prof. Michael Oppenheimer, who made it so.

My committee members: Prof. George Scherer for his careful reading and insights, and Prof. Craig Arnold and Prof. Ilhan Aksay for pushing me.

The Princeton Chemical Engineering Faculty, especially Prof. Kyle Vanderlick for some much-needed support and mentoring, Prof. Richard Register for the excellent input and the use of his lab, and Prof. Debenedetti for the EMP-1 opportunity. Also thanks to Profs. Troian, Schvartsman and Sundaresan for help in preparing for the general exams, as well as graduate students Denis Shcherbakov and Leonard Pease.

The Princeton Chemical Engineering staff: Robin Block, Eric Paul, Ginny Czarnecki, Patti Weiss, Hema Ramamurthy, Don Schoorman, Karen Haskin and Karen Oliver.

The members of Greening Princeton and the Princeton Sustainability Committee.

The Princeton Chemical Engineering graduate students, especially the cohort of 2002 (Jack Tinsley, Bryan Patel, Scott McAllister, Sasha Myers, Greg Reeves, Chris Bristow, Lee Aarons, Jeff Quinn and Judy Hsii), Melanie Webb, Katsuyuki Wakabayashi and Robert Scogna.

NSF MRSEC Princeton Center for Complex Materials Program (DMR 0213706), as well as the WWS/PEI STEP program for funding.

Elsevier, John Wiley & Sons Inc., American Chemical Society, Electrochemical Society, American Society for Mechanical Engineers, Warren Hogarth, Craig Gittleman, Steven Kyriakides, Jonathan Mann and Hitoshi Ota for permission to reprint figures.

Table of Contents

List of Figures

List of Tables

List of Constants & Variable Names

A	Surface area of membrane (chapter 3)
a_w	Activity of water
a_T	Time-temperature superposition shift factor (unitless) (chapter 2)
a_S	Time-strain superposition shift factor (unitless) (ch 2)
B	Bulk modulus [MPa] (ch 4)
Bi	Biot number (ch 3)
β	Stress-relaxation rate (ch 3)
C	Concentration of water in membrane (ch 3)

C_0 Concentration of water in membrane at the beginning of a water (de)sorption experiment [g] (ch 3)
C_t Concentration of water in membrane during a water (de)sorption experiment [g] (ch 3)
C_∞ Concentration of water in membrane at the end of a water (de)sorption experiment [g] (ch 3)
d Exponential power term in Kohlrausch-Williams-Watts equation (ch 3)
D Diffusion coefficient [cm^2/s] (ch 3)
De Deborah number (ch 3)
E Young's modulus or elastic modulus [MPa, unless otherwise noted]
E' Storage modulus [MPa, unless otherwise noted]
E_x (x = 0, 1, 2, or 3) – modulus values used to fit stress-relaxation graphs
E_A Activation energy [kJ/mol] (ch 3)
EW Equivalent weight of membrane [g polymer/mol SO_3^-]
ε Strain [% or fraction]
ΔH_{sorp} Enthalpy of sorption of water by the membrane (ch 4)
ℓ Membrane thickness
η Viscosity [GP] (ch 2)
η_x (x = 0, 1, 2, or 3) – viscosity values used to fit stress-relaxation graphs
λ Membrane water content [mol H_2O/mol SO_3^-]
$K_{equilbrium}$ Equilibrium constant (ch 3)
k Inverse time constant [s] or 'characteristic life'in Kohlrausch-Williams-Watts equation (ch 2)
k_{int} Interfacial mass transport coefficient [cm/s] (ch 3)
M Membrane mass [g]
M_{dry} Membrane mass after drying 24 h at 170°C [g]
M_0 Membrane mass at the beginning of a water (de)sorption experiment [g] (ch 3)
M_t Membrane mass during a water (de)sorption experiment [g] (ch 3)
M_∞ Membrane mass at the end of a water (de)sorption experiment [g] (ch 3)
μ_w Chemical potential of water (ch 4)
ν Poisson's ratio (ch 4)
Π Swelling pressure (ch 4)
P_{resp} Pressure response as membrane swells (ch 4)
p_{app} Pressure applied (ch 4)
p_{solv} Chemical pressure of solvation [MPa] (ch 4)
$p_{w,sol't}$ Vapor pressure of water over a solution (ch 4)
R Gas constant [8.314 kJ/mol-K]
σ Stress [MPa, unless otherwise noted] (ch 2)
T Temperature
T_g Glass transition temperature [°C] (ch 2)
T_{ref} Reference temperature for time-temperature superposition, here 30°C (ch 2)
τ Time constant [s] (ch 2)
τ_x (x = 0, 1, 2, or 3) – time constants values used to fit stress-relaxation graphs (ch 2)
φ Quasi-equilibrium sorption value (ch 3)
V_w Molar volume of water (ch 5)

1 Introduction

1.1 PEMFCs: Applications, Components & Construction

The polymer electrolyte membrane fuel cell (PEMFC) is widely regarded as a key technology in building a hydrogen fuel-based renewable energy economy. Fuel cells convert chemical energy to electricity, working like a battery with continuous fuel and oxidant feeds. In an economy running on renewable energy sources these devices could be used for portable power or load-leveling, generating electricity in mobile or stationary applications at times of high demand and low supply from hydrogen that is created and stored when electricity is more available. PEM fuel cells are seeing early application in extended-life power supplies for laptop computers and cellular phones as well as automobiles. However, a number of basic engineering questions in fuel cell design remain unresolved.

A diagram of a PEM fuel cell appears in Figure 1.1 [1].

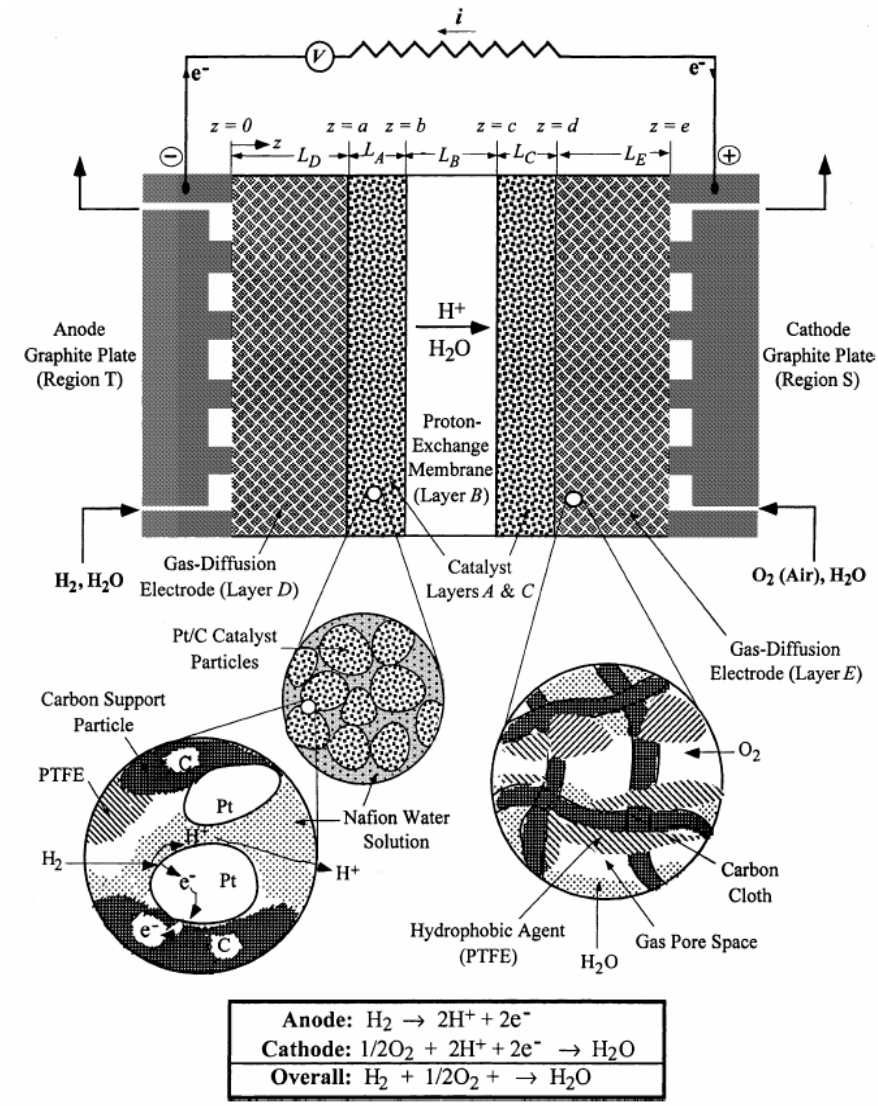

Figure 1.1: Drawing of fuel cell components. Figure reprinted from [1] with permission from Elsevier, © 2001.

As the cell operates, hydrogen enters at the anode (Region *T* in Figure 1.1), flowing through gas flow channels and diffusing toward the membrane through a porous carbon gas diffusion layer (GDL, referred to as "Gas-Diffusion Electrode, Layer *D*" in Figure 1.1). Between the GDL and the membrane, the hydrogen encounters a platinum catalyst, Layer *A* in Figure 1.1. It adsorbs onto the catalyst and loses its electrons. The protons move through the membrane (Layer *B*) to the cathode side while the electrons (excluded by the negatively charged membrane) are carried through the carbon GDL to the current

collector plate (Region *T*) and out through an external circuit to the cathode side (Region *S*). At the cathode catalyst layer (Layer *C*), the hydrogen and electrons react with supplied oxygen to form water. The reaction, which is essentially the combustion of hydrogen, is exothermic, and by separating the reactants across a charge-permeable membrane, the fuel cell creates a voltage across its electrodes, generating electricity from the chemical energy of the reaction.

Pictures of the interior of a cell and of an assembled cell appear in Figure 1.2.

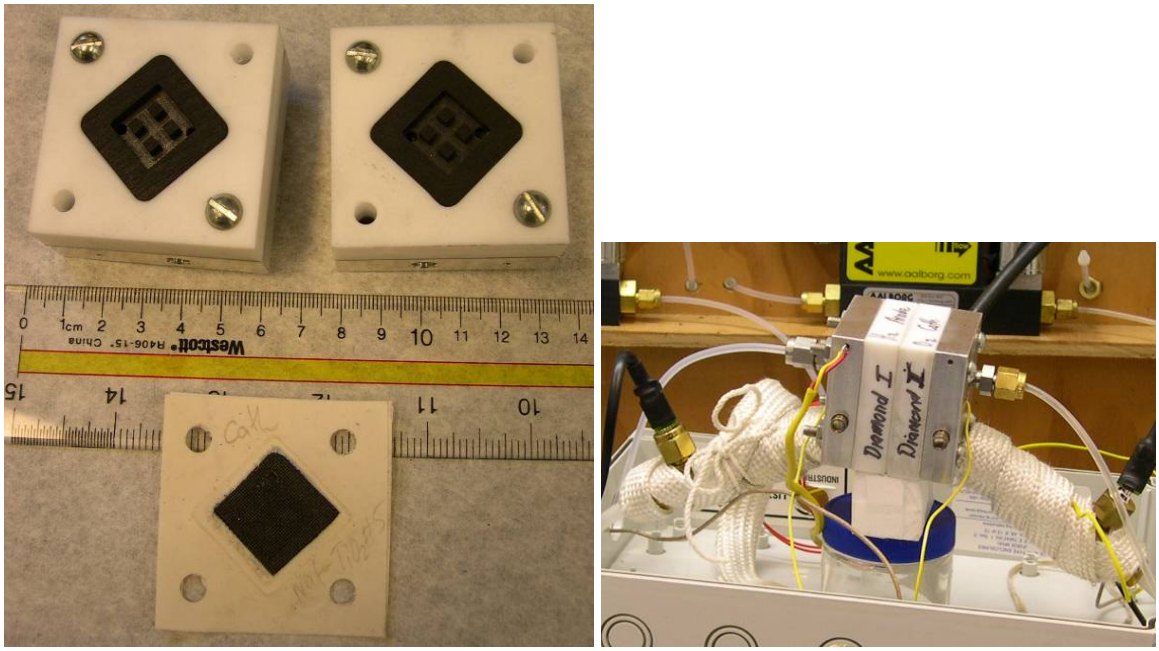

Figure 1.2: Left: Interior of a fuel cell typically used in this lab, also showing membrane-electrode assembly (MEA) with gasketing material. Right: Fuel cell assembled and operating. Both images courtesy of Dr. Warren Hogarth

The current collector plates (Regions *T* & *S* in Figure 1.1) are usually graphite, machined to create flow channels, and the GDL (Layers *D* & *E*) are either carbon cloth or paper (our lab uses cloth). The surface of the GDL that will contact the membrane is coated in a layer of fine carbon particles (Layers *A* & *C*) that support the platinum catalyst.

When fabricating a membrane electrode assembly (MEA), the membrane-contacting surfaces of the gas diffusion/electrode layers are painted with a solubilized

form of the membrane, then sandwiched with the membrane and hot-pressed at 140°C and 10MPa for approximately 90 seconds, which causes the GDL and membrane to adhere, forming the MEA. Both the hot-pressing and painting steps are an effort to extend and improve the contact area between the membrane and electrode, also known as the three-phase interface (gas, electrode/catalyst & membrane). The three-phase interface is the only place where the reactions can take place and is critical to the MEA performance: without gas present there is no fuel or oxidant supply, without the electrode and catalyst there is no reaction site or pathway for electrons and without the membrane there is no pathway for protons to enter or exit the reaction site. While the steps taken during MEA fabrication help ensure good contact between the membrane and electrode, it is suspected that the interface is dynamic, changing during cell operation as the membrane shrinks and swells with water gain and loss and, on a slower time-scale, as the membrane creeps into or away from the pores of the GDL.

The membrane material used in our lab and studied in this work is Nafion®, a product developed by DuPont in the late 1960's for use in the chlor-alkali process. While not ideal in any one respect, Nafion has a good balance of properties of interest for fuel cells–conductivity, chemical stability and mechanical toughness–and consequently has become the most commonly-used fuel cell membrane material, as well as the benchmark for new materials. A picture of its structure appears in Figure 1.3.

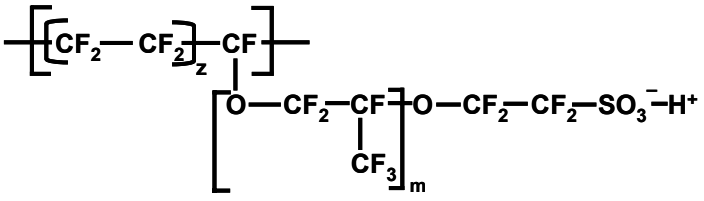

Figure 1.3: Molecular structure of Nafion. Based on drawings in [2-5]

Nafion is a perfluoronated ionomer consisting of a fluorinated-carbon backbone with fluoro-ether side chains ending in sulfonic acid groups. The amount of polymer per mole of sulfonic acid groups (the equivalent weight) of Nafion produced today is approximately 1100 grams, corresponding to values of z =14 and m = 1 in Figure 1.3 [5], and different equivalent weight membranes (1000-1500) have been produced in the past [2, 4, 5]. By convention membranes are named by a combination of their equivalent weight and thickness: "Nafion 112" is equivalent weight 1100, 0.002 inches thick. Currently, Nafion 112, 1135 (0.0035"), 115, 117 and 1110 (0.010") are available commercially as well as solutions of Nafion 1100 equivalent weight in alcohol, which is used for recasting membranes and for painting the GDL before hot-pressing.

The exact morphological structure of Nafion is still debated in literature, and an excellent and extensive historical review of theories and findings can be found in [5]. Generally it is held that the hydrophilic and hydrophobic portions of the polymer phase-separate. However, the shape of the structures formed by the two phases is still debated, and though it is accepted that the two phases change and possibly rearrange as the membrane hydrates, the exact nature of the rearrangement is another point of contention.

The earliest and longest-lasting model for Nafion microstructures is that proposed by Gierke et al.[3, 6] in the early 1980's. Small-angle X-ray diffraction (SAXS) work on Nafion at different hydrations and found a peak indicating a Bragg spacing of 3 nm in dry Nafion which increased in intensity and shifted to longer spacing at greater water content. The peak was attributed to a clustering of the hydrophilic groups, and Geirke proposed a model of spherical ionic clusters, roughly 3-5 nm in diameter, spaced about 5 nm apart and connected by small channels. Their model was also supported by stained TEM

images indicating circular clusters throughout the membrane. From the shift in spacing with water content, the authors concluded that the clusters expand, rearrange and reduce in number with increasing hydration. Later works, described in [5] have suggested other geometries for the inclusions such as rods [7, 8] or "sandwich" style structures [9], and no definitive answer has been reached.

However, it is generally held that the hydrophilic/hydrophobic phase separation creates pathways in the ionic region for the protons to travel from anode to cathode as the cell operates. Protons travel via two mechanisms: Grotthuss hopping, which dominates at high membrane water contents and hydronium ion migration, which dominates at lower water contents[10]. The hydrophilic groups cause the membrane to absorb water, and the membrane becomes more conductive to protons and able to perform better in the fuel cell. This increase in conductivity has been measured in our lab, and appears in Figure 1.4 [11].

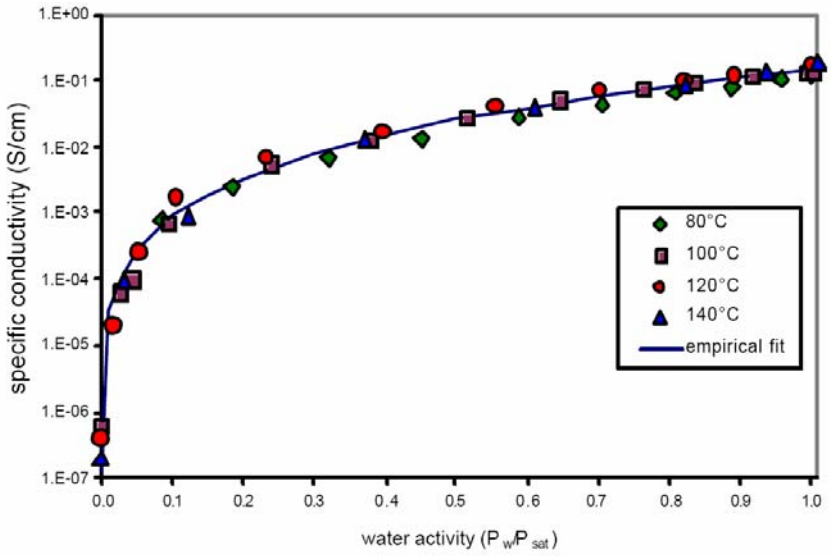

Figure 1.4: The variation of conductivity of Nafion (127 μm thick) with surrounding water activity. Equation of empirical fit: conductivity $=1.3\times10^{-7}\exp(14\cdot a_w^{0.2})$ S/cm.[11] Figure reprinted from [11] with permission from Elsevier, © 2004.

The water content of the membrane increases with the humidity in its surroundings, which is the independent variable in Figure 1.4. The water content of Nafion is frequently expressed as its λ-value, which is the number of water molecules present in the membrane for each sulfonic acid group. In Nafion, λ can vary from 0 under extreme drying conditions to between 12 and 14 in vapor at 100% humidity [12-14] and 22 when submerged in liquid water [14, 15].

(This difference in water content between immersion in 100% humidity and in liquid water, both situations in which water activity is 1, is well-documented in Nafion and several other polymers and known as Schroeder's Paradox[14-16]. No single explanation has been widely accepted within the field, and there is still debate about whether the phenomenon is the result of kinetics or thermodynamics or simply an experimental artifact. Some researchers have observed that the vapor-equilibrated water content can be approached from both directions: a submerged membrane removed to a 100% humidity environment appears to lose water[14]. It has been suggested[14, 15] that the Teflon-like backbone's hydrophobic surface properties resist vapor condensation, but are overcome by exposure to liquid water. However, this has not been proven experimentally, and is a microscopic argument that does not logically scale to macroscopic proportions[17] or explain the occurrence of Schroeder's paradox in other materials. A more recent study[16] has explained Schroeder's paradox as the result of two thermodynamically stable water content states, similar to the "Van der Waals loop." The two states result from multiple solutions to a water sorption equation proposed by the authors that balances endothermic elastic contributions with exothermic chemical interactions, described using the Flory-Huggins polymer-solvent interaction parameter.)

The dependence of the membrane's proton conductivity on its water content means that any changes in humidity within the fuel cell can affect the cell's performance. Increased water content also likely causes it to swell into the pores of the electrode, improving reaction area and the over-all conductivity of the MEA. The presence of a critical membrane water content for successful cell performance was clearly demonstrated in our lab by attempting to start a fuel cell after preconditioning the membrane at different humidities, seen in Figure 1.5 [18].

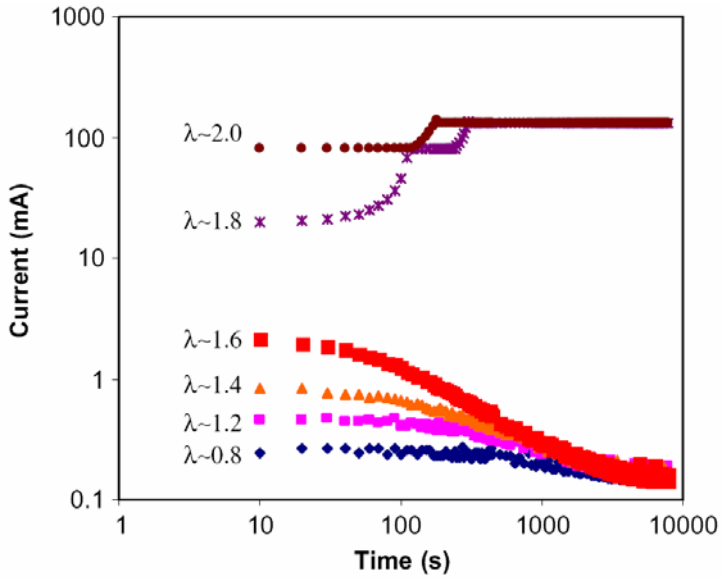

Figure 1.5: Current production by a PEM fuel cell starting with membrane equilibrated to different states of hydration (λ= mol H_2O/SO_3). Temperature is 50°C and load is 5 Ω[18]. Figure reprinted from [18] with permission from Elsevier © 2003.

When the membrane was preconditioned at a higher humidity and equilibrated at a λ-value of 1.8, the cell successfully ignited, but when the membrane was preconditioned at lower humidities to a λ-value of 1.6 or lower, the cell failed to ignite and gradually extinguished.

The cells operated in this lab are autohumidified, meaning that the water generated by reaction within the cell hydrates the membrane, creating a positive feedback where the membrane becomes more hydrated (and more conductive) as the cell operates.

More conventional work in fuel cells has used humidified feed streams due to the belief that the membrane dries at the anode side where water is not generated [19, 20]. However, humidified streams flood the cell, hindering gas transport and requiring higher fuel flow rates to remove excess water [21]. The balance of plant also becomes larger as a result of this approach; using high-flow rate humidified streams requires extra equipment to humidify the streams and to recycle the excess fuel [21].

1.2 Influence of PEM Mechanical Properties on Fuel Cell Performance

1.2.1 Fuel Cell Performance and Longevity

Mechanical properties are an important quality of the polymer membranes used in fuel cells [11, 22-36]. Tough, durable membranes improve fuel cell longevity, as repeated changes in membrane water content and temperature during operational cycling can cause stress-buildup and membrane failure in areas of concentrated stress [29-31]. Creep thinning [23] in which the membrane creeps away from stress points, can also lead to membrane failure, thinning the membrane to the point of hole formation or reactant crossover.

In addition to promoting cell longevity, membrane mechanical properties play an important role in cell performance. They govern the amount of water that the membranes can hold [22, 25, 33, 37] (affecting their conductivity) as well as the speed with which they can take up that water [26-28, 37-39]. Meanwhile, water uptake by the membrane can drastically change its mechanical properties [24, 33, 40, 41].

Improvements in fuel cell performance and longevity witnessed for new composite membranes are suspected to be due to their enhanced mechanical properties. Composite membranes created by adding metal oxide nanoparticles to Nafion perform

better in fuel cells, particularly at higher temperatures and reduced humidities [11, 34, 35, 42-44]. These conditions are desirable for design consideration such as improved CO tolerance and heat management, but are hostile to Nafion membranes, causing dehydration and decreasing the lifespan. Measurements of other membrane properties of interest such as conductivity and water retention do not definitively explain the enhanced performance [11, 34, 35, 45]. Mechanical properties are often suspected of playing a role [11, 34, 35, 42-44], but have only been examined in a limited number of studies [35, 43, 46-55]. A hypothesis put forth by this lab has suggested that the improvement in cell performance is due to scaffolds constructed by the metal oxide particles within the microstructure of the composite membrane, improving its dimensional stability and enhancing the mechanical properties[11].

1.2.2 Fuel Cell Dynamics

In addition to the overall level of performance, membrane mechanical properties can also affect the dynamic responses of fuel cells to changing operating conditions. An interesting feature of the cell behavior depicted in Figure 1.5 is the time needed for the cell to fully ignite or fully extinguish: between 100 and 10,000 seconds.

A widely held assumption is that fuel cells respond instantaneously to changes in operating conditions such as feed flow rate or electrical load, an attribute that would make them suitable for applications such as automobiles that require immediate power response [32]. However, work by this lab has revealed the contrary [32, 36]. In order to design a cell which could be easily modeled mathematically, this lab built a 1-dimensional cell, created after the 'continuous stirred tank' reactor design in which perfect mixing is assumed, meaning there are no spatial concentration or temperature gradients. As seen in

Figure 1.6, this was a break from conventional cell designs that use complex serpentine flow channels in which massive gradients in reactant and water concentrations and temperature can exist.

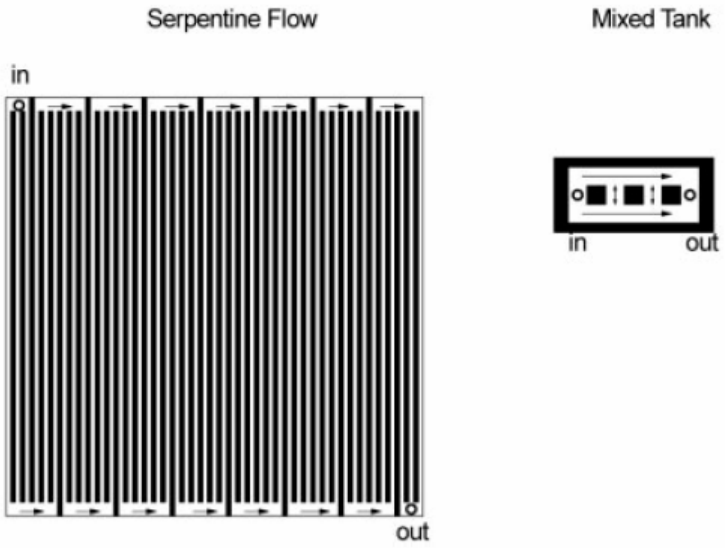

Figure 1.6: Flow channel pattern of a standard (GlobeTech) PEM fuel cell and of the continuous stirred tank PEM cell. The drawings are to scale; the serpentine pattern is 5cm^2 in area, five times that for the stirred tank cell. Figure reprinted from [32] with permission from John Wiley & Sons, Inc © 2004. The STR PEM design has since been replaced with the diamond configuration pictured in Figure 1.2.

The 1-d design gives the investigator much more accurate and meaningful information about an operating cell. Unless segmented electrodes are used [56-61] there is only one output of a cell, providing an integral measurement of the entire cell. This integration over disparate spatial conditions in the serpentine flow channels can obscure temporal variations, but an STR fuel cell removes special variations, revealing the time-dependent dynamic behavior.

These dynamic behaviors have been published [18, 32, 36, 62] and some examples appear in Figure 1.7 and Figure 1.8.

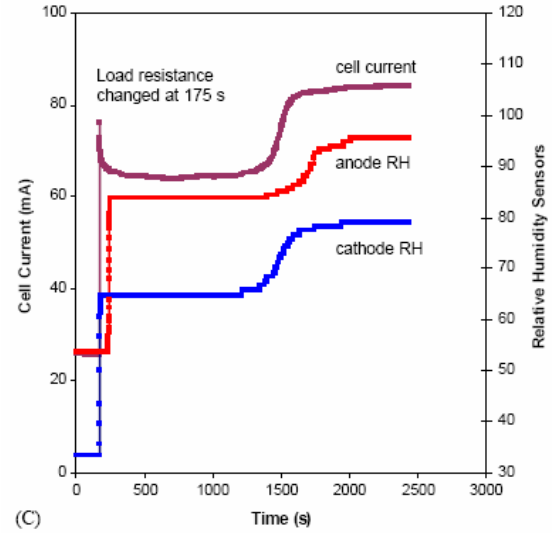

Figure 1.7: Behavior of fuel cell (current output and humidity of anode and cathode effluents) after step decrease in resistive load. Load is initially 25Ω and is decreased to 5Ω at time = 175 s. Temperature is 95°C.[36] Figure reprinted from [36] with permission from Elsevier, © 2005.

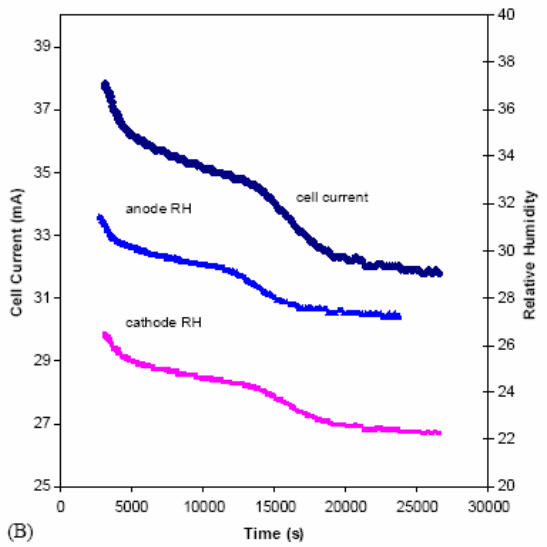

Figure 1.8: Behavior of fuel cell (current output and humidity of anode and cathode effluents) after step increase in resistive load. Load is initially 2Ω with a current output of 175 mA (not shown) and is increased to 20Ω at time = 3300 s. Temperature is 95°C.[36] Figure reprinted from [36] with permission from Elsevier, © 2005.

In Figure 1.7 the load resistance of the cell was decreased abruptly at 175 seconds, and the cell responded quickly by increasing the current production. The higher current is indicative of a faster rate of water-production reaction within the cell, and the humidity of the effluent from the cathode (where the water was generated) rose in tandem with the cell current. The humidity increase in the anode effluent occurred about 100 seconds later, or roughly the amount of time expected for water produced at the cathode to move across the membrane to the anode. However, the second and more gradual increase in current, approximately 1000 seconds later (with no further changes to the operating conditions) was entirely unexpected.

In Figure 1.8 an operation opposite to that done in Figure 1.7 was performed: the resistance was increased at 3300 seconds (where the data collection starts). The current decreased abruptly from 175 mA (before data collection) to 38 mA, and then continued to

decay, along with the effluent humidities, for ~25,000 seconds before starting to level out. The results of another such experiment appear in Figure 1.9.

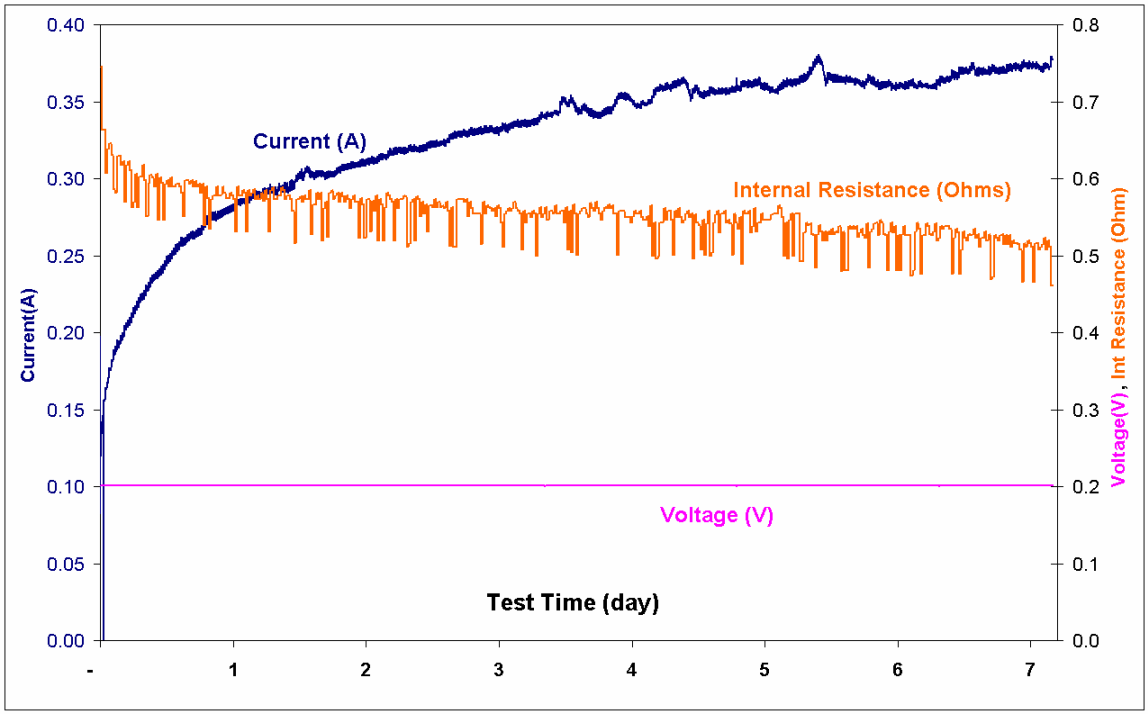

Figure 1.9: Start-up of a dry cell operating at 60 °C with voltage control of 0.2 V. Flow rates are 3.5 cc/min O_2, 7 cc/min H_2.

Figure 1.9 depicts the start-up of a dried cell at 60 °C under voltage control with just enough water to retain some proton conductivity. The cell took over 600,000 seconds (approximately a week) to reach steady operation in this case, and results on a similar time scale have been published by our lab in [62]. These long (10^3-10^5 second) dynamic approaches to steady-state operation after single step changes in operating parameters were surprising and were believed to be caused by chemical-mechanical coupling, particularly the dynamics of changing membrane water content and polymer mechanical relaxations [32, 36].

This work begins to examine that hypothesis and investigate the membrane's role in dynamic behavior of fuel cells. The dynamics of Nafion membrane water sorption and

desorption as well as stress-relaxation at different temperatures and humidities are investigated. Mechanical stress-strain properties are also measured with tensile stress-strain tests at conditions relevant to fuel cells to understand how these properties change under different operating conditions. The pressure exerted by a constrained Nafion membrane as it swells to take up water is also investigated, as membranes are constrained in fuel cell environments. In addition, because mechanical properties of composite membranes are often suspected of improving fuel cell performance, but have only been measured in a limited number of studies, this work also begins to examine those suspicions. The mechanical and water-sorption properties of unmodified Nafion are compared to those of Nafion/TiO_2 composite membranes developed by collaborators in the Princeton Chemistry Department.

1.3 References

1. Thampan, T.; Malhotra, S.; Zhang, J. X.; Datta, R., PEM fuel cell as a membrane reactor. *Catalysis Today* **2001,** 67, (1-3), 15-32.
2. Yeo, S. C.; Eisenberg, A., Physical properties and supermolecular structure of perfluorinated ion-containing (Nafion) polymers. *Journal of Applied Polymer Science* **1977,** 21, (4), 875-898.
3. Gierke, T. D.; Munn, G. E.; Wilson, F. C., The morphology in Nafion perfluorinated membrane products, as determined by wide-angle and small-angle X-ray studies. *Journal of Polymer Science Part B-Polymer Physics* **1981,** 19, (11), 1687-1704.
4. Pushpa, K. K.; Nandan, D.; Iyer, R. M., Thermodynamics of water sorption by perfluorosulfonate (Nafion-117) and polystyrene-divinylbenzene sulfonate (Dowex 50w) ion-exchange resins at 298 +/- 1-K. *Journal of the Chemical Society-Faraday Transactions I* **1988,** 84, 2047-2056.
5. Mauritz, K. A.; Moore, R. B., State of understanding of Nafion. *Chemical Reviews* **2004,** 104, (10), 4535-4585.
6. Hsu, W. Y.; Gierke, T. D., Elastic theory for ionic clustering in perfluorinated ionomers. *Macromolecules* **1982,** 15, (1), 101-105.
7. Lee, E. M.; Thomas, R. K.; Burgess, A. N.; Barnes, D. J.; Soper, A. K.; Rennie, A. R., Local and long-range structure of water in a perfluorinated ionomer membrane. *Macromolecules* **1992,** 25, (12), 3106-3109.
8. Rollet, A. L.; Diat, O.; Gebel, G., A new insight into Nafion structure. *Journal of Physical Chemistry B* **2002,** 106, (12), 3033-3036.
9. Haubold, H.-G.; Vad, T.; Jungbluth, H.; Hiller, P., Nano structure of Nafion: a SAXS study. *Electrochimica Acta* **2001,** 46, 1559-1563.
10. Kreuer, K. D., On the complexity of proton conduction phenomena. *Solid State Ionics* **2000,** 136, 149-160.
11. Yang, C.; Srinivasan, S.; Bocarsly, A. B.; Tulyani, S.; Benziger, J. B., A comparison of physical properties and fuel cell performance of Nafion and zirconium phosphate/Nafion composite membranes. *Journal of Membrane Science* **2004,** 237, (1-2), 145-161.
12. Jalani, N. H.; Choi, P.; Datta, R., TEOM: A novel technique for investigating sorption in proton-exchange membranes. *Journal of Membrane Science* **2005,** 254, (1-2), 31-38.
13. Futerko, P.; Hsing, I. M., Thermodynamics of water vapor uptake in perfluorosulfonic acid membranes. *Journal of the Electrochemical Society* **1999,** 146, (6), 2049-2053.
14. Zawodzinski, T. A.; Derouin, C.; Radzinski, S.; Sherman, R. J.; Smith, V. T.; Springer, T. E.; Gottesfeld, S., Water-uptake by and transport through Nafion$^{(R)}$ 117 membranes. *Journal of the Electrochemical Society* **1993,** 140, (4), 1041-1047.
15. Choi, P. H.; Datta, R., Sorption in proton-exchange membranes - An explanation of Schroeder's paradox. *Journal of the Electrochemical Society* **2003,** 150, (12), E601-E607.
16. Vallieres, C.; Winkelmann, D.; Roizard, D.; Favre, E.; Scharfer, P.; Kind, M., On Schroeder's paradox. *Journal of Membrane Science* **2006,** 278, (1-2), 357-364.

17. Benziger, J., email communication: "Re: latest version of intro". In Satterfield, M. B., Ed. Princeton, NJ, 2007.
18. Moxley, J. F.; Tulyani, S.; Benziger, J. B., Steady-state multiplicity in the autohumidification polymer electrolyte membrane fuel cell. *Chemical Engineering Science* **2003,** 58, (20), 4705-4708.
19. Eikerling, M.; Kharkats, Y. I.; Kornyshev, A. A.; Volfkovich, Y. M., Phenomenological theory of electro-osmotic effect and water management in polymer electrolyte proton-conducting membranes. *Journal of the Electrochemical Society* **1998,** 145, (8), 2684-2699.
20. Zawodzinski, T. A.; Davey, J.; Valerio, J.; Gottesfeld, S., The water-content dependence of electro-osmotic drag in proton-conducting polymer electrolytes. *Electrochimica Acta* **1995,** 40, (3), 297-302.
21. Hogarth, W. H. J.; Benziger, J. B., Operation of polymer electrolyte membrane fuel cells with dry feeds: Design and operating strategies. *Journal of Power Sources* **2006,** 159, (2), 968-978.
22. Choi, P.; Jalani, N. H.; Thampan, T. M.; Datta, R., Consideration of thermodynamic, transport, and mechanical properties in the design of polymer electrolyte membranes for higher temperature fuel cell operation. *Journal of Polymer Science Part B-Polymer Physics* **2006,** 44, (16), 2183-2200.
23. Liu, D.; Kyriakides, S.; Case, S. W.; Lesko, J. J.; Li, Y. X.; McGrath, J. E., Tensile behavior of Nafion and sulfonated poly(arylene ether sulfone) copolymer Membranes and its morphological correlations. *Journal of Polymer Science Part B-Polymer Physics* **2006,** 44, (10), 1453-1465.
24. Kundu, S.; Simon, L. C.; Fowler, M.; Grot, S., Mechanical properties of Nafion$^{(TM)}$ electrolyte membranes under hydrated conditions. *Polymer* **2005,** 46, (25), 11707-11715.
25. Choi, P.; Jalani, N. H.; Datta, R., Thermodynamics and proton transport in Nafion - I. Membrane swelling, sorption, and ion-exchange equilibrium. *Journal of the Electrochemical Society* **2005,** 152, (3), E84-E89.
26. Rivin, D.; Kendrick, C. E.; Gibson, P. W.; Schneider, N. S., Solubility and transport behavior of water and alcohols in Nafion$^{(TM)}$. *Polymer* **2001,** 42, (2), 623-635.
27. Morris, D. R.; Sun, X., Water-sorption and transport properties of Nafion 117 H. *Journal of Applied Polymer Science* **1993,** 50, (8), 1445-1452.
28. Takamatsu, T.; Hashiyama, M.; Eisenberg, A., Sorption phenomena in Nafion membranes. *Journal of Applied Polymer Science* **1979,** 24, (11), 2199-2220.
29. Hector, L. G.; Lai, Y. H.; Tong, W.; Lukitsch, M. J., Strain accumulation in polymer electrolyte membrane and membrane electrode assembly materials during a single hydration/dehydration cycle. *Journal of Fuel Cell Science and Technology* **2007,** 4, (1), 19-28.
30. Huang, X. Y.; Solasi, R.; Zou, Y.; Feshler, M.; Reifsnider, K.; Condit, D.; Burlatsky, S.; Madden, T., Mechanical endurance of polymer electrolyte membrane and PEM fuel cell durability. *Journal of Polymer Science Part B-Polymer Physics* **2006,** 44, (16), 2346-2357.
31. Budinski, M.; Gittleman, C. S.; Lai, Y. H.; Litteer, B.; Miller, D., Characterization of perfluorosulfonic acid membranes for PEM fuel cell mechanical durability. In *AIChE*

Annual Meeting, Austin, TX, 2004; Presentation slides used at 2004 AIChE Annual Meeting.
32. Benziger, J.; Chia, E.; Karnas, E.; Moxley, J.; Teuscher, C.; Kevrekidis, I. G., The stirred tank reactor polymer electrolyte membrane fuel cell. *AIChE Journal* **2004,** 50, (8), 1889-1900.
33. Satterfield, M. B.; Majsztrik, P. W.; Ota, H.; Benziger, J. B.; Bocarsly, A. B., Mechanical properties of Nafion and titania/Nafion composite membranes for PEM fuel cells. *J. Polymer Science B: Polymer Physics* **2006,** 44, (16), 2327-2345.
34. Thampan, T. M.; Jalani, N. H.; Choi, P.; Datta, R., Systematic approach to design higher temperature composite PEMs. *Journal of the Electrochemical Society* **2005,** 152, (2), A316-A325.
35. Bauer, F.; Willert-Porada, M., Zirconium phosphate Nafion® composites - a microstructure-based explanation of mechanical and conductivity properties. *Solid State Ionics* **2006,** 177, (26-32), 2391-2396.
36. Benziger, J.; Chia, E.; Moxley, J. F.; Kevrekidis, I. G., The dynamic response of PEM fuel cells to changes in load. *Chemical Engineering Science* **2005,** 60, (6), 1743-1759.
37. Newns, A. C., The sorption and desorption kinetics of water in a regenerated cellulose. *Transactions of the Faraday Society* **1956,** 52, (11), 1533-1545.
38. Krtil, P.; Trojanek, A.; Samec, Z., Kinetics of water sorption in Nafion thin films -- Quartz crystal microbalance study. *Journal of Physical Chemistry B* **2001,** 105, 7979-7983.
39. Bagley, E.; Long, F. A., 2-Stage sorption and desorption of organic vapors in cellulose acetate. *Journal of the American Chemical Society* **1955,** 77, (8), 2172-2178.
40. Bauer, F.; Denneler, S.; Willert-Porada, M., Influence of temperature and humidity on the mechanical properties of Nafion(R) 117 polymer electrolyte membrane. *Journal of Polymer Science Part B-Polymer Physics* **2005,** 43, (7), 786-795.
41. Tang, Y. L.; Karlsson, A. M.; Santare, M. H.; Gilbert, M.; Cleghorn, S.; Johnson, W. B., An experimental investigation of humidity and temperature effects on the mechanical properties of perfluorosulfonic acid membrane. *Materials Science and Engineering A: Structural Materials Properties Microstructure and Processing* **2006,** 425, (1-2), 297-304.
42. Adjemian, K. T.; Srinivasan, S.; Benziger, J.; Bocarsly, A. B., Investigation of PEMFC operation above 100°C employing perfluorosulfonic acid silicon oxide composite membranes. *Journal of Power Sources* **2002,** 109, (2), 356-364.
43. Chalkova, E.; Pague, M. B.; Fedkin, M. V.; Wesolowski, D. J.; Lvov, S. N., Nafion/TiO_2 proton conductive composite membranes for PEMFCs operating at elevated temperature and reduced relative humidity. *Journal of the Electrochemical Society* **2005,** 152, (6), A1035-A1040.
44. Sacca, A.; Carbone, A.; Passalacqua, E.; D'Epifanio, A.; Licoccia, S.; Traversa, E.; Sala, E.; Traini, F.; Ornelas, R., Nafion-TiO_2 hybrid membranes for medium temperature polymer electrolyte fuel cells (PEFCs). *Journal of Power Sources* **2005,** 152, (1), 16-21.
45. Damay, F.; Klein, L. C., Transport properties of Nafion(TM) composite membranes for proton-exchange membranes fuel cells. *Solid State Ionics* **2003,** 162, 261-267.

46. Shao, P. L.; Mauritz, K. A.; Moore, R. B., [Perfluorosulfonate Ionomer] [Mixed Inorganic Oxide] Nanocomposites via polymer in-situ sol-gel chemistry. *Chemistry of Materials* **1995,** 7, (1), 192-200.
47. Shao, P. L.; Mauritz, K. A.; Moore, R. B., [Perfluorosulfonate ionomer] [SiO_2-TiO_2] nanocomposites via polymer-in situ sol-gel chemistry: Sequential alkoxide procedure. *Journal of Polymer Science Part B-Polymer Physics* **1996,** 34, (5), 873-882.
48. Shao, Z. G.; Xu, H. F.; Li, M. Q.; Hsing, I. M., Hybrid Nafion-inorganic oxides membrane doped with heteropolyacids for high temperature operation of proton exchange membrane fuel cell. *Solid State Ionics* **2006,** 177, (7-8), 779-785.
49. Jalani, N. H.; Dunn, K.; Datta, R., Synthesis and characterization of Nafion$^{(R)}$-MO_2 (M = Zr, Si, Ti) nanocomposite membranes for higher temperature PEM fuel cells. *Electrochimica Acta* **2005,** 51, (3), 553-560.
50. Adjemian, K. T.; Dominey, R.; Krishnan, L.; Ota, H.; Majsztrik, P.; Zhang, T.; Mann, J.; Kirby, B.; Gatto, L.; Velo-Simpson, M.; Leahy, J.; Srinivasan, S.; Benziger, J. B.; Bocarsly, A. B., Function and characterization of metal oxide-naflon composite membranes for elevated-temperature H_2/O_2 PEM fuel cells. *Chemistry of Materials* **2006,** 18, (9), 2238-2248.
51. Kwak, S. H.; Yang, T. H.; Kim, C. S.; Yoon, K. H., Nafion/mordenite hybrid membrane for high-temperature operation of polymer electrolyte membrane fuel cell. *Solid State Ionics* **2003,** 160, (3-4), 309-315.
52. Kim, Y. M.; Choi, S. H.; Lee, H. C.; Hong, M. Z.; Kim, K.; Lee, H. I., Organic-inorganic composite membranes as addition of SiO_2 for high temperature-operation in polymer electrolyte membrane fuel cells (PEMFCs). *Electrochimica Acta* **2004,** 49, (26), 4787-4796.
53. Smitha, B.; Sridhar, S.; Khan, A. A., Proton conducting composite membranes from polysulfone and heteropolyacid for fuel cell applications. *Journal of Polymer Science Part B-Polymer Physics* **2005,** 43, (12), 1538-1547.
54. Liu, Y. H.; Yi, B. L.; Shao, Z. G.; Wang, L.; Xing, D. M.; Zhang, H. M., Pt/CNTs-Nafion reinforced and self-humidifying composite membrane for PEMFC applications. *Journal of Power Sources* **2007,** 163, (2), 807-813.
55. Rhee, C. H.; Kim, Y.; Lee, J. S.; Kim, H. K.; Chang, H., Nanocomposite membranes of surface-sulfonated titanate and Nafion$^{(R)}$ for direct methanol fuel cells. *Journal of Power Sources* **2006,** 159, (2), 1015-1024.
56. Benziger, J. B.; Chia, E. S.; De Decker, Y.; Kevrekidis, I. G., Ignition and front propagation in polymer electrolyte membrane fuel cells. *Journal of Physical Chemistry C* **2007,** 111, (5), 2330-2334.
57. Kimball, E.; Whitaker, T.; Kevrekidis, I.; Benziger, J., Drops, slugs and flooding in PEM fuel cells. *AIChE Journal* **2007**, (Submitted).
58. Lu, G. Q.; Liu, F. Q.; Wang, C. Y., An approach to measuring spatially resolved water crossover coefficient in a polymer electrolyte fuel cell. *Journal of Power Sources* **2007,** 164, (1), 134-140.
59. Berg, P.; Promislow, K.; Stumper, J.; Wetton, B., Discharge of a segmented polymer electrolyte membrane fuel cell. *Journal of Fuel Cell Science And Technology* **2005,** 2, (2), 111-120.
60. Hakenjos, A.; Hebling, C., Spatially resolved measurement of PEM fuel cells. *Journal of Power Sources* **2005,** 145, (2), 307-311.

61. Natarajan, D.; Van Nguyen, T., Current distribution in PEM fuel cells. Part 1: Oxygen and fuel flow rate effects. *AIChE Journal* **2005,** 51, (9), 2587-2598.
62. Hogarth, W. H. J.; Benziger, J. B., Dynamics of autohumidifed PEM fuel cell operation. *Journal of the Electrochemical Society* **2006,** 153, (11), A2139-A2146.

2 Viscoelastic Properties of Nafion Membranes at Elevated Temperature and Humidity

2.1 Abstract

Stress-strain properties of Nafion have been obtained under various states of humidity and temperature. Stress-relaxation tests have also been performed on Nafion in humidified and dry conditions at different temperatures and imposed strains, and a limited set of creep tests have been performed in humidified conditions at different temperatures and applied stresses. Stress-relaxation of Nafion has been modeled as a sum of three time constants and with the stretched-exponential Kohlrausch-Williams-Watts equation. Time-temperature superposition as well as time-strain (relaxation) and time-stress (creep) superposition master curves have been constructed. Stress-strain results indicate that Nafion's Young's modulus decreases with increasing temperature at low water contents, and decreases with increasing water content at room temperature. However, the temperature dependence is weaker for hydrated membranes, such that hydrated membranes are stiffer than dry membranes at elevated temperatures. The plastic modulus and yield, proportional and ultimate stresses decrease with increasing temperature and change little with water content. Proportional, yield and ultimate strains increase with increasing temperature, and the yield strain and, to a lesser extent, the proportional strain also increase with increasing water content. Stress-relaxation rates were found to follow two characteristic shapes, depending on strain, temperature and water content. The shift factors applied to form master curves of dry and humidified membranes also depend on strain, temperature and water content. Both phenomena support the idea that the addition of water slows down stress-relaxation rates.

2.2 Introduction

Researchers have recently begun studying the mechanical properties of fuel cell membranes as a way to understand fuel cell behavior and improve membrane and cell longevity [1-17]. Prolonged build-up of stresses from changes in temperature and membrane water content during dynamic cell operation has been identified as a key cause of mechanical failure of the membrane, either due to the formation of pin holes or delamination of the membrane from the electrode material [1-9], and work to improve Nafion or find alternatives has begun to expand its original focus on membrane conductivity and perm-selectivity to include durability and mechanical properties [5, 6, 10-12]. The Young's modulus is also known to govern equilibrium swelling and water sorption [10, 13-15], and stress-relaxation to govern water sorption dynamics [15-20].

However, as noted by many researchers [4-6, 10], there is a dearth of comprehensive information about the viscoelastic properties of fuel cell membranes, particularly at conditions relevant to fuel cell operation: elevated temperature and humidity. This scarcity is not surprising, as most mechanical testing equipment can easily be configured to operate over a range of temperatures, but has little allowance for humidity control, leaving the investigator with a limited choice of conditions: dry, ambient humidity or submersion in liquid water.

2.2.1 Stress-Strain and Young's Modulus

A summary of all work on elastic moduli reported through 2005 appears in Table 2.1. Generally, membranes at higher temperatures and higher water content exhibit a lower Young's modulus. Numbers with the ~ sign indicate values read from published curves.

Table 2.1: Summary of reported values for Elastic Modulus (Young's Modulus) of Nafion.

Researcher, Year	Material	Apparatus	Method	Water Content	Temp	Elastic Modulus [MPa]
DuPont Product Information [21]	Nafion PFSA Membranes, N-112, NE-1135, N-115, N-117, NE-1110		ASTM D 882	50% RH	23°C	249
				water soaked	23°C	114
					100°C	64
Werner, Jorissen et al. 1996 [22]	Nafion 117, 50 mm length	Zwick 1445 Universalprüf-maschine	Strain rate: 0.20/min in machine direction	Dry	25°C	~100
				"completely humidified"	25°C	~50
				Unspecified	200°C	~1
Kawano, Wang et al. 2002 [23]	Nafion 117, Aldrich, acid form, 25 mm length x 6mm	T.A. Instruments DMA 2980, controlled force mode, tension	Preload force: 0.005N, soak time: 1 min, force ramp rate: 0.500 N/min, upper force: 18.00N	water soaked, 24h	27°C	95
				boiling water soaked, 1h	27°C	128
				as-received	27°C	200
					60°C	147
					90°C	44
					120°C	5
					150°C	3
					180°C	2
				dry: vacuum oven 70°C, 24h	27°C	210
					60°C	176
					90°C	80
					120°C	13
					150°C	4
					180°C	2
Kundu, Simon et al. 2005 [6]	Solution Cast Nafion 117, 5mm gauge length x 6mm	Rheometrics DMTA V, tension	Preload force: 0.1N, strain rate: 0.001/min, max strain: 0.015-0.024.	water soaked	80°C	~45
	Solution Cast Nafion 112					~35
Fujimoto, Hickner et al. 2005 [24]	Nafion 117, 30mm gauge x 9mm	Com-Ten Industries 95T series load frame equipped, load cell: 200 lbf	Strain rate: 0.17/min	Ambient	RT	200
				soaked in water until tested	RT	52
Kyriakides 2005 [25]; Liu, Kyriakides et al. 2006 [5]	Nafion 117; pretreated boiling 0.5 M H_2SO_4 2h & boiling DI water 2h, dried 70 °C vacuum, 40 mm gauge length x 12mm	Instron 4468 screw-driven universal testing machine, load cell: 1kN	Strain rate: 0.7/min	equilibrated at 23°C, 40%RH 72h, water concentration: 5.3+/-1.5%	23°C	270 ± 4
			Strain rate: 0.3/min			253 ± 7
			Strain rate: 0.12/min			256 ± 18
			Strain rate: 0.07/min			263 ± 10
			Strain rate: 0.025/min			250 ± 5

Stress-strain behavior at different temperatures and humidities have also been investigated by Solasi et al. [8], though modulus values were difficult to estimate from the published curves.

Recently, work has expanded to cover more temperature and humidity combinations. Tang et al. [3] used a custom temperature and humidity chamber installed on an MTS Alliance RT/5 material testing system, and tested Nafion 112 in 16 different environments: 25, 45, 65, 85°C and 30%, 50%, 70% and 90% relative humidity. The Nafion was pre-treated in boiling 3% H_2O_2, 0.5M H_2SO_4 and deionized water for 1 hour each, dried at room temperature for 24 h and cut to 100 mm x 10 mm in transverse and machine extrusion directions. The gauge length for each run started at 50 mm but increased by varying amounts depending on the membrane's degree of pre-equilibration swelling and was tested at a uniform extension rate of 0.2 mm/min or, based on the original gauge length, roughly 0.004/min (0.4%)/min. Tang reported results for Young's modulus, ultimate stress and strain and "proportional limit" stress and strain, which was defined as the yield point is typically defined[26]. Their results for Young's modulus appear in Figure 2.1[3].

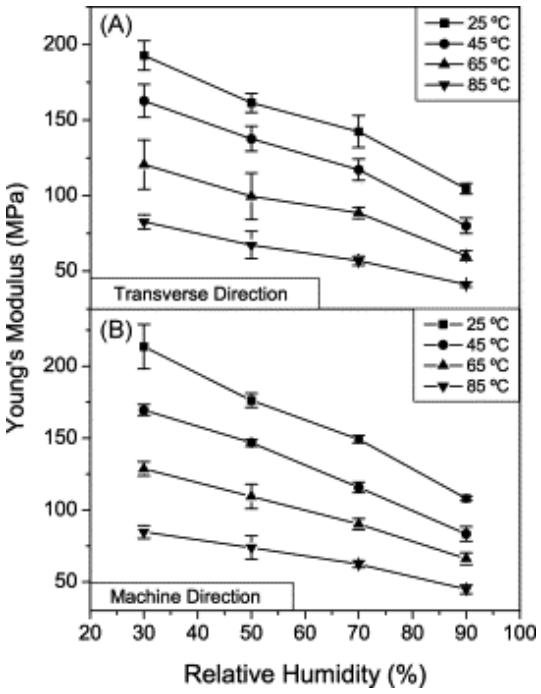

Figure 2.1: Variation of Nafion's Young's modulus with humidity at different temperatures, tested in direction of extrusion (machine direction) and perpendicular to extrusion (transverse direction) Figure reprinted from [3] with permission from Elsevier © 2006.

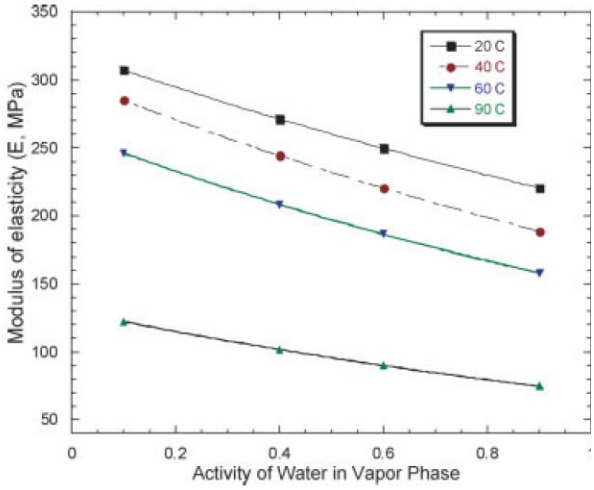

Figure 2.2: "Experimental variation of Young's modulus versus the activity of water vapor for Nafion." Figure & caption reprinted from [10] with permission from John Wiley & Sons, Inc. © 2006

Choi and Jalani et al. [10] used an optoelectronic holography technique, described in [27] on Nafion 112 with varying sample length and a pre-experiment environmental conditioning period of 1h. Their results for Young's modulus at temperatures of 30 and 90°C and humidities of 0%, 20%, 40%, 60%, 80% and 100% humidity appear in [27] and [28]. Their expression for Young's modulus E as a function of the dry modulus (E_0 = 316 MPa) and ε_w, the volume fraction of water in the polymer:

$$E = E_0 \exp\left[-2.1753\varepsilon_w\right] \tag{2.1}$$

appear in [10], as well as data at 20°C, 40°C, 60°C and 90°C and 10%, 40%, 60% and 90%, shown in Figure 2.2. The results of Tang et al. and Choi and Jalani et al. both agree with previous findings that increasing water and temperature decreases membrane stiffness.

2.2.2 Dynamic Mechanical Analysis

Dynamic Mechanical Analysis has yielded storage and loss moduli for Nafion at different temperatures and water contents. Bauer et al. [4] used a TA Instruments DMA 2980, adding a custom-built humidity cell that maintained relative humidities of 0%, 15%, 50%, 85% and 100% between room temperature and 100°C. They tested Nafion 117 samples, 30 mm length x 6 mm width, pre-treated in boiling 10% nitric acid 2h, rinsed in DI water & stored over DI water at room temp. The test parameters were 0.25N static force, frequency of 1 Hz and amplitude 15μm. Their results for storage modulus under different conditions appear in Figure 2.3.

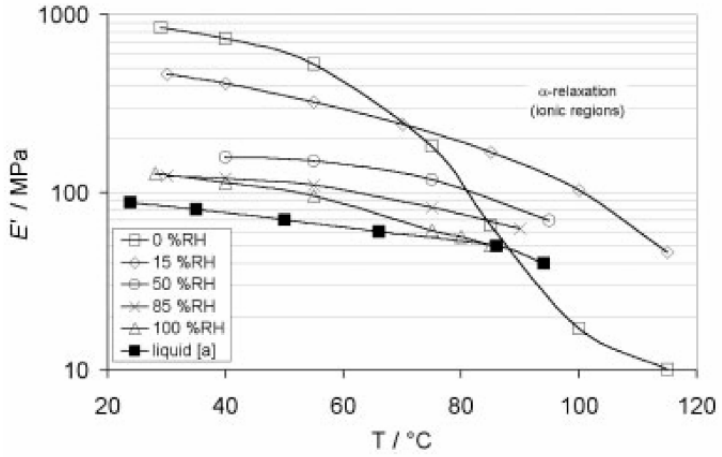

Figure 2.3: "E' of Nafion 117-H versus temperature at different RHs. [a] Uan-Zo-Li 2001." Figure & Caption reprinted from [4] with permission from John Wiley & Sons, Inc. © 2005

They found that the storage modulus of Nafion increased with decreasing water content at low temperatures, and that the storage modulus at all humidities decreased with increasing temperature. However the modulus of the membrane tested at 0% RH decreased much faster with temperature than those at any humidity, eventually becoming significantly lower than the hydrated membranes.

Budinski and Gittleman et al. [9] also performed dynamic tests on Nafion, using a both dry and wet Nafion 112. The test parameters were 0.020 N static force, 0.140N dynamic force, a frequency of 1Hz and a temperature ramp rate of 1°C/min for wet membranes and 10°C/min for dry. Typical results appear in Figure 2.4. [9]

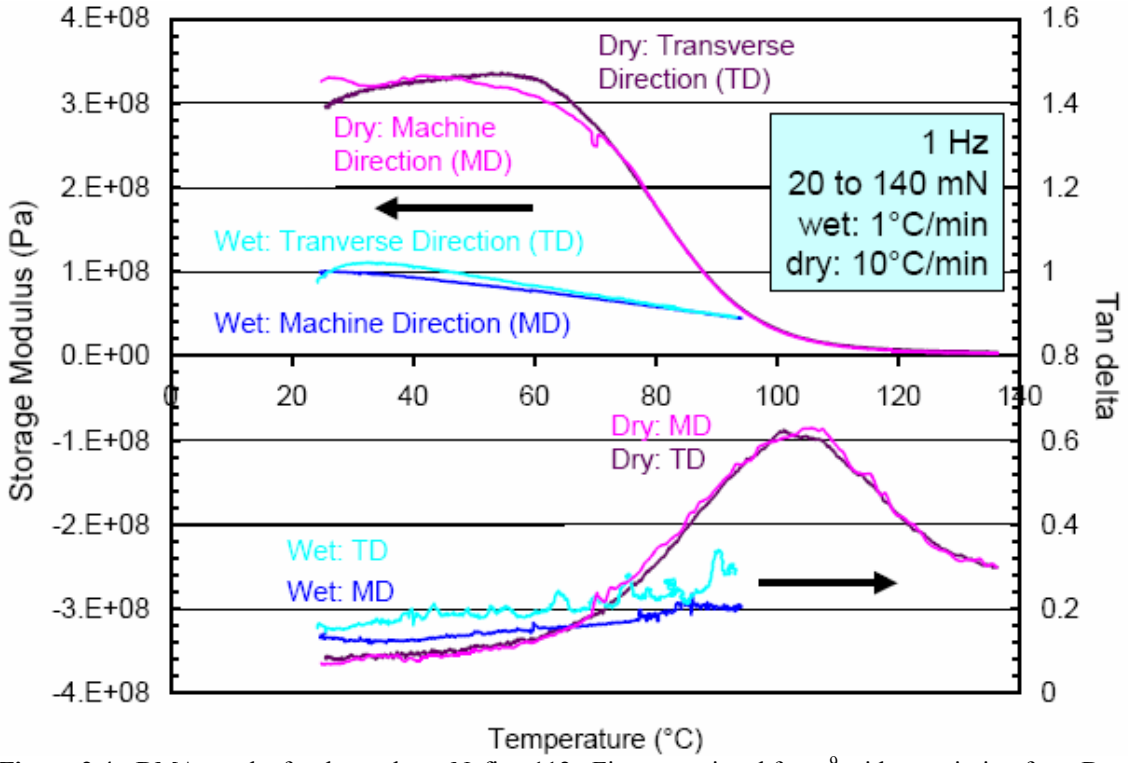

Figure 2.4: DMA results for dry and wet Nafion 112. Figure reprinted from [9] with permission from Dr. Craig Gittleman © 2004.

These findings agree with those of Bauer et al. [4] and Uan-Zo-Li [29] (which are plotted in Figure 2.3). The storage modulus of the saturated samples (blue lines) decreases with increasing temperature, but not as fast as that of the dry samples (pink & purple lines). The saturated test ended at roughly 95°C, at which point testing a sample in wet conditions at atmospheric pressure became impossible, but the saturated storage modulus was on course to cross and stay greater than the dry modulus. Also, the glass transition temperature, which for dry Nafion is at roughly 110°C, does not appear to be lowered (at

least to a temperature below 95°C) by the addition of water and may in fact be raised, a result also reported by Bauer et al. [4]. It should be noted that no glass transition temperature for well-hydrated Nafion has been reported, leading to the suspicion that there may not be a glass transition in hydrated Nafion. Yeo and Eisenberg [30] performed dynamic studies on Nafion 1365, dry and with a water content of $\lambda = 3$ H_2O/SO_3^- and reported that the glass transition temperature was essentially unchanged, though it is not clear how they controlled the water content, and water may have been driven off during the course of the test.

Because the goals of prolonging fuel cell life and understanding fuel cell behavior and water sorption dynamics require knowledge of membrane properties at elevated temperature *and* humidity, the extent to which these combined elastic modulus studies provide information for fuel-cell relevant conditions is depicted in Figure 2.5, which maps the data listed above on a temperature-water content space.

The water content λ, number of water molecules in the membrane per sulfonic acid group, has been estimated for the reported conditions with equation (2.2), an empirical third order polynomial fit to a Nafion sorption isotherm at 30°C [31].

$$\lambda = 0.043 + 17.81a_w - 39.85a_w^2 + 36.0a_w^3 \qquad (2.2)$$

Where a_w is the activity of water (relative humidity) in the test environment. Sorption of water has generally been found to increase slightly with temperature [32], especially at higher water activities[28], but for the simple purposes of estimation here, that effect will be neglected.

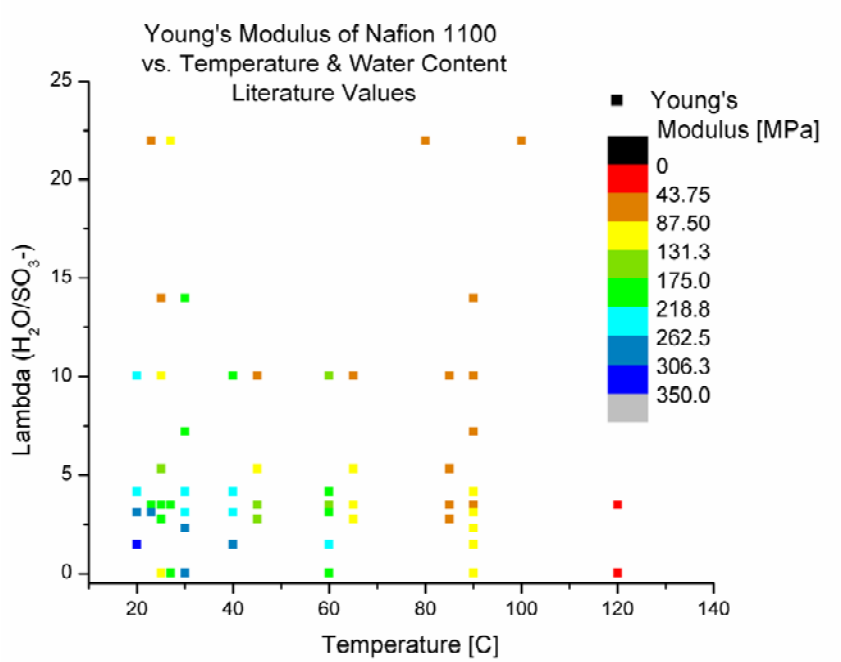

Figure 2.5: Young's Modulus of Nafion 1100 measured through stress-strain tests or optoelectronic holography at different humidities and temperatures, as reported in literature. [3, 5, 6, 10, 21-24, 27, 28]

Similar treatment for the storage modulus from DMA tests appears in Figure 2.6.

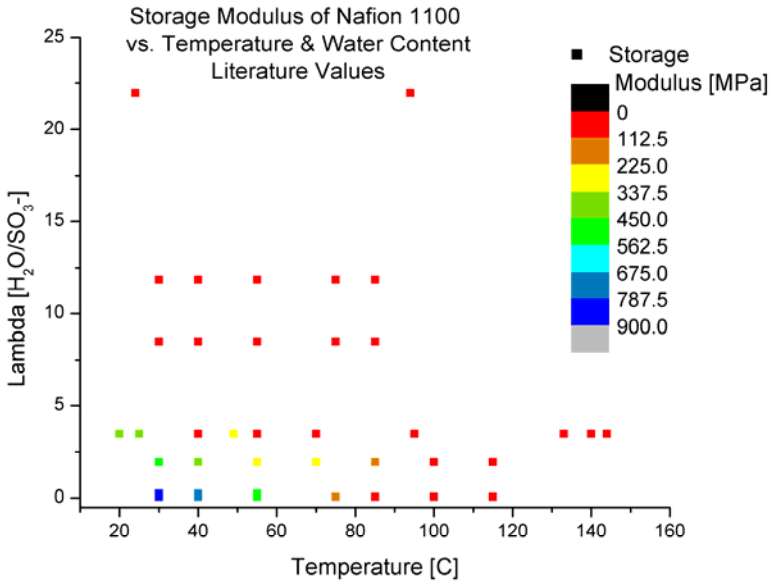

Figure 2.6: Storage Modulus of Nafion 1100 measured through DMA at different temperatures and humidities, as reported in literature. [4, 29]

From these property maps, it appears that the effect of water and temperature act together to reduce the elastic modulus of Nafion membranes (Figure 2.5), but that the storage

modulus of hydrated membranes is roughly constant with temperature (albeit constantly low).

2.2.3 Stress-Relaxation & Creep

Yeo & Eisenberg [30] performed stress-relaxation tests on Nafion 1365. They noted a large distribution of relaxation times, characterized by a broad stress-relaxation master curve Figure 2.7 and that the addition of a small amount of water (0.5 H_2O/SO_3^-) increased the stress-relaxation rate (Figure 2.8). Although it appears that the stress-relaxation master curve has simply changed shape with the addition of water, the authors reported that time-temperature superposition "broke down" with the addition of water, particularly at long times, and that while a master curve could be generated for dry Nafion, only a pseudo-master curve was produced for hydrated Nafion. This behavior was attributed to the influence of ionic clusters in the membrane and a small degree of crystallinity: water acted to plasticize the ionic domains, possibly adding or triggering another relaxation mechanism when introduced into the completely dry Nafion.

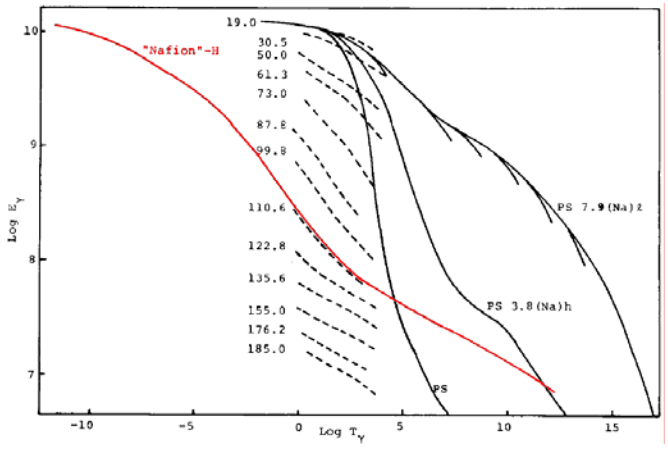

Figure 2.7: "Original stress-relaxation curves and master curve for Nafion-H as well as master curves for polystyrene PS and two styrene ionomers PS 3.8 (Na)h and PS 7.9(Na) $T_{ref}=T_g$" Figure and Caption reprinted from [30] with permission from John Wiley & Sons, Inc. © 1977. Color added. E in dyn/cm^2

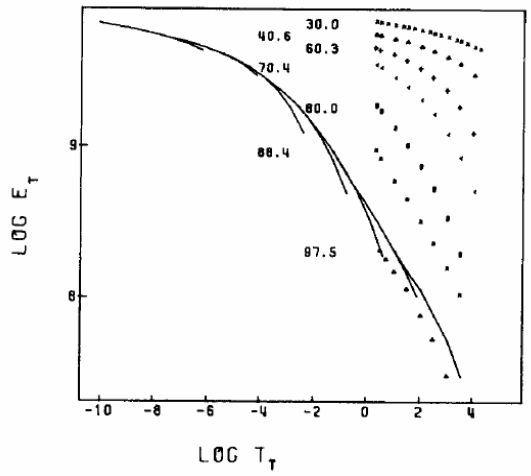

Figure 2.8: "Original stress-relaxation curves and pseudomaster curve for Nafion-H with 0.5 H_2O/SO_3H $T_{ref}=T_g$" Figure and Caption reprinted from [30] with permission from John Wiley & Sons, Inc. © 1977. E in dyn/cm^2

Kyu and Eisenberg reported stress-relaxation behavior of Nafion 1200-equivalent weight, dry and under water [33] and under methanol [34] in acid form and neutralized by Na^+ ions. Time-temperature superposition master curves for dry samples exhibited differences between the acid and sodium forms (the Na-neutralized sample relaxing more slowly), while acid and Na^+ curves obtained from samples immersed in water appeared very similar. They concluded that the strength of the effective crosslinking created by the ionic clusters was reduced when the clusters were hydrated, and that the presence of water eliminated the ionic interactions that cause dry Na-form Nafion to have a higher T_g and slower relaxation than dry acid-form Nafion [33, 34]. They also found that Na-form membranes stored in liquid water at 70°C for 3 days had much lower relaxation rates than 'fresh' samples in the temperature region tested (20-70°C), though the 10-second moduli were unchanged [34]. For the tests performed under water, the time-temperature superposition shift factor was plotted against 1/T, and, in the temperature range studied (20-70°C), exhibited Arrhenius behavior with an activation energy of 160 kJ/mol [34]. Stress-relaxation tests on Na^+-form Nafion under methanol produced stresses an order of

magnitude lower than under water tests, but similar stress-relaxation rates. This observation agreed with their conclusion that the magnitude of the stress response is due to the polymer matrix and the relaxation rate depends on the ionic clusters. Methanol interacts more with the polymer matrix than water but has a similar amount of interaction with the clusters [34].

Recently, stress-relaxation tests have been performed by Liu and Kyriakides [5] under ambient conditions (23°C & 40% RH) at different strains and strain rates [5] and underwater or at ambient conditions at two different strains by Liu and Hickner [7]. Nafion 117 was pretreated in boiling 0.5 M H_2SO_4 2h and boiling deionized water for 2h, and then either dried overnight at 70°C in vacuum for testing under ambient conditions or stored in deionized water at room temperature for underwater testing. An Instron 4468 testing machine with a 1 kN load cell was used for ambient condition testing, and a Tytron 250 MTS machine performed the underwater tests.

For ambient tests, samples were equilibrated for 72h in ambient conditions prior to testing to achieve water contents of 5.3 +/- 1.5%, or λ-values of approximately 3. For the degree-of-strain tests, samples were strained at 0.12 %/min to strains of 1, 3, 6, 7.5, 25, 50, 100, and 200% [5]. For strain-rate tests, samples were strained to either 3% or 50% at rates of 0.7, 0.3, 0.12, 0.07 and 0.025/min [5]. Ambient and underwater tests were performed at strains of 25% or 50% and underwater at 30°C or in air at 23°C (room temperature) [7].

The ambient degree-of-strain tests resulted in a time-strain superposition master curve, shown in Figure 2.9.

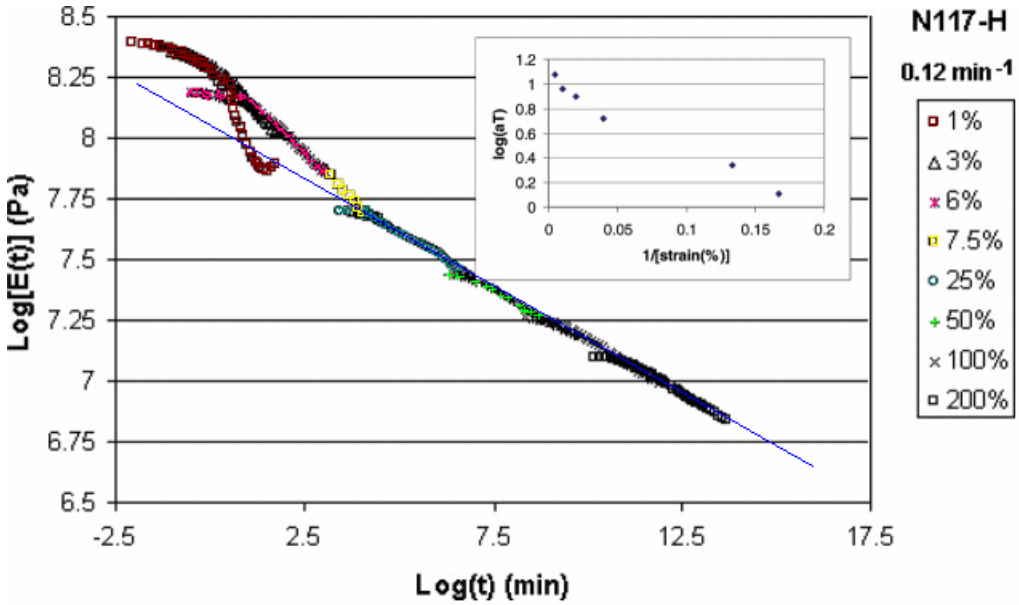

Figure 2.9: "Shifted logarithm plot of E(t) versus t (min) for N117-H films and plot of log a_T versus 1/[strain (%)]."Figure and Caption reprinted from [5] with permission from John Wiley & Sons, Inc. © 1977. Colors & blue line added.

At strains at and below the yield point of 7.6%, the authors noted divergence from the linear behavior observed at higher strains (blue line in Figure 2.9), with a faster relaxation rate. They postulated that this increased relaxation rate was due to "the softening effect of a small amount of water uptake at the beginning of the stress-relaxation process", causing strains on the order of the strains imposed by the test [5]. They also reported on the effect of strain-rate tests. Different strain rates showed little effect on membranes when the imposed strain was only 3% (below the yield point). For the membranes strained to 50% (well beyond the yield point), the relaxation rates were similar, but the modulus values were slightly higher, producing lines of similar slopes but different intercepts on a log-log plot. This rate-independence below the yield point agreed with the findings of their stress-strain tests at different strain rates [5]: the elastic (pre-yield) modulus was independent of rate, but the yield stress increased with strain rate while the yield strain decreased.

The ambient and underwater stress relaxation results [7] appear in Figure 2.10 and were fit to three exponential terms:

$$\sigma = \sigma_\infty + \sigma_1 e^{-t/\tau_1} + \sigma_2 e^{-t/\tau_2} + \sigma_3 e^{-t/\tau_3} \qquad (2.3)$$

Where σ is the stress at some time t, σ_∞ is the equilibrium or residual stress and the σ_i and τ_i terms refer to the elastic and viscous components (respectively) which make up the time-dependent response. The resulting time constants are summarized in Table 2.2.

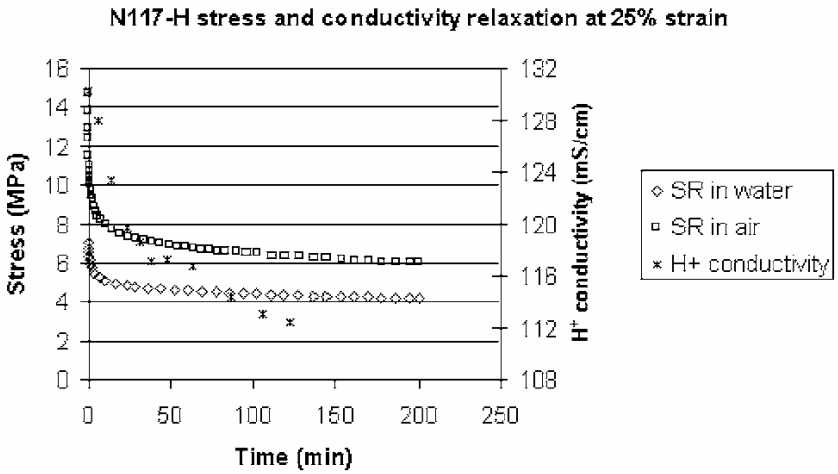

Figure 2.10: Stress relaxation (SR) of Nafion 117. 30°C and 25% strain. Figure reprinted from [7] with permission from ASME © 2006.

Table 2.2: Stress-relaxation rates of Nafion at different applied strains in air and water. Reported in [7]

Strain	Conditions	τ_1 (sec)	τ_2 (sec)	τ_3 (sec)
25%	Water, 30°C	41	407	5874
	Air, 23°C	20	346	2478
50%	Water, 30°C	22	539	25680
	Air, 23°C	20	170	1644

The stresses were not reported in the work, but on the basis of work done here (discussed below), the stresses are probably about equal, with a slightly higher weighting of the shorter time constant, and sum to the initial stress. In Figure 2.10 it is clear that the absolute stress of the submerged sample was lower, and the stress-relaxation rates shown in Table 2.2 are slower for the submerged sample. The authors postulate that because water plasticized the membrane and reduced the stress, the driving force for stress

relaxation was lower, causing the slower rate [7]. The result that stress-relaxation is slowed in hydrated Nafion, combined with results from Bauer et al. [4] and Uan-Zo-Li [29] that the glass transition temperature of Nafion appears to increase (or disappear, as believed by this lab) highlights an unpredicted influence of water on the viscoelastic properties of Nafion that will be further explored in this work.

Kyriakides [25] also investigated creep and recovery behavior of Nafion 117 over a time period of 2 hours under ambient humidity and temperatures of 10°C to 130°C by using dynamic mechanical analyzers from TA Instruments with a preload stress of 0.5 MPa. The compliance results were used to generate a time-temperature superposition master curve, shown in Figure 2.11.

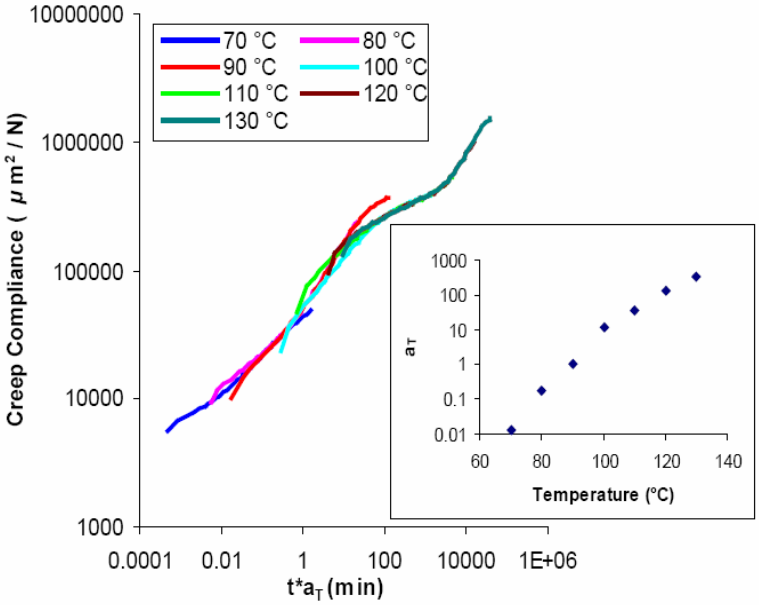

Figure 2.11: "Nafion 117 creep compliance master curve." Figure & caption reprinted from [25] with permission from S. Kyriakides © 2005.

The work presented here further expands on the data published in these previous and concurrent works, providing more detailed and extensive information.

2.3 Procedure

Extruded Nafion® 115 films (DuPont product, equivalent weight 1100 g polymer/mol SO_3^-, 127 μm thickness) were obtained from Ion Power (New Castle, Del). All membranes were cleaned and ion-exchanged by boiling for 1 hour in 3% H_2O_2 in water, 20 minutes in de-ionized (DI) water, 1 hour in 1 M sulfuric acid and 20 minutes in DI water.

This is a standard procedure for treating received Nafion before use in a fuel cell. The step of boiling in 3% H_2O_2 is meant to eliminate organic matter collected from the atmosphere by the sulfonic groups and removes a yellow-brown tinge from the membranes, turning them clear and colorless. They are then ion-exchanged by boiling for approximately 1 hour in 1 molar sulfuric acid, which removes any other counter-ions from the membrane and replaces them with H^+, forming what is commonly called acid-form or H-form Nafion. Nafion can also be ion-exchanged into other forms (Li^+, Na^+, K^+, Cs^+, etc.) for research purposes by soaking in the appropriate salt solution. This procedure for ion-exchanging Nafion by boiling in acid is an accepted standard in this lab. Other labs sometimes use nitric acid, hydrochloric acid or different concentrations of sulfuric acid and different treatment times, but the conversion to acid-form is universally accomplished. Experiments in this lab [13, 35] and others [36, 37] that measured the equivalent weight of newly-developed membrane materials have re-exchanged acid for sodium by soaking in NaCl and then titrated the solution to determine the number of protons released during exchange. When Nafion is used as a control for those experiments the equivalent weight of nearly 1100 g polymer per mole acid is reproduced, indicating a near 100% exchange of ions.

After cleaning and ion-exchanging, the membranes were stored at room temperature and 100% relative humidity. Membranes were die-punched into dogbone samples, overall dimensions: 3.81cm x 1.59cm, gauge dimensions: 2.25cm x 0.475cm. Because Nafion's dimensions can change with water content, care was taken to equilibrate the Nafion at the water content of interest before die-punching.

2.3.1 Stress-Strain

Stress-strain experiments were performed in an Instron 1122 tensile tester, with an Instron model 3111 environmental chamber, pictured in Figure 2.12.

Figure 2.12: Instron 1122 & environmental chamber used for stress-strain tests

To test membranes at room temperature and varying water activity, membranes were conditioned over saturated salt solutions at humidities of 6% (LiBr), 6% (NaOH), 9% (KOH), 29% ($CaCl_2$), 33% ($MgCl_2$), 38% (NaI), 51% ($Ca(NO_3)_2$), 60% ($NaNO_2$), 63% ($MnCl_2$), 75% (NaCl), 84% (KCl), 94% ($CuSO_4$), and 97% (K_2SO_4) [38, 39] for at least two

weeks. Four membranes were tested at each pre-equilibrated water content. Three membranes were also tested after each of: 1 day of immersion in liquid water, 1 hour of immersion in boiling water and 1 day and 2 weeks of equilibration with water vapor at 100% humidity. In all cases samples were then removed and tested under ambient conditions. Testing was completed in ~2 minutes, and membranes were weighed before and after the test, with the average weight used to determine their water content during the test. The wettest membranes (boiled in water) lost at most 10.3% of their initial weight, which translates to λ changing from 24 to 15, while the dry membranes gained at most 2.5% of their initial weight, or changing λ-value from 2.6 to 4.0. Average weight loss was 4.3% and average weight gain was 1.3%.

To test membranes at elevated temperatures and ambient humidity, samples were cut and loaded into the testing apparatus. The chamber was then heated to the desired temperature, and the test was run immediately. Because a well-hydrated piece of Nafion can lose all of its water in the time typically needed for the oven to come up to temperature [40], only the weight of the membranes after the test was used for water content determination. At least four membranes were tested at each temperature, from 40°C to 120°C by 10°C increments. Of the membranes tested in these elevated-temperature runs, roughly half were stretched in the machine direction and the other half in the transverse direction (parallel and perpendicular to direction of extrusion, respectively). Four membranes were also tested at elevated temperature (~75°C) after being stored in liquid water. Their weights after the test were recorded and showed that they retained some hydration during the test, and they appear with slightly elevated water contents in the results section.

To better test membranes at elevated temperature and humidity, samples were placed in a 1-gallon sealed plastic bag with ~100 mL of water & clamped into the Instron machine through the bag, as pictured in Figure 2.13.

Figure 2.13: Instron 1122 outfitted with plastic bag vapor barrier for elevated humidity tests.

The bag was kept slack so as not to interfere with the test, and runs with an empty bag at different temperatures indicated that the effects of the bag on the reading were minimal, amounting to only a few percent of the results. Three tests were run under humidified conditions at each temperature: 50°C, 60°C, 70°C, 80°C and 90°C, and the water content was assumed to be ~13, the λ value typically achieved at 100% RH [41].

As seen in Table 2.1, there is no agreed-upon value for strain rate within the field. For these experiments, the elevated-temperature stress-strain tests were run at a constant extension rate of 50 mm/min (2.28/min strain rate) and room-temperature tests were run at an extension rate of 12.7 mm/min (0.57/min strain rate). Because the results of different strain rates showed little difference from each other at room temperature, their results are treated equally. A limited set of tests were performed at different extension

rates: 2.5 and 0.5 mm/min at room temperature and ambient humidity, and will be discussed.

2.3.2 Stress-Relaxation

Relaxation tests were performed in an Instron 5865 testing machine with an Instron 3111 environmental chamber. Samples were either run at ambient humidity or in the sealed bag at ~100% RH or ~0% RH (with Drierite® desiccant) at different temperatures. For the elevated humidity tests, Nafion was stored at room temperature and 100% RH after being cleaned, then removed and cut to the dogbone size. The sample & bag were then loaded into the Instron and allowed to equilibrate for at least 2h at the test temperature. For dry tests, Nafion was dried at 70°C over drierite for 2h after being cleaned, stored at room temperature over Drierite, then removed and cut to dogbone size. Equilibration after loading the sample and bag into the Instron was shorter: about 10 to 15 minutes, or roughly the time needed for well-hydrated Nafion 115 to lose water at the test temperature [40, 42]. After equilibration the gauge length was adjusted until the sample appeared taut. The gauge length was then re-adjusted, the load cell baseline 'zeroed' on the Instron console, and the test was started. The membranes were strained at 50%/sec to pre-selected strains of 2%, 5%, 10% and 20% and held while the relaxing stress was monitored. The initial stress recorded for the 2% and 5% tests was also used to determine Young's modulus and added to the data gained through constant strain-rate tests. Although some runs were repeated, generally one membrane was tested at each strain, temperature and humidity condition. Again, several tests on a bag with no membrane indicated that the bag affected the readings by only a few percent.

Further, tests on the membranes heated (which created dry conditions) but not in a bag agreed well with tests of membranes heated and tested in a bag with drierite.

2.3.3 Creep

Tests of membrane creep were performed in a custom-built apparatus, pictured in Figure 2.14 (room temperature tests) and Figure 2.15 (elevated temperature tests).

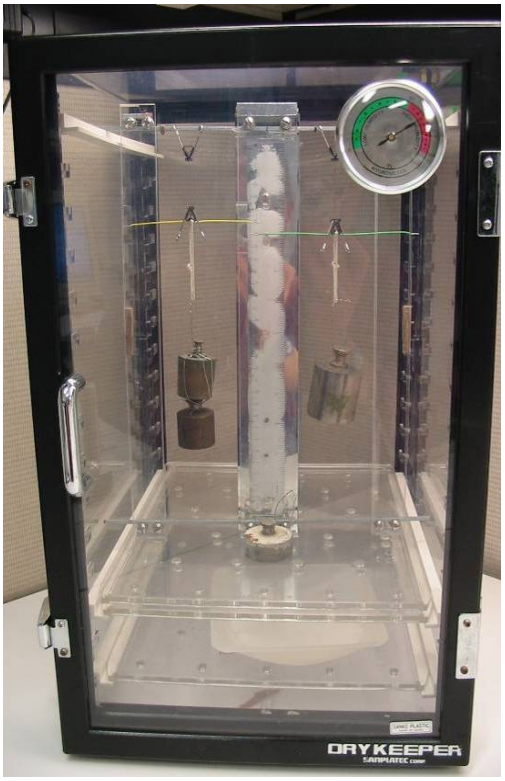

Figure 2.14: Controlled-humidity creep experiment.

Figure 2.15: Controlled humidity & temperature creep experiment

Membranes were held by clips and allowed to equilibrate for a period of several days. To begin the test, weights were hung from the bottom clip and the extension was recorded over time by reading the needle position from the accompanying ruler. The entire assembly was constructed within a desiccator box to control the humidity, and the box was placed inside an oven to run elevated temperature & humidity tests. Initial stresses between 1.24 and 8.1 MPa were applied. One membrane was tested at each temperature and stress.

2.4 Data Treatment & Analysis

2.4.1 Stress-strain

Young's modulus was calculated from the slope of the stress-strain curve in the elastic (small strain) region. Proportional stress and strain were the first points to deviate from the linear region. Yield stress and strain were taken either from a local maximum in the transitions region between elastic and plastic deformation or, when a local maximum did not occur, as the point where the maximum rate of change of slope occurred, determined from the intercept of the third derivative of a 4th-order polynomial fit to the data in that region. The plastic modulus was calculated from the linear portion of the stress-strain curve after yielding and the ultimate stress and strain were the final point before breaking. Figure 2.16 shows a sample of two representative stress-strain curves.

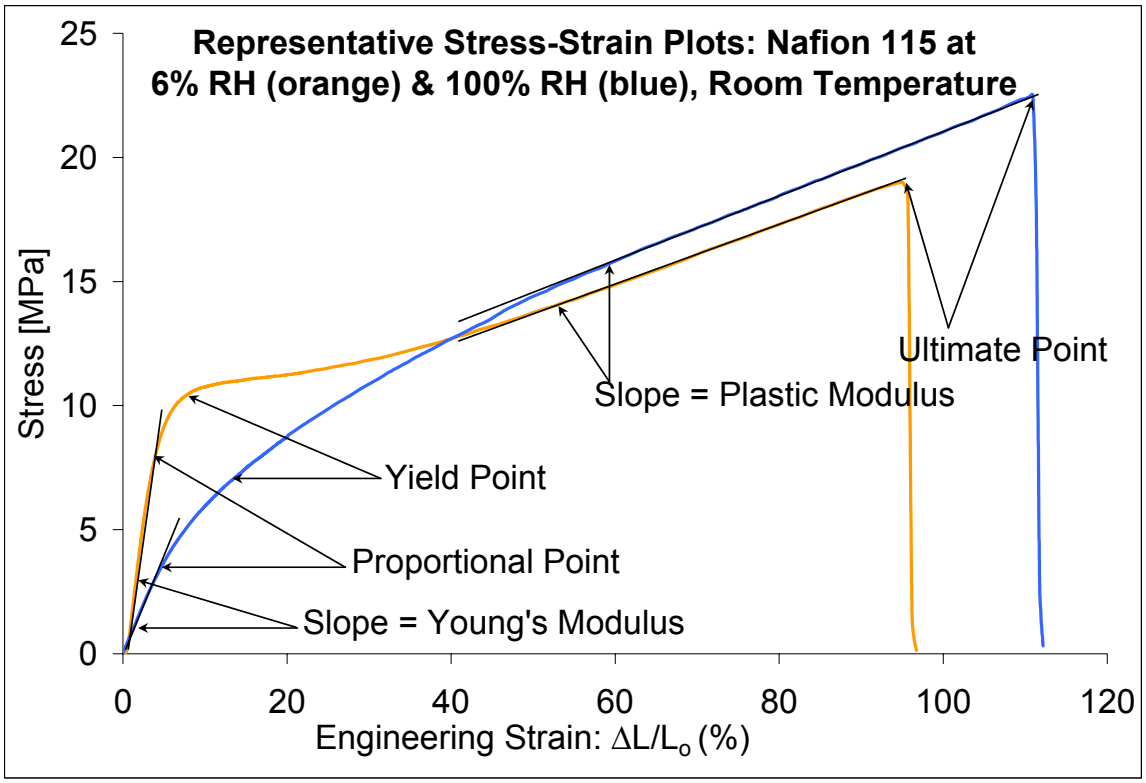

Figure 2.16: Sample analysis of stress-strain curves on Nafion 115

2.4.2 Stress-relaxation

Stress-relaxation data were analyzed using three spring and dashpot elements in parallel, based on the model of an infinite number of parallel elements called the Generalized Maxwell Element by Rosen [43] or the Maxwell-Wiechert Model by Alkonis and MacKnight [44]. Three parallel elements were found to capture the membrane's behavior well without introducing excessive complexity, and a spring in series was added to account for residual stress observed in the samples. This is the same model proposed independently by Liu and Hickner [7]. Figure 2.17 shows the mechanical description:

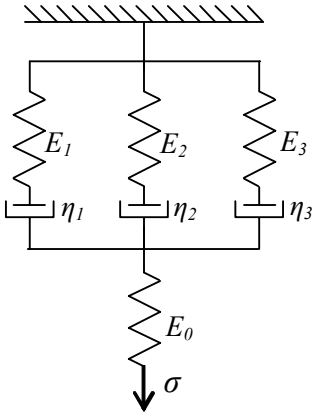

Figure 2.17: Stress relaxation spring & dashpot model: 3 parallel Maxwell elements & a residual stress spring in series

In this model, each dashpot element is represented mathematically by:

$$\frac{d\varepsilon}{dt} = \frac{\sigma}{\eta} \tag{2.4}$$

where η is the viscosity, ε is the imposed strain, and σ is the measured stress.

Each spring element is represented by:

$$\sigma = \varepsilon E \tag{2.5}$$

where E is the elastic modulus.

Placed in parallel, these elements give the solution:

$$E(t) = \frac{\sigma}{\varepsilon} = E_0 + E_1 \exp\left[\frac{-E_1}{\eta_1} t\right] + E_2 \exp\left[\frac{-E_2}{\eta_2} t\right] + E_3 \exp\left[\frac{-E_3}{\eta_3} t\right] \quad (2.6)$$

where $E(t)$ is the stress-relaxation modulus, the measured stress divided by the constant imposed strain. Each E_i/η_i element is equivalent to an inverse time constant τ_i, used by Liu and Hickner [7].

Were an infinite series of parallel elements being considered, the solution would be

$$E(t) = \frac{\sigma}{\varepsilon} = \sum_{i=1}^{\infty} E_i \exp\left[\frac{-E_i}{\eta_i} t\right] \quad (2.7)$$

Stress-relaxation was also fit with the stretched exponential Kohlrausch-Williams-Watts or Weibull equation, commonly applied to relaxation in polymers [45-48]

$$E(t) = \frac{\sigma}{\varepsilon} = E_0 + (E_i - E_0)\exp\left[-(kt)^d\right] \quad (2.8)$$

Where E_i is the initial modulus, E_0 is the residual (final) modulus, and k and d are empirical values, sometimes called the "characteristic life" and "shape" parameters, respectively[46]. All fits were performed in the graphing program Origin.

Time-temperature superposition was applied to the stress-relaxation results for each strain. Time-temperature superposition makes use of accelerated relaxation or creep kinetics at higher temperatures to predict long-term behavior of the polymer at lower temperatures. By dividing the time by a shift factor a_T, the log(modulus) vs. log(time) curves are shifted along the log(time) axis with respect to a curve generated at some reference temperature (here 30°C) to form a master curve. Higher temperatures are shifted to longer times, and the shift factor is expected to decrease with temperature. Time-temperature superposition was also performed on the resultant creep data. Further, because a range of strains were investigated in this work (both in and outside of the linear

stress-strain region) and the stress-relaxation behavior was found to depend on imposed strain, not only were the time-Temperature superposition master curves separated by strain, but time-strain superposition was applied to runs performed at each temperature.

Finally, to determine the membrane water content, the membranes were dried 24h at 170°C after testing, and the difference between the dry mass and mass at test time was used to determine the water content, λ [mol H_2O/mol SO_3^-] using equation (2.9).

$$\lambda\left(\frac{\text{mol } H_2O}{\text{mol } SO_3^-}\right)=\frac{\left(M_{Test}-M_{Dry}\right)\cdot\frac{1 \text{ mole } H_2O}{18.015 \text{ g } H_2O}}{M_{Dry}\cdot\frac{1 \text{ mole } SO_3^-}{1100 \text{ g Membrane}}} \tag{2.9}$$

2.5 Results

2.5.1 Stress-Strain

The stress-strain properties exhibited a range of values, depending on membrane water content and temperature. Young's modulus decreases with increasing temperature at low λ-values, and decreases with increasing λ at room temperature. However, the temperature dependence is weaker for hydrated membranes. The plastic modulus and yield, proportional and ultimate stresses decrease with increasing temperature and change little with λ. Proportional, yield and ultimate strains increase at higher temperatures, and the yield and proportional strains increase with increasing λ. Minimum and maximum values of properties obtained in stress-strain tests appear in Table 2.3.

Table 2.3: Minimum & maximum values of tensile stress-strain properties of Nafion 115.

	Young's Modulus [MPa]:	Plastic Modulus [MPa]:	Pro-portional Point Stress [MPa]:	Pro-portional Point Strain:	Yeild Point Stress [MPa]:	Yield Point Strain:	Ultimate Stress [MPa]:	Ultimate Strain:	Toughness [MJ/m^3]:
Min	5	1	0.3	1%	1	8%	5	88%	763
Max	308	15	8	11%	12	46%	29	394%	3563

Again, the large difference between minimum and maximum values of this data is due to differences in temperature and water content, and will be discussed in more detail below, but the average* values are also worth noting: roughly 140 MPa for Young's modulus, 10 MPa for plastic modulus, 3 MPa and 3% strain at the proportional point, 10 MPa and 15% strain at the yield point, 20 MPa and 180% strain at the ultimate point and 2000 MJ/m^3 toughness.

The shapes of the curves change under different conditions. Figure 2.18 shows representative runs for membranes equilibrated at room temperature over different salt solutions to yield different water contents. The ultimate points have been cut short to concentrate on early-strain behavior, but the very high water-content membranes have a lower ultimate stress and similar ultimate strain, as shown later in Figure 2.24.

* Average is an unweighted mean of available data.

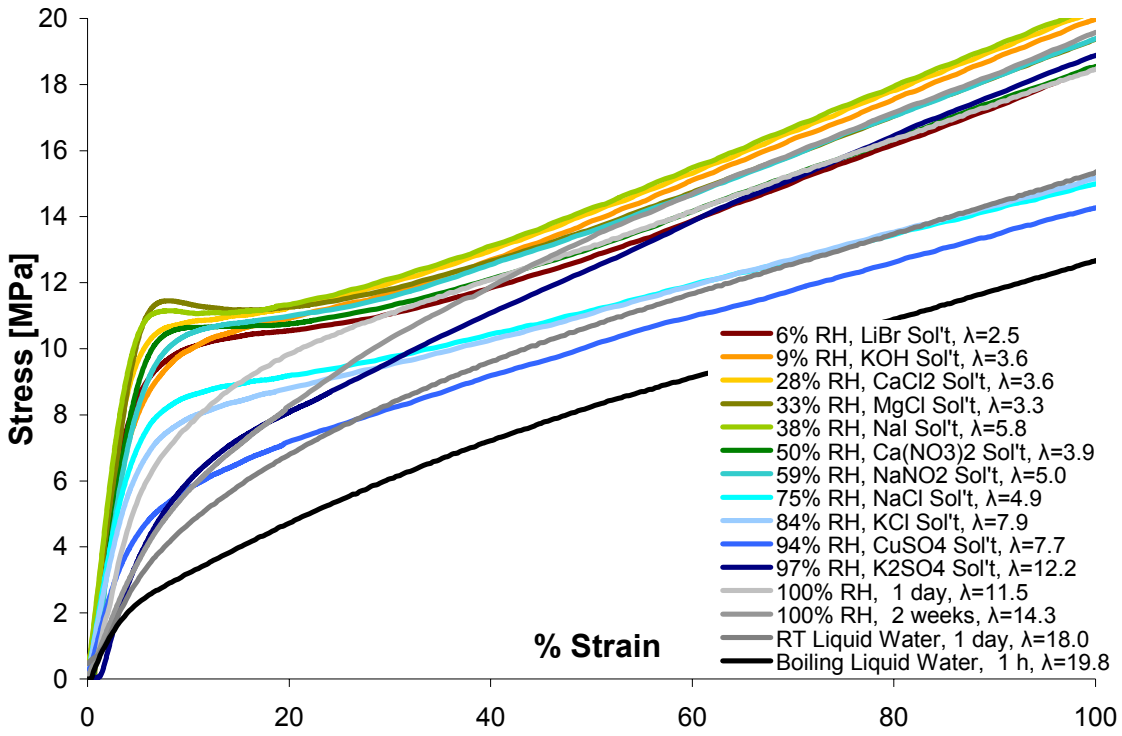

Figure 2.18: Stress-strain curves of room temperature Nafion membranes equilibrated at different hydrations.

Between 28% and 38% humidity there is a distinct local maximum at the yield point, which is not present in drier or wetter membranes. At very elevated humitidies (>95%), no clear yield point can be distinguished at all, a phenomenon also noted by Solasi et al. [8], who suggested that it was a result of changing membrane structure with increased water content. In the absence of a maximum the yield point was defined as the point of greatest rate of change of slope, as discussed in *Data Treatment and Analysis*. Except for the membrane equilibrated in 100% humidity for just 1 day (pale gray line), the membranes all follow a trend of decreasing Young's modulus with increasing hydration. That the one-day equilibration curve does not follow the trend of the membranes equilibrated for 2 weeks indicates that either membrane aging affects the results, or that there is a prolonged time for the membrane structure to equilibrate with the surrounding humidity. However, despite the reduced Young's modulus, the hydrated membrane

curves tend to cross those of the drier membranes. It appears that as well as becoming less defined, the yield point is delayed at humidities >95% (also shown in Figure 2.24), such that even though the Young's modulus is lower, the curves of the more hydrated membranes stay in the elastic (higher slope) region longer, causing them to cross the curves of the drier membranes which have already gone through their plastic transition and changed to a lower modulus.

It is evident from the legend in Figure 2.18 that the values of λ do not exactly match with the humidity at which the membrane was equilibrated. This is due to water gain and loss during the course of the test, which can be affected by different ambient humidity and speed of sample loading and unloading. However, the change in curve shape with pre-equilibration humidity is preserved; a set of four samples was tested at each humidity and, despite sample-to-sample variation in measured λ, exhibited very similar curve shapes. Though λ is admittedly an approximate measurement, it remains the best way to characterize and assign numerical value to the membrane hydration state for purposes of comparison and graphing.

Figure 2.19 shows representative runs for membranes at ambient humidity and increasing temperature.

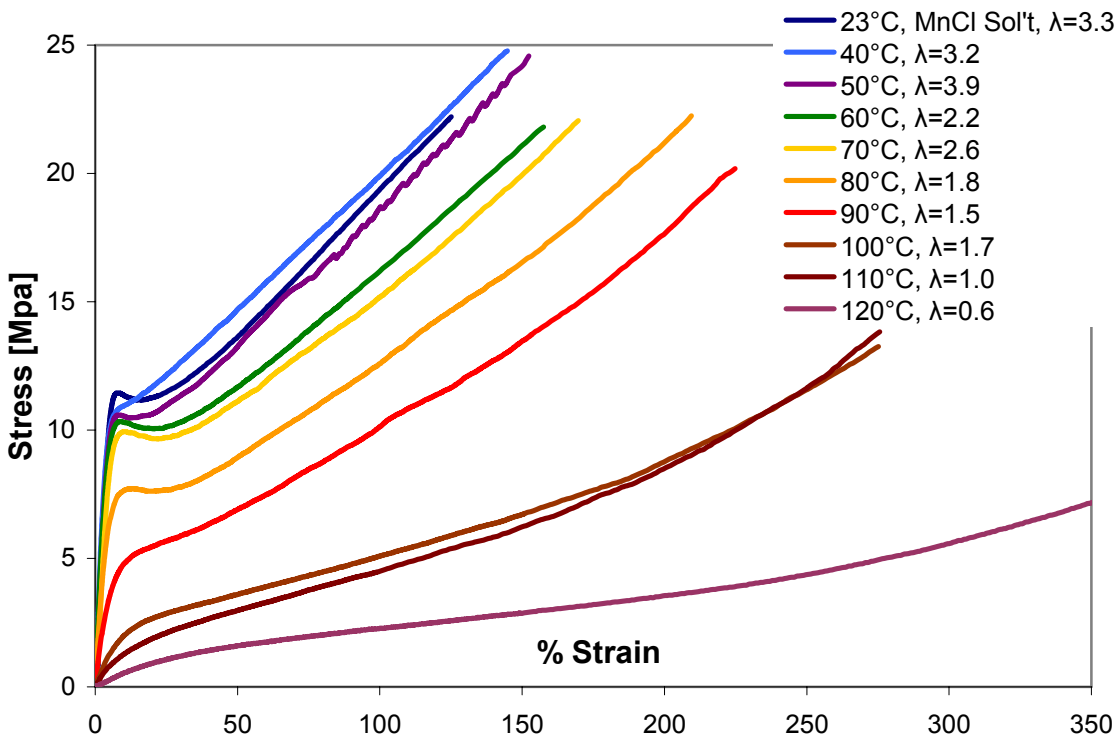

Figure 2.19: Stress-strain curves of Nafion membranes at ambient humidity and different temperatures.

With increasing temperature the Young's modulus and plastic modulus decrease, the local maximum at the yield point disappears, and the linear post-yielding region of the curve begins to turn upwards near the ultimate point, possibly due to membrane crystallization.

Finally, representative curves of Nafion at elevated water content and temperature are presented in Figure 2.20.

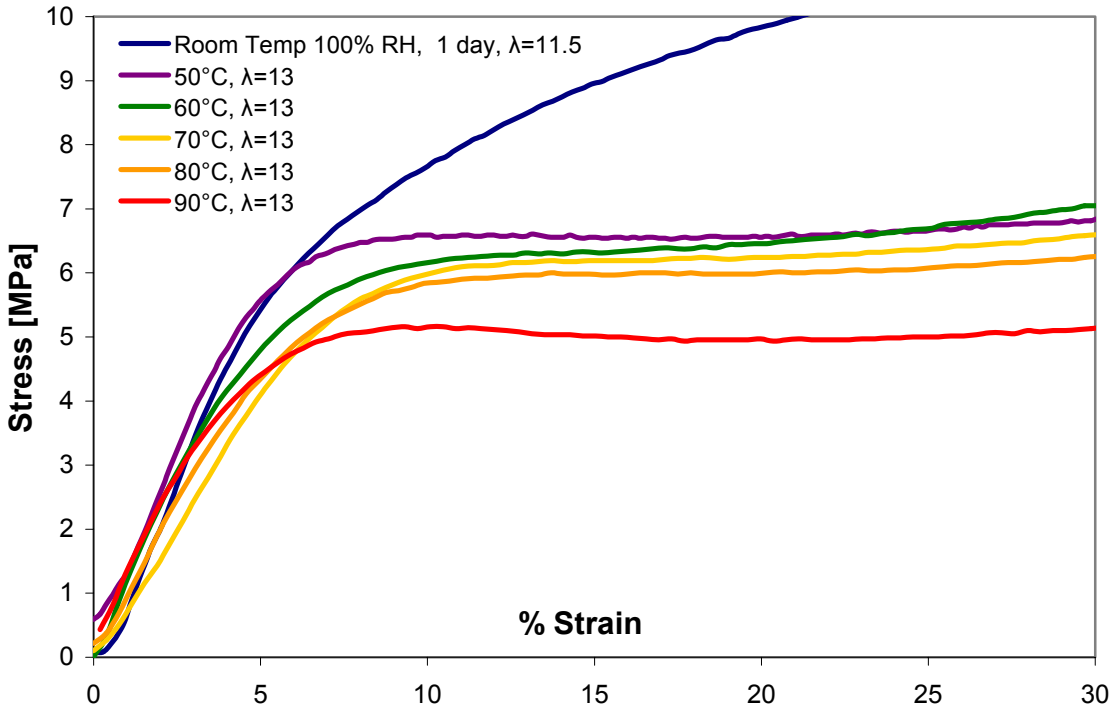

Figure 2.20: Stress-strain curves of Nafion membranes at 100% humidity and different temperatures.

The defining feature of this graph is the lack of a systematic dependence of Young's modulus on temperature. Though there is some spread in the data from run to run, these individual curves contribute to average values of Young's modulus that vary little with changing temperature.

The trends with temperature and humidity that are observed from the stress-strain curves above are extracted to values in the graphs below (shown in terms of color) and mapped on an x-y plane showing different temperature and water content combinations. Values of the Young's modulus, plastic modulus and toughness appear in Figure 2.21, Figure 2.22 and Figure 2.23 respectively. Results for the proportional, yield and ultimate points appear in Figure 2.24. The elevated temperature and humidity graphs have had their temperatures and water contents offset by ± 1°C and ± 0.5 λ, forming a cluster to show the values found in different runs at those conditions.

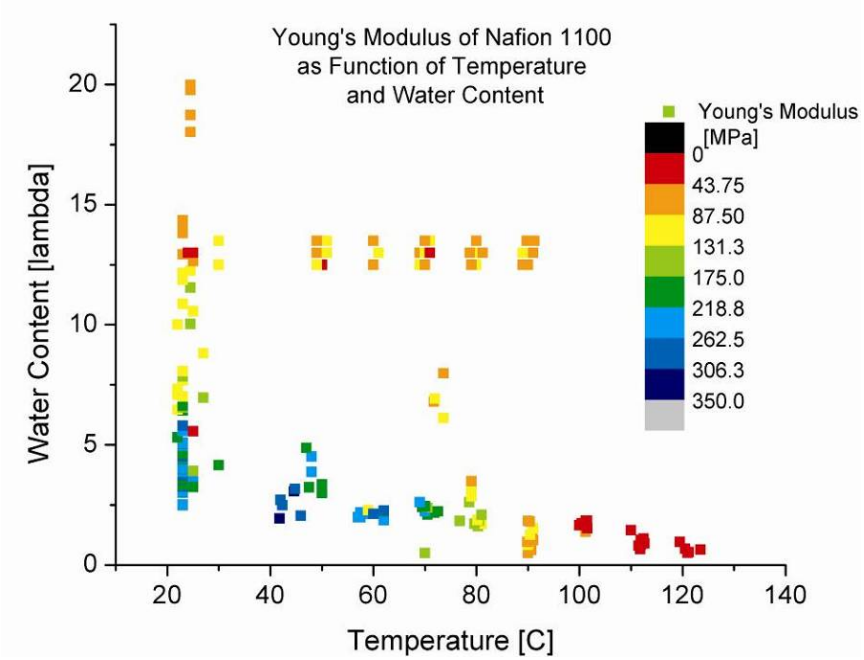

Figure 2.21: Young's modulus measured from stress-strain curves and initial response in relaxation tests

The Young's modulus decreases with both increasing temperature and water content, though increased hydration and temperature do not act together to soften the membrane. In fact, at elevated water content the temperature-dependence of the modulus appears to vanish. The plastic modulus decreases with increasing temperature but does not change significantly with water content.

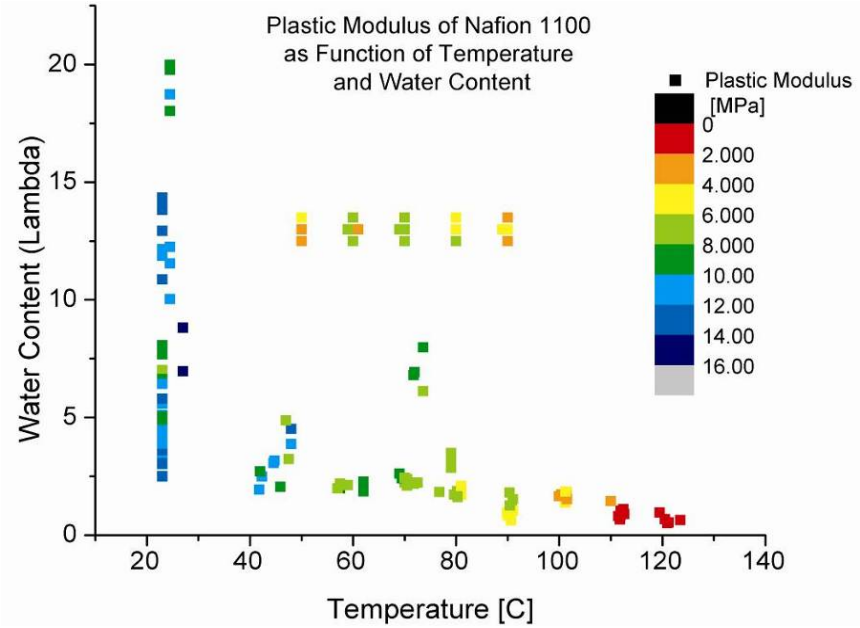

Figure 2.22: Plastic modulus of Nafion 115 measured from stress-strain curves.

The toughness decreases with increasing temperature when dry and water content at room temperature, though the temperature dependence at high-water content is not clear from these results.

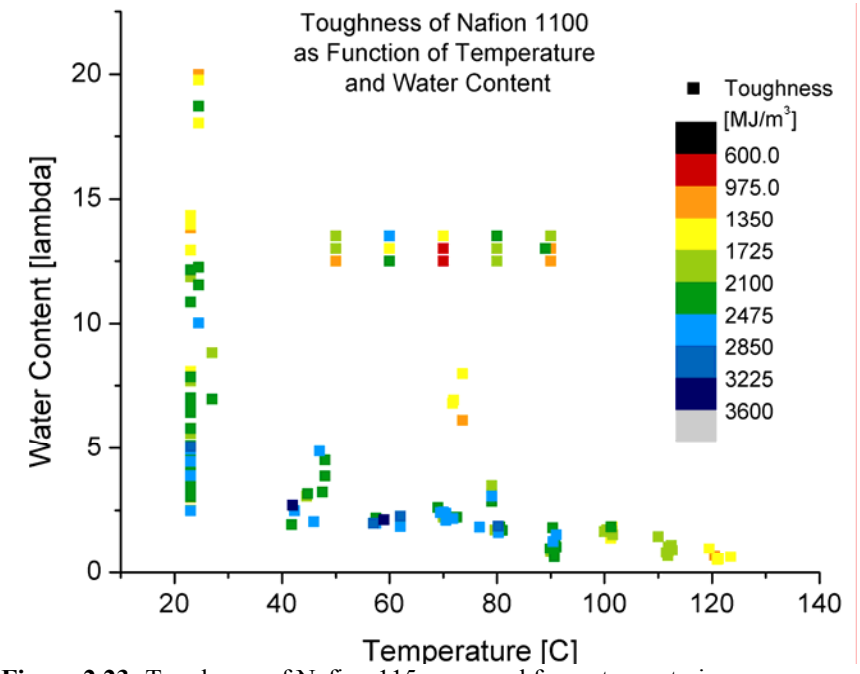

Figure 2.23: Toughness of Nafion 115 measured from stress-strain curves.

Values for the proportional, yield and ultimate points can be seen in Figure 2.24. The proportional point stress decreases and the proportional strain increases steadily with increasing temperature and, to a lesser extent, with increasing hydration. The yield and ultimate stress decrease with increasing temperature but are roughly constant with increasing water content at room temperature. The yield strain increases with both increasing hydration and temperature, as discussed above. However, as with the Young's modulus, the effects on the yield strain do not combine at higher temperatures and elevated humidity. The ultimate strain increases with increasing temperature at all water contents and remains largely unaffected by hydration at all temperatures.

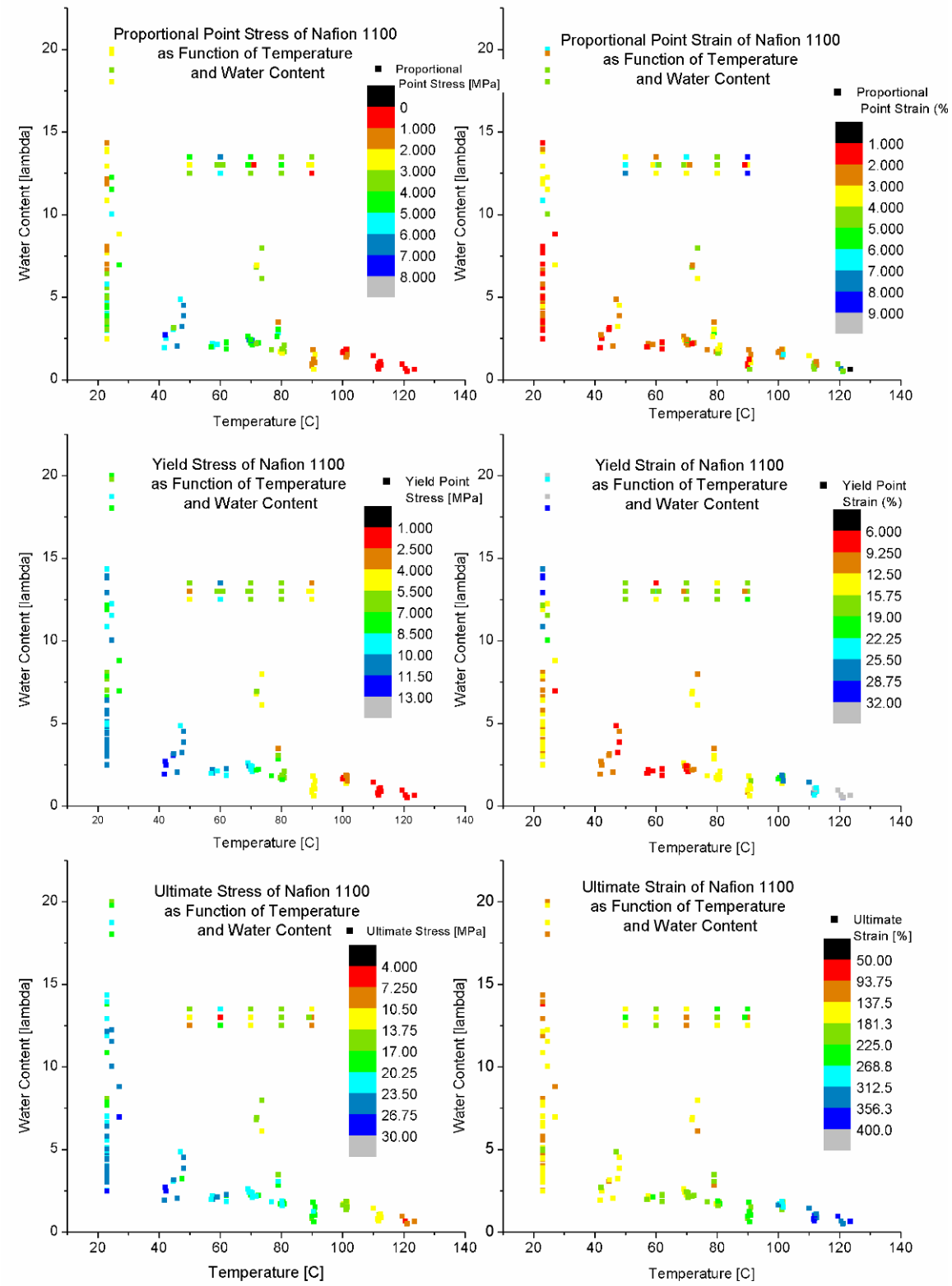

Figure 2.24: Proportional, yield and ultimate stress and strain values for Nafion 115 measured from stress-strain curves.

Testing in the machine and transverse to extrusion directions produced noticeable differences only in post-yielding properties such as plastic modulus and ultimate point. The machine direction produced a slightly higher plastic modulus, also apparent from a slight decreases in ultimate strain and slight increases ultimate stress, as shown in Figure 2.25. These are small differences (~2 MPa or 10%) compared to the differences caused by temperature and humidity, and results from tests in both directions are plotted in Figure 2.22. Young's modulus, proportional, yield and ultimate points showed no clear difference.

Figure 2.25: Plastic modulus & ultimate stress & strain for membranes tested in direction of extrusion (machine) and transverse direction.

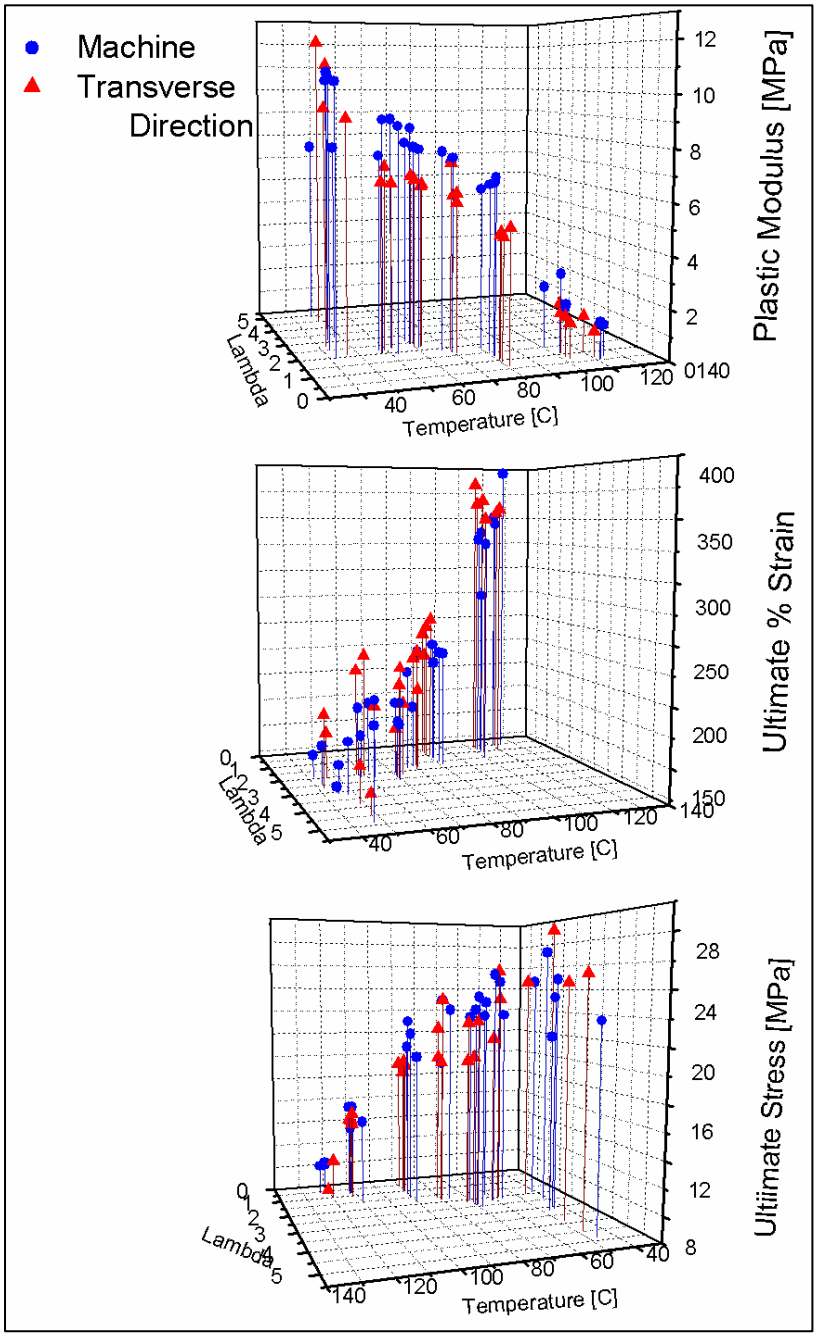

The results of tests at different strain rates appear in Figure 2.26. All tests shown were at room temperature, and the different values are displayed as a function of their water content.

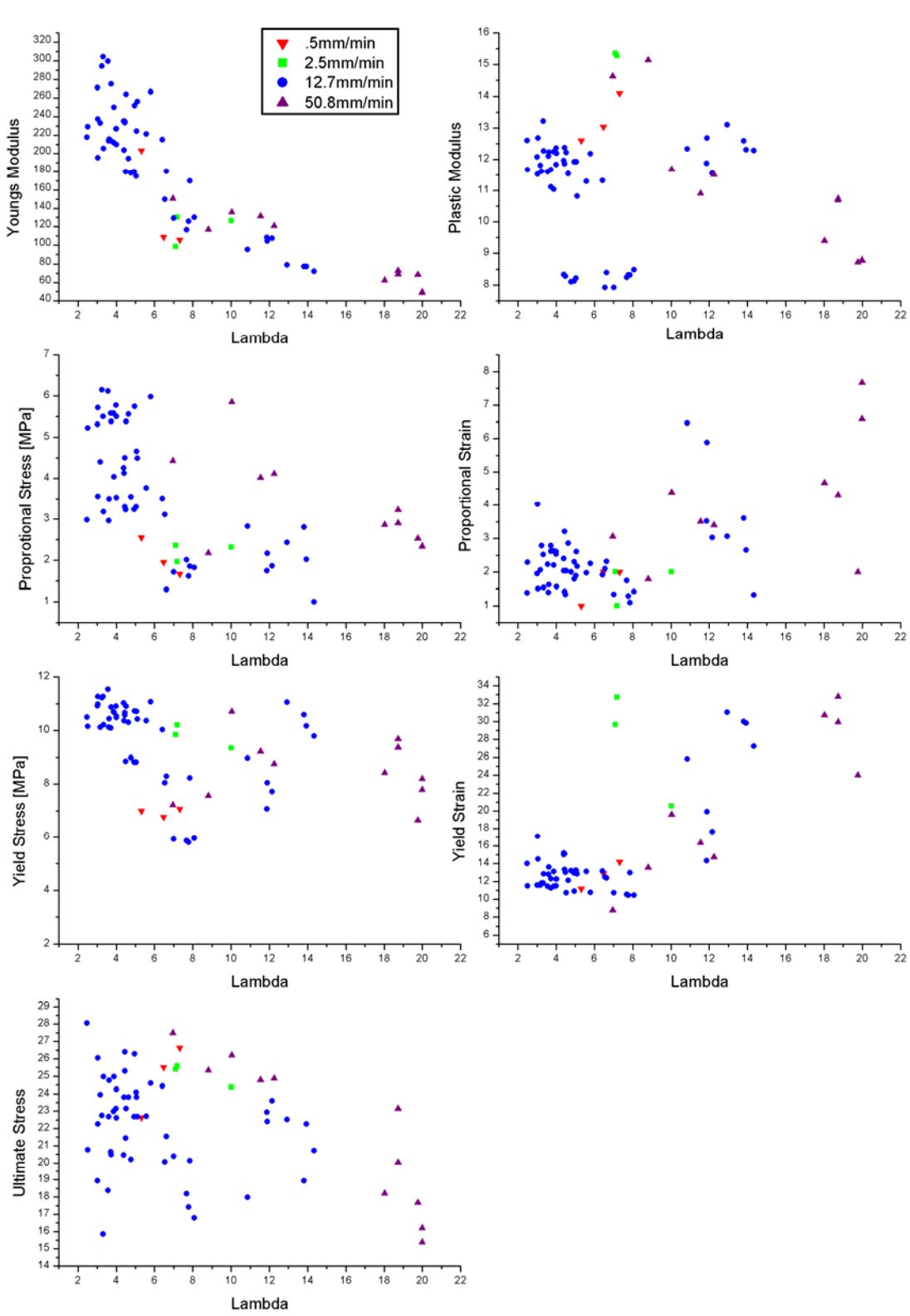

Figure 2.26: Young's, & Plastic Moduli, Proportional & Yield points and ultimate stress for different strain rates at room temperature as a function of water content, lambda. Red: 0.5 mm/min (2%/min); Green: 2.5 mm/min (11%/min); Blue: 12.7 mm/min (57%/min); Purple: 50.8 mm/min (228%/min).

Many points in these results overlap, but it is clear that the Young's modulus is independent of strain rate, while the plastic modulus is slightly higher at lower strain rates, though the difference is small compared to the 2 order of magnitude change in strain rates. The yield and proportional points of the tests run at 0.5 mm/min and 2.5 mm/min (2% and 11%/min) tend to fall close together but do not follow a trend, while the ultimate strain appears slightly lower and the ultimate stress slightly higher. The proportional stress and strain at 50.8 mm/min rate appear slightly higher. The tests run at 0.5 and 2.5 mm/min were not included in Figure 2.21 through Figure 2.24 as a precaution to reduce extra noise that the different strain rates might add to the results, such as those seen in the yield strain and plastic modulus. However, because a substantial number of tests were run at 12.7 and 50.8 mm/min, all of those tests were included.

2.5.2 Stress Relaxation

Figure 2.27 shows the stress-relaxation (modulus vs. time) curves of Nafion 115 at different temperatures in humidified conditions strained to 5% elongation, and Figure 2.28 shows the same experiments at ambient (room) humidity. A strain of 5% is well below the yield point of hydrated Nafion, but approaches the yield point of dry Nafion at temperatures up to about 70°C, as depicted in Figure 2.24. Though the membranes tested at ambient humidity yielded a higher initial modulus than the humidified membranes, the modulus tended to decline much more quickly, especially at higher temperatures.

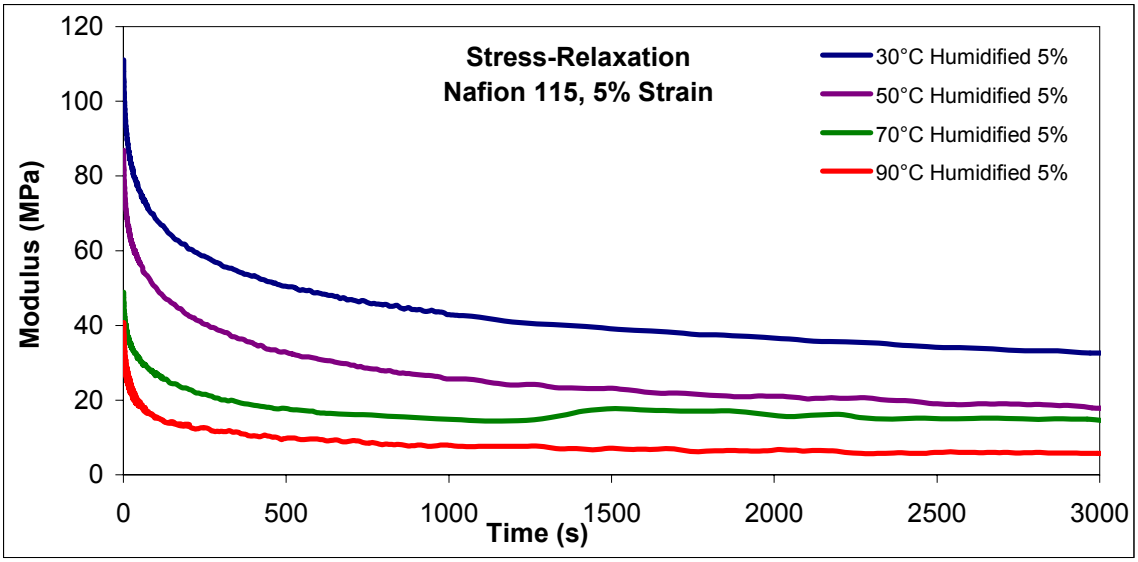

Figure 2.27: Stress relaxation curves of Nafion 115 strained to 5% elongation at different temperatures in humidified conditions.

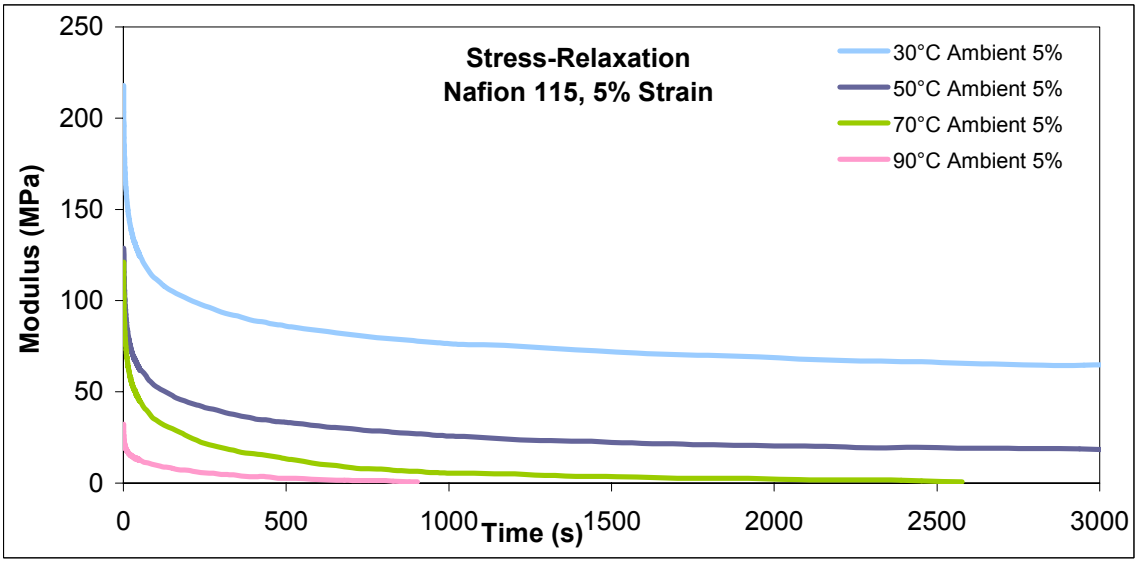

Figure 2.28: Stress relaxation curves of Nafion 115 strained to 5% elongation at different temperatures in ambient conditions.

These and other curves are presented in log(modulus) vs. log(time) format below in order to perform time-temperature and time-strain superposition. Figure 2.29 through Figure 2.40 show results of stress-relaxation tests under humidified and dry (over Drierite®) conditions at 2%, 5%, 10% and 20% strain. For each strain the humidified

and dry results are presented separately, then together for comparison, followed by time-temperature superposition.

The stress-relaxation curves often begin to look jagged and noisy towards the end of the run and sometimes appear to level off. Indeed, an end to relaxation was often observed: the stress decayed to a residual value (represented by the lone spring in series in the model, Figure 2.17). At these long times and low stresses, any fluctuation in the signal is both amplified and compressed in time by the log-log axis, giving the allusion of extraneous noise.

There are two main observations from the stress-relaxation curves. (1) There are two rate regimes: a faster rate that appears as a downward curve in log-log plots and occurs in humidified tests only at lower strains and lower temperatures but appears in dry tests over a greater range of strains and more at higher temperatures. (2) The shift factor needed to make humidified and dry tests fall onto the same master curve is larger in humidified tests at higher temperatures and higher strains and, in dry tests, is larger at lower temperatures and lower strains. The evolution of these two phenomena will be noted in the series of results that follow.

2.5.2.1 2% Strain

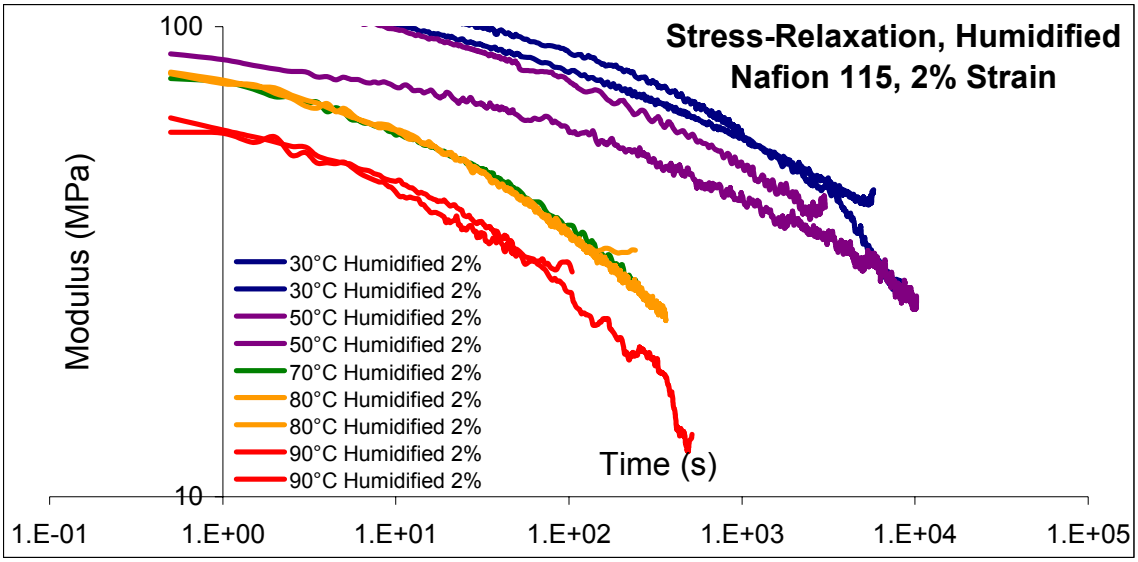

Figure 2.29: Stress-relaxation behavior of Nafion 115 at 2% strain and humidified conditions.

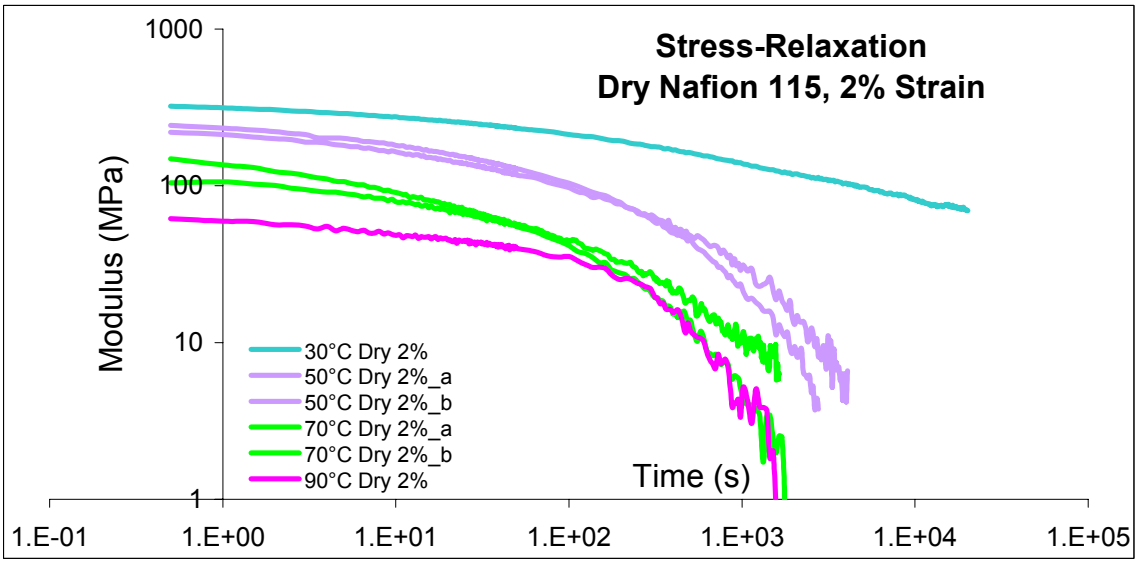

Figure 2.30: Stress-relaxation behavior of Nafion 115 at 2% strain and dry conditions.

At 2% strain all of the stress-relaxation curves follow a distinct downward curve at both humidified and dry conditions.

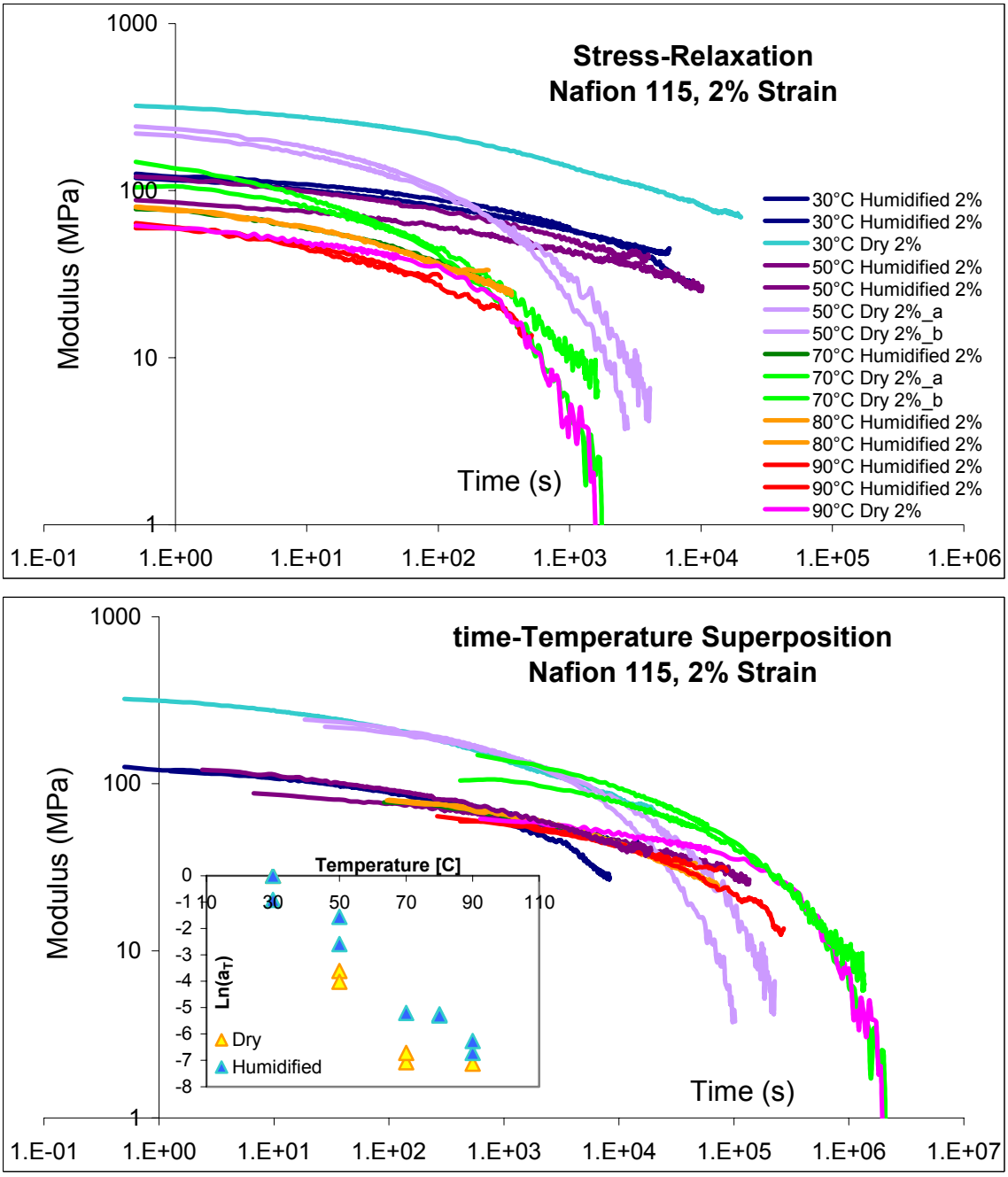

Figure 2.31: Stress-relaxation behavior (top) and time-Temperature superposition master curve (bottom) of Nafion 115 relaxation modulus at 2% strain at both dry & humidified conditions. Inset shows temperature shift factors from the reference curve of 30°C & 100% humidity.

Two separate master curves are created for 2% strain because the modulus values of the dry Nafion are distinctly higher than the humidified Nafion. The increase in modulus for the dry membrane is greater at lower temperatures (up to 70°C), but the dry modulus

actually becomes slightly lower at 90°C – water and temperature do not act together to soften Nafion.

2.5.2.2 5% Strain

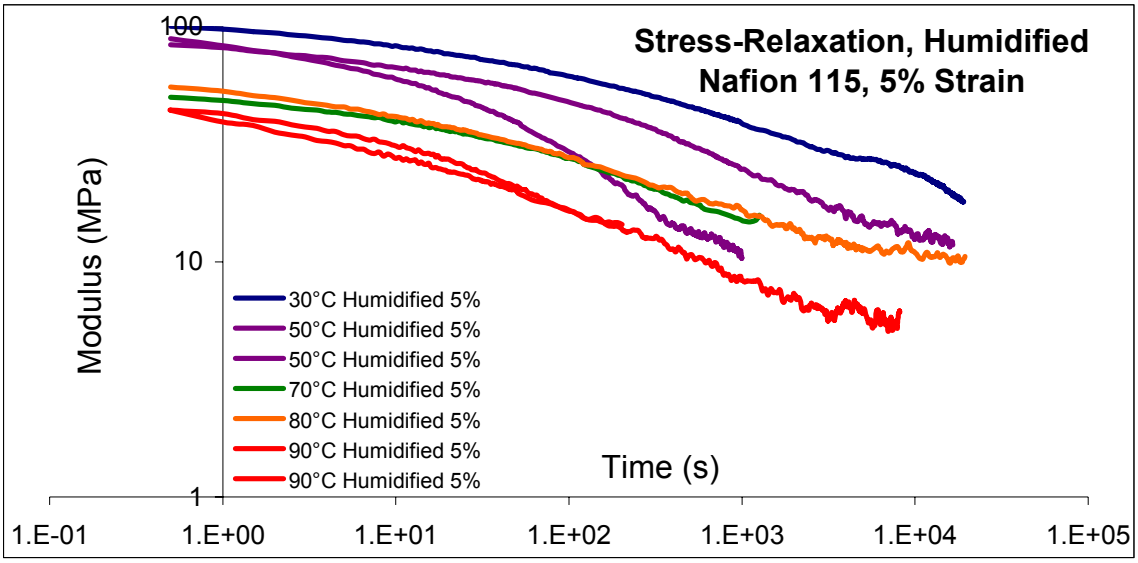

Figure 2.32: Stress-relaxation behavior of Nafion 115 at 5% strain and humidified conditions.

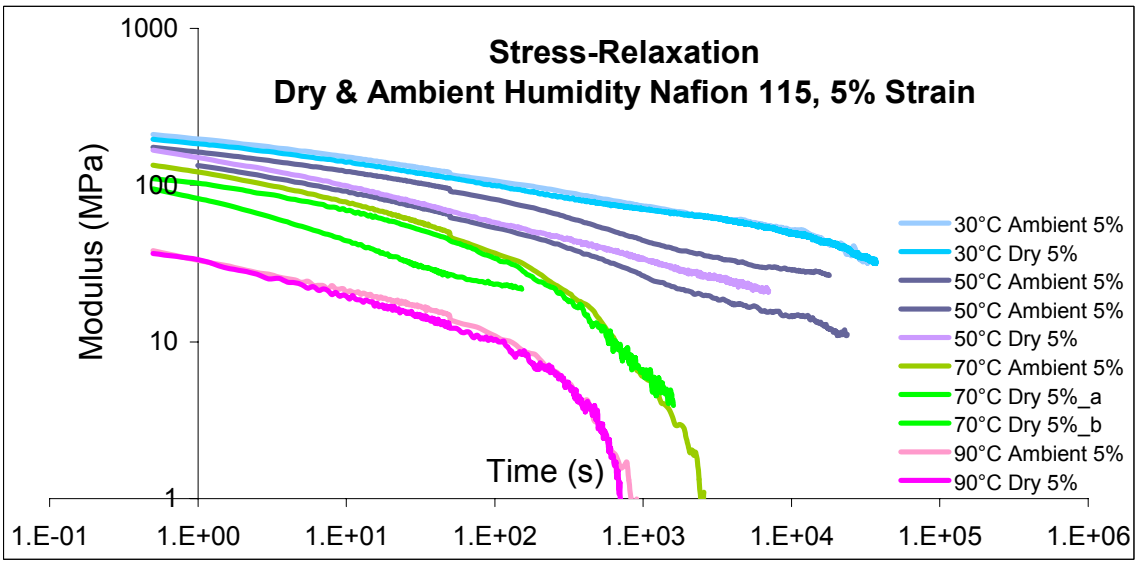

Figure 2.33: Stress-relaxation behavior of Nafion 115 at 5% strain and dry conditions.

At 5% strain the curves tend to turn downwards only at lower temperatures (50°C) in the humidified runs, while for dry Nafion, the curves turn down much faster at higher temperatures.

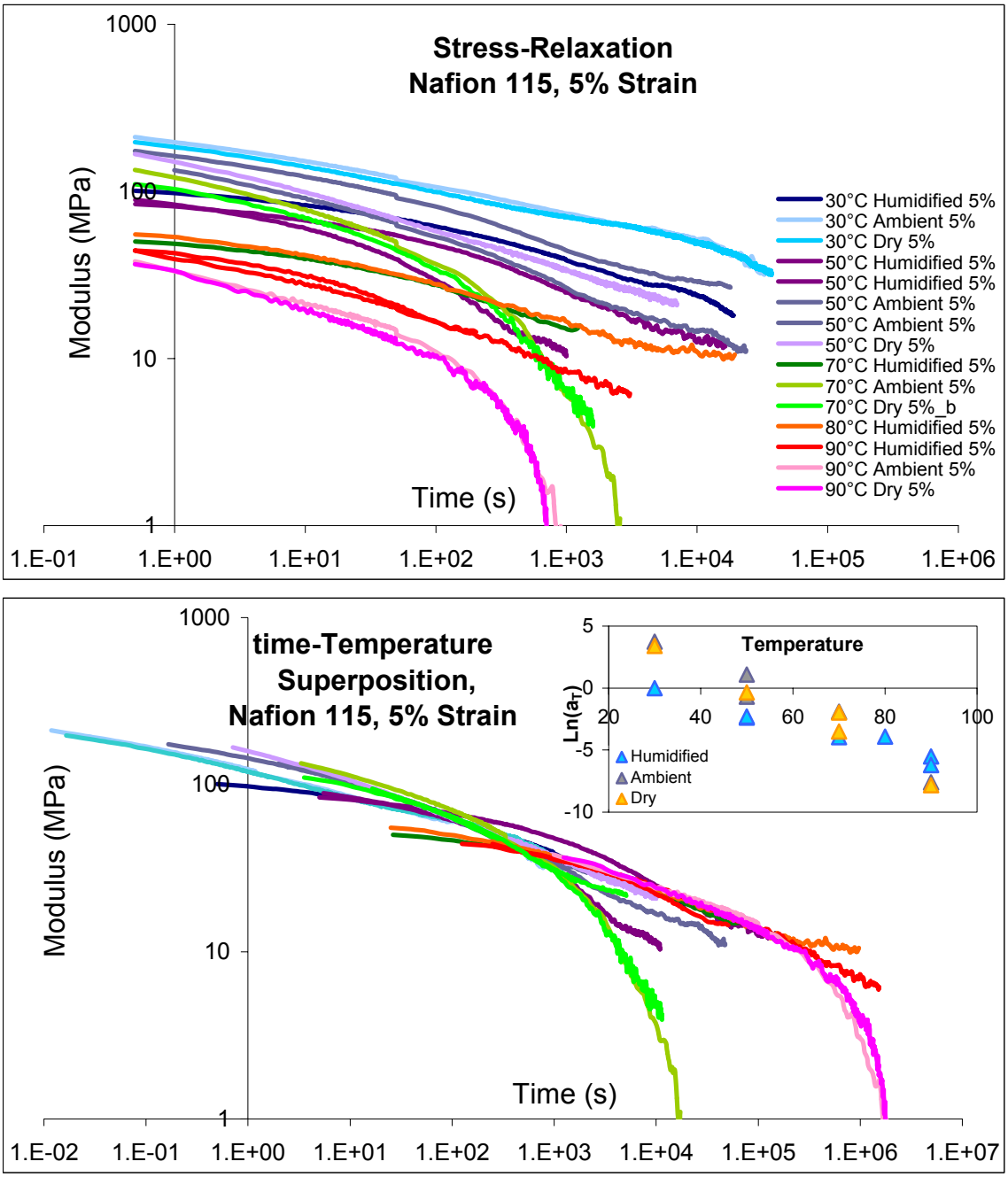

Figure 2.34: Stress-relaxation behavior (top) and Time-temperature superposition master curve (bottom) of Nafion 115 relaxation modulus at 5% strain and dry, ambient & humidified conditions. Inset shows temperature shift factors from the reference curve of 30°C & 100% humidity.

Also, the trend in modulus values is the same at 5% strain as at 2%: humidified membranes have lower modulus values at temperatures up to 70°C, but at 90°C the humidified modulus is higher. The inset $\ln(a_T)$ vs. temperature plot in Figure 2.34. shows that the shift factors of the dry membranes are higher at temperatures up to 70°C. These higher modulus curves must be shifted to shorter times to form a master curve with the humidified membranes. However, at 90°C, the dry and ambient humidity shift factors (and modulus values) are lower, pushing them to longer times.

2.5.2.3 10% Strain

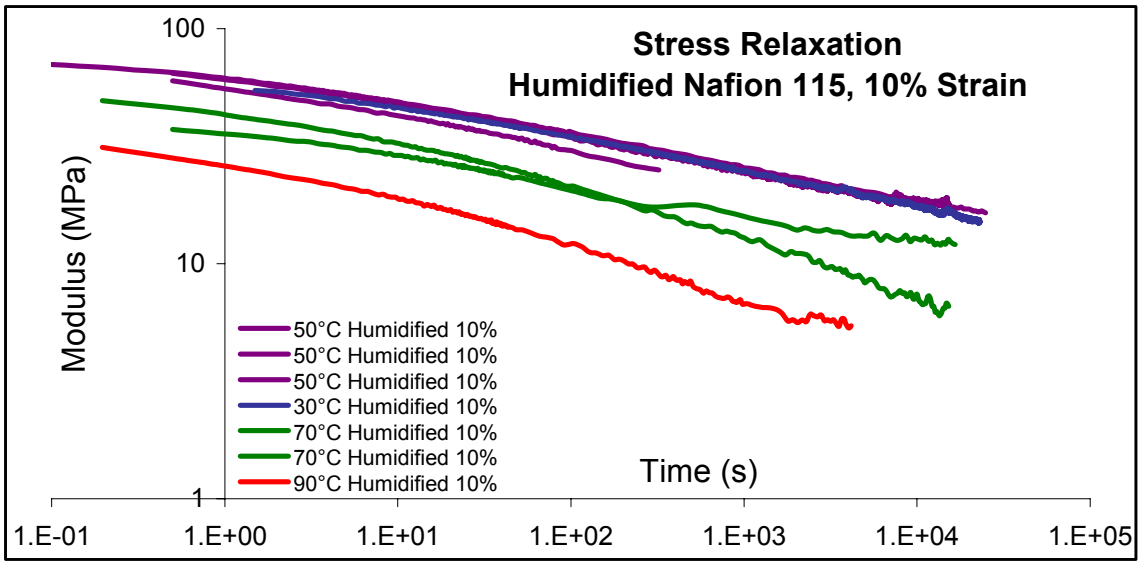

Figure 2.35: Stress-relaxation behavior of Nafion 115 at 10% strain and humidified conditions.

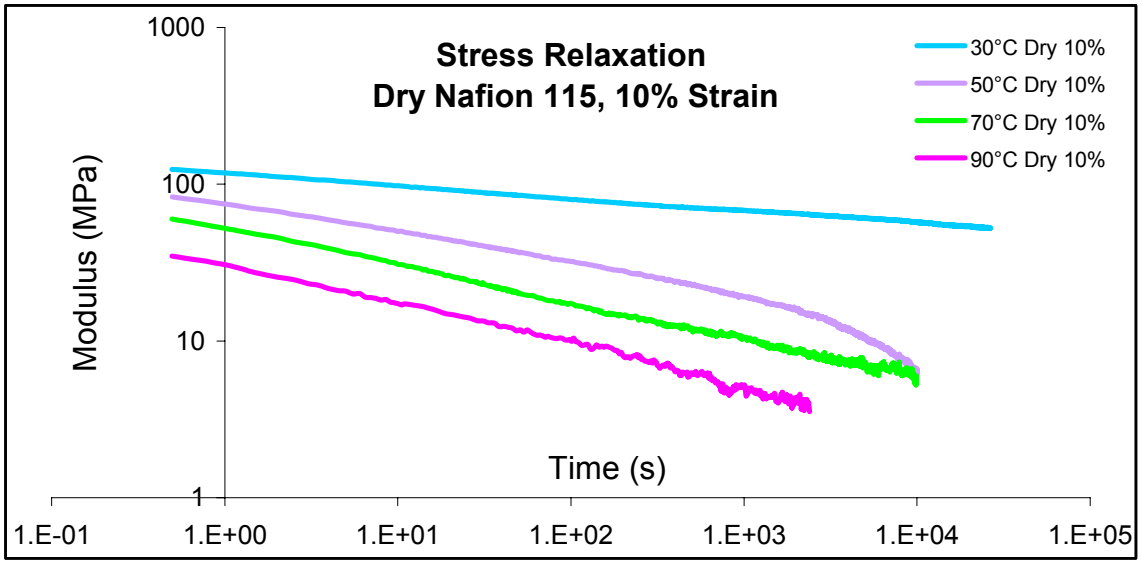

Figure 2.36: Stress-relaxation behavior of Nafion 115 at 10% strain and dry conditions.

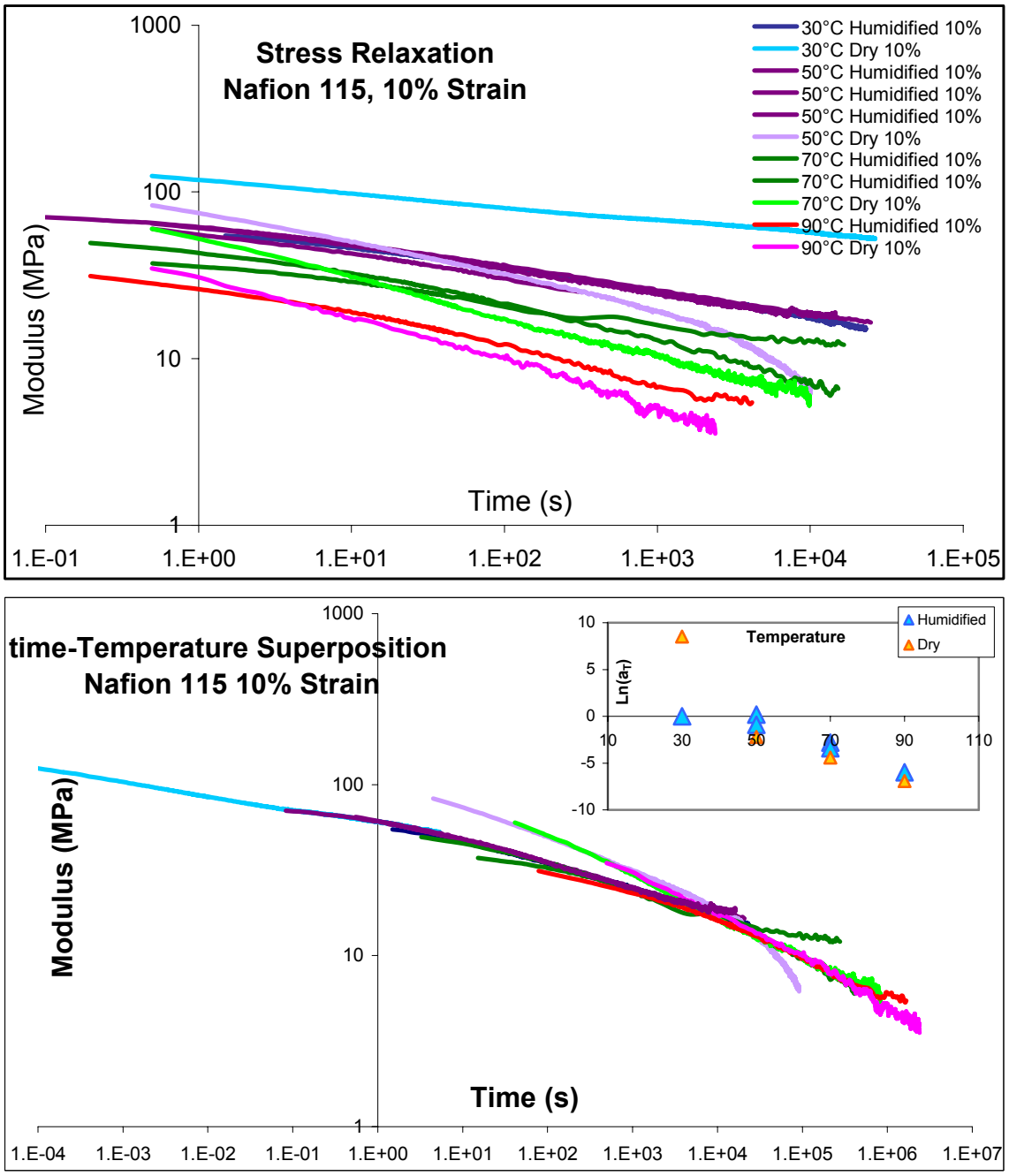

Figure 2.37: Stress-relaxation behavior (top) and Time-temperature superposition master curve (bottom) of Nafion 115 relaxation modulus at 10% strain at both dry & humidified conditions. Inset shows temperature shift factors from the reference curve of 30°C & 100% humidity.

Except at 30°C where the dry modulus is significantly higher than the humidified modulus, the temperature-shift factors are similar between the dry and humidified membranes at 10% strain.

2.5.2.4 20% Strain

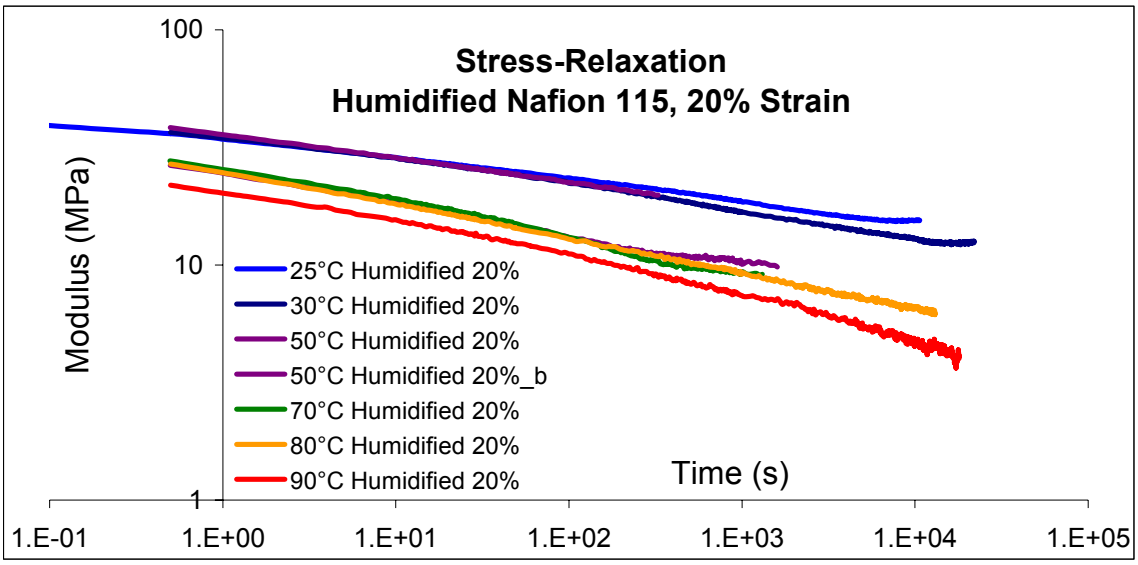

Figure 2.38: Stress-relaxation behavior of Nafion 115 at 20% strain and humidified conditions.

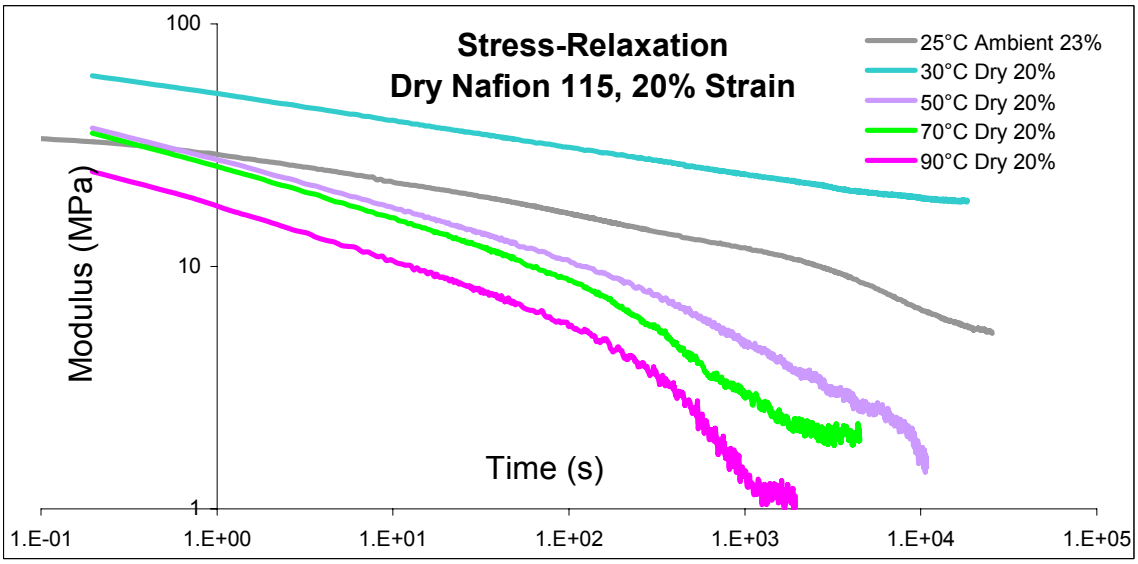

Figure 2.39: Stress-relaxation behavior of Nafion 115 at 20% strain and dry conditions.

At 20% strain the dry Nafion exhibits some of the downward curvature at higher temperatures, while the humidified Nafion has a more linear, gradual decay across all temperatures.

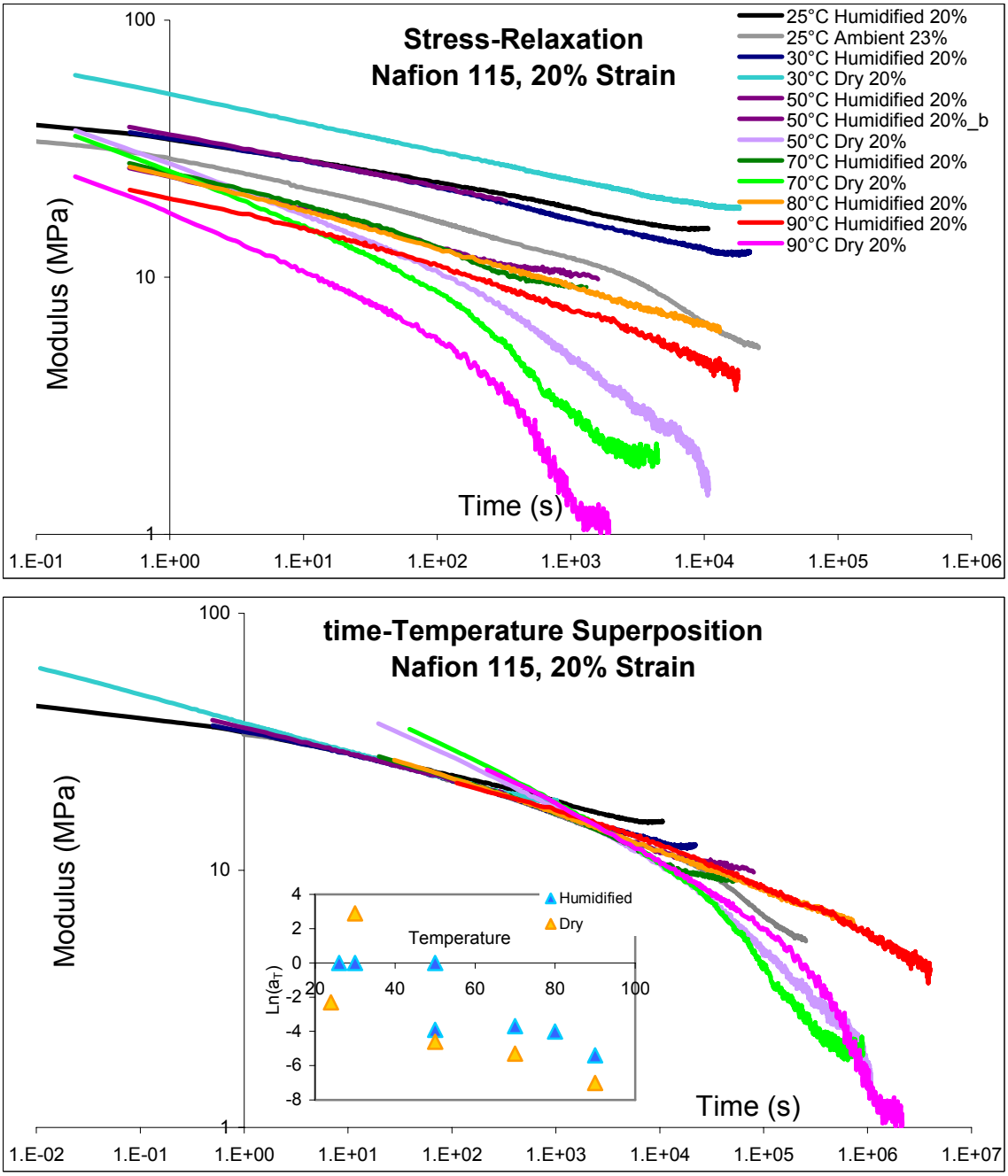

Figure 2.40: Stress-relaxation behavior (top) and Time-temperature superposition master curve (bottom) of Nafion 115 relaxation modulus at 20% strain at both dry & humidified conditions. Inset shows temperature shift factors from the reference curve of 30°C & 100% humidity.

At 20% strain, the modulus values and shift factors are lower for the drier membranes across almost all temperatures.

2.5.2.5 A short summary of the stress relaxation results presented above

Rate Regimes

The stress relaxation behavior follows either a steep downward curve or a linear decrease in stress depending on temperature, humidity level and imposed strain. For the dry samples (Figure 2.30, Figure 2.33, Figure 2.36 and Figure 2.39), the curved shape appears at all strains and tends to increase with increasing temperature. However, in humidified conditions the curved shape appears only at lower strains and temperatures and decreases with increasing temperature. Humidified tests at 2% strain (Figure 2.29) follows the curved shape at all temperatures, while at 5% strain (Figure 2.32) the effect was lessened: only 30°C and 50°C tended to curve downward, either crossing or appearing ready to cross the higher-temperature curves. At 10% and 20% strain (Figure 2.35 and Figure 2.38), the humidified stress-relaxation runs generally followed the gradual linear decay pattern. This strain, temperature and humidity dependence may be the result of water reducing the rate of stress-relaxation, particularly at higher temperatures, while the rate of stress-relaxation in dry membranes increases with increasing temperature, causing the downward curvature.

Shift Factor Regimes

Plots of time-temperature superposition shift factors (Figure 2.31, Figure 2.34, Figure 2.37 and Figure 2.40) show how dry Nafion at lower temperatures and lower strains tends to have a higher shift factor and modulus than humidified Nafion. At 2% strain the dry modulus is higher at all temperatures, creating a distinct master curve for each of the two hydration levels. The effect is less pronounced at greater strains. While two distinct master curves could be created at 5% and 10% strain, the wet and dry runs can also be collapsed. When collapsed to a single master curve, the shift factors are

higher for dry membranes at lower temperatures and strains. However, at higher temperatures and strains dry Nafion has a lower modulus and must be shifted to longer times relative to the humidified runs, the effect of both a lower modulus in dry membranes at higher temperatures and faster relaxation rates of dry membranes.

These two regimes are also visible in Figure 2.41 through Figure 2.44, which organize the same data by temperature rather than by strain and do time-strain superposition. In general, the stiffening/stabilizing effect of water becomes more apparent at higher temperatures and strains. At 30°C the dry shift factor is always greater than the humidified. However, at 50°C, the dry shift factor is greater up to 10% strain and then becomes very similar to the hydrated shift factors, and at 70°C the transition occurs between 5% and 10%. At 90°C the dry shift factor is always less than the humidified; it is shifted to longer times to match the humidified run.

2.5.2.6 30°C

At 30°C the dry modulus and shift factors are higher than the hydrated membranes at all strains.

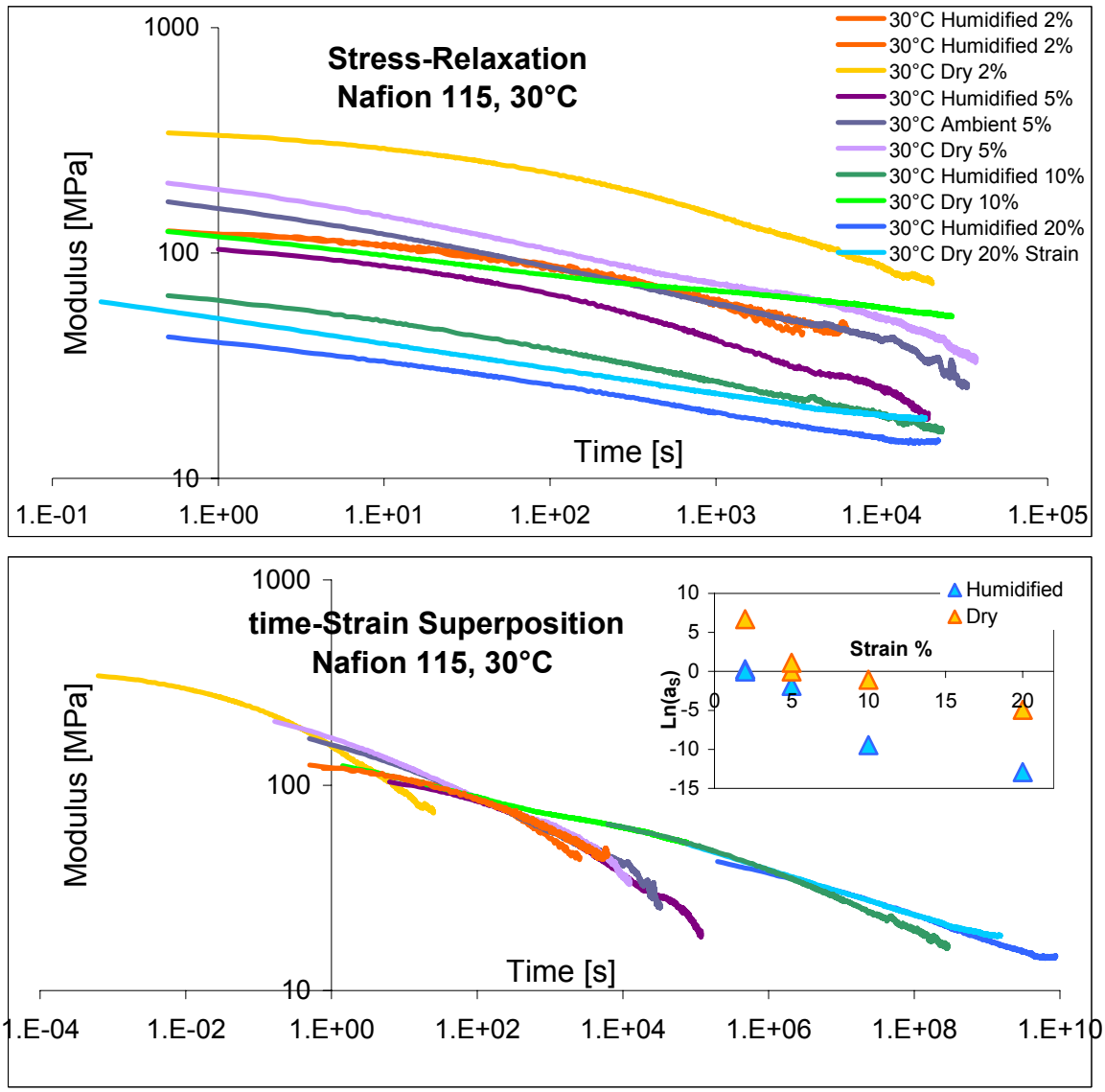

Figure 2.41: Stress-relaxation behavior (top) and time-strain superposition master curve (bottom) of Nafion 115 relaxation modulus at 30°C at both dry & humidified conditions. Inset shows strain shift factors from the reference curve of 2% strain & 100% humidity.

2.5.2.7 50°C

At 50°C the dry shift factor continues to be higher for the dry membrane than the hydrated (though the difference is less than at 30°C). Also, the shift factors begin to agree more closely at higher strains.

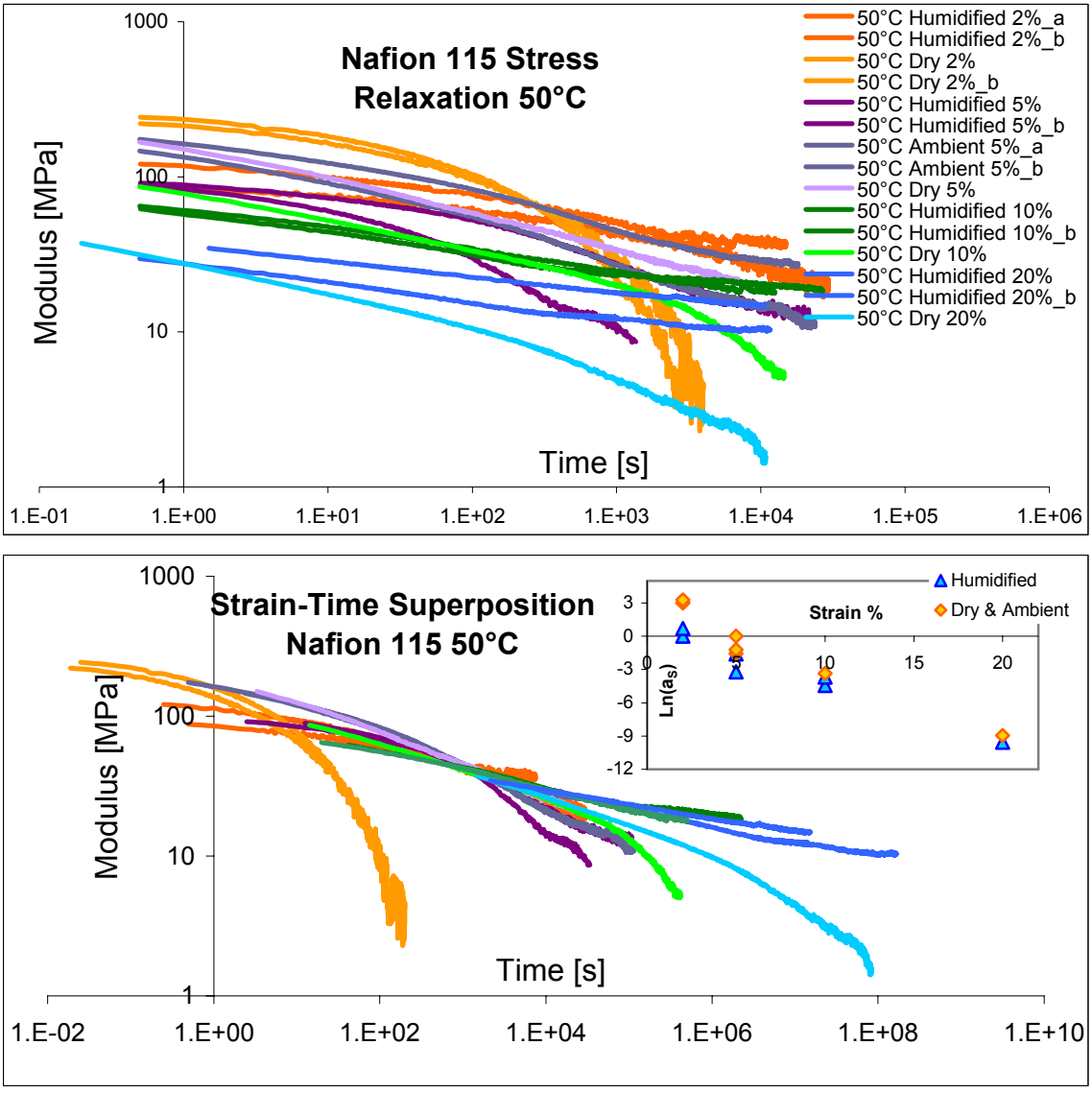

Figure 2.42: Stress-relaxation behavior (top) and time-strain superposition master curve (bottom) of Nafion 115 relaxation modulus at 50°C at both dry & humidified conditions. Inset shows strain shift factors from the reference curve of 2% strain & 100% humidity.

2.5.2.8 70°C

At 70°C the shift factors begin to agree and then cross at lower strains than at 50°C, roughly 5% strain. The stiffening (higher modulus) and stabilizing (lower relaxation rate) effect of water is more apparent at 70°C than at 30°C or 50°C.

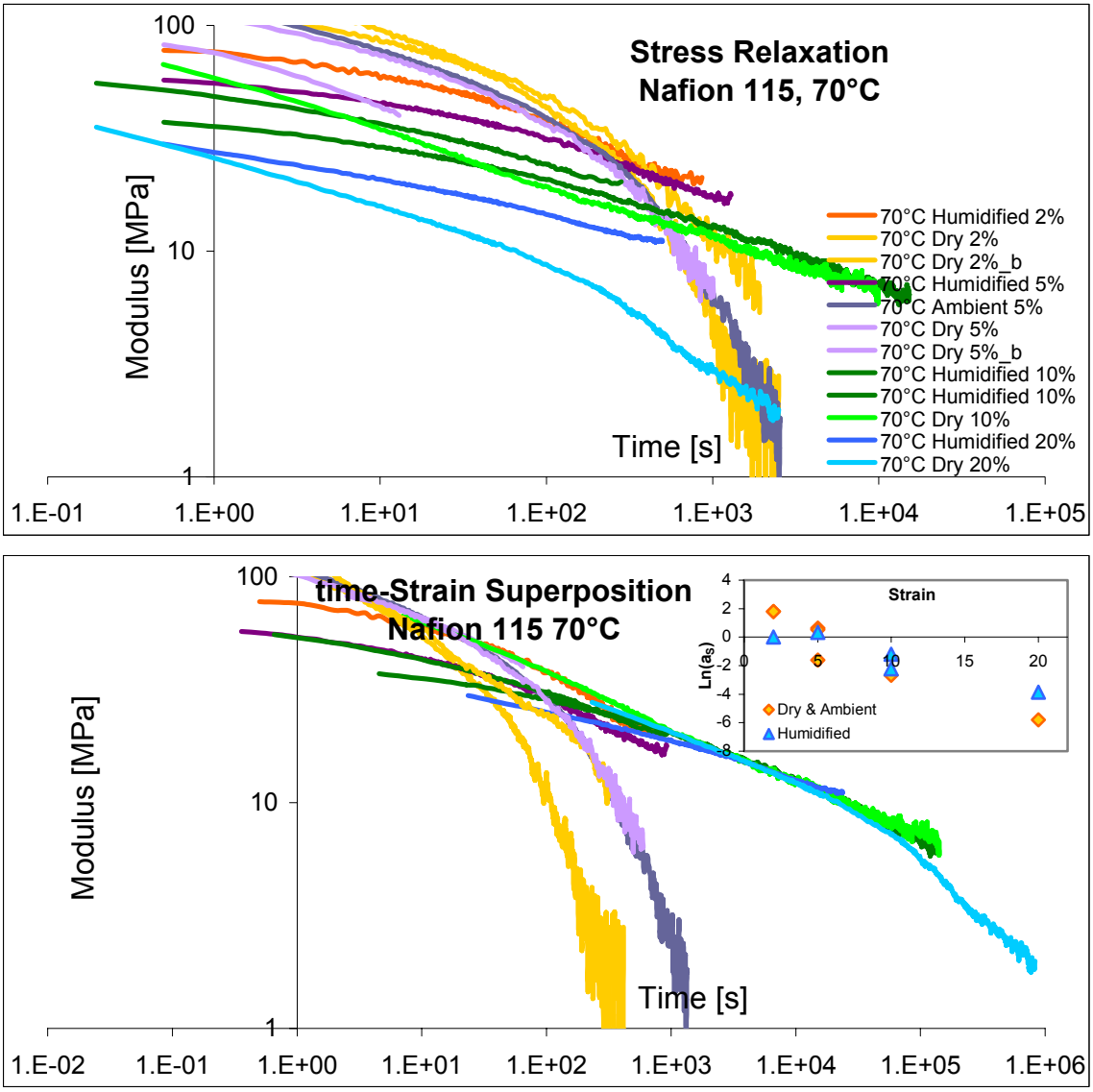

Figure 2.43: Stress-relaxation behavior (top) and time-strain superposition master curve (bottom) of Nafion 115 relaxation modulus at 70°C at both dry & humidified conditions. Inset shows strain shift factors from the reference curve of 2% strain & 100% humidity.

2.5.2.9 90°C

The reinforcing effect of water on Nafion is very apparent at 90°C. The dry membranes show lower modulus values and faster relaxation rates, pushing them to lower shift factors and longer times to match the humidified membranes.

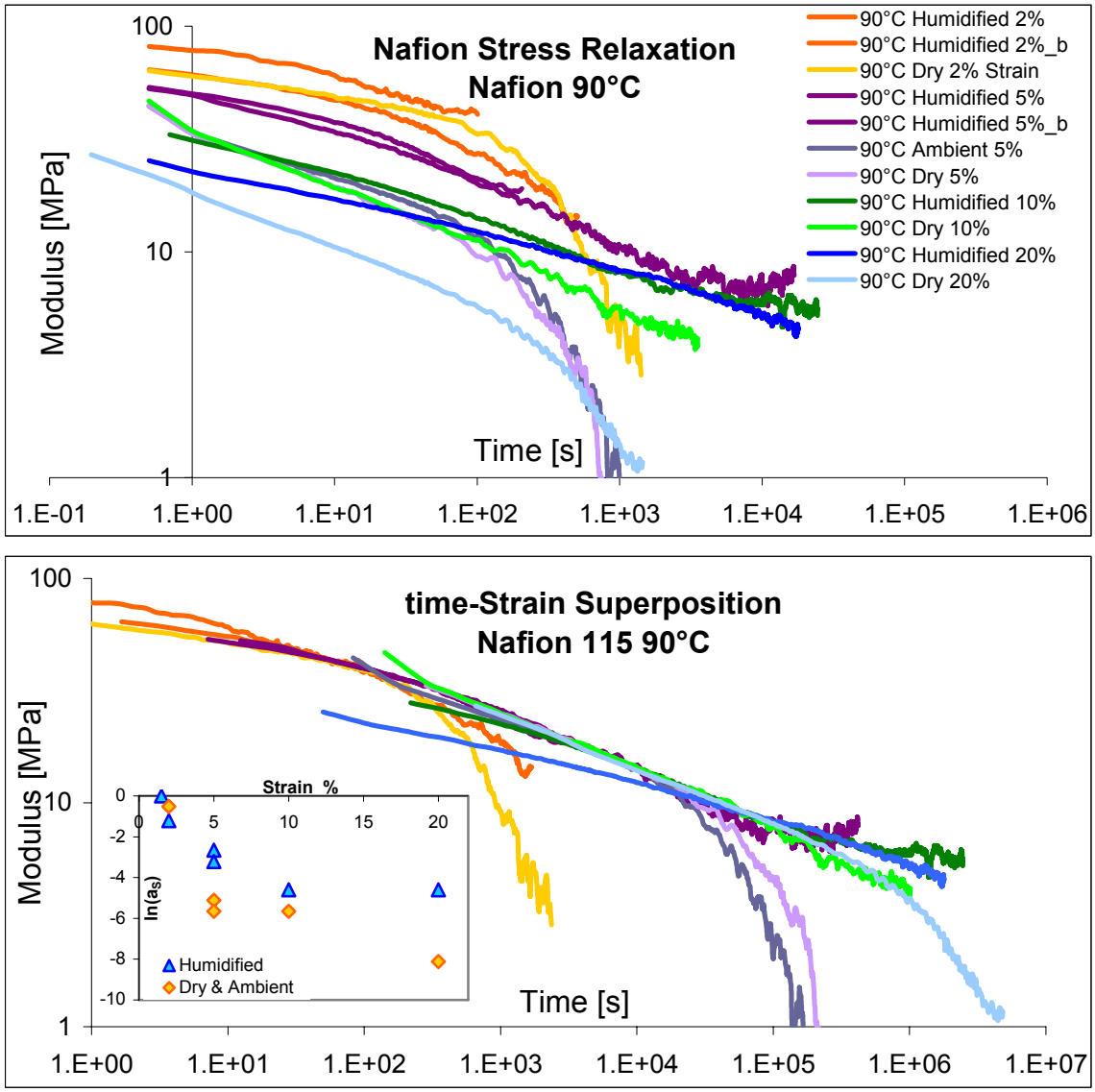

Figure 2.44: Stress-relaxation behavior (top) and time-strain superposition master curve (bottom) of Nafion 115 relaxation modulus at 90°C at both dry & humidified conditions. Inset shows strain shift factors from the reference curve of 2% strain & 100% humidity.

2.5.3 Creep

Figure 2.45 through Figure 2.48 show creep behavior and time-stress superposition for Nafion at room temperature, 35°C, 45°C and 60°C.

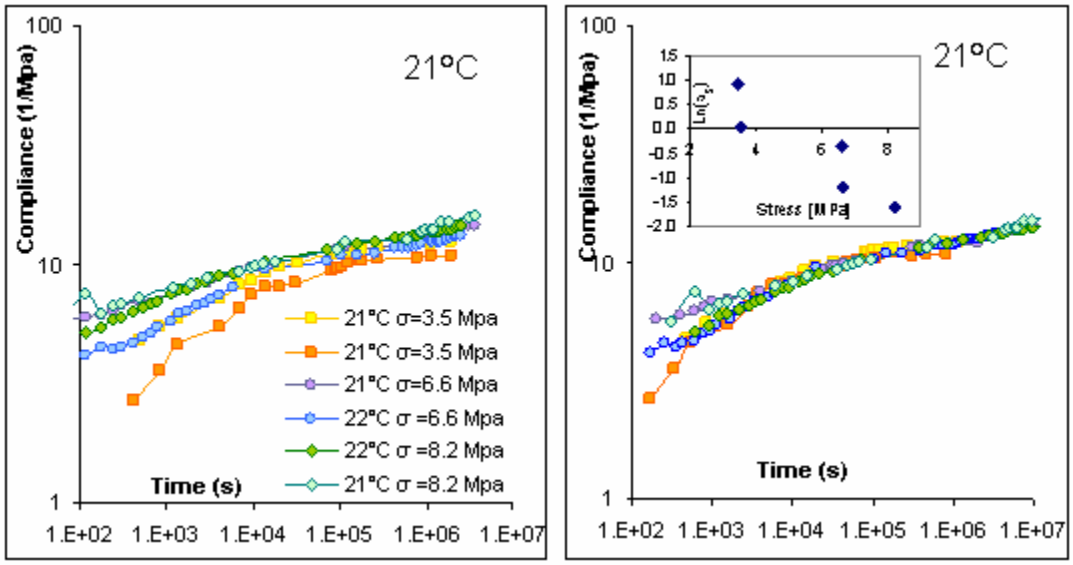

Figure 2.45: Creep behavior (left) and Time-stress superposition master curve (right) of Nafion 115 creep compliance at humidified conditions & room temperature. Inset shows temperature shift factors from the 3.5 MPa reference.

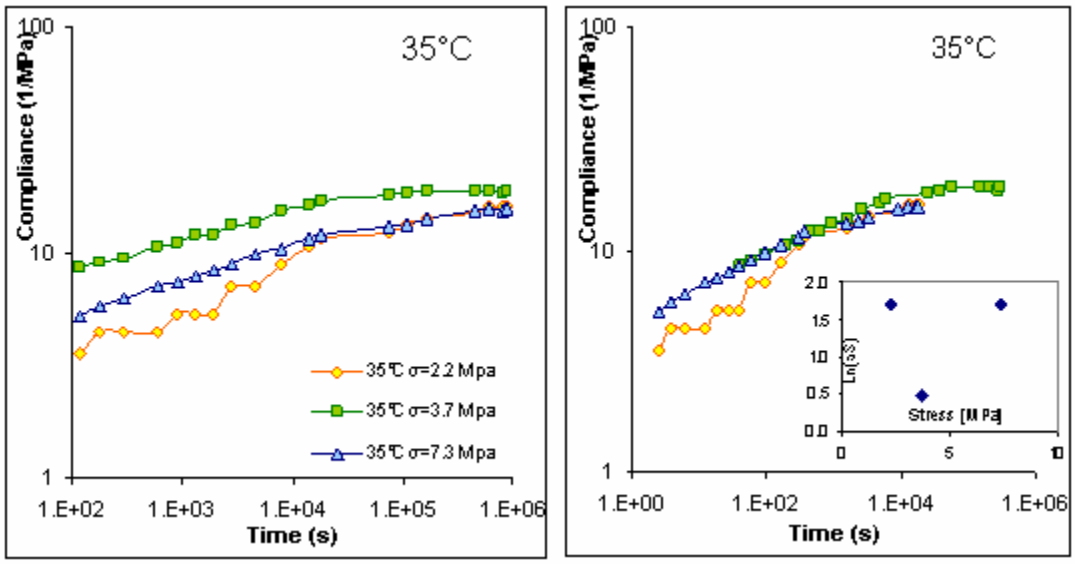

Figure 2.46: Creep behavior (left) and Time-stress superposition master curve (right) of Nafion 115 creep compliance at humidified conditions & 35°C. Inset shows temperature shift factors from the 1.24 MPa reference.

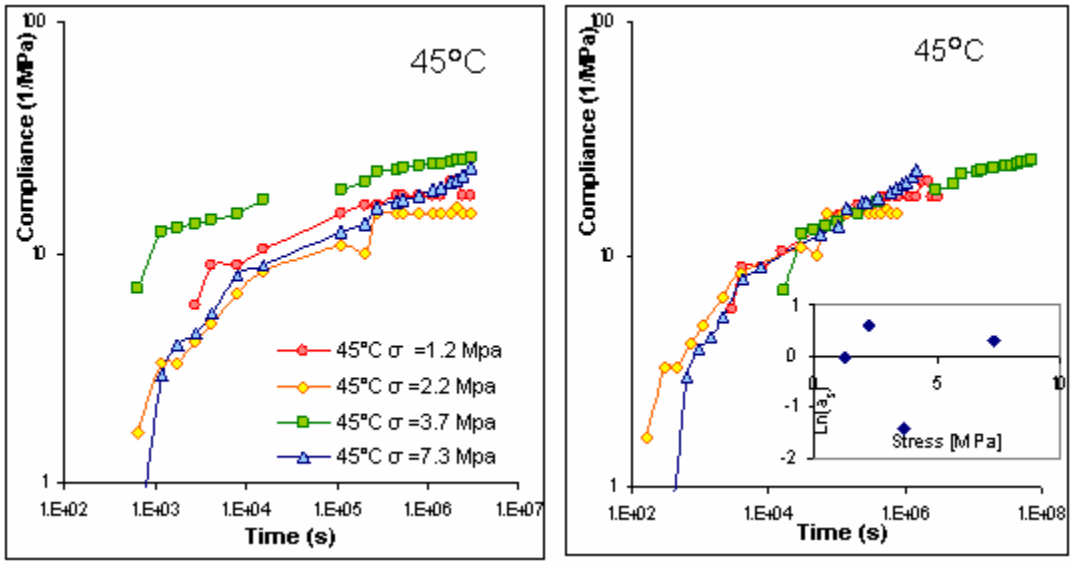

Figure 2.47: Creep behavior (left) and Time-stress superposition master curve (right) of Nafion 115 creep compliance at humidified conditions & 45°C. Inset shows temperature shift factors from the 1.24 MPa reference.

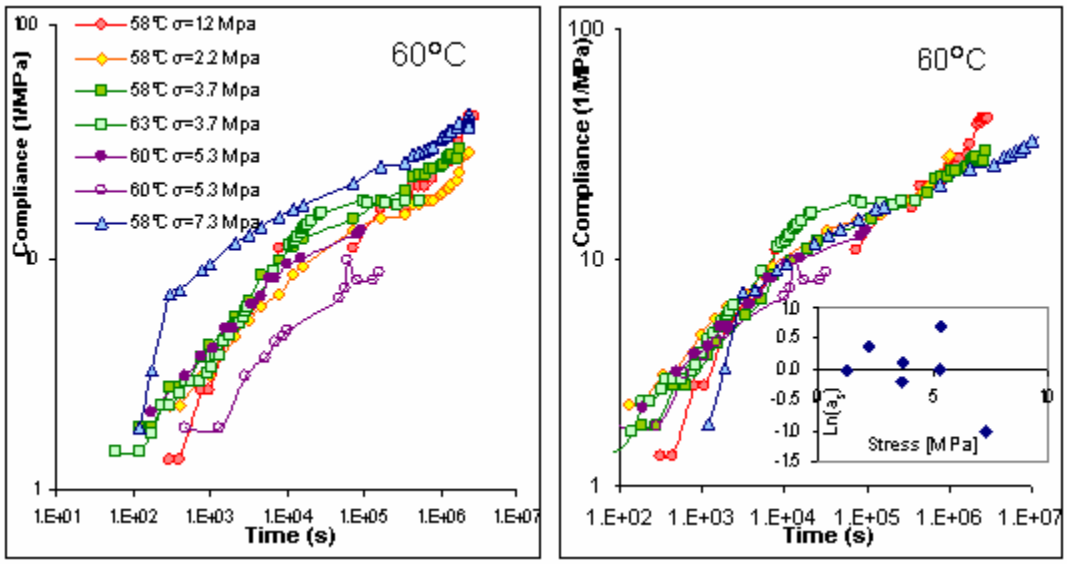

Figure 2.48: Creep behavior (left) and Time-stress superposition master curve (right) of Nafion 115 creep compliance at humidified conditions & ~60°C. Inset shows temperature shift factors from the 1.24 MPa reference.

The creep data here is poorer than the stress-relaxation data, as illustrated by the rough lines and time-stress shift factors that do not always change monotonically with stress. A more sophisticated creep-measurement device has been constructed and is in use by P. Majsztrik. However, two distinct curve shapes are visible with this data as well. At

lower temperatures and stresses the curves are more linear while at higher temperatures and stresses the compliance increases dramatically at short times before the curve levels off and becomes linear. The slope of these linear regions, or the exponent in a power-law fit of the compliance vs. time graphs increases with temperature, as seen in Figure 2.49.

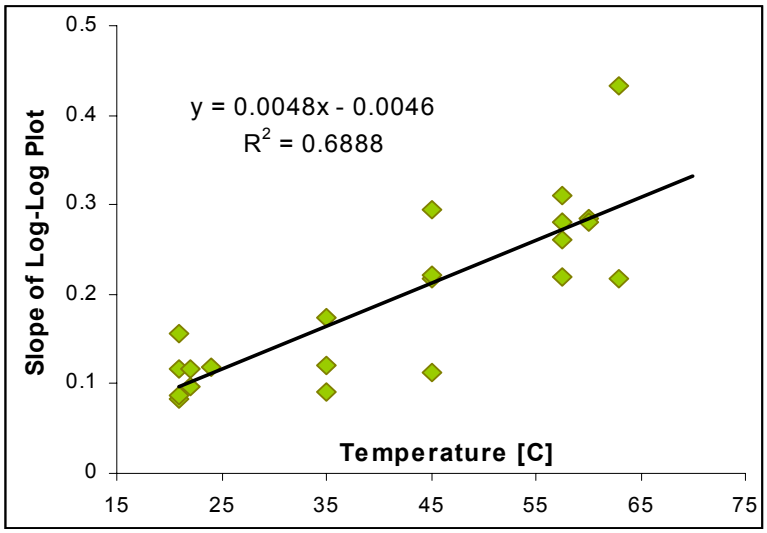

Figure 2.49: Slope of creep compliance vs. time log-log plots (exponent of power law fit) verses Temperature [°C].

2.6 Discussion

2.6.1 Stress-Strain tests

The key results of this work show the strong dependence of elastic modulus on water content and temperature, decreasing significantly as either or both conditions increase. This work agrees well with previously reported values of Young's modulus, and expands the range of conditions tested. A weaker dependence on water content was reported by Choi and Jalani [28], who fit their data for Young's modulus E at room temperature to the expression

$$E = 316\exp\left[-2.1753\varepsilon_w\right] \tag{2.10}$$

where ε_w is the volume fraction of water in the polymer. At room temperature, the data reported here yield the expression:

$$E = 381 \exp[-4.8\varepsilon_w] \tag{2.11}$$

with a higher dry modulus and over twice the rate of decline with increasing water content. This difference could be due to polymer aging, as discussed in relation to Figure 2.18. Here, samples were equilibrated over their respective salt solutions for approximately 2 weeks, rather than on the time scale of the tests, and Figure 2.18 shows that equilibration at 100% humidity for 1 day yields a very different result than equilibration for 2 weeks.

Another key result of this work is that in contrast to properties within the elastic deformation region, those beyond the yield point such as the ultimate stress and strain and the plastic modulus are only weakly dependent on water content, though they do change with temperature. This is a strong indication that the hydrophilic ionic portions (whose properties are expected to change as the membrane water content changes) control the elastic deformation, while the hydrophobic backbone (whose properties would not change with water content) controls the post-yielding deformation. The ionic groups are often suspected of acting like crosslinks within the membrane [33, 34], and these data indicate that at yielding these crosslinks no longer affect the membrane's properties. The decrease in Young's modulus with increasing water content can be explained by water in the ionic regions that shield the ionic interactions and decrease the strength of the effective crosslinks [10, 33, 34].

Another key result is that the Young's modulus does not change with increasing temperature for well-hydrated membranes, such that dry membranes are less stiff than hydrated membranes at higher temperatures. The ionic interactions that decrease the crosslinks at lower temperatures appear to stabilize them at higher temperatures. Also,

the yield and proportional strains are increased by the addition of water, keeping the membrane in the elastic deformation region for longer. That the toughness decreases with increasing temperature and water content is also interesting and of interest for efforts to improve the longevity of fuel cell membranes.

The short investigation into strain rate performed here supports findings by Liu and Kyriakides [5, 25] that strain rate has little effect on the measured elastic modulus or the ultimate points. This result is surprising, because Nafion relaxes on the time-scale of many of the strain rates investigated, meaning that a slower strain rate should yield a lower modulus [49]. Still, strain rates as low as those used by Tang et al. [3] (0.004/min) still produced values comparable to those found here from testing at 2.28/min. These tests also found little to no trend in properties such as yield point, while Liu and Kyriakides found that yielding strains increase and yielding stresses decrease with decreasing strain rate. That effect is seen only to a small degree here and within the uncertainty of the data. The plastic modulus, which is not reported by Liu & Kyriakides, decreases somewhat with increasing strain rate, possibly due to the increasing role of viscous behavior in this deformation region.

Tang et al. [3] and Bauer et al. [4] included a comparison of machine and transverse directional testing in their work. Using dynamic testing, Bauer reported a discernable difference in mechanical properties between the two only at high humidity levels (>80%RH), with testing in the machine direction producing a higher storage modulus, by between 12% and 16% and a lower tanδ. From stress-strain tests, Tang reported that the Young's modulus and yield and break stresses were higher for samples tested in the machine direction across the testing spectrum, though the ultimate strain in the machine

direction was lower. Both researchers reported that machine and transverse test exhibited similar trends in mechanical properties with increasing water and temperature for both membranes. For dimensional changes with swelling, not investigated in this work, both found that swelling occurred significantly more (~20%) in the transverse direction.

A set of stress-strain tests comparing machine and transverse directions between 45°C and 120°C and λ-values between 1 and 5 was performed in this work, (Figure 2.25) yielding no discernable difference in elastic modulus, proportional point or yield point. However, the plastic modulus was noticeably higher for the machine direction, supported by a slightly higher ultimate stress and lower ultimate strain for the samples tested in the machine direction, which agrees with the findings by Tang [3]. Because of the observation that Young's modulus was not affected and difficulty in obtaining and preserving directional information from the manufacturer, directionality of the membrane was largely ignored. It was assumed that the boiling during pretreatment erases most of the directional memory of the polymer by allowing the chains to reorganize. Further, similar tests (reported in chapter 5) on completely isotropic recast Nafion showed little discernable difference in any of the properties, except for an arguably higher plastic modulus. However, Tang and Bauer both used comparable pretreatment procedures and still saw directional differences. One possible explanation is that Tang used a much slower strain rate: 0.04%/min, compared to 228%/min used here. At that testing speed, anisotropic effects may become more apparent.

2.6.2 Stress Relaxation

As discussed in the results section above, there are two main observations from the stress relaxation data. (1) There are two shapes of the stress-relaxation curves, with

the faster relaxation rate curve appearing at low strains and lower temperatures in the humidified membranes but at higher temperatures and a greater range of strains in the dry membranes. (2) The shift factors needed to create a single curve from dry and humidified runs are higher for the humidified samples at higher temperature and strain.

The different regimes of shift factor with temperature appears to be analogous to observations made about humidified and dry Nafion in stress-strain tests above: at higher temperatures the membrane is stiffened by the addition of water, while at lower temperatures it is plasticized. At low temperatures the dry membranes had a higher modulus and were shifted to shorter times (larger a_T or a_S) while at temperatures approaching 90°C the dry membranes had a lower modulus and were shifted to longer times (smaller a_T or a_S) to match humidified conditions. As seen in Figure 2.50, which re-plots data from Figure 2.21, the Young's modulus of dry Nafion starts high and drops precipitously with temperature, but the modulus of humidified Nafion starts low and stays roughly constant with temperature, creating a situation in which at higher temperatures a humidified piece is somewhat stiffer than a dry sample, causing the change in shift factors needed to form a master curve.

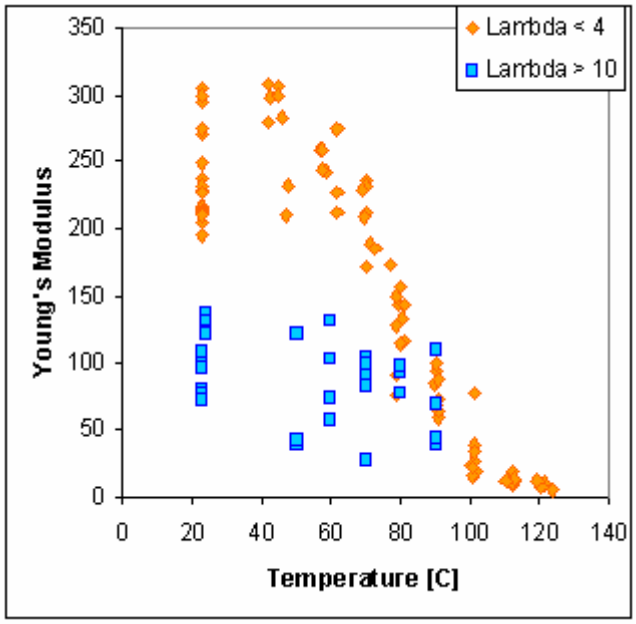

Figure 2.50: Young's modulus vs. temperature for samples under humidified conditions (λ>10, blue squares) and under ambient to dry conditions (λ<4, orange diamonds).

This change in the temperature dependence pattern of the Young's modulus with humidity is also visible from the results of Tang et al. [3] (Figure 2.1) and in the storage modulus measured by Bauer et al. [4] (Figure 2.3). In both cases the modulus of the dry membrane drops much more quickly with increasing water content than the modulus of the wet membrane.

The strain-dependence of the shift factor does not necessarily correlate with the stress-strain curves. The humidified stress-strain curves always lie below the dry curves at temperatures up to 90°C, where they begin to overlap, and the difference between humidified and dry stresses tends to increase with strain for the strains studied here. Thus, an increase in modulus cannot be the only cause of the increase in shift factor with strain. We believe that the addition of water stabilizes the sulfonic acid groups in the membrane, slowing down stress relaxation rates. Kyu and Eisenberg [34] theorized that the stress-relaxation rates were dependent on the ionic groups. So, even though the stress of the humidified membrane is lower than that of dry membranes, which would cause a smaller shift factor (to longer times), its stress-relaxation rate is slower, which causes a larger shift factor (to shorter times). The two effects contribute different amounts at different strains and temperatures. The stabilization or slow down in relaxation rate

(increase in shift factor) becomes most apparent at higher strains and temperatures, conditions that cause the dry membrane stress relaxation to accelerate.

That the addition of water stabilizes the sulfonic acid groups at higher strains and temperatures also explains the pattern of conditions where the downward curving stress-relaxation behavior does and does not occur. In dry membranes the occurrence of the downward curve increases with increasing temperature and decreases with increasing strain, occurring only at low stain at all temperatures and at all strains at higher temperatures. However, stabilized by the addition of water, the stress-relaxation is slowed, such that the curved shape only occurs at lower strains and temperatures.

The effect of water slowing stress-relaxation rates is exactly counter to that observed by Yeo and Eisenberg[30] who observed faster relaxation after the addition of 3 mol H_2O/SO_3^- to Nafion 1365. The different equivalent weight of the membrane might change the results, but probably not the qualitative trends, so it may be that $\lambda=3$ was simply not a high enough water content to cause the change observed here at $\lambda\sim13$. The appearance of two types of relaxation behavior –linear or downward curving – is similar to that reported for Nafion 117 (the same equivalent weight, though slightly thicker) by Liu and Kyriakides [5] (Figure 2.9). They found that at small strains in ambient humidity and room temperature the stress relaxation had a steeper slope and less linear behavior than at larger strains. However, while they attributed this behavior to experimental error, we have seen that it follows a pattern. This investigation also covers a far greater range of experimental conditions, allowing trends to become visible.

The different regimes of dependence on temperature and stress were observed to a degree in the creep data here, though dry creep experiments were not performed. At

lower temperatures and strains the compliance increased linearly with time (on a log-log plot), while at higher temperatures and strains the compliance increased dramatically in the early part of the run, but adopted a linear behavior (again, on a log-log plot) in later time. In this longer-time linear region, the slope of the compliance was lower in the higher-temperature runs than in the lower-temperature runs, though the compliance was higher, and the over-all slopes increased with temperature, as seen in Figure 2.50. The results of these creep experiments is decidedly less conclusive than the stress-relaxation data. However, in performing a more comprehensive and sophisticated creep experiments, colleague Paul Majstrik has also seen different regimes of dependence on temperature, applied stress and humidity that complement the results presented here [50]. Also, stress-relaxation modulus and creep compliance are related through a convolution integral [51], and by using Laplace transforms, one function can be determined from the other. This will be explored as the combined creep and stress-relaxation data are assembled for publication. The creep behavior measured here is not accurate enough for such treatment.

Contrary to the claims of Yeo and Eisenberg [30], the degree of success of time-Temperature superposition for Nafion 115 did not appear to change between dry and humid conditions. However, as may have been found by Yeo and Eisenberg, the functional form of the curves and shift factors was different. Plots of $\ln(a_T)$ for the time-temperature superposition and $\ln(a_s)$ for time-strain superposition yield roughly straight lines when plotted vs. temperature and strain, respectively. However, they did not yield straight lines when fit with the Williams, Landel and Ferry (WLF) equation, which is frequently used to predict $\log(a_T)$ from temperature, using the following equation:

$$\log a_T = \frac{-C_1(T - T_g)}{C_2 + T - T_g} \tag{2.12}$$

Where C_1 and C_2 are material-dependent parameters, usually ~16 and ~50 respectively and T_g is the glass transition temperature [44]. However, the WLF equation is usually only applicable above the polymer's glass transition temperature [43]. Nafion's T_g is well above 90°C, the highest temperature probed in this part of the study, so it is not surprising that the WLF equation fits this data poorly. Values of slope, intercept and R^2 for the fits of $\ln(a_T)$ vs. T (°C) appear in Table 2.4.

Table 2.4: Slope & intercept of $\ln(a_T)$ vs. temperature (°C) for time-temperature superposition

Strain	Slope	Intercept	R^2	Figure
2% humidified	-0.102	2.73	0.96	Figure 2.31
2% dry	-0.125	2.76	0.88	Figure 2.31
5% humidified	-0.090	2.41	0.95	Figure 2.34
5% ambient, matched with humidified	-0.180	9.35	0.94	Figure 2.34
5% dry, matched with humidified	-0.177	8.90	0.95	Figure 2.34
10% humidified	-0.110	4.60	0.87	Figure 2.37
10% dry, matched with humidified	-0.242	13.3	0.85	Figure 2.37
20% humidified	-0.083	2.29	0.75	Figure 2.40
20% dry, matched with humidified	-0.152	5.61	0.80	Figure 2.40

The fact that time-strain superposition works as well as time-temperature superposition suggests that stress-relaxation kinetics are controlled by the stress or strain as well as the temperature. This is also seen in the creep master curves, and indicates that Nafion is a non-linear polymer. Values for slope, intercept and R^2 for the fits of $\ln(a_s)$ vs. strain at 30°C and 80°C, for both stress and modulus appear in Table 2.5.

Table 2.5: Slope & intercept of $\ln(a_S)$ vs. temperature for time-stress superposition

Strain	Slope	Intercept	R^2	Figure
30°C humidified	-0.76	1.17	0.92	Figure 2.41
30°C dry & ambient	-0.52	4.76	0.78	Figure 2.41
50°C humidified	-0.46	0.61	0.92	Figure 2.42
50°C dry & ambient	-0.63	3.18	0.93	Figure 2.42
70°C humidified	-0.23	0.85	0.90	Figure 2.43
70°C dry & ambient	-0.42	2.17	0.90	Figure 2.43
90°C humidified	-0.21	-1.14	0.63	Figure 2.44
90°C dry & ambient	-0.31	-2.37	0.65	Figure 2.44

The time-temperature shift factors presented here often show deviations from linear dependence on temperature, while at constant temperature time-strain shift factors follow a much more monotonic dependence on strain. There is some natural variability in tests like this, as seen in the spread of results for Young's modulus and other properties. However, there are some added experimental difficulties in these tests in which the strain is not known exactly. Prior to testing, the membranes were equilibrated in the plastic bag for 2 hours. During this time the membranes tended to swell, becoming slack in the mounting. The crosshead was adjusted visually—through the window in the oven and the plastic bag-- until slack had disappeared. The load cell and gauge length were then zeroed and the test was started. The process of visually removing the slack could introduce errors by going slightly too far or not far enough, particularly when the applied strain of the test is as low as 2% or 5%. If the membrane is strained before the test starts and the load cell is zeroed, the membrane stress can dip below zero as it relaxes during the test, as was seen several times, or the modulus could start significantly higher or lower depending on whether the strain imposed was more or less than expected. Thus, when performing time-temperature shifts, the curves could all be at slightly different strains, though when doing time-strain shifts, the small difference in strain would only cause a small shift in the abscissa, but not disrupt the general trend of

the data. This discrepancy could also explain why stress-time graphs (not shown) superpose more successfully than the modulus-time graphs. Small differences in strain are magnified by comparing moduli (stress/strain) vs. comparing only stress at roughly the same strain.

The values of E_0, E_1, E_2, E_3 and η_1, η_2 and η_3 determined from fitting the stress-relaxation behavior with the generalized Maxwell equation (2.6) yield inconclusive results. For the humidified tests there is no discernable dependence of the viscosities on temperature or strain, yet the values are not consistent. The residual modulus E_0 tends to decrease with temperature, and all of the modulus values decrease with strain: beyond the yield point the stress-strain relationship falls below the linear elastic slope. The results are presented in Table 2.6. The first row is the average, and the second is the standard deviation.

Table 2.6: Viscosity and modulus values measured from humidified stress-relaxation data, fit with equation (2.6) Viscosity values in GigaPoise, modulus values in MPa.

η_1	η_2	η_3	E_0	E_1	E_2	E_3
15.3	1.1	0.08	14	12.2	16.7	19.2
± 12.4	± 0.7	± 0.06	± 8.4	± 9.4	±8.1	± 5.8

Clearly, these fitting parameters have a great deal of spread: the standard deviation is comparable to the value, even after the removal of 3 of the 32 runs whose fitting parameters fell more than two standard deviations outside the mean, following Chauvenet's criterion[52]. However, it is apparent that the viscosities are orders of magnitude 10, 1 & 0.1 GP and the moduli order 10 MPa, and slightly weight the lower viscosity values. In the dry tests, the viscosities exhibit temperature dependence, as seen in Figure 2.51, which is not seen in the hydrated membranes.

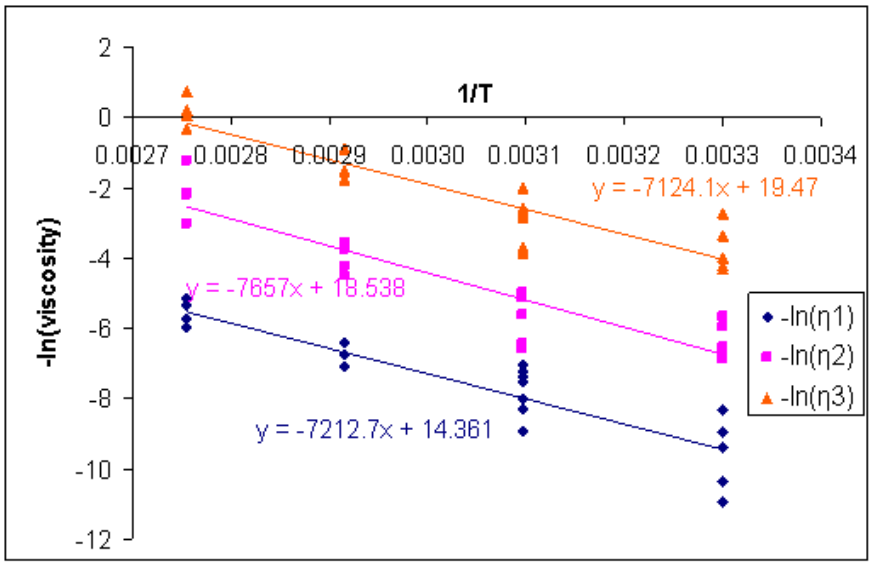

Figure 2.51: Arrhenius temperature-dependence of viscosity in dry Nafion 115. Hydrated Nafion shows little temperature dependence.

The residual modulus of the dry tests (E_0) shows roughly the same temperature-dependence as the humidified tests (decreasing with temperature), though at low temperatures the dry E_0 is slightly higher. The other modulus values do not change with temperature, and in general are higher in the dry membranes, presented in Table 2.7.

Table 2.7: Modulus values measured from dry stress-relaxation data, fit with equation (2.6) Modulus in MPa. Top line is average value, bottom is standard deviation.

E_1	E_2	E_3
28	31	50
± 24	± 23	± 21

The Kohlrausch-Williams-Watts (KWW) equation, equation (2.8) represents dynamic behavior that results from a sum of events with either a broad range of time constants [53] or a time-dependent probability distribution function, $\varphi(t) \sim \frac{1}{t^d}$ [46]. It was developed by Williams and Watts [53] for asymmetrical dielectric relaxation behavior, and

is often applied to stress-relaxation behavior of inhomogeneous materials such as glasses and polymers [45-48, 54, 55]. It is usually considered as an empirical fit to data [45, 54]. However, it has been related to physical phenomena using models with stress-dependent rates [46, 47, 54, 55] such as the Prandtl-Eyring potential energy model in which probability distribution function approximates the different heights of energy barriers [46]. Other models, such as one proposed by Soules [46] in which the transfer of energy from stressed to unstressed sights in a strained glassy material happens at a rate proportional to $1/R^6$ (R distance between sites) also arrive at the KWW equation. A mechanical model of this behavior meant to complement the Voigt-Kelvin and Maxwell spring and dashpot models has also been constructed, in which a series of latches or switches are thrown by springs with time constants whose distribution is given by $1/t^d$ [47].

The stress-relaxation curves could be fit with the KWW equation with as much success as the generalized three-term Maxwell equation (average R^2=0.986 and 0.991 for Maxwell). In the KWW model *d* or the 'shape parameter' lies between 0 and 1 for rates that decrease with time, or can be greater than 1 if the rate increases with time [45, 48]. It is also indicative of the width of relaxation time distribution, being smaller for broader distributions[46, 48]. The average value of *d* for the humidified samples was 0.30 with a standard deviation of 0.10. For the dry samples, the values of *d* tend to be slightly lower, with an average of 0.26, standard deviation 0.12, indicating a broader distribution of relaxation times, which may have been the result of the temperature-dependence of the viscosities in the dry membranes. In both cases the values decreased with increasing strain, as seen in Figure 2.52, and increased weakly with increasing temperature.

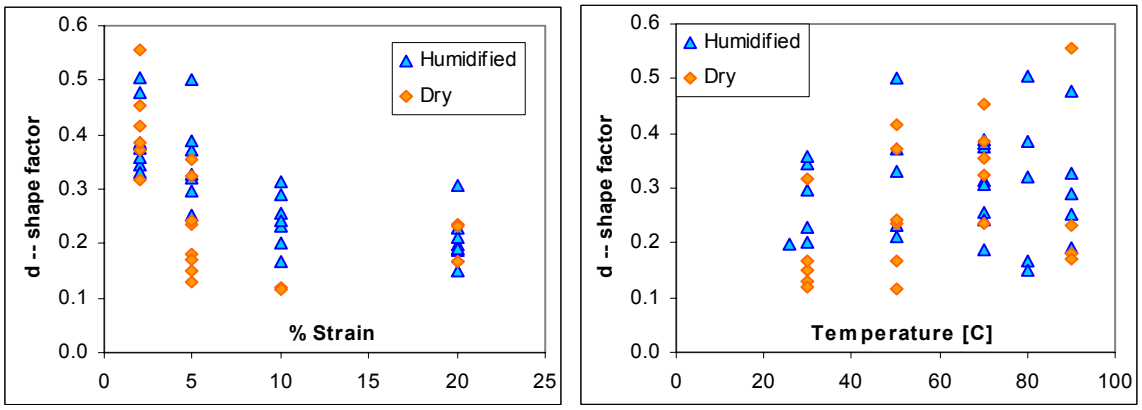

Figure 2.52: Dependence of d, the KWW shape factor, on strain (left) and temperature (right).

The changes in *d* with strain and temperature imply that the width of the relaxation spectrum increases at higher strains and decreases with temperature. The value of *k*, the inverse time constant, also tends to increase with both temperature and strain, as seen in Figure 2.53.

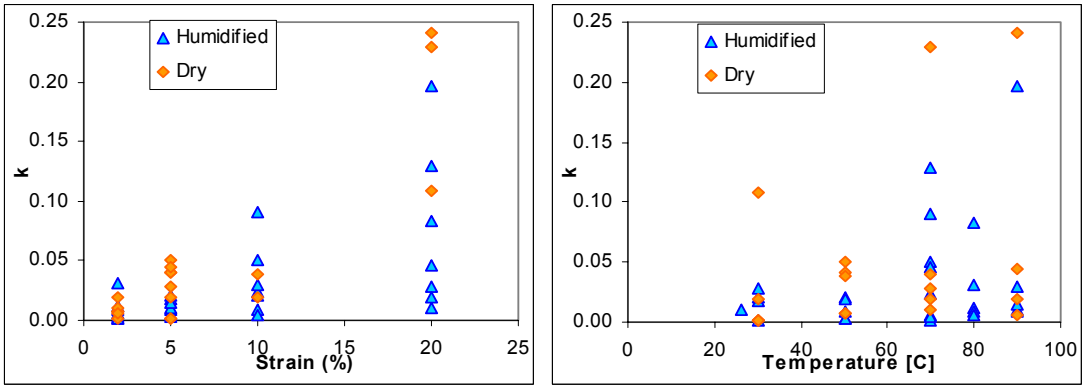

Figure 2.53: Dependence of k the KWW time constant, on strain (left) and temperature (right).

The combined strain and temperature-dependence of the time constant, similar to that found with the time-temperature and time-strain superposition, indicate that both strain and temperature govern the relaxation kinetics.

2.7 Conclusion

Stress-strain and stress-relaxation properties of Nafion have been studied under different temperature and humidity conditions. The Young's modulus of dry Nafion is found to decrease with temperature, while the modulus of wet Nafion is almost independent of temperature. Also, the proportional and yield points of dry and hydrated Nafion follow different trends. The two modulus temperature-dependency regimes are also manifest in stress-relaxation, producing two different regimes of time-temperature shift factors for the hydrated and dry membranes. The stabilizing or stiffening effect of water at higher temperatures also reduces the stress-relaxation rate in hydrated membranes at higher temperatures and strains.

2.8 Acknowledgments

Thanks to Robert Scogna, Dr. Katsuyuki Wakabayashi and Prof. Richard Register for the use of the Instron tensile testing machine as well as excellent instruction and support.

Thanks also to Robert Scogna, Prof. Register and Prof. George Scherer for advice on data treatment and analysis, and to Paul Majsztrik for help constructing the creep experiments and some interesting and informative discussions related to this work.

2.9 References

1. Hector, L. G.; Lai, Y. H.; Tong, W.; Lukitsch, M. J., Strain accumulation in polymer electrolyte membrane and membrane electrode assembly materials during a single hydration/dehydration cycle. *Journal of Fuel Cell Science and Technology* **2007,** 4, (1), 19-28.
2. Huang, X. Y.; Solasi, R.; Zou, Y.; Feshler, M.; Reifsnider, K.; Condit, D.; Burlatsky, S.; Madden, T., Mechanical endurance of polymer electrolyte membrane and PEM fuel cell durability. *Journal of Polymer Science Part B-Polymer Physics* **2006,** 44, (16), 2346-2357.
3. Tang, Y. L.; Karlsson, A. M.; Santare, M. H.; Gilbert, M.; Cleghorn, S.; Johnson, W. B., An experimental investigation of humidity and temperature effects on the mechanical properties of perfluorosulfonic acid membrane. *Materials Science and Engineering a-Structural Materials Properties Microstructure and Processing* **2006,** 425, (1-2), 297-304.
4. Bauer, F.; Denneler, S.; Willert-Porada, M., Influence of temperature and humidity on the mechanical properties of Nafion$^{(R)}$ 117 polymer electrolyte membrane. *Journal of Polymer Science Part B-Polymer Physics* **2005,** 43, (7), 786-795.
5. Liu, D.; Kyriakides, S.; Case, S. W.; Lesko, J. J.; Li, Y. X.; McGrath, J. E., Tensile behavior of Nafion and sulfonated poly(arylene ether sulfone) copolymer membranes and its morphological correlations. *Journal of Polymer Science Part B-Polymer Physics* **2006,** 44, (10), 1453-1465.
6. Kundu, S.; Simon, L. C.; Fowler, M.; Grot, S., Mechanical properties of Nafion$^{(TM)}$ electrolyte membranes under hydrated conditions. *Polymer* **2005,** 46, (25), 11707-11715.
7. Liu, D.; Hickner, M. A.; Case, S. W.; Lesko, J. J., Relaxation of proton conductivity and stress in proton exchange membranes under strain. *Journal of Engineering Materials and Technology-Transactions of the ASME* **2006,** 128, (4), 503-508.
8. Solasi, R.; Zou, Y.; Huang, X.; Reifsnider, K.; Condit, D., On mechanical behavior and in-plane modeling of constrained PEM fuel cell membranes subjected to hydration and temperature cycles. *Journal of Power Sources* **2007,** 167, (2), 366-377.
9. Budinski, M.; Gittleman, C. S.; Lai, Y. H.; Litteer, B.; Miller, D., Characterization of perfluorosulfonic acid membranes for PEM fuel cell mechanical durability. In *AIChE Annual Meeting*, Austin, TX, 2004; p Presentation slides used at 2004 AIChE Annual Meeting.
10. Choi, P.; Jalani, N. H.; Thampan, T. M.; Datta, R., Consideration of thermodynamic, transport, and mechanical properties in the design of polymer electrolyte membranes for higher temperature fuel cell operation. *Journal of Polymer Science Part B-Polymer Physics* **2006,** 44, (16), 2183-2200.
11. Liu, Y. H.; Yi, B. L.; Shao, Z. G.; Xing, D. M.; Zhang, H. M., Carbon nanotubes reinforced Nafion composite membrane for fuel cell applications. *Electrochemical and Solid State Letters* **2006,** 9, (7), A356-A359.
12. Greso, A. J.; Moore, R. B.; Cable, K. M.; Jarrett, W. L.; Mauritz, K. A., Chemical Modification of a Nafion® sulonyl fluoride precursor via in situ sol-gel reactions. *Polymer* **1997,** 38, (6), 1345-1356.

13. Satterfield, M. B.; Majsztrik, P. W.; Ota, H.; Benziger, J. B.; Bocarsly, A. B., Mechanical properties of Nafion and titania/Nafion composite membranes for PEM fuel cells. *J. Polymer Science B: Polymer Physics* **2006,** 44, (16), 2327-2345.
14. Choi, P.; Jalani, N. H.; Datta, R., Thermodynamics and proton transport in Nafion - I. Membrane swelling, sorption, and ion-exchange equilibrium. *Journal of the Electrochemical Society* **2005,** 152, (3), E84-E89.
15. Newns, A. C., The sorption and desorption kinetics of water in a regenerated cellulose. *Transactions of the Faraday Society* **1956,** 52, (11), 1533-1545.
16. Rivin, D.; Kendrick, C. E.; Gibson, P. W.; Schneider, N. S., Solubility and transport behavior of water and alcohols in Nafion(TM). *Polymer* **2001,** 42, (2), 623-635.
17. Morris, D. R.; Sun, X., Water-sorption and transport properties of Nafion 117 H. *Journal of Applied Polymer Science* **1993,** 50, (8), 1445-1452.
18. Krtil, P.; Trojanek, A.; Samec, Z., Kinetics of water sorption in Nafion thin films -- quartz crystal microbalance study. *Journal of Physical Chemistry B* **2001,** 105, 7979-7983.
19. Takamatsu, T.; Hashiyama, M.; Eisenberg, A., Sorption phenomena in Nafion membranes. *Journal of Applied Polymer Science* **1979,** 24, (11), 2199-2220.
20. Bagley, E.; Long, F. A., 2-Stage sorption and desorption of organic vapors in cellulose acetate. *Journal of the American Chemical Society* **1955,** 77, (8), 2172-2178.
21. DuPont DuPont Fuel Cells: DuPont Nafion PFSA membranes N-115, N-117, NE-1110. http://www.dupont.com/fuelcells/pdf/dfc101.pdf
22. Werner, S.; Jorissen, L.; Heider, U., Conductivity and mechanical properties of recast Nafion films. *Ionics* **1996,** 2, (1), 19-23.
23. Kawano, Y.; Wang, Y. Q.; Palmer, R. A.; Aubuchon, S. R., Stress-strain curves of Nafion membranes in acid and salt forms. *Polimeros: Ciencia e Technologia* **2002,** 12, (2), 96-101.
24. Fujimoto, C. H.; Hickner, M. A.; Cornelius, C. J.; Loy, D. A., Ionomeric poly(phenylene) prepared by diels-alder polymerization: Synthesis and physical properties of a novel polyelectrolyte. *Macromolecules* **2005,** 38, (12), 5010-5016.
25. Kyriakides, S. A., Mechanical behavior of Nafion and BPSH membranes. *Journal of Undergraduate Materials Research* **2005,** 1, 11-14.
26. Ward, I. M.; Sweeney, J., 11.1.4 Definition of yield stress. In *An Introduction to the Mechanical Properties of Solid Polymers*, 2nd ed.; John Wiley & Sons: Chichester, England, 2004; pp 249-250.
27. Jalani, N. H.; Mizar, S. P.; Choi, P.; Furlong, C.; Datta, R., Optomechanical characterization of proton-exchange membrane fuel cells. *Proc. SPIE* **2004,** 5532, 316-325.
28. Jalani, N. H.; Choi, P.; Datta, R., TEOM: A novel technique for investigating sorption in proton-exchange membranes. *Journal of Membrane Science* **2005,** 254, (1-2), 31-38.
29. Uan-Zo-li, J. T. Thesis: The effects of structure, humidity and aging on the mechanical properties of polymeric ionomers for fuel cell applications. Master of Science, Virginia Polytechnic Institute and State University, Blacksburg, Virginia, 2001.

30. Yeo, S. C.; Eisenberg, A., Physical-properties and supermolecular structure of perfluorinated ion-containing (Nafion) polymers. *Journal of Applied Polymer Science* **1977,** 21, (4), 875-898.
31. Springer, T. E.; Zawodzinski, T. A.; Gottesfeld, S., Polymer electrolyte fuel-cell model. *Journal of The Electrochemical Society* **1991,** 138, (8), 2334-2342.
32. Gebel, G.; Aldebert, P.; Pineri, M., Swelling study of perfluorosulphonated ionomer membranes. *Polymer* **1993,** 34, (2), 333-339.
33. Kyu, T.; Eisenberg, A., Mechanical relaxations in perfluorosulfonate-ionomer membranes. *ACS Symposium Series* **1982,** 180, 79-110.
34. Kyu, T.; Eisenberg, A., Underwater stress-relaxation studies of Nafion (perfluorosulfonate) ionomer membranes. *Journal of Polymer Science-Polymer Symposia* **1984**, (71), 203-219.
35. Yang, C.; Srinivasan, S.; Bocarsly, A. B.; Tulyani, S.; Benziger, J. B., A comparison of physical properties and fuel cell performance of Nafion and zirconium phosphate/Nafion composite membranes. *Journal of Membrane Science* **2004,** 237, (1-2), 145-161.
36. Sacca, A.; Carbone, A.; Passalacqua, E.; D'Epifanio, A.; Licoccia, S.; Traversa, E.; Sala, E.; Traini, F.; Ornelas, R., Nafion-TiO_2 hybrid membranes for medium temperature polymer electrolyte fuel cells (PEFCs). *Journal of Power Sources* **2005,** 152, (1), 16-21.
37. Bauer, F.; Willert-Porada, M., Zirconium phosphate Nafion (R) composites - a microstructure-based explanation of mechanical and conductivity properties. *Solid State Ionics* **2006,** 177, (26-32), 2391-2396.
38. Vapor Pressure of Saturated Salt Solutions. In *CRC Handbook of Chemistry and Physics, Internet Version 2007*, 87th ed.; Lide, D. R., Ed. Taylor and Francis: Boca Raton, FL, 2007; pp 6-92.
39. Wexler, A., Constant Humidity Solutions. In *CRC Handbook of Chemistry and Physics, Internet Version 2007*, 87th ed.; Lide, D. R., Ed. Taylor and Francis: Boca Raton, FL, 2007; pp 15-33.
40. Majsztrik, P. W.; Satterfield, M. B.; Bocarsly, A. B.; Benziger, J. B., Water sorption, desorption and transport in Nafion membranes. *Journal of Membrane Science* **2007,** 301, (1-2), 93-106.
41. Thampan, T.; Malhotra, S.; Tang, H.; Datta, R., Modeling of conductive transport in proton-exchange membranes for fuel cells. *Journal of the Electrochemical Society* **2000,** 147, (9), 3242-3250.
42. Satterfield, M. B.; Benziger, J. B., NonFickian water sorption dynamic by Nafion membranes. **2007,** forthcoming.
43. Rosen, S. L., *Fundamental Principles of Polymeric Materials*. 2 ed.; John Wiley & Sons, Inc.: New York, 1993; p 407.
44. Aklonis, J. J.; MacKnight, W. J.; Shen, M., *Introduction to Polymer Viscoelasticity*. Wiley-Interscience: New York, 1972.
45. Scherer, G. W., Theories of relaxation. *Journal of Non-Crystalline Solids* **1990,** 123, (1-3), 75-89.
46. Soules, T. F.; Markovsky, A., Direct dipole induced energy-transfer - A microscopic model for glass relaxation. *Journal of Chemical Physics* **1987,** 86, (10), 5874-5880.

47. Fancey, K. S., A latch-based Weibull model for polymeric creep and recovery. *Journal of Polymer Engineering* **2001,** 21, (6), 489-509.
48. Khare, V. P.; Greenberg, A. R.; Krantz, W. B., Investigation of the viscoelastic and transport properties of interfacially polymerized barrier layers using pendant drop mechanical analysis. *Journal of Applied Polymer Science* **2004,** 94, (2), 558-568.
49. Scherer, G. W., In email: re: Thesis. In Satterfield, M. B., Ed. Princeton, NJ, 2007.
50. Majsztrik, P. Thesis. forthcoming.
51. Ferry, J. D., Ch 3, Sec E1. Interrelation of the two transient functions. In *Viscoelastic Properties of Polymers*, 2nd ed.; John Wiley & Sons, Inc.: New York, 1970; p 671.
52. Young, H. D., 9: Gauss distribution, or normal error function and 10: Rejection of data. In *Statistical Treatment of Experimental Data*, McGraw-Hill Book Company: New York, 1962; pp 64-80.
53. Williams, G.; Watts, D. C., Non-symmetrical dielectric relaxation behaviour arising from a simple empirical decay function. *Transactions of the Faraday Society* **1970,** 66, (565P), 80-&.
54. Dobreva, A.; Gutzow, I.; Schmelzer, J., Stress and time dependence of relaxation and the Kohlrausch stretched exponent formula. *Journal of Non-Crystalline Solids* **1997,** 209, (3), 257-263.
55. Fancey, K. S., A mechanical model for creep, recovery and stress relaxation in polymeric materials. *Journal of Materials Science* **2005,** 40, (18), 4827-4831.

3 NonFickian Water Vapor Sorption Dynamics by Nafion Membranes

3.1 Abstract

Water absorption and desorption dynamics for Nafion 1100 EW ionomers have been measured for film thicknesses between 50.8 μm and 606 μm and at temperatures ranging from 30°C to 90°C. The behavior exhibits two distinct nonFickian characteristics: desorption is ten times faster than absorption, and neither absorption nor desorption collapse to a uniform curve when plotted against a reduced time over membrane thickness squared: t/ℓ^2. The data were fit well by models in which interfacial mass transport resistance governs desorption while absorption follows a modified two-stage absorption model in which interfacial mass transport controls early-time sorption and long-time sorption is controlled by polymer chain rearrangement and relaxation.

3.2 Introduction

Nafion® is a sulfonated perfluoroionomer commonly used as an electrolyte in polymer electrolyte membrane (PEM) fuel cells. Its proton conductivity is strongly dependent on its water content [1-3]. This moisture dependent performance is of concern for fuel cell operation in which dynamic conditions may alter the membrane water content. Events such as start-up and shut-down, changes in circuit load and environmental changes in temperature and humidity can cause dynamic conditions that affect cell water production and removal rates and alter the water concentration inside the cell and the membrane.

This likelihood has been confirmed in the lab with experiments comparable to those more ‘real world’ events. Single step changes in operating conditions have been

shown to cause dramatic non-linear dynamic responses on a range of time-scales [4, 5], leading to the suspicion that changing membrane water content contributes to the observed responses. These results underscore the importance of understanding the dynamics of membrane water uptake and loss from environments similar to that in a fuel cell.

Many different researchers have examined water sorption and transport in Nafion over the past 30 years [6-16]. Experiments have generally focused on determining diffusion coefficients or other mass-transfer kinetics via dynamic water uptake and/or loss [6, 9-14], steady-state permeation [8, 11] and NMR diffusion measurements [16]. Majsztrik et al. [17] provides an excellent summary of reported diffusion coefficients and trends.

The standard analysis [18] of the water uptake and loss from Nafion films has employed a Fickian model for diffusion into a slab in which diffusion is the rate-controlling mechanism:

$$\frac{\partial C}{\partial t} = -D\frac{\partial^2 C}{\partial x^2} \tag{3.1}$$

It is commonly assumed that the diffusion coefficient D does not change with concentration, C, that there are no thermodynamic or kinetic effects associated with swelling, and that the concentration at the membrane surfaces (x=0,ℓ) is constant and equal to the concentration in equilibrium with the external fluid phase, C_∞:

$$C = C_\infty, \quad t > 0, \quad x = 0, \ell \tag{3.2}$$

And that, by symmetry, there is no flux through the center of the membrane:

$$\frac{\partial C}{\partial x} = 0, \quad t \geq 0, \quad x = \ell / 2 \tag{3.3}$$

For absorption into a dry membrane the initial conditions are

$$C = C_0 = 0, \quad t = 0, \quad 0 \le x \le \ell \tag{3.4}$$

while for desorption from a hydrated membrane

$$C = C_0 > 0, \quad t = 0, \quad 0 \le x \le \ell \tag{3.5}$$

Assuming Fickian behavior with a constant diffusivity, the resultant equation can be solved:

$$\frac{M_t - M_0}{M_\infty - M_0} = 1 - \frac{8}{\pi^2} \sum_{m=0}^{m=\infty} \frac{1}{(2m+1)^2} \exp\left\{ \frac{-D(2m+1)^2 \pi^2}{4\ell^2} t \right\} \tag{3.6}$$

At short times equation (3.6) can be approximated by:

$$\frac{M_t - M_0}{M_\infty - M_0} = 4\left(\frac{Dt}{\pi \ell^2} \right)^{1/2} \tag{3.7}$$

which yields a commonly used [6, 11, 12] expression for D as a function of $t_{1/2}$, the time to achieve half of the equilibrium mass uptake or loss:

$$D = \frac{0.049\ell^2}{t_{1/2}} \tag{3.8}$$

Using equations (3.6) or (3.7), experimental data for the approach to equilibrium mass uptake $(M_t-M_0)/(M_\infty-M_0)$ or, for desorption, approach to equilibrium mass loss $(M_0-M_t)/(M_0-M_\infty)$ versus time for a given membrane thickness ℓ yields the diffusion coefficient of water in Nafion.

Two defining characteristics of diffusion-controlled water uptake are that sorption and desorption curves should collapse to a universal function of the reduced time over membrane thickness squared: t/ℓ^2 [19] and that, given a constant diffusion coefficient D and that the magnitude of the driving forces (C_0-C_∞ for sorption and C_∞-C_0 for desorption) are equal, the sorption and desorption curves should be symmetric.

Interestingly, even though most investigators [6, 10-12] chose to model water uptake based on Fickian diffusion equations (3.6), (3.7) or (3.8), many have noticed distinct nonFickian behavior, including diffusion coefficients that depend on membrane thickness [6, 8, 9, 11], diffusion coefficients that depend on concentration [6, 10, 11, 16], diffusion coefficients that are different for water sorption from liquid or vapor [8, 11, 16, 20], and different diffusion coefficients for absorption or desorption [10-12, 21].

Burnett et al. [6] and Morris and Sun [10] analyzed sorption tests and concluded that the diffusion coefficient increased with membrane water content, up to a maximum at an intermediate hydration level and then decreased. Zawodzinski [16] reported similar findings for diffusion measured through NMR experiments, and Rivin [11] reported similar behavior for water uptake and loss experiments, but found in permeation experiments that the diffusion coefficient steadily increases with increasing concentration. Ge et al. [8] also found that permeation increased with water activity but suggested that the maximum in D persists and that the decrease in diffusivity at higher water contents was offset by a decrease in interfacial mass transport resistance.

Burnett [6] and Ge [8] attributed the decline in D at higher concentrations to it being augmented by the presence of an activity gradient, while Rivin [11] attributed this behavior to localized temperature effects in which heat released during the exothermic sorption process depresses the rate of water uptake, an effect which is enhanced in the steep upper reaches of the water sorption isotherm. The concentration-dependent maximum in D could help explain faster desorption rate [10] but, as Rivin [11] points out, desorption remains faster than absorption over the entire range of water concentrations, and the localized

temperature effect also would not explain the difference between sorption and desorption rates, counteracting both processes equally.

Several researchers have suggested that interfacial mass transport may be responsible for the differences between vapor and liquid water uptake [8, 11, 16, 20], sorption and desorption [9, 11] and varying membrane thickness [8, 9, 11]. Ge [8] noted the importance of interfacial mass transfer in permeation experiments and modeled results to yield interfacial mass transport rates k dependent on the volume fraction of water f_V:

$$k_a = 1.14 \times 10^{-3} f_V \exp\left[2416 \cdot \left(1/303 - 1/T\right)\right] \text{ cm/s} \tag{3.9}$$

for sorption and

$$k_d = 4.59 \times 10^{-3} f_V \exp\left[2416 \cdot \left(1/303 - 1/T\right)\right] \text{ cm/s} \tag{3.10}$$

for desorption. They attributed the larger desorption rate to the hydrophobic surface slowing condensation during sorption and localized temperature effects from the latent heat of sorption. Permeation experiments were also performed in our lab with membranes of different thicknesses that clearly showed that interfacial mass transport between water vapor and the Nafion membrane is the rate controlling step in permeation at low temperatures and thin membranes [17], but that water diffusion across the membrane also contributes resistance, which accounts for a change in permeation rate with membrane thickness and water content. Krtil et al. [9] noted that a mechanism controlled by diffusion and interfacial mass transport would predict sigmoidal behavior, which had only been reported by Rivin [11]. So, to explain the difference observed between sorption and desorption, Krtil adopted a model using a reversible water immobilization reaction—a bulk mechanism, which accounted for their observed thickness-independent sorption

rates. They attributed the faster desorption reaction rate to the expanded pores of the swollen membrane [9].

Several researchers have pointed to ways in which structural changes and polymer chain rearrangement mechanisms might govern water uptake and loss dynamics, particularly the difference between sorption and desorption rates [9-12]. Takamatsu et al. [12] found Fickian behavior for sorption of acid-form and neutralized Nafion 1155 from liquid water but, for partially neutralized membranes they reported distinct nonFickian trends such as a "secondary absorption process" which they associated with a structural rearrangement which would be slow compared to diffusion for completely neutralized Nafion (cation hindered chain movement) and fast compared to diffusion for acid-form Nafion.

We recently proposed that water sorption and transport may be controlled by interfacial mass transport and polymer relaxation dynamics [17]. We present here more detailed studies that explore the roles of temperature and membrane thickness on sorption and desorption rates, proposing a model which combines the observed effects of diffusion, polymer relaxation and interfacial mass transport in the sorption of water. We have fit our data to this model and extract interfacial mass transfer coefficients and polymer relaxation rates.

3.3 Procedure

Extruded Nafion® 1100 equivalent weight films of 50.8 μm, 127 μm and 254 μm (DuPont product) were obtained from Ion Power (New Castle, Del), and a 606 μm film was recast from the Nafion solution Liquion™ (Ion Power product). We also prepared 125 μm films by recasting from solution and found that after annealing to 140°C for 2

hours recast films exhibited sorption/desorption rates that were identical to extruded 125 μm films. All membranes were cleaned and ion-exchanged by boiling for 1 hour in 3% hydrogen peroxide in water, 20 minutes in de-ionized water, 1 hour in 1 M sulfuric acid and 20 minutes in DI water. Afterwards membranes were stored at room temperature and 100% relative humidity.

Experiments were carried out using the set-up pictured in Figure 3.1 through Figure 3.3. Before absorption experiments, membranes were dried over drierite at 70°C for 2h. They were then introduced into a 100% relative humidity environment, and their weight recorded over time. After the membranes had reached equilibrium with the humid environment they were immediately transferred to a dry environment at the same temperature and their weight was recorded over time as they dried.

To record weight while in the controlled environments, membranes hung on a hook into the chamber from below a bottom-weighing balance, Ohaus AR0640, accurate to 10^{-4} g. The scale interfaced with a computer, and the weight was recorded by the program LabTech every 2 seconds.

Figure 3.1: Water Sorption Set-up: Membrane hung from a bottom-weighing scale into the controlled-atmosphere chamber and weight was continuously recorded. Figure reprinted from [17] with permission from Elsevier © 2007. Image has been cropped & text box removed.

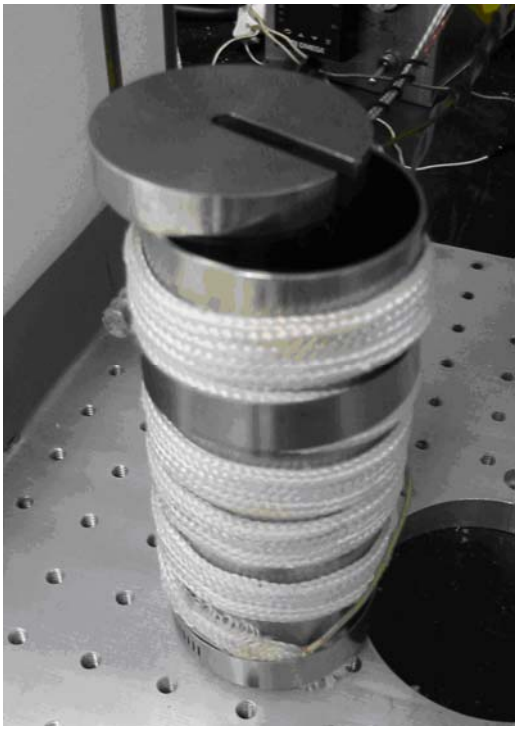

Figure 3.2: Water absorption environment filled with water to just below the membrane. The body and top of chamber were heated by heating tape and a cartridge heater, respectively.

The humidity chamber, seen in Figure 3.2, was a stainless steel vessel, 15 cm tall and 6 cm in diameter, filled with water to a height just below the membrane. The lid was stainless steel 13 mm in thickness with a slot allowing it to slide easily into place around the membrane's hook. The vessel was heated with heating tape, and the lid with a cartridge heater. To prevent condensation on the hook at the chamber exit, the lid was heated to ~2°C above the temperature of the vessel. Even with the heated lid, liquid condensation on the wire was a problem. A heat lamp was used to illuminate the support wire which effectively prevented condensation. We assumed that 100% relative humidity in the chamber was maintained. There were small temperature differences (~2°C) between vessel and lid but the membrane hung far enough from the lid that we

ignored that small correction.

Additionally, membranes were put in a sealed jar over water in an oven overnight and the mass uptakes were within5% of those achieved during the sorption experiment.

Sorption experiments at 80°C and 90°C had uptakes that were 10-15% less than the values obtained from a sealed jar, an indication that the RH was less than 100% at the higher temperatures.

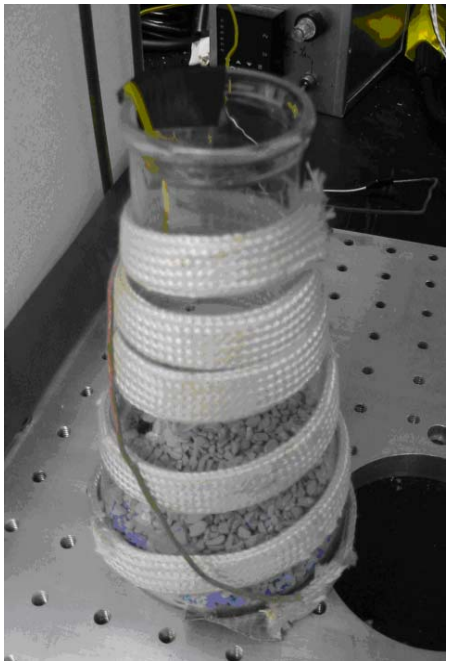

Figure 3.3: Water desorption environment containing drierite. Heating tape controlled the interior temperature.

The drying chamber, seen in Figure 3.3, consisted of an Erlenmeyer flask partially filled with Drierite® and heated with heating tape.

3.4 Results:

Figure 3.4 to Figure 3.9 depict the measured water uptake and loss curves for Nafion at 50°C, represented as approach to final mass change: $(M_t-M_0)/(M_\infty-M_0)$ for absorption and $(M_0-M_t)/(M_0-M_\infty)$ for desorption. Each line is the result of a single experiment. In Figure 3.4 and Figure 3.5, absorption and desorption are plotted against time. Absorption and desorption occur with dramatically different rates; while the absorption runs approach equilibrium over ~5000 s, the desorption runs reach equilibrium in ~500 s. If water sorption was controlled by Fickian diffusion the absorption and

desorption rates should be identical. In Figure 3.7 and Figure 3.9, the departure from Fickian behavior is exhibited: the curves do not collapse to a uniform line when plotted against the reduced time over membrane thickness squared: t/ℓ^2, as predicted by the solution of the Fickian model in Equation (3.6). However, in Figure 3.6 and Figure 3.8, the absorption and desorption runs for different membrane thicknesses appear to collapse to single curves when plotted against time over thickness: t/ℓ.

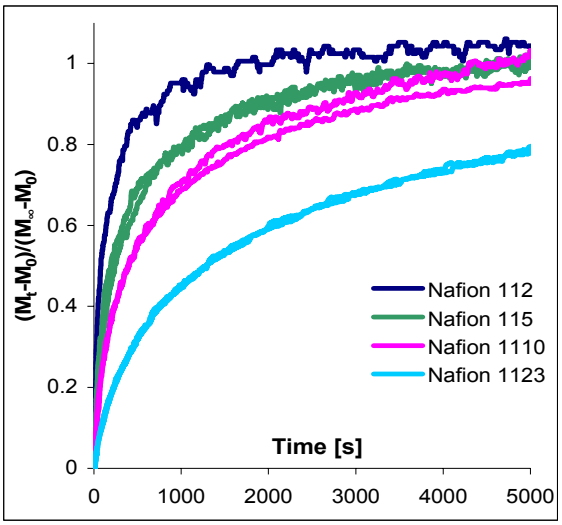

Figure 3.4: Absorption: approach to equilibrium water uptake vs. time. Nafion 1100 EW, 50°C, different film thicknesses.

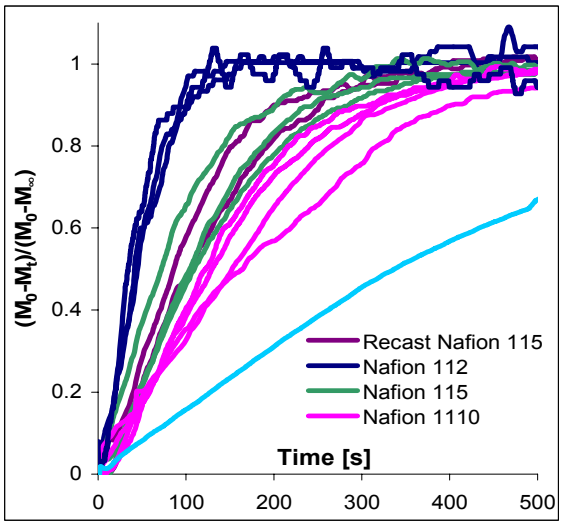

Figure 3.5: Desorption: approach to equilibrium water loss vs. time. Nafion 1100 EW, 50°C, different film thicknesses.

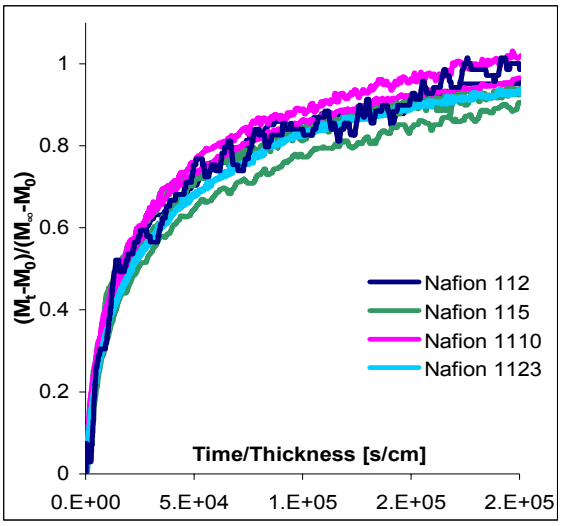

Figure 3.6: Absorption: approach to equilibrium water uptake vs. time/membrane thickness. Nafion 1100 EW, 50°C

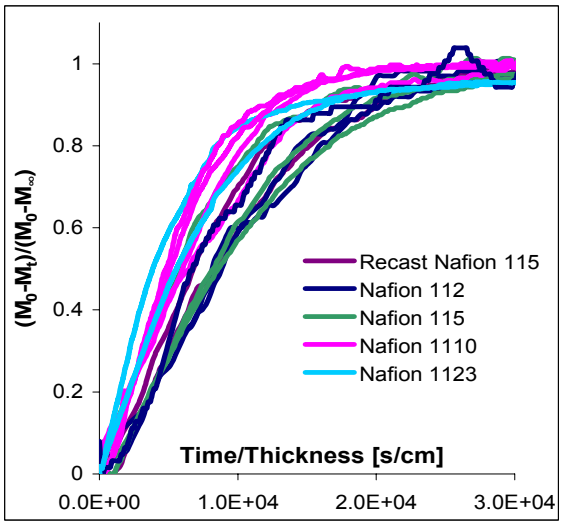

Figure 3.7: Absorption: approach to equilibrium water uptake vs. time/membrane thickness^2 Nafion 1100 EW, 50°C

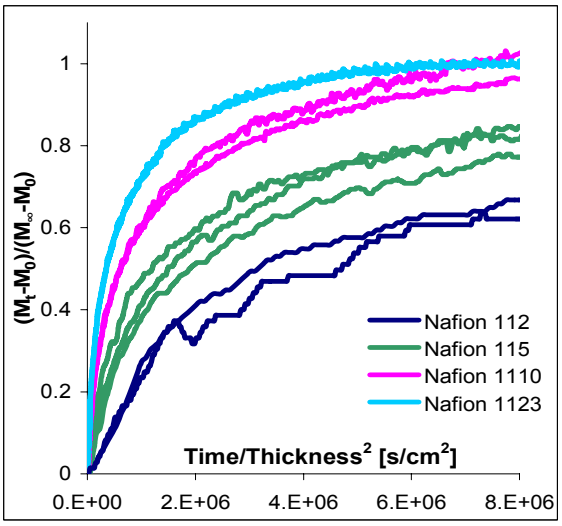

Figure 3.8: Desorption: approach to equilibrium water loss vs. time/thickness. Nafion 1100 EW, 50°C

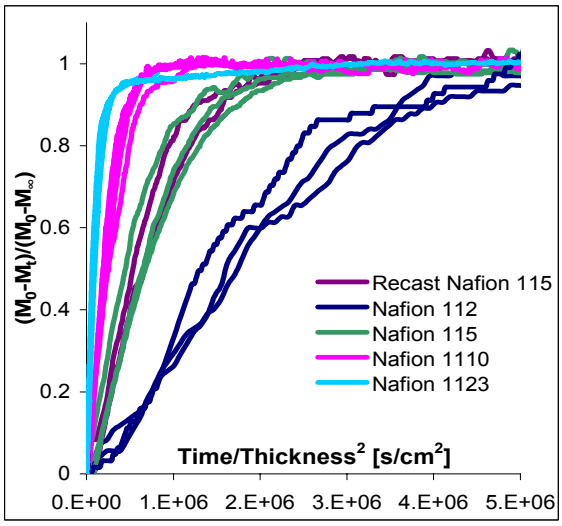

Figure 3.9: Desorption: approach to equilibrium water loss vs. time/membrane thickness^2 Nafion 1100 EW, 50°C

These behavioral trends are the same across all temperatures tested in this work (30°C-90°C): desorption is 10x faster than absorption and curves collapse not against t/ℓ^2 but against t/ℓ. The kinetics for both absorption and desorption get significantly faster with increasing temperature, as illustrated in Figure 3.10 and Figure 3.11, where

absorption and desorption curves are plotted for a single film thickness: Nafion 1110 (254 μm) at different temperatures.

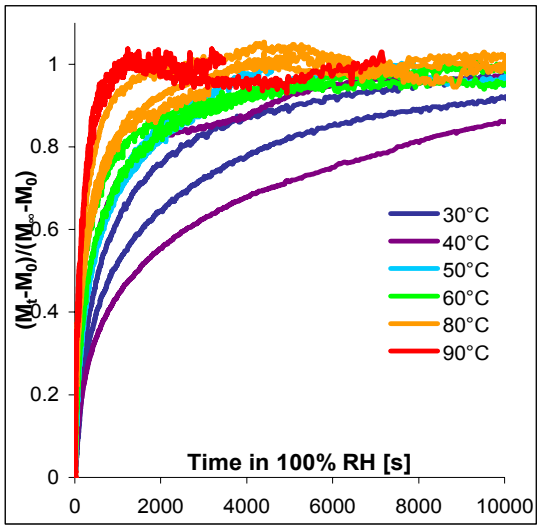

Figure 3.10: Absorption: approach to equilibrium water uptake vs. time, Nafion 1110, different temperatures.

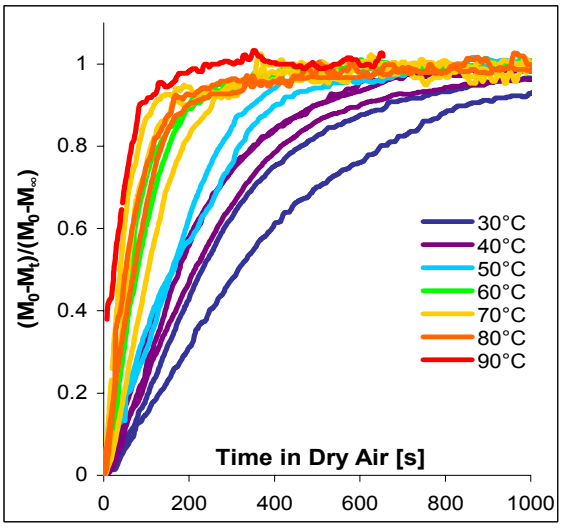

Figure 3.11: Desorption: approach to equilibrium water loss vs. time, Nafon 1110, different temperatures.

3.5 Discussion:

Apparent diffusion coefficients can be calculated assuming Fickian behavior and using equations (3.6) and (3.7). As would be expected from the lack of agreement when plotted vs t/ℓ^2, these apparent diffusion coefficients are very different depending on membrane thickness. At 30°C, the 254 μm thick membrane has apparent diffusion coefficients of ~5 x 10^{-8} cm^2/s (absorption) and 4.5 x 10^{-7} cm^2/s (desorption) which are more than an order of magnitude greater than the apparent diffusion coefficients calculated for the 51μm thick films: 5x10^{-9} cm^2/s (absorption) and 1x10^{-8} cm^2/s (desorption). The variation of apparent diffusion coefficient with membrane thickness grows more pronounced at higher temperatures.

Diffusion coefficients in the range of 10^{-9} to 10^{-7} at 30°C agree with other investigations of sorption and desorption from water vapor [6, 7, 10, 12], but are significantly lower than diffusion coefficients found with permeation, sorption from liquid water or NMR experiments. Diffusion coefficients determined through permeation experiments are between $1.3x10^{-7}$ and $2.6x10^{-6}$ cm^2/s at 32°C [11], depending on surrounding water activity of 0.2 to 1, respectively. Sorption from liquid water using the Arrhenius parameters identified by Takamatsu et al. [12] yields a diffusion coefficient of $2.3x10^{-6}$ at 30°C for Nafion equivalent weight 1155, 1300 μm thick. Similarly, *D* values adjusted from NMR self-diffusion coefficients in Nafion 117 at 30°C range from $1.3x10^{-6}$ to $4.2x10^{-6}$ cm^2/s for membrane water contents of λ=2 and 3, respectively [16].

These inconsistencies in diffusion coefficients determined by different experimental measurement techniques suggest that diffusion is significantly faster than the actual rate-controlling mechanism in water vapor uptake and loss. Combined with the large discrepancy between sorption and desorption, these results give clear indication that both processes are controlled by different mechanisms, and that neither absorption nor desorption is simple Fickian diffusion.

3.5.1 Comparison with other NonFickian Mechanisms

NonFickian sorption behavior is frequently reported for polymer systems [19, 20, 22-26]. While diffusion tends to be Fickian in rubbery polymers, nonFickian behavior commonly occurs in situations similar to the Nafion/water system considered here: glassy polymers insoluble in the surrounding environment with a dilute penetrant that is below its critical temperature [19, 23]. Characteristic nonFickian behaviors [23, 26] include sorption and desorption curves that are not symmetric, though usually cross at some point,

sorption curves for different thicknesses which do not collapse to a single curve with t/ℓ^2, and sorption curves that display an inflection point when plotted either against time or $t^{1/2}$ [26, 27], or are linear or curve upwards with time.

Though the membrane becomes thicker as it swells, deviations from Fickian behavior are not due to changes in membrane thickness during sorption. As long as the thickness length is defined as a length that contains a specified mass of polymer per unit area, it can be treated as constant [26]. Using this length scale, concentration is defined as the amount of solvent per unit mass of polymer, diffusion is through a reference frame that moves with the advancing polymer thickness, such that there is always the same mass of polymer inside the reference frame and the same functional form for diffusion is maintained.

NonFickian behaviors are attributed to a number of physical deviations from Fick's idealized case. Situations in which the diffusion coefficient D is dependent on penetrant concentration can often cause asymmetry in sorption and desorption rates [27]. For D increasing with penetrant concentration, the initial sorption is slower than desorption but with an increasing rate such that it crosses the desorption curve and reaches equilibrium more quickly. For D decreasing, the observed desorption curve is always slower than sorption [26, 28]. In the Nafion-water system the desorption is always faster than sorption, which cannot be described by a concentration-dependent D. History-dependent diffusion coefficients [26] have also been proposed as an explanation for nonFickian behavior in which gradual polymer rearrangements following an increase in solvent content control the rate at which the diffusion coefficient reaches its equilibrium value for that concentration. In this case desorption could be much faster than

absorption, as the diffusion coefficient would remain high throughout desorption, decaying more slowly than solvent is lost.

Other typical nonFickian sorption mechanisms are usually categorized as two-stage, Case-II, super Case-II or as somewhere between Fickian and Case-II. [19, 29, 30] In Case-II type behaviors, the solvent profile in the absorbing polymer is discontinuous and appears as a propagating front into the dry polymer, different from the continuous parabolic concentration profile predicted by Fick's law. This class of behaviors produces sorption curves that are linear when plotted against t^n, where n=1 for Case II (linear with time), n>1 for super-Case II (curves upwards with time), or 0.5<n<1 for behavior between Fickian (or Case I in which n=0.5) and Case II. None of the Case II characteristic behaviors are exhibited in the Nafion-water system, which maintains a downward curvature with both time and $t^{1/2}$.

Two-stage absorption, the sort of mechanism which will be proposed here, is distinct from Case-II or super Case-II in that it is not necessarily characterized by a sharp advancing front. Instead there is an initial solvent uptake up to a quasi-equilibrium concentration which is diffusion-controlled, and considered analogous to an elastic response by the polymer, but further approach to equilibrium is controlled by stress-relaxation as the polymer chains rearrange to accommodate more solvent.[19, 22-25, 31] Because the second stage diffusion is fast compared to relaxation, the concentration profile through the sample is essentially flat, with mass uptake controlled almost entirely by relaxation [25]. One of the earliest treatments of this behavior came from Crank and Park [26] who proposed and solved a time-dependent boundary condition similar to that proposed later by Long and Richman [25] and noted that this mechanism explains why

desorption can be faster than absorption, as chain rearrangement and relaxation is not necessary for penetrant to leave the polymer.

3.5.2 Desorption

The data from Figure 3.6 and Figure 3.8 have been re-plotted in Figure 3.12 and Figure 3.13 using a natural log scale.

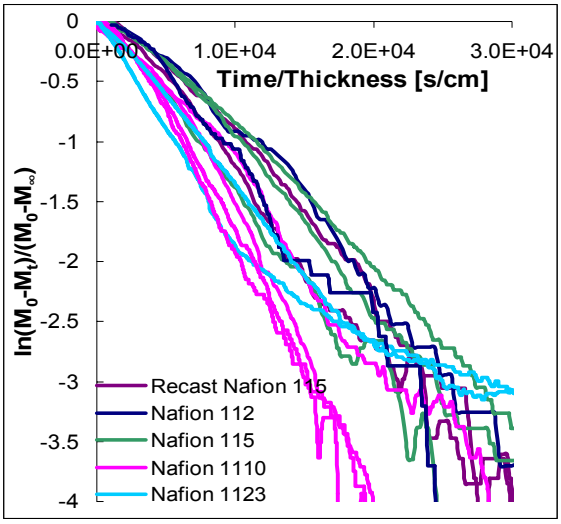

Figure 3.12: Desorption: $\ln[(M_0-M_t)/(M_0-M_\infty)]$ vs. t/ℓ Nafion 1100, 50°C

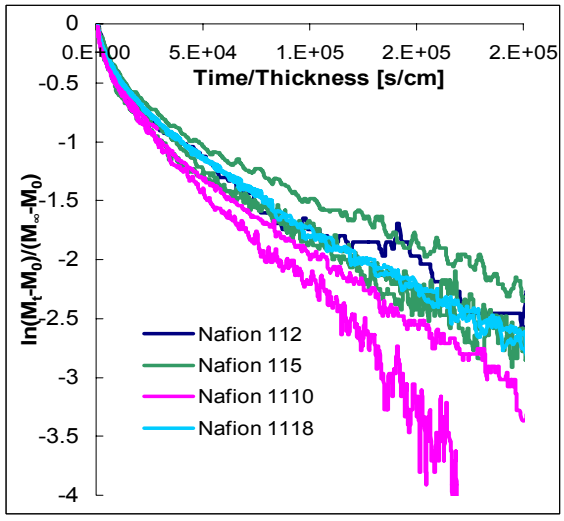

Figure 3.13: Sorption: $\ln[(M_0-M_t)/(M_0-M_\infty)]$ vs. t/ℓ Nafion 1100, 50°C

The slope of the log of normalized mass change as a function of time/thickness is the effective mass transport coefficient for water. The desorption curves in Figure 3.12 display a single slope through most of the process and collapse reasonably well, a functional form that can be explained by assuming that interfacial mass-transport mechanism is the rate-controlling mechanism.

Interfacial mass transport is accommodated in water absorption/desorption analysis by changing the boundary condition at the membrane/environment interface. The constant concentration boundary condition, equation (3.2), is replaced by a flux boundary condition, equation (3.11)

$$D\frac{dC}{dx} = k_{\text{int}}\left(C - C_{ext}\right), \quad t > 0, \quad x = 0, \ell \tag{3.11}$$

where k_{int} is the interfacial mass transport coefficient. The Biot number, $Bi = k_{\text{int}}\ell/2D$, represents the ratio of characteristic times of the (external) mass transfer to the (internal) diffusion. For $Bi<1$, the characteristic time of mass transfer, $2k_{int}/\ell$, is greater than that of diffusion, $4D/\ell^2$, and interfacial mass transfer is the controlling mechanism. The complete analytic solution for the diffusion equation with the flux boundary condition is presented in Majsztrik et al.[17].

For a completely interfacially-controlled process, ($Bi<<1$), the Fickian mass-transport equation (3.1) can be replaced by an equation for flux across the area A:

$$A\ell\frac{dC}{dt} = -Ak_{\text{int}}(C - C_{\infty}) \tag{3.12}$$

Since diffusion is much faster than interfacial mass transport the concentration inside the membrane C is nearly uniform across the membrane, and approaches the equilibrium concentration C_∞ at long times.

$$C = C_{\infty}, \quad t \to \infty \tag{3.13}$$

The mass-loss curve when interfacial mass transport is the dominant resistance ($Bi<<1$) is given by:

$$\frac{M_0 - M_t}{M_0 - M_{\infty}} = 1 - \exp\left[-\frac{k_{\text{int}}t}{\ell}\right] \tag{3.14}$$

The interfacial mass transfer coefficients k_{int} calculated from equation (3.12) for water desorption from Nafion are plotted as functions of temperature for different membrane thicknesses in Figure 3.14:

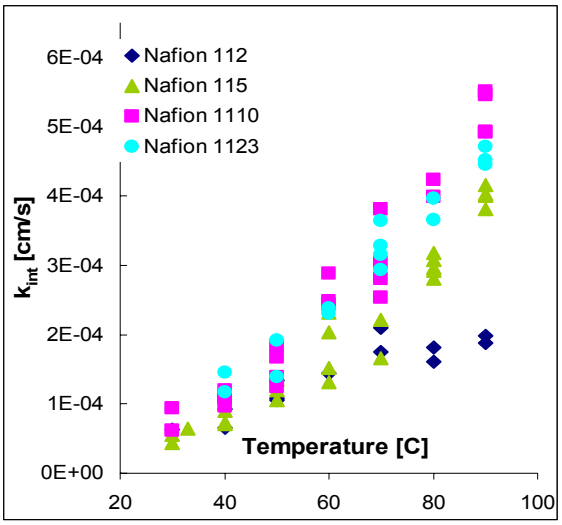

Figure 3.14: Interfacial Mass Transport Resistance, k_{int} of Nafion 1100 EW Membranes & Water, Determined from Desorption Tests.

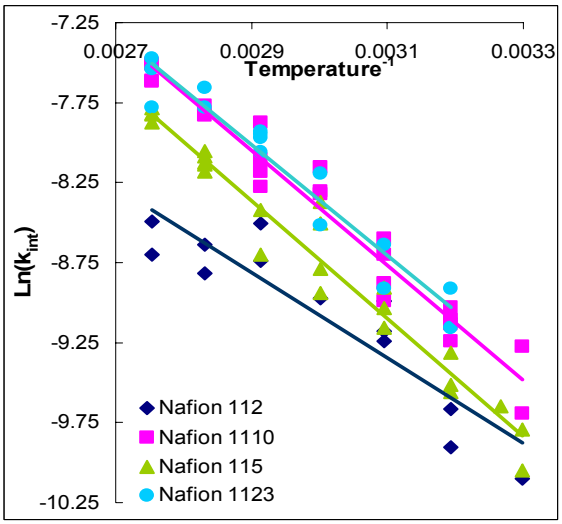

Figure 3.15: $Ln(k_{int})$ vs. Inverse Temperature: Arrhenius behavior.

The values of k_{int} increase with temperature from $0.5x10^{-4}$ at 30°C to $5x10^{-4}$cm/s at 90°C. The values found here are lower than those reported by Ge [8] based on permeation experiments. However, the mass transport coefficients determined based on Equation (3.14) neglect any diffusional resistance for water transport in the membrane, so the values are expected to be lower. The mass transfer coefficients follow an Arrhenius behavior, as shown in Figure 3.15, yielding pre-exponential factors and activation energies for different membranes:

Membrane Name, Thickness [μm]	$k_{int,0}$ [cm/s]	E_A [kJ/mol]
112, 50.8	0.35	22.2
115, 127	10.2	30.6
1110, 254	10.6	29.8
1123, 606	7.6	28.8

Table 3.1: Arrhenius parameters for k_{int} determined through water desorption

The kinetic parameters for the 127 μm, 254 μm and 606 μm films are all very similar. The thinnest membrane showed some deviations from the others, especially at higher temperatures. This may be the result of experimental uncertainty due to the smaller mass

and rapid decrease in water concentration in thinner membranes. The activation energy for interfacial mass transport ($E_{act,kint}$ ~30 kJ/mol) is larger than the activation energy for the diffusion coefficient determined by Takamatsu [12], Morris [10] and Yeo and Eisenberg [14], $E_{act,D}$ ~20 to 23 kJ/mol.

The difference in temperature dependencies of the two mass transfer mechanisms creates a situation in which diffusion becomes relatively more important at higher temperatures and with thicker membranes. Thus, the Biot number increases with both increasing membrane thickness and temperature, as described in Equations (3.15) and (3.16).

$$\frac{\partial Bi}{\partial T} \sim Bi \frac{\left(E_{A,k_{\text{int}}} - E_{A,D}\right)}{RT^2} > 0 \tag{3.15}$$

$$\frac{\partial Bi}{\partial \ell} \sim \frac{Bi}{\ell} > 0 \tag{3.16}$$

A similar conclusion was reached by Majsztrik et al. from permeation results [17].

The Biot number signals the relative importance of interfacial mass transport to diffusion. We have used the Arrhenius values for the interfacial mass transport coefficient in Table 3.1 and the form of temperature-dependent diffusion coefficient reported by Takamatsu [12]:

$$D = 8 \times 10^{-3} \exp\left(-20.5 kJ/RT\right) \tag{3.17}$$

(confirmed by Morris & Sun [10] and yielding D values consistent with Zawodzinski [16], Ge [8] and Rivin [11]), to determine the Biot number at different temperatures and with different membrane thicknesses. For thin membranes at low temperatures, Bi <<1 (0.06 for Nafion 112, ℓ=50 μm, at 30°), meaning that interfacial mass transport is the rate-limiting mechanism for water desorption. For the thickest membranes and highest temperatures

studied, Bi>1 (1.85 at 90°C for Nafion 1123, ℓ=600 μm), meaning that diffusion is comparable to interfacial mass transport. For higher temperatures and thicker membranes the functional form for desorption described in Majsztrik et al. [17] is appropriate, as it combines interfacial transport resistance and diffusion effects. However, for membranes ≤127 μm thick at temperatures relevant to fuel cell operation (≤90°C), the Biot number is small; interfacial mass transport is the rate controlling process for water desorption, and the concentration of water inside the membrane will be nearly uniform.

3.5.3 Sorption

In contrast to the constant slope of $\ln[(M_t-M_0)/(M_\infty-M_0)]$ vs. time/thickness displayed by desorption in Figure 3.12, the sorption curves in Figure 3.13 show a rapid early response with a slope similar to the desorption runs, but bend into a slower linear approach to equilibrium, which makes the absorption rate constant for water vapor ten times slower than the water desorption rate constant. If both absorption and desorption were limited by only diffusion or interfacial mass transport the two rates would be the same. Further, if absorption/desorption were an equilibrium limited process the rate constant for absorption would be greater than that for desorption. ($K_{equilibrium}=rate_{ads}/rate_{des}>1$ when absorption is thermodynamically favored.) We conclude that the rate of water absorption into Nafion films is not controlled entirely by transport (diffusion or interfacial transport) or by thermodynamics.

Because water absorption is accompanied by the swelling of the membrane, we posit that after an initial amount of water uptake, the rate of water sorption becomes controlled by polymer chain rearrangement and relaxation. We do not know the molecular details of the structural changes accompanying water absorption, but based on

the cluster model of Gierke [32] the hydrophilic domains expand while the "teflonic" continuum is stretched, creating stress which subsequently relaxes by viscous flow. The stress induced by water absorption increases with the amount of water absorbed. The swelling stress (or swelling pressure) and the subsequent stress relaxation has been measured as described by us previously [33]. We have recently extended those studies and measured the rates of tensile stress relaxation as functions of water activity, temperature and strain, reported in chapter 2 of this thesis.

The water entering during the early part of absorption does not impose enough stress to push the membrane beyond its elastic deformation region. Hence, during the early part of water sorption the membrane responds elastically, or instantaneously, to accommodate the entering water. During this portion we propose that the sorption rate, like desorption, is controlled by interfacial mass transport.

A simple and successful model of water vapor absorption by Nafion membranes can be constructed by combining equation (3.14), which describes a process controlled by interfacial mass transport, with equation (3.18), which describes a process controlled by relaxation:

$$\frac{M_t - M_0}{M_\infty - M_0} = 1 - \exp\left[-\beta t\right] \tag{3.18}$$

where β is the relaxation rate constant. A weighted sum of equations (3.14) and (3.18) provides a model which accounts for both mechanisms:

$$\frac{M_t - M_0}{M_\infty - M_0} = \varphi\left\{1 - \exp\left[-\frac{k_{\text{int}} t}{\ell}\right]\right\} + (1-\varphi)\left\{1 - \exp\left[-\beta t\right]\right\} \tag{3.19}$$

where φ controls the weighting of each mechanism. The parameter is frequently referred to as the 'quasi-equilibrium' point in similar models [20, 22-24], in that for water uptake less

than φ the first mechanism predominates and comes to equilibrium before the next mechanism takes over at uptakes larger than φ. When fitting equation (3.19) to experimental data, changing φ changes the value of mass uptake at which the curve shifts from one slope to another.

Long and Richman [25] developed a similar model to account for stress relaxation. They also introduced the concept of two-stage water uptake by designating a critical concentration below which there was no stress relaxation in the polymer and above which the stress relaxation was first order. The primary difference between this model and theirs is that diffusion remained relevant in their system. They retained the Fickian diffusion equation, and chose to incorporate polymer stress relaxation into the boundary condition at the polymer interface. They also did not account for interfacial mass transport resistance at the fluid polymer interface. Stress relaxation is not a surface phenomenon, so it is more appropriate to include it in the mass transfer equation.

The model for water uptake presented in equation (3.19) relies on three parameters, the interfacial mass transfer coefficient, $k_{int,}$ the relaxation rate β, and the weighting factor φ. We have fit equation (3.19) to the experimental data and found the model fits to be superior to any of the standard Fickian diffusion model fits. Using the interfacial mass-transport coefficients k_{int} calculated from the desorption data above and a weighting factor of $\varphi = 0.35$, the only remaining fitting parameter is β. Example fits of the 50°C sorption curves shown in Figure 3.4 appear in Figure 3.16 and fits of sorption curves at 80°C appear in Figure 3.17:

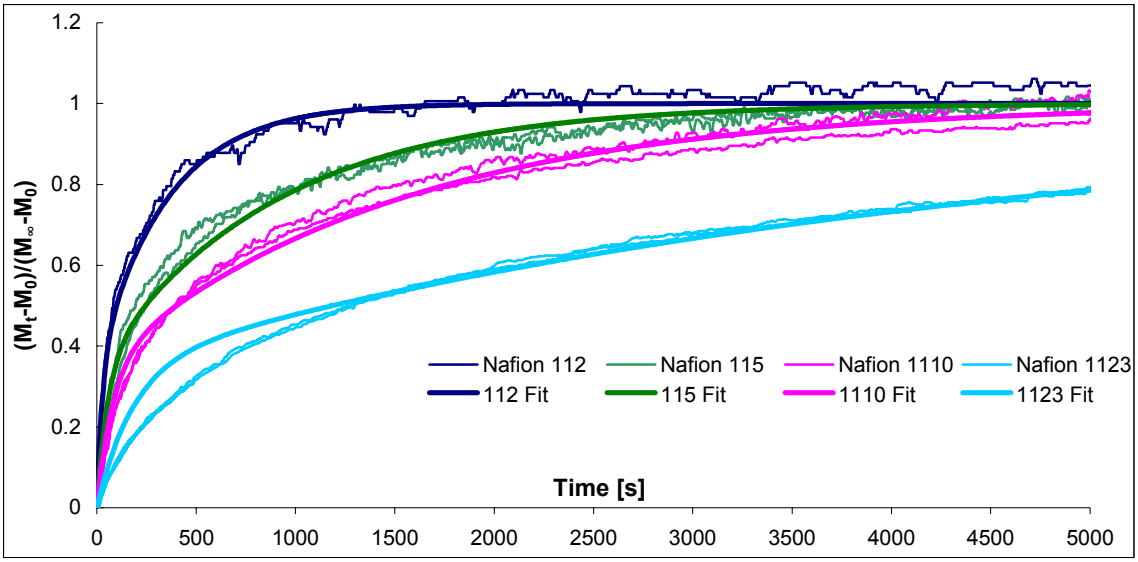

Figure 3.16: Modified two-stage sorption model fit to Nafion water vapor uptake curves at 50°C

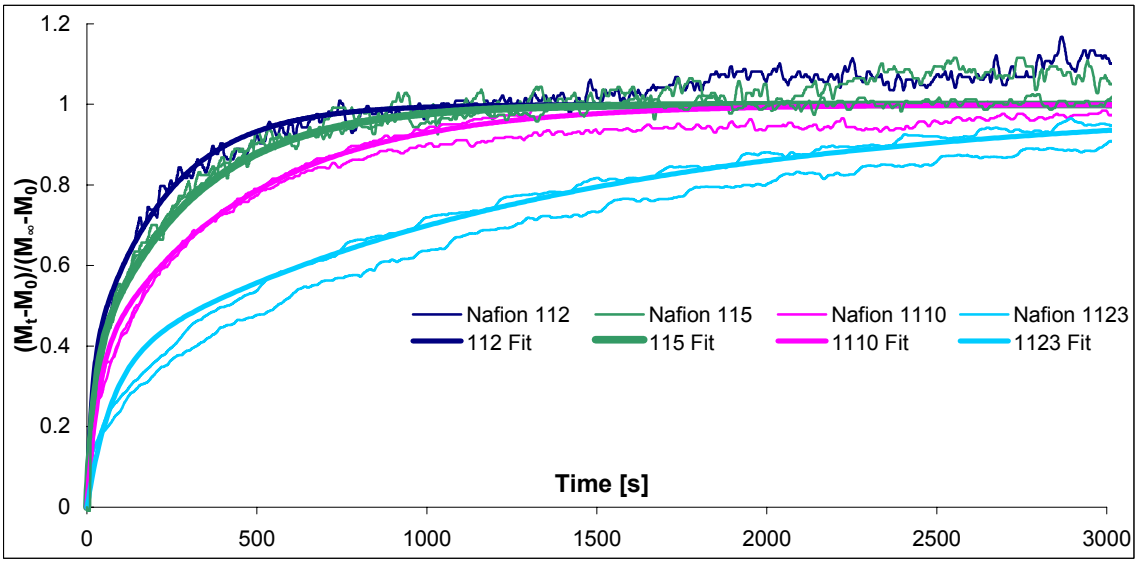

Figure 3.17: Modified two-stage sorption model fit to Nafion water vapor uptake curves at 80°C

The parameters and their physical significance will be discussed in more detail below.

3.5.3.1 Weighting factor or Quasi-Equilibrium Uptake: φ

The quasi-equilibrium uptake is frequently considered to be equivalent to an elastic response of the membrane while the second-stage rate is relaxation controlled. [20, 22-24] Newns [22] equated the osmotic stress to the change in volume at quasi-equilibrium

uptake multiplied by the bulk modulus. In this system the change in volume at quasi-equilibrium (taken as 0.35 of equilibrium uptake) is roughly 10%, which, assuming isotropic swelling, imposes a strain of 3% to 4% in each dimension. This strain is in the vicinity of the proportional limit measured from independent tensile tests: 2% to 3%, a good indication that after the quasi-equilibrium point the change in volume is no longer an elastic response.

3.5.3.2 Relaxation Rate: β

Approximate values of β needed to fit the data using equation (3.19) are shown in Figure 3.18. They fall between $5x10^{-3}$ s^{-1} and $2x10^{-4}$ s^{-1}, or between 200 and 5000 seconds, with longer relaxation times for lower temperatures and thicker membranes.

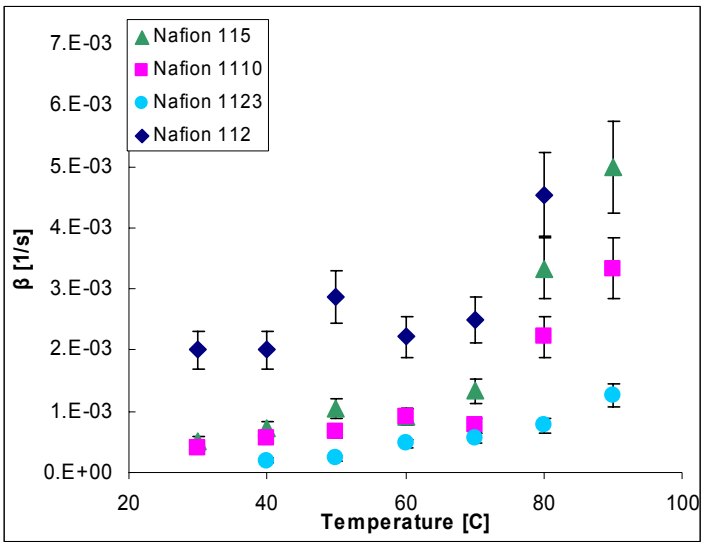

Figure 3.18: Values of relaxation kinetic term β, determined through simulation of water sorption curves, error bars are ±15%.

The increase of stress relaxation rates with temperature is an expected result for polymer systems. That the relaxation rates also increase for thinner membranes may be explained by unconstrained flow at the surface permitting more rapid relaxation, or by the idea that instead of being a truly bulk mechanism, relaxation acts as the water penetrates into the

membrane, exhibiting something like the Case-II sorption phenomena proposed in Majsztrik et al. [17].

Relaxation times for well-hydrated Nafion under uniaxial tensile strain have been independently measured at temperatures of interest here and have been reported in chapter 2. Because of Nafion's structure, it is subject to a range of relaxation frequencies, and the single frequency used in this model is a significant simplification. In general, uniaxial relaxation can be successfully fit with three relaxation times, which average ~3000 s, ~200 s and ~10 s. The shorter relaxation times are approximately the time during which the interfacial mass transport controlled portion of the membrane's water uptake occurs, possibly creating a situation in which the faster relaxation frequencies fade during the early sorption and long-term sorption is controlled by the slower frequencies. It is tempting to propose that sorption is entirely relaxation-controlled, but a simple bulk mechanism would not explain the thickness dependence observed here.

3.5.3.3 Interfacial Mass Transport k_{int}

We speculate that the surface of Nafion is phase separated to minimize the surface energy. When exposed to a vapor the low surface energy hydrophobic domains will segregate to the surface, and water must go through this hydrophobic skin to enter the polymer membrane. This model is consistent with previous observations that water sorption is faster from liquid water than water vapor [8, 11, 16, 20]. Liquid water will cause the hydrophillic domains to segregate to the surface reducing the interfacial transport resistance.

3.5.3.4 Deborah and Biot Numbers

The Deborah number, $De = 4D/\beta\ell^2$, compares the characteristic time for relaxation, $1/\beta$, to $4D/\ell^2$, the time for diffusion [19, 23, 25, 34]. The values of the Deborah number determined from fitting the experimental data to equation (3.19) and using diffusion coefficients found by Takamatsu [12] are between order 10 for thick membranes at higher temperatures and order 10^2 for thinner membranes and lower temperatures, meaning that diffusion is fast compared to relaxation across all temperatures and membrane thicknesses studied here.

In earlier models that have considered polymer stress-relaxation, the Deborah number was used to predict the behavior [25, 35]. For $De<<1$ or $\beta >> \ell^2/4D$ any changes in the polymer are fast compared to diffusion, and water uptake is diffusion-controlled. For $De>>1$ or $\beta << \ell^2/D$, the uptake is also diffusion controlled, but physically resembles a solvent diffusing in a medium that does not relax or flow during diffusion. For $\beta \sim \ell^2/D$, polymer relaxation is on a time scale relevant to diffusion and leads to classic two-stage sorption described by Long and Richman [25].

However, in the Nafion-water vapor system the Deborah number is >>1 and behavior is still not diffusion controlled. But because the Biot number is <1 diffusion is rapid compared to interfacial mass transport, so instead of relaxation and diffusion, relaxation and interfacial mass-transport are the two governing phenomena. The relationship between these two mechanisms can be represented as a third dimensionless parameter, the product of the Biot and Deborah numbers: $BiDe = 2k_{\text{int}}/\beta\ell$.

As discussed in relation to desorption, the Biot numbers for these experiments range from a value of <<1 to ~1 as temperature and membrane thickness increase.

Meanwhile the Deborah numbers range from ~10 to ~100 as temperature and membrane thickness decrease. As a result, water absorption is limited by polymer relaxation for Nafion membranes <500 μm thick below 90°C.

3.5.4 Comparison with traditional Two-stage Sorption

Two-stage sorption is generally characterized by a Deborah number ~1, such that diffusion and relaxation are both controlling mechanisms and typically describes a sigmoid shape in the sorption curve, or Fickian behavior up to the quasi-equilibrium concentration after which the sigmoid shape appears [19, 22-25, 31, 35]. Here, although two distinct slopes are visible in Figure 3.13, the plots in Figure 3.4 do not have a sigmoid shape and appear Fickian except for the thickness and sorption/desorption anomalies. Further, the Deborah number predicts Fickian diffusion. However, the relevant mechanisms here include mass-transfer resistance instead of diffusion. Adapting the interfacial mass transport equation to include stress relaxation can predict the mass-uptake behavior using physically realistic parameters.

This sort of behavior, in which individual mass uptake curves appear Fickian but yield different diffusivities for different thicknesses is termed 'pseudo-Fickian' [30]. This behavior has been reported for other polymer-solvent systems [34, 35] and attributed to viscoelastic effects within the polymer, with the observation that different thicknesses are often not tested due to time constraints and that a valid diffusion coefficient can only be determined by extrapolating the effect of thickness on D to an infinite thickness.

3.6 Conclusion

The water uptake by Nafion membranes follows a modified two-stage absorption pattern, in which the rapid first stage is not diffusion-controlled, but governed instead by interfacial mass-transport limitations, similar to Nafion water-desorption. The second, slower stage is then relaxation-controlled, with the relaxation rate dependent on the water content of the membrane. An abrupt transition between the two stages is not immediately apparent in $(M_t-M_0)/(M_\infty-M_0)$ vs. time plots. However, plots of $\ln(M_t-M_0)/(M_\infty-M_0)$ vs. time/ℓ reveal a rapid (high slope) early response, which bends into a slower (low slope) linear approach to equilibrium. Comparison with similar plots for desorption behavior reveal a much more nearly linear behavior, consistent with our surface-controlled model.

3.7 References

1. Yang, C.; Srinivasan, S.; Bocarsly, A. B.; Tulyani, S.; Benziger, J. B., A comparison of physical properties and fuel cell performance of Nafion and zirconium phosphate/Nafion composite membranes. *Journal of Membrane Science* **2004,** 237, (1-2), 145-161.
2. Gavach, C.; Pamboutzoglou, G.; Nedyalkov, M.; Pourcelly, G., AC Impedance investigation of the kinetics of ion-transport in Nafion perfluorosulfonic membranes. *Journal of Membrane Science* **1989,** 45, (1-2), 37-53.
3. Sone, Y.; Ekdunge, P.; Simonsson, D., Proton conductivity of Nafion 117 as measured by a four-electrode AC impedance method. *Journal of the Electrochemical Society* **1996,** 143, (4), 1254-1259.
4. Benziger, J.; Chia, E.; Karnas, E.; Moxley, J.; Teuscher, C.; Kevrekidis, I. G., The stirred tank reactor polymer electrolyte membrane fuel cell. *AIChE Journal* **2004,** 50, (8), 1889-1900.
5. Benziger, J.; Chia, E.; Moxley, J. F.; Kevrekidis, I. G., The dynamic response of PEM fuel cells to changes in load. *Chemical Engineering Science* **2005,** 60, (6), 1743-1759.
6. Burnett, D. J.; Garcia, A. R.; Thielmann, F., Measuring moisture sorption and diffusion kinetics on proton exchange membranes using a gravimetric vapor sorption apparatus. *Journal of Power Sources* **2006,** 160, (1), 426-430.
7. Gates, C. M.; Newman, J., Equilibrium and diffusion of methanol and water in a Nafion 117 membrane. *AIChE Journal* **2000,** 46, (10), 2076-2085.
8. Ge, S. H.; Li, X. G.; Yi, B. L.; Hsing, I. M., Absorption, desorption, and transport of water in polymer electrolyte membranes for fuel cells. *Journal of the Electrochemical Society* **2005,** 152, (6), A1149-A1157.
9. Krtil, P.; Trojanek, A.; Samec, Z., Kinetics of water sorption in Nafion thin films -- quartz crystal microbalance study. *Journal of Physical Chemistry B* **2001,** 105, 7979-7983.
10. Morris, D. R.; Sun, X., Water-sorption and transport properties of Nafion 117 H. *Journal of Applied Polymer Science* **1993,** 50, (8), 1445-1452.
11. Rivin, D.; Kendrick, C. E.; Gibson, P. W.; Schneider, N. S., Solubility and transport behavior of water and alcohols in Nafion$^{(TM)}$. *Polymer* **2001,** 42, (2), 623-635.
12. Takamatsu, T.; Hashiyama, M.; Eisenberg, A., Sorption phenomena in Nafion membranes. *Journal of Applied Polymer Science* **1979,** 24, (11), 2199-2220.
13. Tsonos, C.; Apekis, L.; Pissis, P., Water sorption and dielectric relaxation spectroscopy studies in hydrated Nafion (R) (-SO3K) membranes. *Journal of Materials Science* **2000,** 35, (23), 5957-5965.
14. Yeo, S. C.; Eisenberg, A., Physical-properties and supermolecular structure of perfluorinated ion-containing (Nafion) polymers. *Journal of Applied Polymer Science* **1977,** 21, (4), 875-898.
15. Zelsmann, H. R.; Pineri, M.; Thomas, M.; Escoubes, M., Water self-diffusion coefficient determination in an ion-exchange membrane by optical measurement. *Journal of Applied Polymer Science* **1990,** 41, (7-8), 1673-1684.
16. Zawodzinski, T. A.; Neeman, M.; Sillerud, L. O.; Gottesfeld, S., Determination of water diffusion-coefficients in perfluorosulfonate inomeric membranes. *Journal of Physical Chemistry* **1991,** 95, (15), 6040-6044.

17. Majsztrik, P. W.; Satterfield, M. B.; Bocarsly, A. B.; Benziger, J. B., Water sorption, desorption and transport in Nafion membranes. *Journal of Membrane Science* **2007,** 301, (1-2), 93-106.
18. Hartley, G. S.; Crank, J., Some fundamental definitions and concepts in diffusion processes. *Transactions of the Faraday Society* **1949,** 45, (9), 801-818.
19. Carbonell, R. G.; Sarti, G. C., Coupled deformation and mass-transport processes in solid polymers. *Industrial & Engineering Chemistry Research* **1990,** 29, (7), 1194-1204.
20. Zawodzinski, T. A.; Derouin, C.; Radzinski, S.; Sherman, R. J.; Smith, V. T.; Springer, T. E.; Gottesfeld, S., Water-uptake by and transport through Nafion$^{(R)}$ 117 membranes. *Journal of the Electrochemical Society* **1993,** 140, (4), 1041-1047.
21. Uan-Zo-li, J. T. Thesis: The effects of structure, humidity and aging on the mechanical properties of polymeric ionomers for fuel cell applications. Master of Science, Virginia Polytechnic Institute and State University, Blacksburg, Virginia, 2001.
22. Newns, A. C., The sorption and desorption kinetics of water in a regenerated cellulose. *Transactions of the Faraday Society* **1956,** 52, (11), 1533-1545.
23. Sanopoulou, M.; Roussis, P. P.; Petropoulos, J. H., A detailed study of the viscoelastic nature of vapor sorption and transport in a cellulosic polymer.1. Origin and physical implications of deviations from Fickian sorption kinetics. *Journal of Polymer Science Part B-Polymer Physics* **1995,** 33, (7), 993-1005.
24. Bagley, E.; Long, F. A., 2-Stage sorption and desorption of organic vapors in cellulose acetate. *Journal of the American Chemical Society* **1955,** 77, (8), 2172-2178.
25. Long, F. A.; Richman, D., Concentration gradients for diffusion of vapors in glassy polymers and their relation to time dependent diffusion phenomena. *Journal of the American Chemical Society* **1960,** 82, (3), 513-519.
26. Crank, J.; Park, G. S., Diffusion in high polymers - Some anomalies and their significance. *Transactions of the Faraday Society* **1951,** 47, (10), 1072-1084.
27. Crank, J.; Henry, M. E., Diffusion in media with variable properties.1. The effect of a variable diffusion coefficient on the rates of absorption and desorption. *Transactions of the Faraday Society* **1949,** 45, (7), 636-650.
28. Crank, J., A theoretical investigation of the influence of molecular relaxation and internal stress on diffusion in polymers. *Journal of Polymer Science* **1953,** 11, (2), 151-168.
29. Petropoulos, J. H.; Roussis, P. P., The influence of transverse differential swelling stresses on kinetics of sorption of penetrants by polymer membranes. *Journal of Membrane Science* **1978,** 3, (2-4), 343-356.
30. Frisch, H. L., Sorption and transport in glassy-polymers - Review. *Polymer Engineering and Science* **1980,** 20, (1), 2-13.
31. Long, F. A.; Bagley, E.; Wilkens, J., Anomalous diffusion of acetone into cellulose acetate. *Journal of Chemical Physics* **1953,** 21, (8), 1412-1413.
32. Gierke, T. D.; Munn, G. E.; Wilson, F. C., The morphology in Nafion perfluorinated membrane products, as determined by wide-angle and small-angle X-ray studies. *Journal of Polymer Science Part B-Polymer Physics* **1981,** 19, (11), 1687-1704.

33. Satterfield, M. B.; Majsztrik, P. W.; Ota, H.; Benziger, J. B.; Bocarsly, A. B., Mechanical properties of Nafion and titania/Nafion composite membranes for PEM fuel cells. *J. Polymer Science B: Polymer Physics* **2006,** 44, (16), 2327-2345.
34. Vogt, B. D.; Soles, C. L.; Lee, H. J.; Lin, E. K.; Wu, W. L., Moisture absorption and absorption kinetics in polyelectrolyte films: Influence of film thickness. *Langmuir* **2004,** 20, (4), 1453-1458.
35. Vrentas, J. S.; Jarzebski, C. M.; Duda, J. L., A Deborah number for diffusion in polymer-solvent systems. *AIChE Journal* **1975,** 21, (5), 894-901.

4 Membrane Swelling Behavior Under Constraint

4.1 Abstract

Measurements of pressure exerted by Nafion when absorbing water in a confined space under pressure have been undertaken in this work. The goal of these measurements was to help build the body of knowledge about stresses inside fuel cells. Fuel cell membranes frequently succumb to stress-induced failures as they swell and shrink in the confined space of a sealed fuel cell, while the porous carbon gas diffusion layer can be crushed by excess pressure and the gas-tight seal can be compromised by changing dimensions or stresses. Results indicate that the pressure exerted by swelling Nafion membranes increases with increasing applied pressure, temperature and membrane thickness and is on the order of other stresses in fuel cells. The pressures measured here are distinct from the well-known concept of osmotic or swelling pressure. The swelling pressure exists in the membrane as a balance between energy (pressure) of acid solvation and the constraining pressure exerted by the polymer, which can be estimated using measured values of elastic modulus.

4.2 Introduction

To assemble a fuel cell, the membrane electrode assembly (MEA), gasket and flow field plates are sandwiched together under pressure to ensure good electrical contact and to prevent the leakage of fuel and oxidant gases [1]. A drawing of the different layers of a cell appears in Figure 4.1.

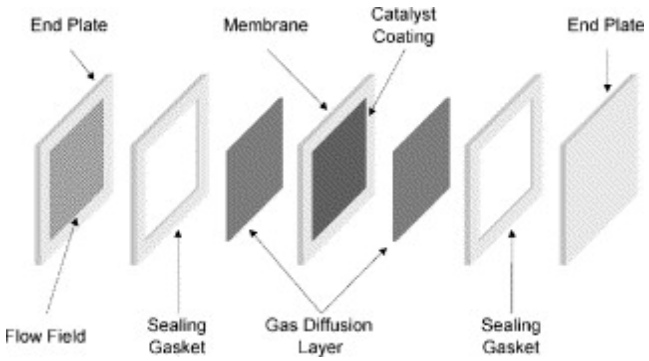

Figure 4.1: Components of a typical fuel cell: MEA, gaskets & flow field plates. Figure reprinted from [2] with permission from Elsevier © 2004.

The need to seal cells and the question of how much pressure to use is becoming more widely addressed in the literature [1, 3-12]. Compression increases electrical contact and decreases resistivity [1, 3-8]. However, too much force can collapse the gas diffusion layer and lead to unfavorable gas and water permeability [1, 6-12]. The presence of an optimum compressive sealing pressure was reported in our lab by Dr. Joanne Chia, as shown in Figure 4.2 [13], and similar results have been reported by others [5, 7, 8].

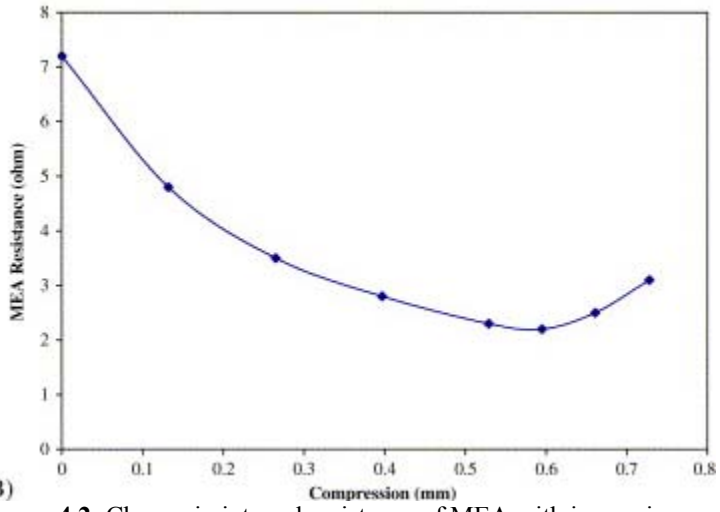

Figure 4.2: Change in internal resistance of MEA with increasing compression. Compression was increased by tightening the bolts sealing the cell a set number of turns past finger tight. Figure reprinted from [13] with permission from Elsevier © 2005.

For cells in this lab, the pressure is usually applied with bolts at each of the four corners of the cell, though elsewhere other mechanisms such as straps, springs or pistons are

sometimes used [1]. Springs or pneumatic pistons offer the benefit of constant pressure as the dimensions of the cell change due to thermal expansion [7] or membrane swelling.

In general, the sealing process does not place significant pressure on the membrane within the active operating area where the gas diffusion layer (GDL) is, but pins the edges of the membrane where they overlap with the gasketing material [1]. Inside the active area, the membrane's water content is subject to change with changing fuel cell conditions, and it shrinks and swells accordingly. This area is somewhat stabilized against in-plane dimensional changes by the carbon cloth GDL to which it is hot-pressed during MEA fabrication, though it can shrink or swell out-of-plane (perpendicular to the membrane surface) into the pores of the catalyst and GDL, as seen in Figure 4.3, or become delaminated from the GDL, as seen in Figure 4.4. Both of these phenomena affect the performance of the cell. They change the amount of contact between membrane and catalyst/GDL layer, and loss of contact increases resistance in the MEA [14, 15].

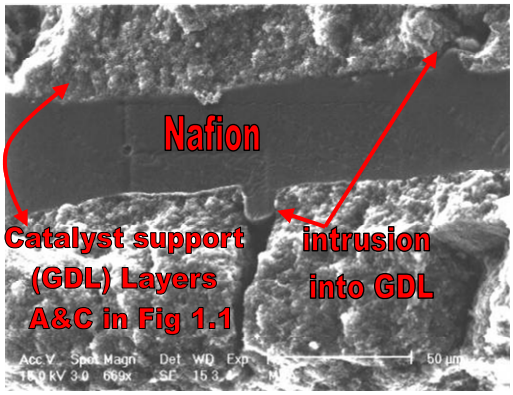

Figure 4.3: SEM image of cross-section of MEA after operation in a fuel cell, showing Nafion intrusion into pores of GDL. Courtesy of Dr. Jonathan Mann, labels added.

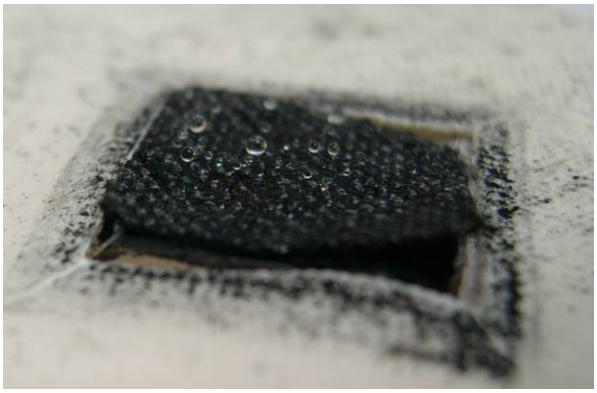

Figure 4.4: GDL delamination from Nafion membrane after operation in a fuel cell. Courtesy of Dr. Warren Hogarth

Even within the active area, in-plane tension due to membrane shrinking is reported to cause holes to form in the membrane, particularly at stress points such as the cracks in the carbon powder coating [16], which are visible in Figure 4.5.

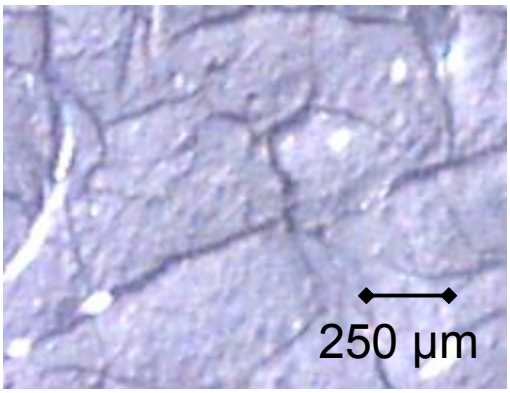

Figure 4.5: Surface of the gas diffusion layer (GDL) which contacts the membrane when assembled into an MEA. At this surface, the carbon cloth is coated with carbon-powder supported platinum catalyst. Magnification is 60x.

Stresses can also build up at the edge of the active area where the membrane is pinned by the gasket and no longer supported by the GDL [17, 18], producing holes such as those seen in Figure 4.6. Holes can allow gas cross-over and reduce the voltage sustained by the cell.

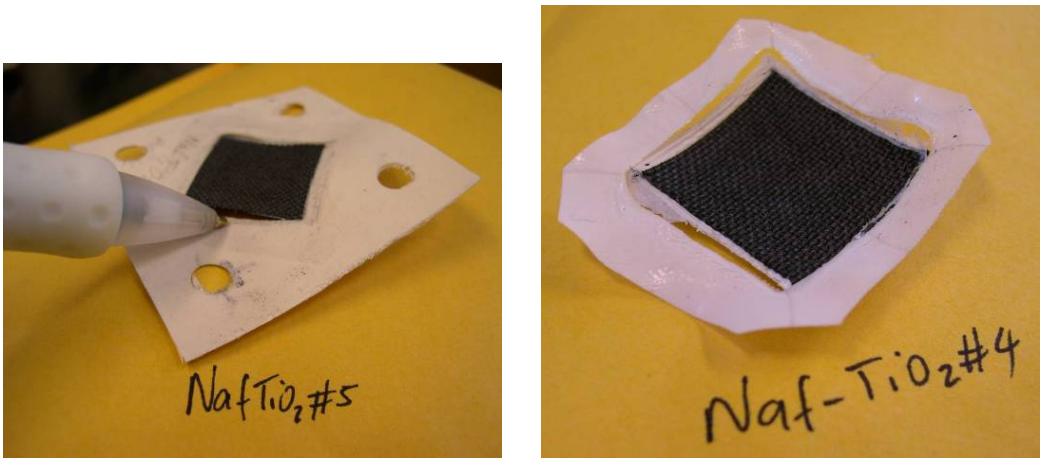

Figure 4.6: Membranes that have failed mechanically between the gasketed area (removed at right) and the GDL/active area. Courtesy of Dr. Warren Hogarth.

However, while it is known that membrane mechanical failure has been reported to be hastened by operational cycling, [17-21] only a limited amount of experimental work

has focused on this issue. Recent work using finite-element analysis models using tensile stress-strain mechanical properties measured by Tang et al. [22] have predicted out-of-plane stresses up to 8 MPa and in-plane stresses of ~ 10-20 MPa on membranes 25-50μm thick during a hydration and heating cycle similar to fuel cell start-up in cells tightened with bolts [18-21]. However, the latest of these models [21] acknowledges a limitation in failing to include time-dependent behavior such as creep and stress-relaxation. Experimental work has found in-plane stresses of 2.25 MPa upon moving from liquid water at 80°C to dry air 23°C [17], and two works have tracked in-plane strains during drying [16, 21]. There remains a need for experimental information regarding out-of-plane (perpendicular) stresses and dynamic, time-dependent behavior.

Knowledge of pressures inside a fuel cell and how the membrane behaves under constraint in an environment with changing water content will improve understanding of the stresses and strains it experiences in (and exerts *on*) an operating fuel cell. Work to extend the life of membranes, by reengineering the membrane material, changing the design of the cell or changing its operating parameters could benefit from enhanced knowledge of the forces the membrane experiences in and exerts on its environment.

4.3 Procedure

4.3.1 Pressure exerted by a swelling Nafion membrane

To test the swelling properties of Nafion under load in a confined space, a controlled-environment chamber was constructed in which the membrane was constrained by a screw drive between a load cell and a porous frit. A picture and drawing of the chamber appear in Figure 4.7. In addition the chamber was surrounded by an insulated wooden box to reduce temperature gradients.

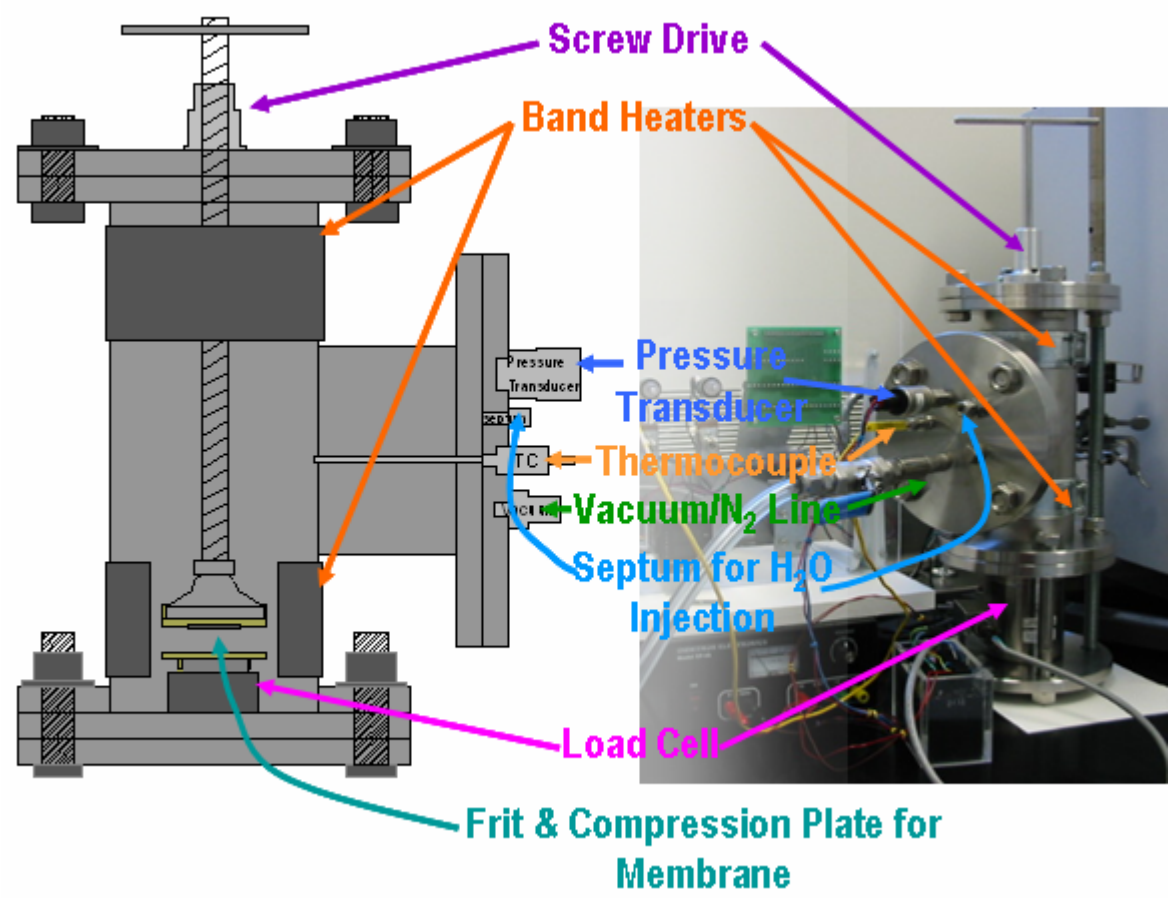

Figure 4.7: Controlled-environment chamber for compression & swelling experiment.

Pictures of the frit and compression plate that holds the membrane sample and sits on top of the load cell appear in Figure 4.8.

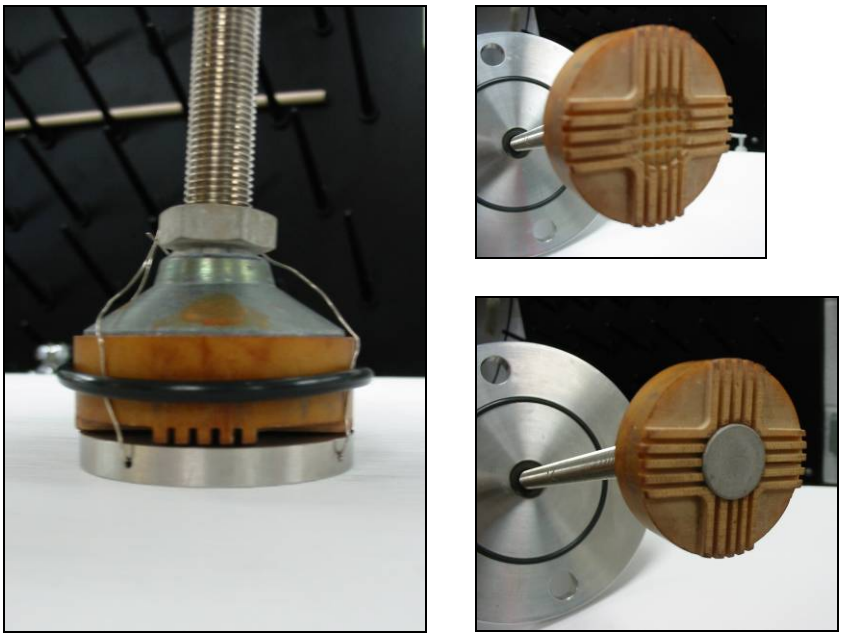

Figure 4.8: Compression plate: side view of plate assembled (left) and view (right) of top plate with & without fritted disk, showing channels for water vapor movement.

The bottom plate was flat, either stainless steel (as seen in picture) or garolite-10 (an extremely hard plastic) and rested on the load cell. The top plate was garolite-10, mounted on a stainless steel leveling swivel pad, which was attached to the screw drive, and held a stainless steel frit. The frit surface contacted the membrane, allowing water in the chamber to reach the top surface of the membrane. In addition, groves were machined out of the top plate. The mean pore size of the frit was 5.0 μm, with 39% open area, per manufacturer part specifications [23]. This approximately, though not exactly, matches the pore size of the gas diffusion and catalyst layers, whose pore sizes range from 0.01 μm to 100 μm [3, 24-26]. The membrane was not constrained in the lateral direction, except by friction, and measurements of sample diameter before and after the test typically did not show lateral expansion.

To prepare for a typical experiment, the membrane was cleaned following standard procedures (boiling 1 h in 3% H_2O_2, 20 min in dionized water, 1 h in 1 M H_2SO_4 and 20 min in DI water) and then stored at 100% humidity and room temperature until

testing. Prior to testing, the sample was die-punched using a circular punch 14.3 mm (9/16 inch) diameter and dried in an oven. Drying conditions were either 130°C or 70°C over drierite for 1-2 hours. During this time the chamber was pre-heated to 110°C and purged with dry air to drive off water. After drying, the sample was weighed and measured and then loaded into the frit & compression plate assembly and lowered into the chamber. The chamber was sealed, evacuated and filled with dry nitrogen. The chamber was then allowed to equilibrate to the testing temperature for several hours, as gradients in temperature and transients were found to affect readings. The signals from the load cell, pressure transducer, a relative humidity sensor (not pictured), and several thermocouples placed in and around the chamber were recorded during this time to verify equilibration and stable signals.

To start the test, the screw drive was turned, constraining the membrane against the load cell. A considerable amount of relaxation occurred afterward, and several hours elapsed until the force stopped changing. After the reading from the load cell appeared level, liquid water was injected through the septum into the chamber. The amount injected was the amount calculated to raise the humidity in the chamber to 100% at the chosen temperature for testing, and temperatures ranged between room temperature and 90°C. The signals from the load cell, pressure transducer, relative humidity sensor and thermocouples were recorded during the test using the computer program Lab Tech. Different membrane thicknesses were tested, either Nafion 115 (127 μm), 1110 (254 μm) or 4 stacked sheets of 115. Several non-ionomers were also tested, including Teflon, polystyrene butadiene blend and polyethylene. In addition, the test procedure was carried out with no polymer sample at all.

4.3.2 Pressure distribution in a fuel cell

The distribution of stresses across the cell was measured in a short experiment performed and analyzed in conjunction with Paul Majsztrik. One of our lab's fuel cells was assembled with a pressure-sensitive film between the membrane and the GDL. The four 10-32 bolts at the corners of the cell were tightened to ~2.94 N-m (the standard value used by our lab) by means of a torque wrench. No washers were used. The clamping force F in Newtons was calculated from the torque on the bolts using the following expression [1] $F = \frac{nT}{kd}$, where n is the number of bolts, T is the torque on the bolts in Nm, k is the bolt friction coefficient (0.2 for unlubricated, 0.17 for lubricated) and d is the diameter of the bolts in meters (#10 = 4.826×10^{-3} m).[1] The total force was ~12,200 N, or an average pressure of ~4 MPa across the cell [5.5 cm x 5.5 cm = 3.0×10^{-3} m^2], with an estimated error of ± 15-30% [27].

4.4 Results

A photograph of the pressure-sensitive film upon removal appears in Figure 4.9, with a photo of the interior of a similar cell. The pressure felt by the portion of the membrane in the active area in contact with the posts was between 25 and 37% of the film's pressure range, or between 0.6 and 0.89 MPa, with no pressure in the flow channels.

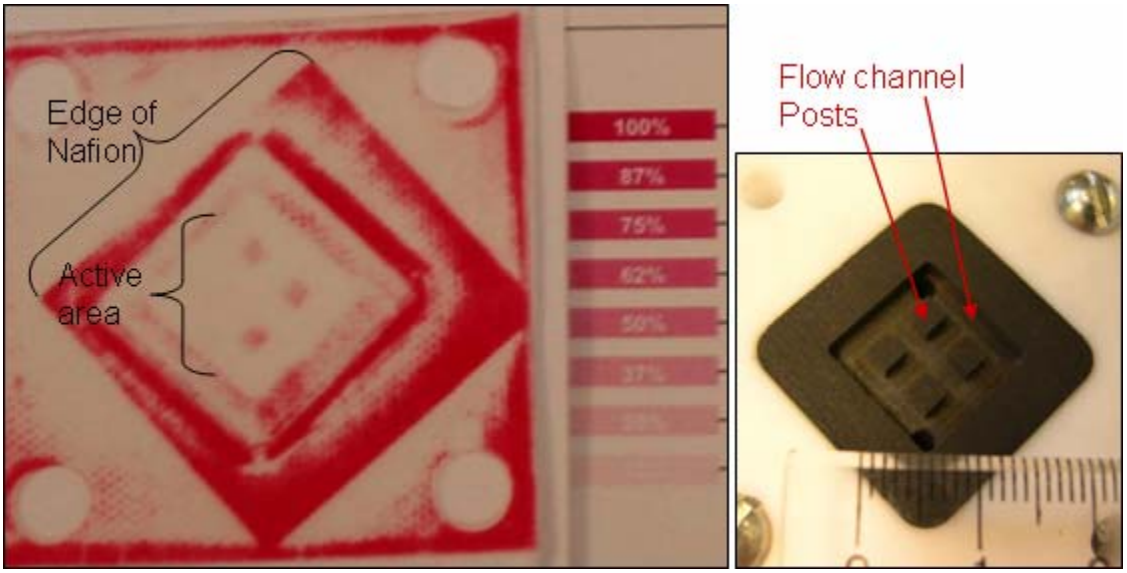

Figure 4.9: Left: Pressure-sensitive film after removal from cell with pressure scale comparison. Right: interior of similar cell, showing gas flow channels & posts, courtesy of Dr. Warren Hogarth, with text and arrows added.

However, the pressure applied to the membrane in the gasketed area (around the perimeter of the electrode area) maxed out the film's indicating range of 2.4 MPa. The Nafion extends into the gasket region only far enough to help ensure a gas-tight seal, but where the two overlap is where the most pressure is exerted.

Figure 4.10 and Figure 4.11 show the results of two swelling runs. The pressure (force read by the load cell divided by the measured area of the sample), the vapor pressure inside the chamber and temperatures inside and outside the chamber are recorded with time. The injection of water into the chamber appears as an abrupt increase in vapor pressure, followed by an increase in the pressure read by the load cell.

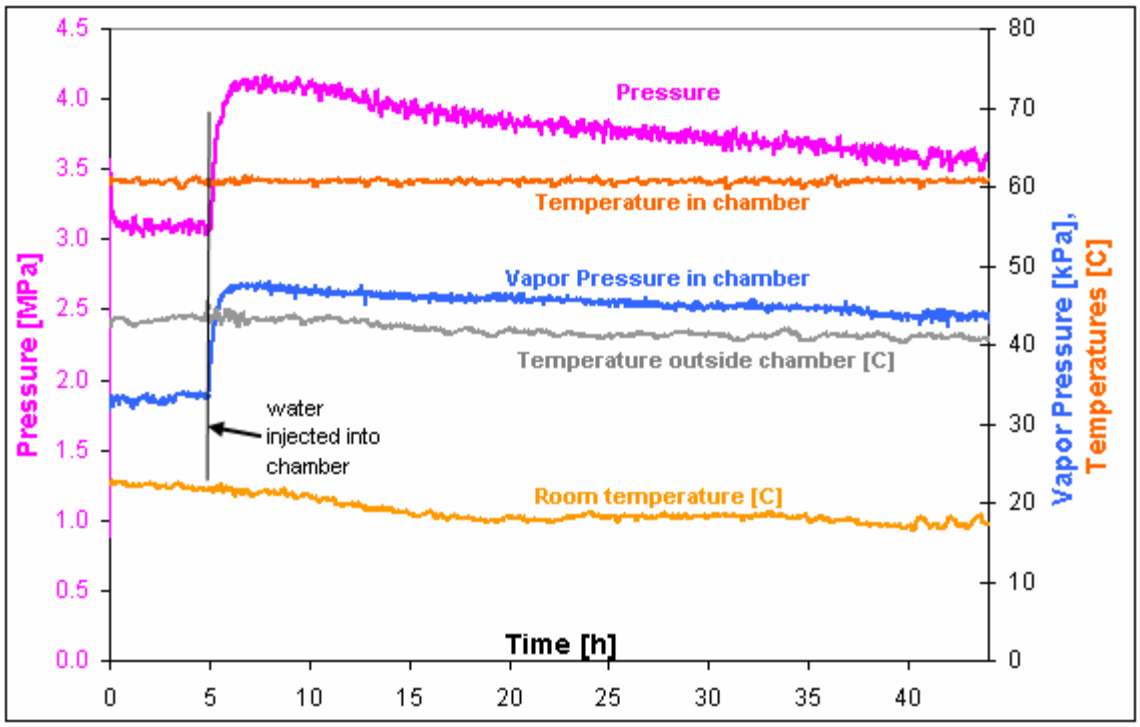

Figure 4.10: Pressure exerted by Nafion 1110 in response to step increase in humidity from 0% to 100% at time =5 h. Test temperature = 60°C.

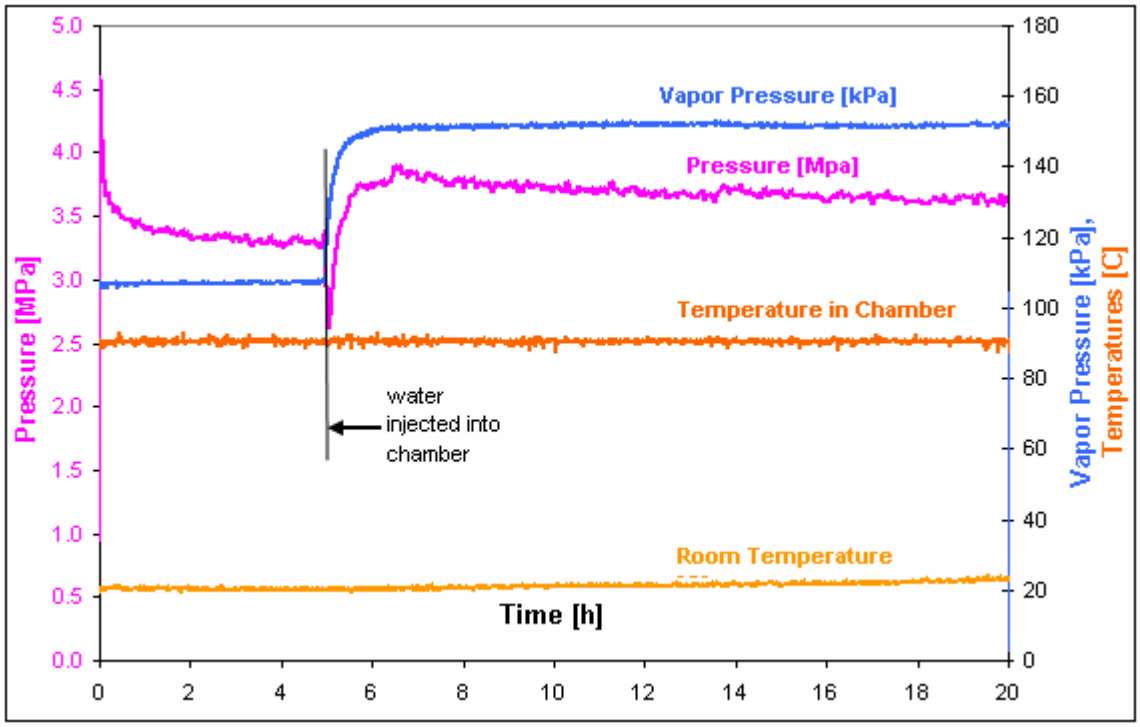

Figure 4.11: Pressure exerted by Nafion 115 in response to step increase in humidity from 0% to 100% at time = 5 h. Test temperature = 90°C.

The increase in pressure on the load cell is distinct to Nafion. Non-hydrophilic polymers were tested and did not exhibit any swelling response. Figure 4.12 shows an identical experiment performed on a similarly-sized sheet of Teflon.

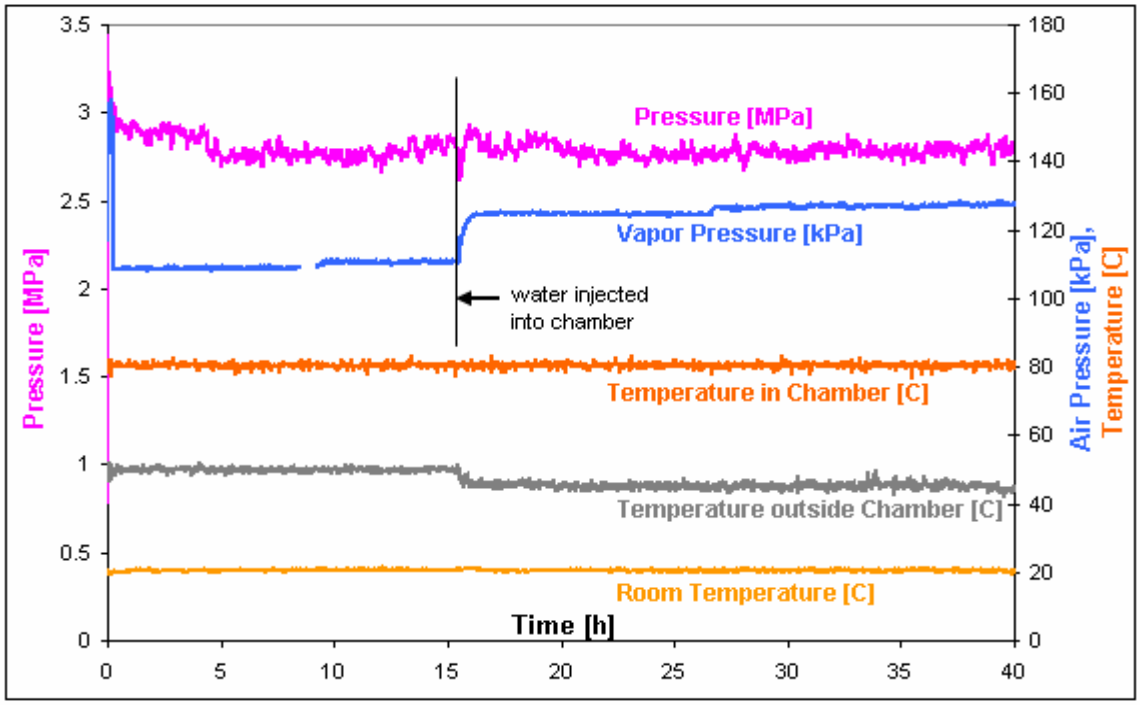

Figure 4.12: Pressure exerted by Teflon (127 µm thick) in response to step increase in humidity from 0% to 100% at time = 15 h. Test temperature = 80°C.

4.5 Discussion

Four aspects of these graphs yield potentially valuable information pertaining to Nafion and fuel cells: (1) the rate of relaxation after initially constraining the membrane, (2) the swelling response time, (3) the rate of relaxation after swelling and (4) the value of the pressure response. It should be mentioned that there were some significant difficulties with this experiment: temperature and vapor pressure variations within the chamber as well as temperature variations in the surrounding lab were found to affect the reading of the load cell, sometimes causing long time responses that proved difficult to control. Nevertheless, general conclusions can be drawn from the results.

4.5.1 Initial Relaxation

The first stress-relaxation rate yields time constants on the order of 100's to 1000's of seconds, which are similar to the longer time constants observed with tensile stress relaxation reported in chapter 2. The total amount of relaxation seen during tests was variable and increased with pressure applied but averaged about 30%. It is likely that this was the result of membrane relaxation, but there was also some relaxation within the screw drive assembly and load cell. Blank runs (without a polymer) have shown relaxation time constants of ~1000, ~10 and ~1 seconds and relaxation amounts of ~5% at room temperature and 10-15% at 80°C, meaning that relaxation in the screw drive was a significant effect, particularly at higher temperatures.

4.5.2 Swelling Response Time

The amount of time from water injection to the maximum in pressure response in this data ranges from about 2000 to 12,000 seconds, with an average of about 5000 seconds. This is roughly the same amount of time observed for unconstrained water sorption from vapor in chapter 3 and, as discussed in chapter 3, does not scale with the thickness of the membrane *squared*, but more closely with the membrane thickness. However, though this data is significantly less accurate, the swelling response time here actually becomes slightly slower with increasing temperature, the opposite of what was observed in unconstrained sorption experiments.

4.5.3 Post-swelling Relaxation Rates

The rate of relaxation after swelling has a time-constant on the order of 10^5 to 10^6 seconds. This rate of relaxation is significantly slower than that observed during tensile stress-relaxation and has been observed to persist for 40 hours, at which point temperature and signal drift began affecting data. The relaxation rate could simply be an

artifact of signal drift, or it may be associated with membrane creep, as the membrane slowly moves further into the pores of the frit, expands laterally or rearranges internally. Membrane creep during fuel cell operation is suspected of playing a significant part in cell failure [17].

4.5.4 Magnitude of Pressure Response

The values of the pressure responses of individual runs, normalized for a membrane thickness of 127 μm are pictured in Figure 4.13, which shows two viewing angles of the same 3-dimensional plot.

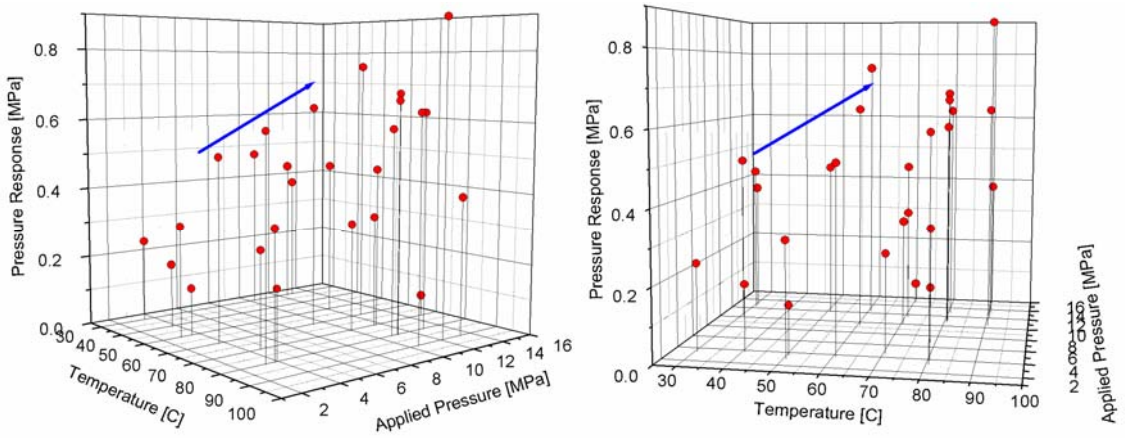

Figure 4.13: Dependence of water sorption pressure response on applied pressure (left) and temperature (right).

The pressure response exhibits an increasing trend with both applied pressure and temperature. Also, while the pressure response increases with applied pressure, it also appears to scale to some degree with membrane thickness, as seen in Figure 4.14. At an applied pressure of roughly 10 MPa, the pressure response increases with thickness (left) and can be brought into closer agreement by normalizing the response to a thickness of 127μm (right). The same is the case at ~3 MPa of applied pressure.

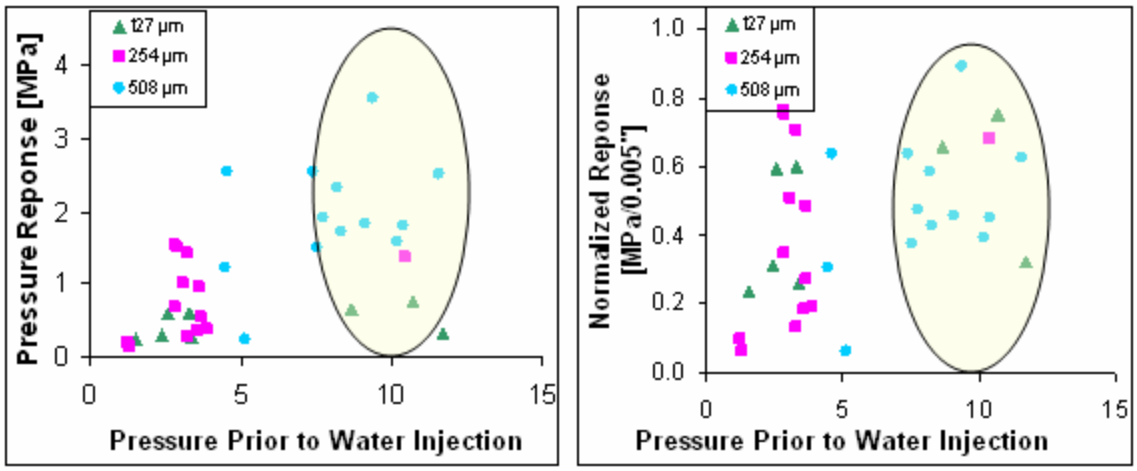

Figure 4.14: Dependence of water sorption pressure response on applied pressure for different membrane thicknesses. All temperatures are included.

This phenomenon is also apparent when the pressure responses are plotted against temperature, seen in Figure 4.17 (left) and then normalized for a single sheet of Nafion 115 (right).

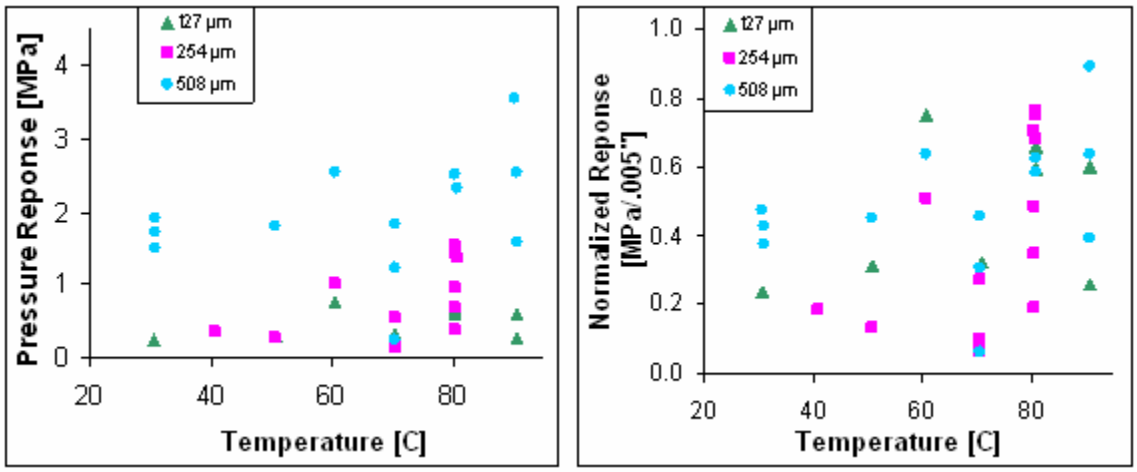

Figure 4.15: Dependence of water sorption pressure response on temperature for different membrane thickness. All applied pressures are included.

The physical significance of the pressure response of the membrane is not completely clear. The swelling pressure is the pressure that must be applied to a solution (in this case the membrane) to keep it from taking in more solvent. Here, the membrane

does take on more solvent--there was a measurable increase in weight--and this measurement is the pressure exerted while that is happening.

The measurement is also subject to dynamic behavior such as membrane creep and stress-relaxation. It is a transient measurement, and so not a measurement of swelling (or osmotic) pressure, which is an equilibrium property. An integral form of the pressure response might be a more accurate representation of swelling pressure, but this measurement provides information that is in many ways more relevant to fuel cells.

However, a further complication of this measurement is the use of a porous frit to constrain a deformable membrane. While a porous surface was necessary to allow access to the water, it complicates interpretations of pressure exerted by the swelling membrane, as the membrane can easily swell into the pores without detection by the load cell. An example of this is seen in Figure 4.17, which shows the surface of the frit (left) and then how the Nafion has deformed into it (left) during a typical test. (A membrane that has not been compressed does not show any of the ridges pictured here.)

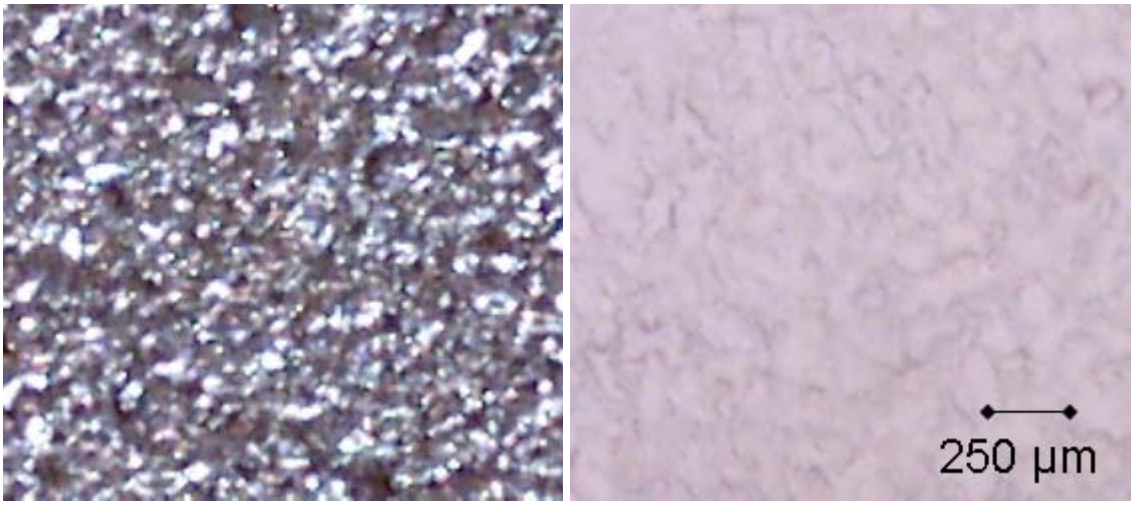

Figure 4.16: Pictures of frit surface (left) and surface of Nafion (right) after removal from a typical test. Magnification is 60x.

If the pores of the frit are idealized as hemispherical openings of radius 5μm, then the volume of a single pore is $\frac{2}{3}\pi r^3$, or ~260 μm^3. The volume of membrane underneath the pore is that of a cylinder with thickness ℓ: $\pi r^2 \ell$, or ~1000 μm^3 for the thinnest membrane tested (127 μm). Further, because the membrane material can move laterally as well as vertically, the total amount of volume available to intrude into the pore could include the surrounding membrane as well, which can be modeled as a concentric cylinder, radius r_2 surrounding the pore. This frit has an open area fraction of 0.39 and a pore radius of 5μm, corresponding to an outer radius r_2 of 8 μm, or a volume of ~25,500 μm^3.

The amount of intrusion into the pores depends on the volumetric strain, which is dependent on the pressure applied and the modulus. For an isotropic material the bulk modulus can be estimated from the elastic modulus, *E,* using equation (4.1) [28]

$$E = 3B(1-2\nu) \tag{4.1}$$

where ν is Poisson's ratio, the ratio of contraction in the membrane's width to extension in its length at it is stretched. Poisson's ratio has been measured to be about 0.40 in Nafion [21]. Because the membrane begins the test in a dry state, the Young's modulus can be modeled with a simple linear dependence on temperature: E = 504.5 - 4.6·T (°C), derived from the low-water content data presented in chapter 2.

These calculations indicate that at low applied pressures (~3MPa), the volumetric strain ranges from 0.4% at room temperature to 2% at 90°C (increasing with temperature as the modulus decreases). Assuming the entire volume of 25,500 μm^3 is available to extrude into the pore, this corresponds to a volume of ~100 to 500 μm^3 of membrane extruding into the pore. For higher applied pressures (~10 MPa) the strain increases from

1.5% at room temperature to 7% at 90°C, or a volume of 390 to 1700 μm^3 extruding into the pore. These volumes are doubled or quadrupled for the higher thickness of membrane.

However, the pores are only ~260 μm^3 in volume, meaning that at higher pressures, temperatures and sample thicknesses, they could easily be filled before water is injected into the chamber. This explains why the pressure response increases with applied pressure, temperature and membrane thickness: at lower values of each of these the pores may not be completely filled, and the membrane can swell by filling the pores. But, when the pores are already filled by the membrane, it must push against its constraints to swell. If a frit with higher porosity were used, the pressure could be expected to be lower.

Of course, this is an idealization of the pore conditions. They are inter-connected and not as limited in volume as described here. A membrane undoubtedly has more volume to swell into (and later creep into, causing the post-swelling relaxation rates described above) than a simple half-sphere. However, it is unlikely that the membrane will move through the more tortuous paths in the frit, so it is reasonably valid to assume that only the outermost layer of pores is readily available to the membrane.

The pressure registered by the load cell is the result of the work of expansion exerted by the swelling membrane. The load cell measures pressure from the deformation of its diaphragm, or the expansion of the membrane from swelling. Thus, while ideally the membrane is totally constrained by the apparatus, volume expansion is necessary for the load cell to measure pressure.

From a simple thermodynamic heat/work balance, the change in thickness of the membrane can be found by equating the work done by the membrane upon swelling, $P_{resp} A_{mem} \Delta \ell_{mem}$, to the enthalpy of water absorption, $\Delta H_{sorp}[\mathrm{MJ/m^3}] A_{mem} \ell_{mem}$, yielding the expression

$$P_{resp} \Delta \ell = -\Delta H_{sorp} \ell \tag{4.2}$$

where ΔH_{sorp} is the enthalpy of water sorption per volume of membrane, $\Delta \ell$ is the change in membrane thickness upon swelling, and A_{mem} is the area of the membrane. Equation (4.2) may contribute to the explanation of the dependence of pressure response on temperature; the enthalpy of solvation increases with increasing temperature. Though the solvation of the sulfonic acid groups is an exothermic process and should shift equilibrium uptake towards less water content at higher temperatures, the polymer stretching to accommodate water is an endothermic process. Following the model described in[29], as well as experimental observations[30-32], equilibrium shifts towards higher water uptake at higher temperatures; the enthalpy of sorption becomes larger (more negative), contributing to the higher pressure response by the swelling membrane. Water uptake could not be measured accurately enough to independently confirm a higher water uptake at higher temperatures.

The magnitude of the pressure response (~0.5 MPa for a membrane of thickness 127 μm) is important information for fuel cell manufacturers, particularly that the force response of the membrane increases with increasing applied pressure and temperature and with reduced porosity of its surroundings. To the author's knowledge, none of these features (pressure, surroundings or temperature dependence) have yet been accounted for in existing models or cell designs.

Knowledge of the possible expansion forces exerted by the membrane should inform the choice of gasketing material and bolts or other compression devices used to keep the fuel cell sealed. The amount of pressure exerted on the membranes in these compression tests was in the region of that measured with the pressure-sensitive film in the gasketed area of the fuel cell (>2.4 MPa), and while Nafion in the gasketed area probably does not change water content as abruptly as in the active area, water diffusion into the non-active area of the membrane will occur.

In the active area the membrane swelling forces may affect the GDL. That the membrane pressure response is dependent on the porosity of the surface to which it is exposed is important information for those working to optimize the design of membrane-electrode assemblies and construction of the GDL. Since degradative GDL compression has been noted to result from cell clamping, it may also be important to study the effect of the membrane swelling forces on the GDL during typical cell operational cycling.

4.6 Swelling Pressure Calculations

The pressure response reported here is distinct from the swelling pressure of the membrane, Π, which is defined [33-36] in equation (4.3).

$$\Pi = p_{app} - p_{solv} = \frac{RT}{V_w} \ln \frac{a_{w,external}}{a_{w,sol't}} \tag{4.3}$$

This equation describes the difference between the applied (p_{app}) and solvation (p_{solve}) pressures of a system when at equilibrium, and the pressure response experiments did not measure an equilibrium, but, rather pressure exerted upon approach to equilibrium.

Escoubes et al. [37] reported measurements of the swelling pressure of Nafion 1200 (equivalent weight: 1200 g Nafion/mol SO_3^-) using a system that constrained the membrane with a piston between a porous plate and a piece of metal foil. Upon exposure

to liquid water, the pressure was determined from the deformation of the foil to be 30 MPa. These results agree reasonably well with those from Pushpa et al.[35] who determined a swelling pressure for Nafion 117 at 25°C by comparing Nafion's water sorption isotherm to a reference polymer with weaker crosslinking (after [36] and [38]) and reported a value of 19.6 MPa.

With a few approximations, it is possible to work in the other direction of Pushpa and draw a sorption isotherm from some simple thermodynamic calculations and knowledge of mechanical properties. Equation (4.3) predicts how much pressure must be exerted on a system which wants to take up water (here the sulfonic acid groups) in order to maintain equilibrium, or stop the sulfonic acid groups from absorbing water. The necessary pressure depends on the temperature, T, gas constant R, molar volume of water V_w and activities of water in the membrane ($a_{w,sol't}$) and in its environment ($a_{w,external}$). In the system of interest here $a_{w,external}$ is simply the relative humidity of the surroundings, while $a_{w,sol't}$ can be estimated from the activity of water in a sulfuric acid solution, for which vapor pressure depression data is available in the literature [39, 40].

To find the activity of water in solution from the vapor pressure depression, the chemical potential of water in liquid solution is equated with that of the water in the vapor above it ($\mu^{g}_{w,sol't} = \mu^{\ell}_{w,sol't}$), giving an expression for the activity of water in the sulfuric acid solution as a function of the partial pressure of water over it [41]:

$$\mu^{g}_{w,pure} + RT\ln\left(\frac{p_{w,sol't}}{p_{tot}}\right) = \mu^{\ell}_{w,pure} + RT\ln\left(a_{w,sol't}\right) \tag{4.4}$$

or, equivalently:

$$a_{w,sol't} = \frac{p_{w,sol't}}{p_{tot}} \times \exp\left[\frac{\mu^{g}_{w,pure} - \mu^{\ell}_{w,pure}}{RT}\right] \qquad (4.5)$$

($p_{w,sol't}$, $\mu^{g}_{w,pure}$ and $\mu^{\ell}_{w,pure}$ are available or calculable from reference tables [39, 40, 42], and 1 atmosphere is assumed for p_{tot}.) Using the range of data available, the solvation pressure (p_{solv}) exerted by sulfuric acid at different temperatures, solution concentrations and humidities ($a_{w,external}$) can be estimated using equations, (4.4), (4.5) and (4.3), assuming no constraining pressure, p_{app}. Figure 4.17 shows the solvation pressure for different temperatures and concentrations at 100% relative humidity. The solution concentration is expressed in terms of membrane water content or λ.

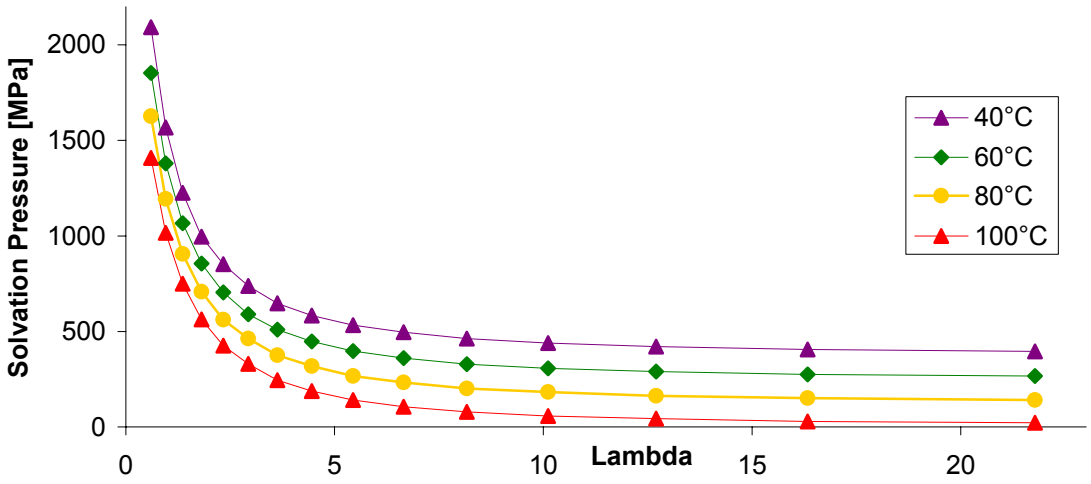

Figure 4.17: Solvation pressure of water solvating Nafion in a 100% humidity environment, as a function of temperature and amount of water already in the Nafion.

Clearly, for low temperatures and very dry membranes the solvation pressure is enormous: over 2000 MPa, evidence of the hydrophilic nature of Nafion.

In the Nafion system, the applied pressure (p_{app}) that balances the solvation pressure is the elastic force of the polymer, which is expressed in terms of the bulk modulus, B, the change in pressure per unit change in volume at constant temperature [41]:

$$B = -V\left(\frac{\partial P}{\partial V}\right)_T \tag{4.6}$$

As discussed above, the bulk modulus can be calculated from the tensile modulus using equation (4.1), yielding the bulk modulus and solvation pressure balance in terms of tensile modulus:

$$\frac{E}{3(1-2\nu)} = \frac{RT}{V_w}\ln\frac{a_{w,external}}{a_{w,sol't}} \tag{4.7}$$

This determines the membrane water activity $a_{w,sol't}$ at which the system will be at equilibrium at a given temperature and humidity, and the membrane water content λ can be correlated to the literature data for solution concentrations that yield that activity. For simplicity the Young's modulus is again modeled with a simple linear dependence on temperature: (E = 504.5 - 4.6·T). Using 0.40 for the Poisson's ratio yields a rough sorption isotherm, seen in Figure 4.18.

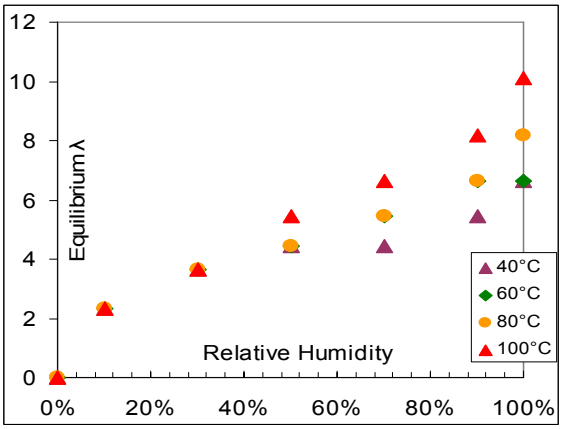

Figure 4.18: Water sorption isotherm found through balance of swelling and elastic forces in Nafion.

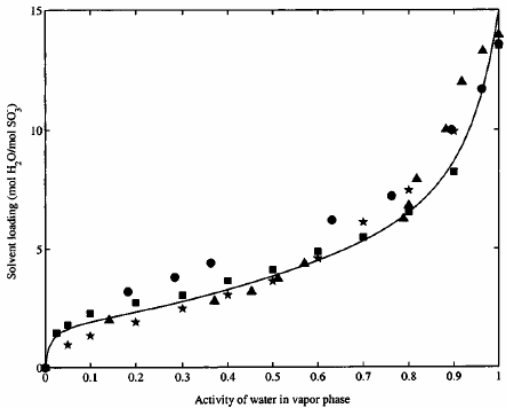

Figure 4.19: Sorption isotherm experiment & model predictions at room temperature.[33] Experimental data from: triangles[43], squares[44], stars[45], circles[35] Figure reprinted from [33] reprinted pending permission from The Electrochemical Society © 2003.

While this is not as exact as similar modeling approaches [32, 33, 46] (shown in Figure 4.19) that employ more complicated thermodynamic considerations for sorption and elastic

stretching, this simple estimation gives a reasonable agreement using fits of elastic moduli measured and reported in chapter 2. The equilibrium values of water-uptake predicted here are somewhat low compared to experimentally-observed values. This is probably due to the effect of water content on elastic modulus (particularly for the lower temperatures) and relaxation in the polymer as it absorbs water, the phenomenon discussed in chapter 3.

4.7 Conclusion

The pressure exerted by a dry 127 μm-thick Nafion membrane absorbing water from a 100% RH environment has been measured as a function of applied constraining pressure and temperature. The pressure applied was on the order of pressures that could be experienced by the membrane in the gasketed region of the cell. The pressure response was found to increase with applied pressure and temperature, while the time for response (~5000 s) agreed roughly with that found for water absorption in an unconstrained environment. The post-swelling relaxation times (order 10^5 to 10^6 s) provide potentially important information about membrane creep rates in constrained environments. Finally, the swelling pressure in the membrane can be estimated with a simple thermodynamic model and measured values of elastic modulus.

4.8 Acknowledgements

Thanks to Dr. James Nehlsen for lots of help and advice in building the instrument used here, and to Prof. George Scherer for some excellent advice in interpreting the effect that pores in the frit produced on my results (page 139).

4.9 References

1. Barbir, F., 6.6 Stack Clamping. In *PEM Fuel Cells: Theory & Practice*, Elsevier Academic Press: Boston, 2005; pp 196-203.
2. Banerjee, S.; Curtin, D. E., Nafion® perfluorinated membranes in fuel cells. *Journal of Fluorine Chemistry* **2004,** 125, (8), 1211-1216.
3. Mathias, M.; Roth, J.; Fleming, J.; Lehnert, W., Diffusion media materials and characterisation. In *Handbook of Fuel Cells - Fundamentals, Technology and Applications*, Vielstich, W.; Gasteiger, H. A.; Lamm, A., Eds. John Wiley & Sons, Ltd: 2003; Vol. Volume 3: Fuel Cell Technology & Applications, pp 1-21.
4. Barbir, F., 4.5.2 Main cell components, materials properties and processes, bipolar plate, properties. In *PEM Fuel Cells: Theory & Practice*, Elsevier Academic Press: Boston, 2005; pp 102-110.
5. Ge, J. B.; Higier, A.; Liu, H. T., Effect of gas diffusion layer compression on PEM fuel cell performance. *Journal of Power Sources* **2006,** 159, (2), 922-927.
6. Lee, S. J.; Hsu, C. D.; Huang, C. H., Analyses of the fuel cell stack assembly pressure. *Journal of Power Sources* **2005,** 145, (2), 353-361.
7. Hentall, P. L.; Lakeman, J. B.; Mepsted, G. O.; Adcock, P. L.; Moore, J. M., New materials for polymer electrolyte membrane fuel cell current collectors. *Journal of Power Sources* **1999,** 80, (1-2), 235-241.
8. Lee, W.-k.; Ho, C.-H.; Zee, J. W. V.; Murthy, M., The effects of compression and gas diffusion layers on the performance of a PEM fuel cell. *Journal of Power Sources* **1999,** 84, 45-51.
9. Ihonen, J.; Mikkola, M.; Lindbergh, G., Flooding of gas diffusion backing in PEFCs - Physical and electrochemical characterization. *Journal of The Electrochemical Society* **2004,** 151, (8), A1152-A1161.
10. Bazylak, A.; Sinton, D.; Liu, Z. S.; Djilali, N., Effect of compression on liquid water transport and microstructure of PEMFC gas diffusion layers. *Journal of Power Sources* **2007,** 163, (2), 784-792.
11. Gostick, J. T.; Fowler, M. W.; Pritzker, M. D.; Ioannidis, M. A.; Behra, L. M., In-plane and through-plane gas permeability of carbon fiber electrode backing layers. *Journal of Power Sources* **2006,** 162, (1), 228-238.
12. Lim, C.; Wang, C. Y., Development of high-power electrodes for a liquid-feed direct methanol fuel cell. *Journal of Power Sources* **2003,** 113, (1), 145-150.
13. Benziger, J.; Chia, E.; Moxley, J. F.; Kevrekidis, I. G., The dynamic response of PEM fuel cells to changes in load. *Chemical Engineering Science* **2005,** 60, (6), 1743-1759.
14. Foulkes, F. R.; Graydon, W. F., Transport in membrane fuel cells. *Electrochimica Acta* **1971,** 16, 1577-1591.
15. Scherer, G. G., Interfacial aspects in the development of polymer electrolyte fuel cells. *Solid State Ionics* **1997,** 94, (1-4), 249-257.
16. Hector, L. G.; Lai, Y. H.; Tong, W.; Lukitsch, M. J., Strain accumulation in polymer electrolyte membrane and membrane electrode assembly materials during a single hydration/dehydration cycle. *Journal of Fuel Cell Science and Technology* **2007,** 4, (1), 19-28.
17. Budinski, M.; Gittleman, C. S.; Lai, Y. H.; Litteer, B.; Miller, D., Characterization of perfluorosulfonic acid membranes for PEM fuel cell mechanical durability. In *AIChE*

Annual Meeting, Austin, TX, 2004; p Presentation slides used at 2004 AIChE Annual Meeting.
18. Huang, X. Y.; Solasi, R.; Zou, Y.; Feshler, M.; Reifsnider, K.; Condit, D.; Burlatsky, S.; Madden, T., Mechanical endurance of polymer electrolyte membrane and PEM fuel cell durability. *Journal of Polymer Science Part B-Polymer Physics* **2006,** 44, (16), 2346-2357.
19. Kusoglu, A.; Karlsson, A. M.; Santare, M. H.; Cleghorn, S.; Johnson, W. B., Mechanical response of fuel cell membranes subjected to a hygro-thermal cycle. *Journal of Power Sources* **2006,** 161, (2), 987-996.
20. Tang, Y. L.; Santare, M. H.; Karlsson, A. M.; Cleghorn, S.; Johnson, W. B., Stresses in proton exchange membranes due to hygro-thermal loading. *Journal of Fuel Cell Science and Technology* **2006,** 3, (2), 119-124.
21. Solasi, R.; Zou, Y.; Huang, X.; Reifsnider, K.; Condit, D., On mechanical behavior and in-plane modeling of constrained PEM fuel cell membranes subjected to hydration and temperature cycles. *Journal of Power Sources* **2007,** 167, (2), 366-377.
22. Tang, Y. L.; Karlsson, A. M.; Santare, M. H.; Gilbert, M.; Cleghorn, S.; Johnson, W. B., An experimental investigation of humidity and temperature effects on the mechanical properties of perfluorosulfonic acid membrane. *Materials Science and Engineering a-Structural Materials Properties Microstructure and Processing* **2006,** 425, (1-2), 297-304.
23. Small Parts Inc, Catalog 22. http://www.engineeringfindings.com/cat22/cat22pg136.pdf
24. Thoben, B.; Siebke, A., Influence of different gas diffusion layers on the water management of the PEFC cathode. *Journal of New Materials for Electrochemical Systems* **2004,** 7, 13-20.
25. Xie, J.; More, K. L.; Zawodzinski, T. A.; Smith, W. H., Porosimetry of MEAs made by "thin film decal" method and its effect on performance of PEFCs. *Journal of The Electrochemical Society* **2004,** 151, (11), A1841-A1846.
26. Jordan, L. R.; Shukla, A. K.; Behrsing, T.; Avery, N. R.; Muddle, B. C.; M., F., Effect of diffusion-layer morphology on the performance of polymer electrolyte fuel cells operating at atmospheric pressure. *Journal of Applied Electrochemistry* **2000,** 30, 641-646.
27. Majsztrik, P., Comment about error in estimation of force applied through torque on bolts. In email communication ed.; Satterfield, M. B., Ed. 2007.
28. Ward, I. M.; Sweeney, J., 2.3 The generalized Hooke's Law. In *An Introduction to the Mechanical Properties of Solid Polymers*, 2nd ed.; John Wiley & Sons, Ltd: Chichester, England, 2004; pp 24-25.
29. Satterfield, M. B.; Majsztrik, P. W.; Ota, H.; Benziger, J. B.; Bocarsly, A. B., Mechanical properties of Nafion and titania/Nafion composite membranes for PEM fuel cells. *J. Polymer Science B: Polymer Physics* **2006,** 44, (16), 2327-2345.
30. Jalani, N. H.; Choi, P.; Datta, R., TEOM: A novel technique for investigating sorption in proton-exchange membranes. *Journal of Membrane Science* **2005,** 254, (1-2), 31-38.
31. Gebel, G.; Aldebert, P.; Pineri, M., Swelling study of perfluorosulphonated ionomer membranes. *Polymer* **1993,** 34, (2), 333-339.

32. Choi, P.; Jalani, N. H.; Thampan, T. M.; Datta, R., Consideration of thermodynamic, transport, and mechanical properties in the design of polymer electrolyte membranes for higher temperature fuel cell operation. *Journal of Polymer Science Part B-Polymer Physics* **2006,** 44, (16), 2183-2200.
33. Choi, P. H.; Datta, R., Sorption in proton-exchange membranes - An explanation of Schroeder's paradox. *Journal of the Electrochemical Society* **2003,** 150, (12), E601-E607.
34. Rosen, B., Some mechanical aspects of swelling and shrinking of polymeric solids.1. external and internal restraints. *Journal of Polymer Science* **1962,** 58, (166), 821-&.
35. Pushpa, K. K.; Nandan, D.; Iyer, R. M., Thermodynamics of water sorption by perfluorosulfonate (Nafion-117) and polystyrene-divinylbenzene sulfonate (Dowex 50w) ion-exchange resins at 298 +/- 1-K. *Journal of the Chemical Society-Faraday Transactions I* **1988,** 84, 2047-2056.
36. Helfferich, F., Swelling pressure and solvent activity. In *Ion Exchange*, McGraw-Hill Book Company, Inc: New York, 1962; pp 109-112.
37. Escoubes, M.; Pineri, M.; Robens, E., Application of coupled thermal-analysis techniques to thermodynamic studies of water interactions with a compressible ionic polymer matrix. *Thermochimica Acta* **1984,** 82, (1), 149-160.
38. Nandan, D.; Gupta, A. R., Solvent sorption isotherms, swelling pressures and free energies of swelling of polystyrenesulfonic acid type cation exchangers in water and methanol. *The Journal of Physical Chemistry* **1977,** 81, (12), 1174-1179.
39. Liley, P. E., Vapor Pressures of Solutions Table 3-13 Vapor Pressures, Normal Boiling Points, and Latent Heats of Vaporization for Aqueous Solutions of H_2SO_4. In *Perry's Handbook for Chemical Engineers*, 5th ed.; Perry, R.; Chilton, C. H., Eds. McGraw-Hill: New York, 1973.
40. Liley, P. E.; Thomson, G. H.; Friend, D. G.; Daubert, T. E.; Buck, E., Physical and Chemical Data, Table 2-12: Water Partial Pressure, bar, over Aqueous Sulfuric Acid Solutions. In *Perry's Chemical Engineer's Handbook*, Perry, R. H.; Green, D. W.; Maloney, J. O., Eds. McGraw-Hill: New York, 1997; pp 2--78.
41. Denbigh, K., *The Principles of Chemical Equilibrium*. 4th ed.; Cambridge University Press: Cambridge, United Kingdom, 1997; p 494.
42. Moran, M. J.; Shapiro, H. N., Table A-2 Properties of Saturated Water (Liquid-Vapor): Temperature Table. In *Fundamentals of Engineering Thermodynamics*, 2000; pp 804-805.
43. Zawodzinski, T. A.; Springer, T. E.; Davey, J.; Jestel, R.; Lopez, C.; Valerio, J.; Gottesfeld, S., A comparative-study of water-uptake by and transport through ionomeric fuel-cell membranes. *Journal of the Electrochemical Society* **1993,** 140, (7), 1981-1985.
44. Morris, D. R.; Sun, X., Water-sorption and transport properties of Nafion 117 H. *Journal of Applied Polymer Science* **1993,** 50, (8), 1445-1452.
45. Rivin, D.; Kendrick, C. E.; Gibson, P. W.; Schneider, N. S., Solubility and transport behavior of water and alcohols in Nafion$^{(TM)}$. *Polymer* **2001,** 42, (2), 623-635.
46. Choi, P.; Jalani, N. H.; Datta, R., Thermodynamics and proton transport in Nafion - I. Membrane swelling, sorption, and ion-exchange equilibrium. *Journal of the Electrochemical Society* **2005,** 152, (3), E84-E89.

5 Mechanical Properties, Water Sorption Dynamics & Confined Swelling Behavior of Nafion/TiO_2 Composite Membranes

5.1 Abstract

Composite fuel cell membranes of Nafion and inorganic particles have shown enhanced performance and lifetime in fuel cells operating at elevated temperatures and reduced humidity. These more extreme operating conditions are desirable for design considerations but cause mechanical failure or loss of proton conductivity in unmodified Nafion. However, the changes that occur in Nafion with the addition of inorganic particles to create these more successful membranes are not well understood, and expected properties of interest such as ion exchange capacity, proton conductivity and water uptake do not always correlate with behavior inside the cell. It is suspected that the addition of inorganic composite materials to Nafion changes its microstructure, and previous work has suggested that mechanical properties and rigidity of the membranes contribute to their success in fuel cells. This work begins to test that hypothesis, comparing properties of recast Nafion/TiO_2 composite membranes to unmodified Nafion. Membrane mechanical properties are measured through stress-strain tests and stress-relaxation, and water-sorption pressure response and water sorption/desorption kinetics are also measured. Results of stress-strain tests indicate that, compared to unmodified Nafion, Nafion/TiO_2 composite membranes have a slightly higher Young's modulus and toughness as well as a lower ultimate stress and higher ultimate strain, creating a lower plastic modulus after yielding. The higher Young's modulus also appears in stress-relaxation tests: at low strains the composite membranes require a greater shift factor to form a master curve with unmodified Nafion, though at higher strains the difference is

less pronounced. Stress-relaxation rates appear unchanged. Sorption and desorption rates of composite membranes are also unchanged, and swelling pressure is slightly higher.

5.2 Introduction

The ability to operate fuel cells at temperatures of 130°C to 145°C has been a goal for many fuel cell developers. At these temperatures the cell's platinum catalyst is less susceptible to poisoning by feed-stream carbon monoxide, which is a byproduct of steam-reforming hydrocarbons to create hydrogen. Elevated operating temperatures also increase cell reaction kinetics and membrane conductivity and, on a larger design scale, would facilitate heat management and create higher quality waste heat that could be utilized more easily. However, the lifetime of the Nafion membrane within the cell is shortened at higher temperatures because it becomes softer and can develop tears or holes [1-3]. Also, at atmospheric pressure, temperatures above 100°C drive off water, drying out the membrane and reducing its conductivity and the cell performance. Options such as pressurizing the cell and humidifying the gas feed streams contribute to the complexity of the system, making it more expensive, bulkier and more difficult to maintain. Thus, a design goal for new fuel cell membrane materials is durability and humidity-insensitive performance at higher temperatures.

The addition of inorganic particles to Nafion is a promising step towards this goal. Their enhanced performance is sometimes [4-7], but often not visible under "ideal" operating conditions of 80°C and fully humidified streams [4-6] but becomes particularly visible at low relative humidities [4-6, 8-11] and elevated temperatures [5, 6, 8-10] Their improved performance has been largely attributed to increased water retention [1, 4, 6, 9-14]

and management [12], ion exchange capacity [14], mechanical durability and robustness [1, 6, 10, 13, 14], proton conductivity [5, 13-15] and resistance to fuel cross-over [4, 13-15], particularly in direct-methanol fuel cell (DMFC) applications [15-17]. However, data derived from tests outside of the fuel cell that would support these suggestions is scattered and inconclusive, and systematic comparisons are made difficult by the myriad material and loading combinations as well as different procedures for membrane fabrication and testing [13].

5.2.1 Methods of Membrane Fabrication

Membranes are usually made by either sol-gel processing [1, 5, 12, 18, 19] or by recasting in solution [1, 3, 6, 9, 10, 16, 17]. In sol-gel processes an existing Nafion membrane is swollen in a solvent to allow infiltration of either solutions of precursors of the desired additive or the additive itself. The precursors are then reacted to form the desired product, either by the addition of another reactant, or by reaction with the sulfonic acid groups in the membrane [20]. In recasting procedures, a solution of Nafion in a solvent such as isopropyl alcohol, dimethyl sulfoxide or ethanol is mixed with particles of the desired filler. The solvent is then evaporated away and the resulting membrane is annealed and cleaned.

Membranes with homogeneous phase distributions and successful fuel cell characteristics have been reported for both procedures [1, 19, 21], though Thampan et al. [13] reported much more homogeneous membranes with smaller ZrO_2 particles when forming membranes with sol-gel processing than with recasting. Alberti and Casciola [20] also point out that achieving a uniform distribution of unagglomerated nanoparticles is difficult with the recasting procedure, even after enhanced mixing with sonication. These

observations make sense: the sol-gel procedure forms the particles inside the membrane while recasting essentially forms the membrane around the particles.

5.2.2 Water Uptake

It has been proposed [12, 18] that the addition of metal oxides such as SiO_2 or TiO_2 to the fuel cell membrane would enhance water uptake and retention because of the hygroscopic nature of metal oxides, and reported investigation of membrane water uptake generally indicates that Nafion recast with metal oxide particles enhances equilibrium water uptake at full hydration. However, it is not clear that these membranes exhibit an enhanced retention of water in conditions mimicking an under-humidified fuel cell.

Saccà et al. [10] measured percent water uptake of Nafion recast with 3 wt % TiO_2 particles (5-20 nm). The water uptake of the composite membrane between drying 2h at 80°C in a vacuum oven and immersion for 24h immersion in liquid water at room temperature was 29% by weight, compared to 27% for extruded Nafion. Similarly, Shao et al. [3] measured % water uptake of Nafion recast with 10 wt % TiO_2, SiO_2, WO_3 or SiO_2/phosphotungstic acid (PWA) between drying 24h in a vacuum oven at 70°C and boiling in water for 24 h. They found that water uptake increased in the order listed, with TiO_2 absorbing 34% by weight, compared to 26% by extruded Nafion and 37% by the WO_3 composite.

Yang et al. [5] found that water vapor uptake at 80°C increased with the addition of 25 wt % zirconium phosphate to Nafion via sol-gel processing, particularly at humidities > 30%, going from a λ-value of 11 [mol H_2O/SO_3^-] for Nafion at 100% RH to λ =19, a result consistent with that found by Bauer and Willert-Porada [14]. Yang et al. also reported that water uptake from liquid water at room temperature was the same for

Nafion and the composite, and that the flux of water across the membrane was inhibited by the addition of the composite, decreasing the flux to just over half that of Nafion at a comparable thickness.

Jalani et al. [22] measured water uptake of Nafion/ZrO_2, SiO_2 and TiO_2 (created via sol-gel synthesis) at 90°C and at 120°C [19] using a tapered element oscillating microbalance (TEOM) to produce water-sorption isotherms for each membrane. They found composites had a higher % weight water uptake, particularly at higher humidities, but with similarly-shaped isotherms for all membranes, which they interpreted as indicating that the water-sorption mechanism was unchanged by the addition of composite materials. Sorption was as follows: 33-35% increase over unmodified Nafion for the ZrO_2 composite, 20-25% for TiO_2, and 0-120% for SiO_2 at 90°C and 120°C respectively. Similar measurements at 120°C of Nafion/ZrO_2 prepared via sol-gel processing (3-4 wt %) or 5 wt % prepared via recasting showed both methods for making composites enhanced the water uptake, but the composite formed with a sol-gel method showed the greatest [13] and exhibited much more uniform distribution within the membrane.

Uchida et al. [18] found that introducing 2 wt % TiO_2 particles into Nafion 112 via sol-gel processing *doubled* equilibrium water uptake between drying 3h at 80°C in a vacuum oven and humidified air (95% RH) 2 h at 60°C, a result the authors claimed was also consistent with Nafion/TiO_2 membranes created via recasting. This result, however, is much more of an improvement than usually reported for water sorption enhancement.

However, to test the widely-made assertion that composite membranes retain and manage water better under drying conditions, Damay and Klein [11] performed water

sorption/desorption kinetic tests at room temperature and humidities between 10% and 70% on 10-15 wt % Nafion/$7SiO_2$-$2P_2O_5$-ZrO_2 (SPZ gel), Nafion/ SiO_2+H_3PO_4 (iHPO gel), Nafion/SiO_2+$H_3PW_{12}O_{40}$ (iHPW gel) and Nafion/ZrP (zirconium phosphate) composites prepared via the sol gel method. They found little difference in sorption and desorption kinetics between their composites and bare Nafion and concluded that Nafion's water retention capabilities, and not those of the inorganic fillers' governed the composite properties.

Work in this lab [7] on Nafion recast with 3 wt % TiO_2 (21 nm particles from Degussa-Huls) found that water uptake between drying 3h at 80°C in a vacuum oven and immersion for either 24h in room temperature water or 1 h in boiling water was slightly lower for the composite than for extruded or recast Nafion (27.7% vs. 29% for room temperature water and 47% vs. 54% for sorption from boiling water), but the difference was within experimental error.

5.2.3 Ion Exchange Capacity

Researchers tend to report that the addition of inorganic materials slightly enhances the acidity or ion exchange capacity of the membrane, due to the contribution of ion exchange capacity from the metal oxide. Saccà et al. [10] measured the ion exchange capacity of Nafion recast with 3 wt % TiO_2 particles (5-20 nm), and found it was 2% to 4% greater than their control recast and extruded Nafions. Yang et al. [5] found the ion exchange capacity of 25 wt % Nafion 115/zirconium hydrogen phosphate prepared via sol-gel processing to be enhanced 40-50% by the additive. Thampan et al. [13] measured the ion exchange capacity of Nafion/ZrO_2 (created via sol-gel synthesis) and 5, 10 and 20 wt % ZrO_2 recast membranes, finding that the equivalent weight (g polymer per mol H^+)

decreased by 8% for the sol-gel membrane (indicating greater acidity or ion exchange capacity) and decreased by 2% for the 5 wt % recast, yet increased slightly for the 10% and 20 wt % recast membranes, a result attributed to the larger particle sizes found in the recast membranes. Jalani et al. [19] measured equivalent weight of ZrO_2, SiO_2 and TiO_2 composites formed via a sol-gel method and reported that only ZrO_2 improved the membrane acidity. Bauer and Willert-Porada [14] also found that the equivalent weight of Nafion recast with 10 wt % TiO_2 was higher, indicating lower acidity. Work in this lab [7] has found that the ion exchange capacity of Nafion recast with 3 wt % TiO_2 (21 nm particles from Degussa-Huls) was increased by 1% - 2% over extruded and recast Nafion, but the findings were within experimental error.

5.2.4 Proton Conductivity

Researchers report differing results for measurements of conductivity outside of the cell, and it has often been pointed out that results of IEC, water uptake and proton conductivity do not correlate with each other or with fuel cell performance [5, 13, 14].

Saccà et al. [10] found the in-plane conductivity measured with AC impedance of Nafion recast with 3 wt % TiO_2 particles (5-20 nm) to be 25-30% greater than their control recast and extruded Nafions and that the performance of the membranes in the cell was improved at temperatures between 80°C and 130°C. Similar results were found by this lab [7] for Nafion recast with 3 wt % TiO_2 (21 nm particles from Degussa-Huls), with the composite improving conductivity by ~30% over extruded Nafion and 14% over recast. In contrast, Shao et al. [3] measured the proton conductivity at 100% RH of Nafion recast with 10 wt % TiO_2, SiO_2, WO_3 or SiO_2/phosphotungstic acid (PWA), and found it was *lower* for all of the composite membranes, particularly TiO_2, though the conductivity

of all of the composites except TiO_2 approached that of Nafion at higher temperatures. However, measured in the fuel cell at 70% RH, all of the composites produced higher conductivities than extruded Nafion, ordered: TiO_2<SiO_2<WO_3<SiO_2/PWA. The TiO_2 composite was ~10% higher and the SiO_2/PWA composite was over 3 times higher. [3]

Wang et al. [12] measured proton conductivity of Nafion/TiO_2 composites (3 wt % formed via sol-gel processing) at 30°C and different water contents and reported that for completely humidified conditions the composite and unmodified Nafion had similar conductivities but that while both membranes' conductivities decreased linearly with decreasing water content, the composite membrane's conductivity decreased less. The composite membrane also outperformed extruded Nafion in fuel cell tests at 40°C with no feed humidification.

Damay and Klein [11] measured conductivity using in-plane ac impedance of Nafion/$7SiO_2$-$2P_2O_5$-ZrO_2 (SPZ gel), Nafion/ SiO_2+H_3PO_4 (iHPO gel), Nafion/SiO_2+$H_3PW_{12}O_{40}$ (iHPW gel) and Nafion/zirconium phosphate (ZrP) composites (10-15 wt % prepared via the sol gel method) at several temperatures and RH's between 10% and 70%. At 25°C, the Nafion/iHPO and Nafion/iHPW composites showed higher conductivity than Nafion, while Nafion/ZrP, the only non-gel composite, showed lower. At 75°C and 130°C the gel silica network-based composites showed only minor improvement in conductivity, though the authors note that it was not enough to explain the enhanced cell performance, and Nafion/ZrP remained significantly worse. Nafion and Nafion/gel composite's conductivity improved more with humidity and temperature than did the zirconium phosphate composites. It was suggested that the ZrP particles

blocked pathways for proton conduction, and that the structure of the composite played a role in governing membrane behavior[11].

The decrease in conductivity with the addition of ZrP was also observed by Bauer and Willert-Porada [14] and Yang et al. [5]. Yang found that the proton conductivity of Nafion/ZrP, (25 wt% zirconium phosphate via sol-gel processing) was lower over the temperature range 80-140°C at all humidities, while the cell performance was improved at higher temperatures and lower humidities.

Thampan et al. [13] looked at conductivity of Nafion/ZrO_2 (created via sol-gel synthesis) and 5%, 10% and 20% (ZrO_2 by weight) recast membranes. The sol-gel prepared composite exhibited greater conductivity than Nafion at 90°C and 120°C, 10% and 40% RH, while the recast composites were less conductive. [13] Among the different weight loadings of recast composites, the 10 wt % appeared the most successful, with the highest conductivity. Jalani et al. [19] performed conductivity measurements of sol-gel derived SiO_2, ZrO_2 and TiO_2 membranes at 90°C and 120°C and found that only ZrO_2 actually increased the conductivity of the membrane. However, both TiO_2 and ZrO_2 composite membranes performed better in fuel cells.

5.2.5 Powder Properties & Surface Area

Many believe that the performance of the membrane is changed by the interfacial interactions of composite materials with the polymer, such that composites of smaller particles[15] or composites with different surface properties [9, 17, 23] would behave differently in the membrane. Alberti and Casciola [20] recommend recasting with colloidal particles rather than nanoparticle powders in order to reduce particle agglomeration and size distribution. Kumar and Fellner [15] point out that the interfaces between ceramic and

polymer may be the active parts of the composite membrane, providing a defect structure and void volume that could hold water and help proton conduction, and that decreasing particle size by a factor of 10 increases the number of sites for particle-polymer interaction by a factor of 1000. Chalkova, et al. [9] formed recast composite membranes of Nafion and 10 wt % rutile TiO_2 with two different types of TiO_2 particles. The second powder had smaller grains, about 5 times the specific surface area, higher zeta potential, more regular crystalline morphology and, when incorporated into a membrane, substantially enhanced cell performance at low humidities and elevated temperatures. This was attributed to an increase in the number of proton adsorption sites, and water molecules at the ceramic/polymer interface. Similarly, Baglio et al. [16] found that recast 5 wt % Nafion/TiO_2 composite membranes performed better in direct methanol fuel cells, and that TiO_2 particles calcined at lower temperatures (yielding higher specific surface areas) performed the best. In a separate study [17], they observed better DMFC performance at 145°C for Nafion membranes recast with 5 wt % TiO_2 powders calcined at 500°C than those calcined at higher temperatures. The powders calcined at 500°C yielded an anatase crystal structure (compared to rutile at higher calcining temperatures) and higher surface area and acidity.

5.2.6 Dimensional Stability

A complementary theory, first proposed by Yang et al. [5], is that in changing the microstructure the addition of particles also changes the membrane's mechanical properties, making them stiffer and more able to absorb and retain water in the confined space of a fuel cell. The authors suggested that the composite absorbed more water than simple Nafion because the zirconium phosphate acts as a scaffold and inhibits shrinkage

when the membrane dehydrates, meaning that upon rehydration the membrane has less swelling work to do, both against the polymer matrix and the sealing pressure exerted on the electrodes. This hypothesis was supported by the fact that enhanced fuel cell behavior was observed for many different metal oxides, regardless of ex-situ conductivity, ion exchange capacity or water uptake. Also, density measurements revealed that the dry ZrP composite membrane has a lower density than both Nafion and the zirconium phosphate, indicating the presence of void volume. SAXS data on Nafion and composites at different humidities further supported the scaffolding idea, indicating that Nafion rearranges more upon hydration: the Bragg spacing of the polymer's ionic regions shifted from 3.7 nm (dry) to 5.1 nm (hydrated) for Nafion and from 4.5 nm (dry) to 5.1 nm (hydrated) for the composite. Because the composite is created in a wet membrane, it would make sense that the scaffolding acts to hold the ionic regions within the Nafion (and thus the SAXS peaks) closer to the 'wet position'—a higher Bragg spacing—when dry[5].

The scaffolding would also increase dimensional stability during the hydration and dehydration accompanying operational cycling. Added dimensional stability would improve membrane durability and help maintain the membrane/electrode interface, which can be lost during dehydration as the membrane shrinks away from the electrode. This effect would explain why composite membranes perform so much better in fuel cells but do not always exhibit improved conductivity when tested outside of a fuel cell. The idea of improving membrane/electrode interface by increasing dimensional stability through better mechanical properities has also been put forth by [1, 20] among others and is

consistent with other observations that dimensional stability during water uptake and loss contributes to membrane performance [2].

Interestingly, however, Thampan et al. [13] found that Nafion/ZrO_2 (3-4 wt %) membranes prepared via sol-gel processing exhibited higher conductivity inside & outside the cell, but performed exactly as well as unmodified Nafion in fuel cell tests at 110°C with an under humidified feed stream (bubbler temperature of 80°C). The authors attributed discrepancy between conductivity and cell performance to a decrease in the electrochemical surface area in the membrane-electrode assembly as the membrane dried at higher temperatures and shrank. Apparently the authors found that the effect of this shrinkage was the same (maybe even more to offset the enhanced conductivity) for the composite membrane. Also, dimensional changes measured in this lab [7] between dry and completely hydrated (either room temperature liquid water 24 h or boiling water for 1 h) were the same for Nafion recast with 3 wt % TiO_2 as they were for unmodified recast Nafion, though the composite membranes performed better in fuel cells. It is possible that a higher mass fraction of inorganic filler is needed to affect dimensional stability. The membranes investigated by Yang et al. [5] carried 25 wt % ZrP, while those tested by Thampan et al. [13] were 3-4 wt %, as were those reported on by this lab [7].

Performance in fuel cells is still enhanced by the addition of only 3 wt % composite material, and the effect of mechanical properties and swelling pressure should be investigated even if effects of dimensional changes are not visible at this low loading.

5.2.7 Mechanical Properties

Mechanical properties are not routinely measured by researchers developing new membrane materials, though they are often credited with enhancing performance and

prolonging the life of the composite membranes. [6] The addition of a ceramic to a polymer generally increases the elastic modulus and the glass transition temperature [15], and most reported findings for fuel cell membranes support this. However, it is still not clear which properties are more important to performance in a fuel cell, and different properties are reported by different groups. Further, groups routinely fail to report the conditions under which the membranes are tested, including membrane preconditioning, water content, temperature, strain rate and number of samples tested. Authors often report on "tensile strength", which can be inferred to mean ultimate stress in some cases [24] [25] [3] but appears to mean elastic modulus in others[26] and is not at all clear in still other cases [27] [28].

Shao et al. [24] created Nafion/[SiO_2-TiO_2] ~7 wt % and Nafion/[SiO_2-Al_2O_3] ~4-6 wt % using in situ sol-gel processing. X-ray energy dispersive spectroscopy on Nafion/[SiO_2-TiO_2] showed Ti/Si intensity ratios that were highest at the surface of the membrane, indicating that TiO_2 had concentrated at the surface, while the Al/Si intensity ratios for Nafion/[SiO_2-Al_2O_3] indicated a fairly uniform distribution through the membrane cross-section. Mechanical tests were performed at 22°C with an MTS 810 Universal Test Machine. The strain rate was 0.1 mm/s and sample dimensions were 3 mm(wide) x 10mm(long). [24] Their results appear in Figure 5.1 and Figure 5.2.

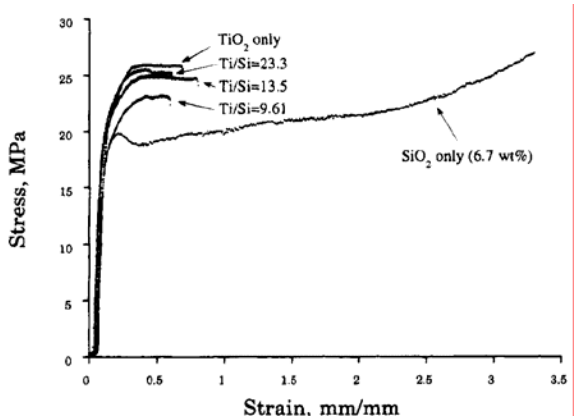

Figure 5.1: Stress/strain behavior of TiO_2-SiO_2/Nafion composite membranes. (roughly equal amounts of both oxides) Figure reprinted from [24] with permission from the American Chemical Society © 1995.

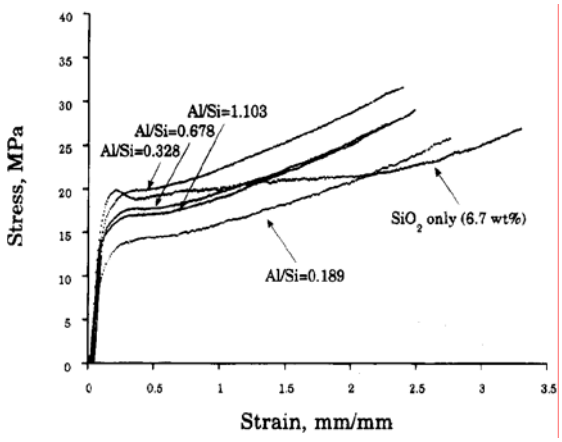

Figure 5.2: Stress/strain behavior of Al_2O_3-SiO_2/Nafion composite membranes . (roughly equal amounts of both oxides) Figure reprinted from [24] with permission from the American Chemical Society © 1995.

The authors comment on the ductility of the membranes, stating that the SiO_2-only composite was as ductile as plain Nafion observed in earlier work and suggest that the SiO_2 concentration is below its percolation threshold, meaning that the polymer matrix is bearing the load. They found that 7% TiO_2 and any mixture of TiO_2/SiO_2 at ~7% causes the membrane to become much more brittle, which they attribute to the formation of a continuous phase -- the high surface concentration of TiO_2 controls the membrane properties. Ultimate strain was found to be roughly similar for all TiO_2/SiO_2 mixtures and the ultimate stress increased with increasing TiO_2/SiO_2 ratios. The modulus was found to be roughly the same across all samples, which the authors attributed to the possibility of poor interfacial bonding, or to the fact that the loading was roughly the same across all composites, and only inorganic loading and interfacial surface area (not composition) would affect the modulus [24].

Similar work [25] in which Nafion/SiO_2-TiO_2 composite membranes were formed from a 2-stage sol-gel process (forming an SiOH and SiOR core then treating with tetrabutyltitanate to form a TiO_2 outer surface) also yielded a membrane with higher

ratios of Ti to Si at the surface. Membranes containing only SiO_2 (having only undergone the first stage of processing) with loadings of either 6.7 or 15.9 wt % had ultimate strains of ~350% and 100% respectively and were more ductile than those that had been through the second stage of processing to contain TiO_2. Membranes with higher ratios of Ti to Si loadings monotonically increased the yield and ultimate stresses, but these membranes were 3 to 5 times more brittle (lower ultimate strain) than similarly-made membranes loaded with only SiO_2. The authors attributed the behavior of the SiO_2 membrane to it not forming a continuous phase within the Nafion and the behavior of the TiO_2/SiO_2 membranes to the resultant formation of a continuous phase at the surface where the Ti/Si loading ratio is highest.

It should be noted that these membranes created by P.L. Shao and Mauritz [24, 25] were not intended for fuel cell application and were not tested in fuel cells. Later research found that the additives in similar membranes leached out during the standard cleaning process. [18]

Z .G. Shao et al. [3] formed Nafion recast with 10 wt % SiO_2, TiO_2, WO_2 and SiO_2/phosphotungstic acid (PWA) for use in high-temperature fuel cells and measured their stress-strain properties at 25°C with an Instron Series IX Automated Material Testing System at a strain rate of 2.5 mm/min on 3 mm x 10 mm samples. Their results are shown in Figure 5.3.

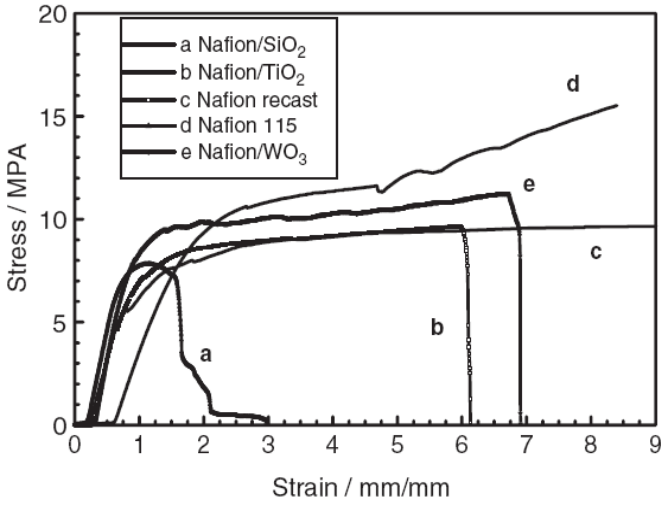

Figure 5.3 Stress/strain behavior of extruded and recast Nafion 115 and composite membranes formed via recasting. Figure reprinted from [3] with permission from Elsevier © 2006.

They note the longer ultimate strain for recast and extruded Nafion (lines c and d) and conclude that the addition of inorganic oxides embrittles the polymer. However, they note the ultimate stress of the composites increases with "order of impregnation", as complementary SEM images showed that SiO_2 (line a) had the largest particles (40-45 um), TiO_2 (line b) had medium-sized particles with a wide distribution of sizes (3-10 um) due to agglomeration and WO_3 (line e) had small uniform particles (~2 um), which appeared unagglomerated and well-impregnated into the membrane, thus improving the amount of inorganic/organic surface area.[3] It is not clear how many samples were tested by the authors, and the results for lines a and d, if not repeatable, would appear to indicate sample slippage in the cross-head grips or the existence of a defect in the gauge length.

Jalani et al. [19] performed dynamic mechanical analysis on Nafion/ TiO_2, SiO_2, and TiO_2 membranes made through the sol-gel process. They reported that the glass transition temperature increased for the composite membranes from 110°C for Nafion to 118°C for SiO_2, 122°C for TiO_2 and 142°C for ZrO_2. From the decreasing height of tanδ, the increasing T_g and increasing degradation temperature measured through TGA, they

predicted that the membranes were more suitable for high-temperature operation than unmodified Nafion, which proved true for the TiO_2 and ZrO_2 composite membranes. Adjemian et al. [23] also reported that the glass transition temperatures of recast SiO_2, TiO_2, Al_2O_3 and ZrO_2 composite membranes increased, which they said was "indicative of a stiffening of the polymer system", and that polymer/oxide interactions may have added crosslinks in the polymer. However, not all of the membranes that exhibited higher T_g's also performed better in cells at the higher temperatures.

Bauer and Willert-Porada [14] reported elastic moduli of Nafion and Nafion/zirconium phosphate (21 wt % ZrP prepared via sol-gel processing) membranes at 75°C and various humidities measured with a dynamic mechanical analyzer (DMA 2980, TA Instruments), equipped with a custom-built humidity chamber. Their results appear in Figure 5.4.

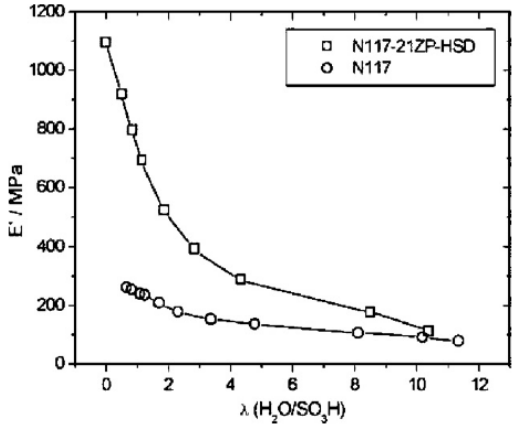

Figure 5.4: Elastic modulus vs. water content (λ) at 75°C. Figure reprinted from [14] with permission from Elsevier © 2006.

They report a substantially (almost 4x) higher elastic modulus for the composite at low water content, but a modulus approaching that of Nafion at higher water content.

Researchers have reported mechanical properties of other composite membrane materials for fuel cells made of different polymer materials.

Kwak et al. [28] formed composite membranes of Nafion and the zeolite mordenite by melting Nafion and H^+-form mordenite powders and hot-pressing them to the desired membrane form. Membranes were cleaned, boiled in NaOH to convert them to the Na-form and dried 6 h at 110°C. Tensile testing was done with an Instron 8848 on 4 cm x 1.5 cm samples at a strain rate of 2 mm/min. They reported 'tensile strength' of the materials, which decreased linearly with increasing mordenite loadings (3, 5, 10, 20 wt %) from 45 MPa for plain Nafion to ~12 Mpa at 20 wt %. They attributed the weakening of the membrane to an increase in membrane porosity as mordenite and polymer surfaces are incompatible. Use of the membranes in fuel cells at 110°C and 130°C with partially humidified feed streams showed an improvement in performance with mordenite content, up to 10 wt %.

Kim et al. [27] formed composite membranes of a fluorinated organic ionomer made of decafluorobiphenyl and 4,4'-(hexafluoroisopropylidene)diphenol and SiO_2 and tested the 'tensile strength' in an Instron 4465 according to ASTM-1708 protocol. Their polymer with no loading had a tensile strength of 32.85 MPa which decreased linearly to ~6 MPa at 10% SiO_2, which they attributed to the SiO_2 interfering with the composite network. The authors compared their new membrane material favorably to Nafion, which they tested to have a tensile strength of 21 MPa, less than half that reported for Nafion by Kwak [28]. The new membrane also performed well in fuel cells at elevated temperature.

Smitha et al. [29] created recast composite membranes of phosphotungstic acid, a heteropolyacid (HPA) and sulfonated polysulfone (SPSF) and performed stress-strain tests on 5 cm samples with a Shimadzu Universal Testing Machine at 12.5 mm/min.

They found the ultimate stress to be over 80 MPa at a strain of ~80% for HPA loadings up to 30%, an increase over plain SPSF that they attributed to hydrogen bonding interactions between HPA and the polymer, though higher loadings caused the membrane to become more brittle. The authors stated that this mechanical reinforcement "confirms the mechanical stability of the membrane in high temperature (>120°C) fuel cell environments", though it is not clear that the membrane was tested in a cell, or that the mechanical properties were tested at elevated temperatures.

Liu et al. [30] created Nafion/Pt-carbon nanotube (40 nm diameter) composite membranes and tested dry (10 h 80°C vacuum oven) samples in a GMT 4503 tension tester at room temperature at a rate of 50 mm/min (gauge length not indicated). The ultimate stress was measured at 33.42 MPa, compared with 27.2 MPa for plain Nafion. The authors suggested that the several-micrometer long nanotubes contributed to crosslinking. These membranes also performed better in fuel cells at 80°C and feed streams both completely or un- humidified.

Rhee et al. [26] formed recast composite membranes of Nafion with HSO_3^- functionalized nanosheets of titanate. Tensile tests were performed in an Instron 4206 on 5 mm x 5 cm samples with a strain rate of 5 mm/min. They reported Young's moduli which improved from Nafion (at ~80 MPa) to ~200 MPa for composites recast with montmorillonite needles, aspect ratio 100:1 and TiO_2 P25 nanoparticles. The plain geometry of the titanates further increased the modulus to ~250 MPa at 3 wt % and up to ~350 MPa for 10 wt %. The functionalized titanate sheets outperformed Nafion and Nation/TiO_2 recast membranes in a methanol cell at 40°C.

5.3 Procedure

The procedures for these experiments have been documented in earlier chapters of this thesis, as well as in Satterfield et al. [7]. Stress-strain and stress-relaxation tests (chapter 2), water sorption and desorption experiments (chapter 3) and swelling pressure measurements (chapter 4) were performed on Nafion/TiO_2 composite membranes created by colleague Paul Majsztrik (Princeton University Department of Chemistry).

A variety of different membranes were tested. The most common membranes used were created from 15 wt % Nafion solution mixed with isopropyl alcohol (IPA) that had been sonicated 1 h with 3 wt % TiO_2 particles, anatase form, nominal size 21 nm purchased from Degussa Huls (DH). These were used in stress-strain tests, stress-relaxation tests, water sorption and swelling pressure tests. Other membranes were prepared similarly but with a 20 wt % TiO_2 loading. These were used in stress-strain and stress-relaxation tests. Stress-strain tests were also performed on a range of membranes, some recast with different solvents: dimethyl sulfoxide (DMSO) or ethanol (EtOH), different loadings: 0.5, 1 or 6 wt % TiO_2, different shapes: 3 wt % nano-sized needles in rutile form or from a different supplier: Alfa Aesar (AA). Water sorption and stress-strain tests were also performed on Nafion prepared using the same recasting procedure without TiO_2 to identify changes in membrane properties that might be due to the recasting procedure and not the addition of TiO_2 nanoparticles.

In the recasting procedure followed by P. Majstrik, the sonicated mixture was cast onto a glass plate in a cylindrical mold and the solvent was evaporated off in a vacuum oven at 70°C (EtOH and IPA) or 80°C (DMSO). The membranes were then annealed at 165°C for 1 hour. The membranes were cleaned and converted to acid form by the same procedure described for extruded Nafion: boiling 1 h in 3% H_2O_2 in water, 20 minutes in

deionized water, 1 h in 1 M H_2SO_4 and 20 minutes in deionized water. Composite membranes were usually stored in sealed plastic bags at roughly ambient conditions after cleaning. Cast (composite and unmodified) and extruded (unmodified) membranes were all of the same dry thickness: 127 μm.

The composite membranes created this way generally did not have a homogeneous distribution of particles. TEM images of the recast composite membranes, shown in Figure 5.5, reveal that the 21 nm particles tended to agglomerate within the membrane. However, these membranes have still exhibited improved performance in fuel cells.

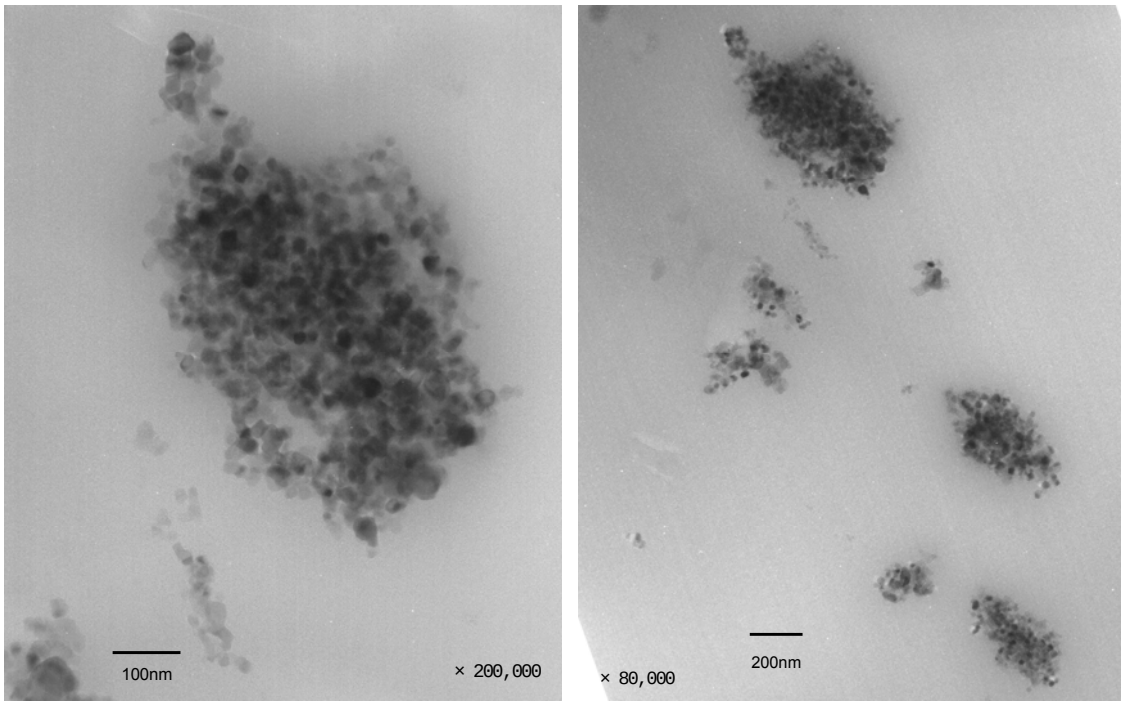

Figure 5.5: TEM images of recast 3 wt% TiO_2/Nafion composite membranes showing ~21 nm particles agglomerated in the polymer. Images made by Dr. Hitoshi Ota.

Stress-strain mechanical properties of composite membranes were obtained at either room temperature or 80°C at ambient humidity using an Instron model 1122 with a model 3111 environmental chamber. Samples were die-punched into dogbone shapes,

gauge dimensions 2.25cm x 0.475 cm and stretched at a rate of 50 mm/min. The resulting stress-strain curves were examined for Young's modulus, plastic modulus, toughness and proportional, yield and ultimate stresses and strains.

Stress-relaxation tests of composite membranes were performed at 100% relative humidity at temperatures of 30°C, 50°C, 70°C, and 90°C and strains of 2%, 5%, 10% and 20% using an Instron model 5865 with a model 3111 environmental chamber. Membranes were die-punched into dogbone shapes described above and placed in a sealed in a plastic bag inside the environmental chamber for ~2 hours to equilibrate. To start the tests the membranes were strained quickly to a pre-determined strain at a rate of 50%/sec, or 670 mm/min and held as the stress was recorded over time. Membranes tested were 3 wt % and 20 wt % TiO_2, anatase form, nominal size 21nm, purchased from Degussa Huls and recast using IPA solvent. Stress-relaxation curves were compared with extruded Nafion in time-temperature and time-strain superposition plots.

Water-sorption tests were performed on membranes recast with 3 wt % TiO_2, anatase form, nominal size 21nm, purchased from Degussa Huls and recast using IPA solvent. They were suspended from a bottom-weighing balance into a heated chamber at ~100% RH and their weight was recorded over time. After the membrane's weight stabilized, the humidified chamber was immediately substituted for a chamber filled partially with drierite and heated to the same temperature. The weight was again recorded over time. Temperatures used ranged from 30°C to 90°C.

Swelling behavior under compressive load in confined space was measured using the controlled-environment compression test described in Chapter 3 and in [7]. Membranes were constrained against a load cell by a screw drive in an initially dry environmental

chamber. Water was added to the chamber, and the load cell measured the force exerted by the membrane as it swelled to absorb the added water.

5.4 Results

Figure 5.6 and Figure 5.7 show sample stress-strain curves of extruded Nafion & Nafion recast with 3 and 20 wt % TiO_2, respectively. The membranes are at room temperature in both plots, and at similar water contents: λ=10.9 [H_2O/ SO_3^-] in Figure 5.6 and λ=13.8 [H_2O/ SO_3^-] in Figure 5.7.

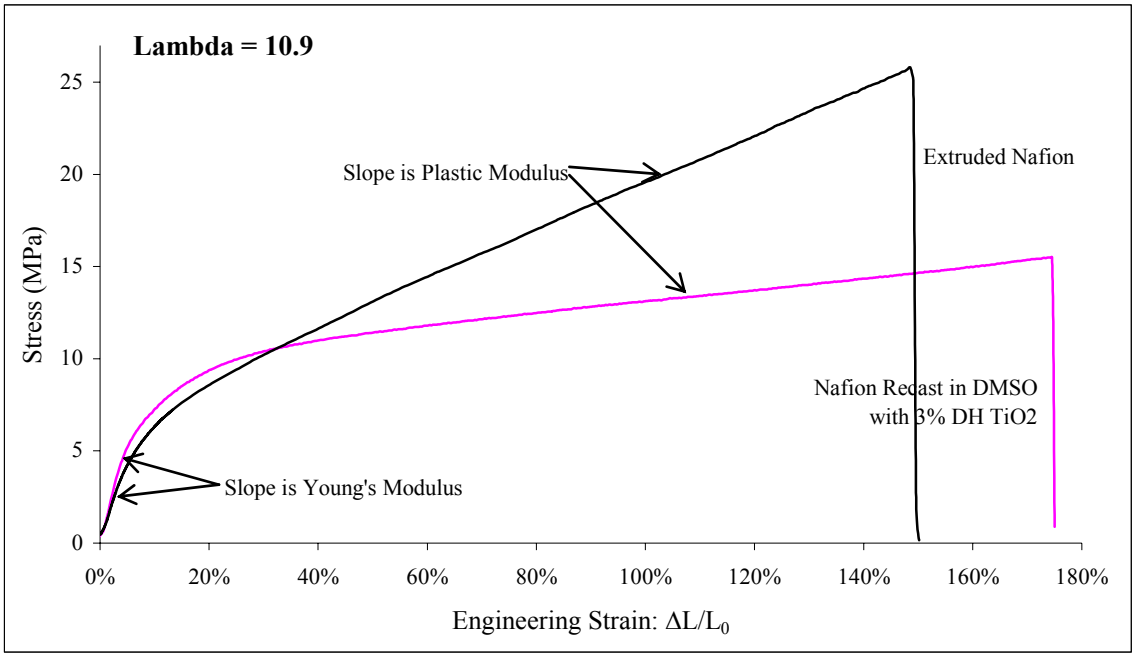

Figure 5.6: Sample stress-strain curves for extruded Nafion & Nafion recast with 3 wt % TiO_2 at room temperature & with similar water contents, showing differences in Young's modulus and in plastic modulus. Figure reprinted from [7] with permission from John Wiley & Sons © 2006.

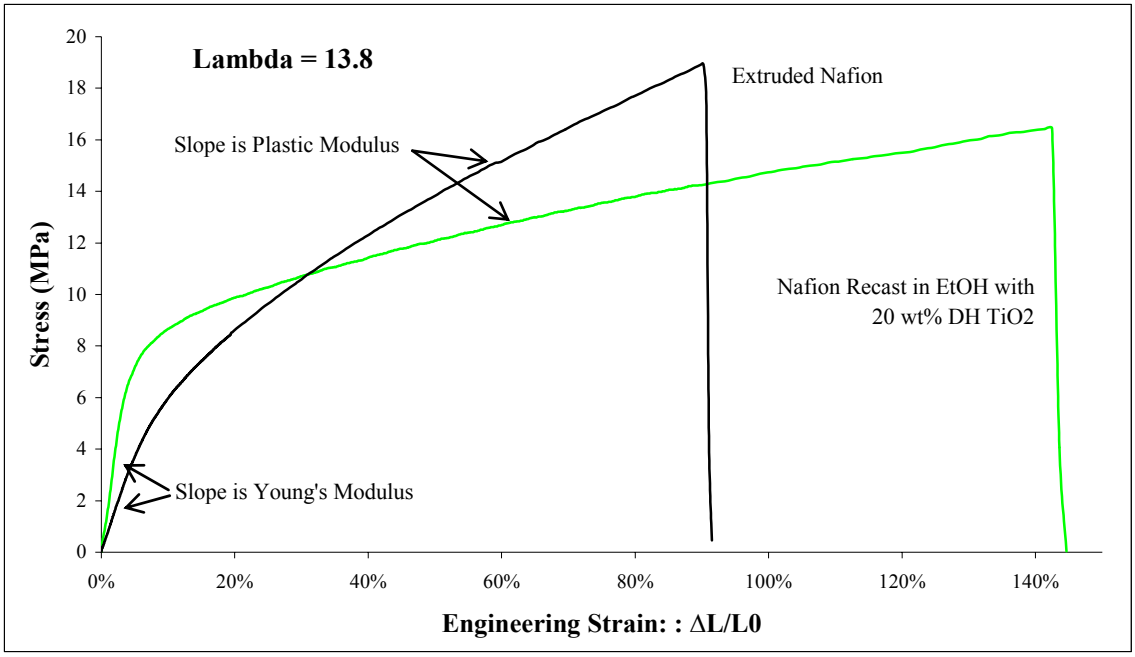

Figure 5.7: Sample stress-strain curves for extruded Nafion & Nafion recast with 20 wt % TiO_2 at room temperature & with similar water contents, showing differences in Young's modulus and in plastic modulus.

A slight increase in Young's modulus with increasing TiO_2 content is visible from these graphs as well as a significant decrease in plastic modulus. Figure 5.8 through Figure 5.11 show how the values of Young's and plastic modulus for extruded Nafion compare with those of the composites. Figure 5.8 shows the change in Young's modulus with water content for samples tested at room temperature, and Figure 5.9 shows the change in modulus with temperature for samples tested in ambient conditions with water contents measured below $\lambda = 4.5$ [mol H_2O/SO_3^-].

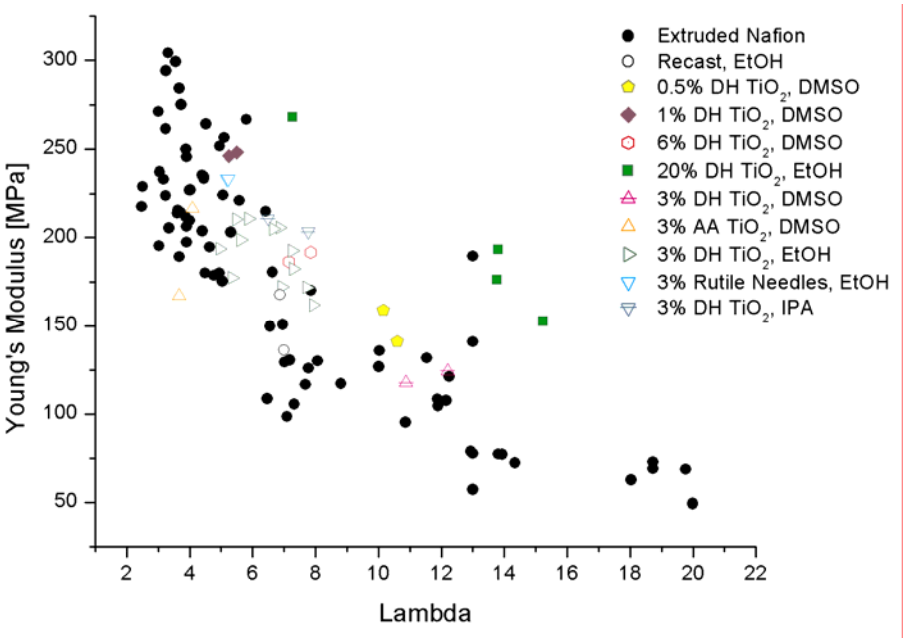

Figure 5.8: Change of Young's modulus with water content, Lambda [mol H_2O/SO_3^-] at room temperature comparing extruded Nafion & composites. AA = Alfa Aesar supplier, DH = Degussa Huls, EtOH = ethanol solvent, IPA = isopropyl alcohol, DMSO = dimethyl sulfoxide.

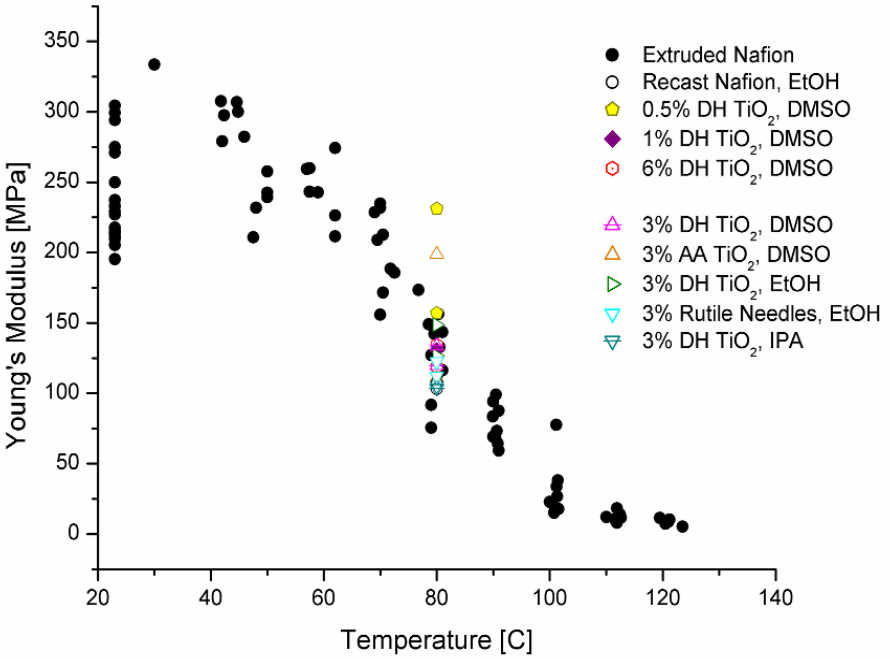

Figure 5.9: Change of Young's modulus with temperature comparing extruded Nafion & composites. Water contents are all below λ=4.5 [mol H_2O/SO_3^-].

Figure 5.8 shows that at room temperature and higher water contents the Young's modulus is increased slightly by the addition of TiO_2 particles, particularly 20 wt %

(green squares). However, at 80°C the composite membranes do not appear to be stiffer than extruded Nafion with only 2 exceptions. The spread in data points among the composites in Figure 5.9 is likely due to sample variability introduced during preparation, as at 80°C no dependence on measured water content was evident. Stress-strain tests are subject to enough error that values are usually reported after tests of 4 to 5 samples at the same condition. However, due to limits in material availability, each point here represents a single test. Also, due to limits in material availability, 20 wt % TiO_2 was only tested at room temperature.

Figure 5.10 shows how the plastic modulus varies with water content at different temperatures while Figure 5.11 shows how it varies with temperature at mid-to-low water content. The decrease in plastic modulus with the addition of TiO_2 is apparent at both room temperature and 80°C.

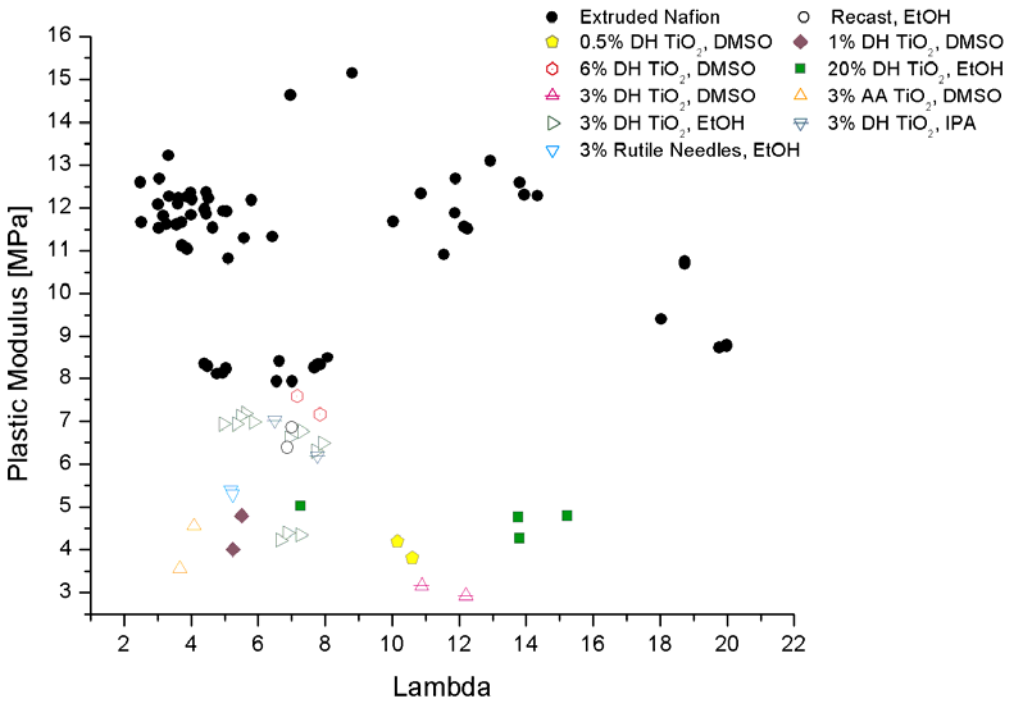

Figure 5.10: Change of plastic modulus with water content at room temperature, Lambda [mol H_2O/SO_3^-] comparing extruded Nafion & composites.

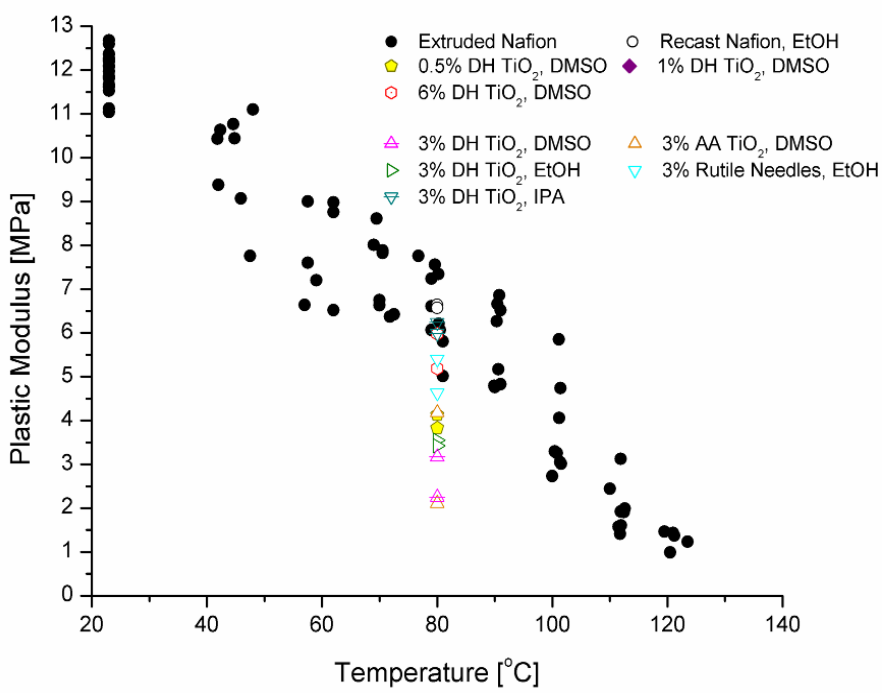

Figure 5.11: Change of plastic modulus with temperature comparing extruded Nafion & composites. Water contents are all below 4.5 [mol H_2O/SO_3^-]. AA = Alfa Aesar supplier, DH = Degussa Huls, EtOH = ethanol solvent, IPA = isopropyl alcohol, DMSO = dimethyl sulfoxide.

Figure 5.12 and Figure 5.13 show how the composite & extruded Nafion's toughness change with water content at room temperature (Figure 5.12) and with temperature at ambient humidity (Figure 5.13). At room temperature the composites appear somewhat tougher than the extruded Nafion, and this difference is even more pronounced at 80°C. This increase in toughness may be a contributing factor for the increased lifetime and performance of composite membranes at higher temperatures.

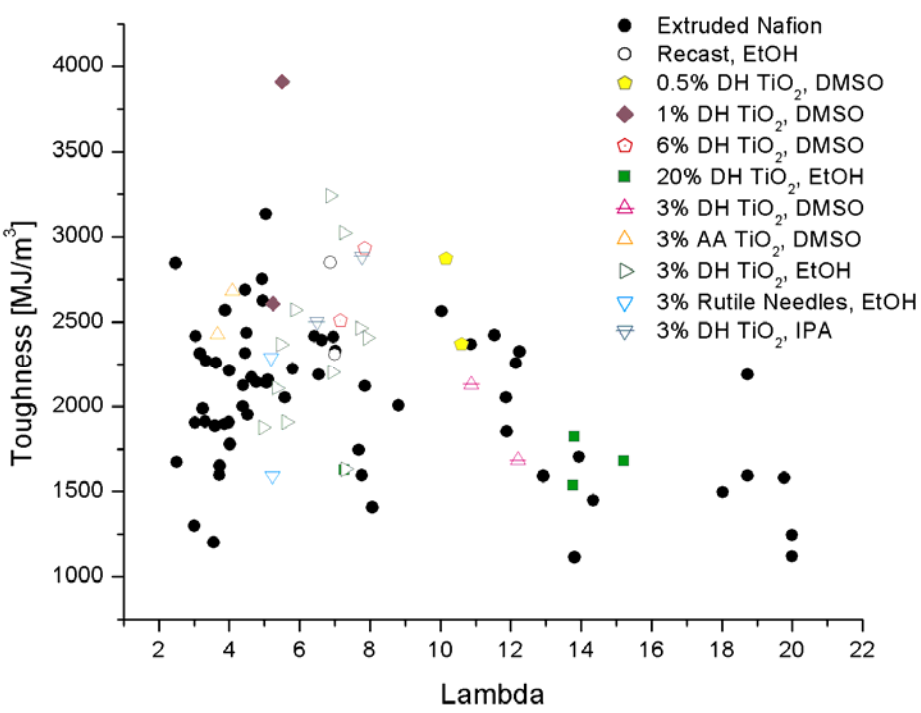

Figure 5.12: Change of toughness with water content at room temperature, Lambda [mol H_2O/SO_3^-] comparing extruded Nafion & composites. AA = Alfa Aesar supplier, DH = Degussa Huls, EtOH = ethanol solvent, IPA = isopropyl alcohol, DMSO = dimethyl sulfoxide.

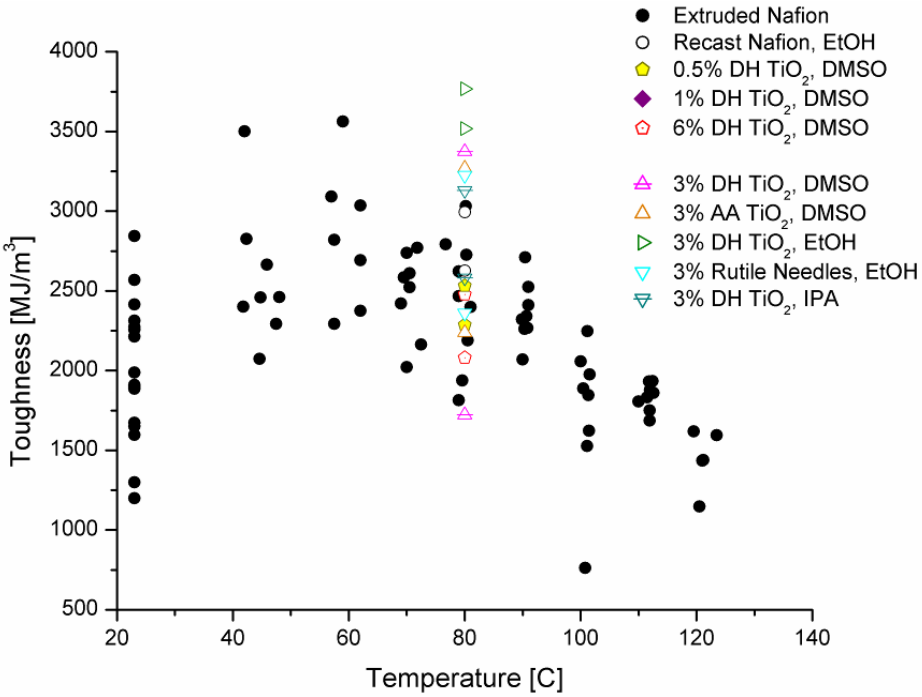

Figure 5.13: Change of toughness with temperature comparing extruded Nafion & composites. Water contents are all below 4.5 [mol H_2O/SO_3^-].

Figure 5.14 and Figure 5.15 show the dependence of proportional, yield and ultimate stresses & strains on water content (Figure 5.14) at room temperature and temperature (Figure 5.15) at ambient humidity. At both room temperature and 80°C the composites stay in the linear elastic region slightly longer than extruded Nafion (higher proportional stress & slightly higher yield stress), though the proportional and yield strains appear unaffected by the addition of the TiO_2 particles. The ultimate stress of the composites is lower than extruded Nafion and the ultimate strain appears higher, which does not tend to agree with reports by other researchers [3, 24, 25] who reported a higher ultimate stress but lower ultimate strain, though their membranes were not prepared similarly. The recast membrane with no TiO_2 particles exhibits the same properties as extruded Nafion.

The scatter in data in Figure 5.12 and Figure 5.14 is due to a combination of natural variability in samples and uncertainty in measuring λ. All measurements presented in these figures were performed at room temperature, the variability of which is not expected to drastically affect findings.

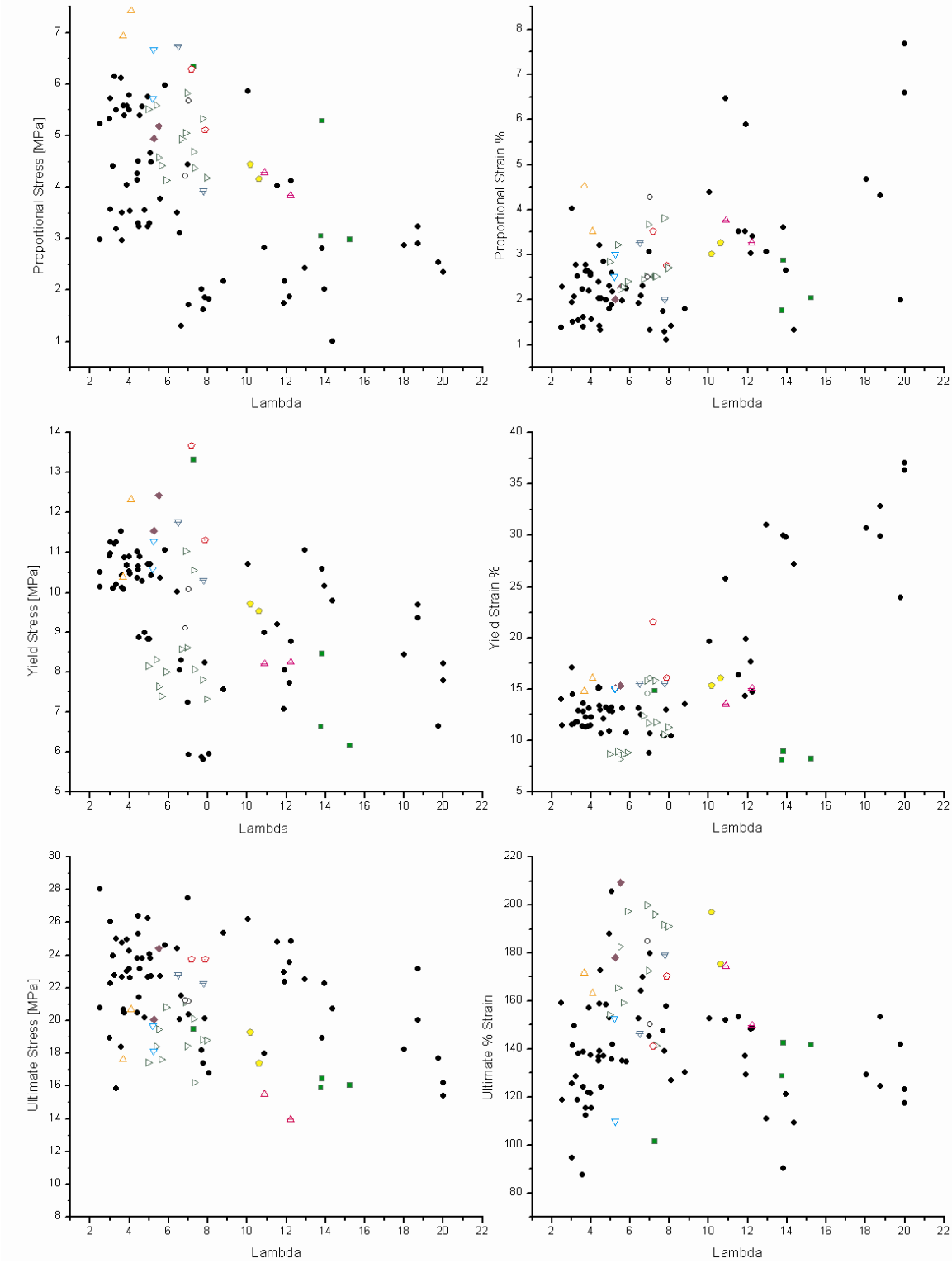

Figure 5.14: Dependence of Proportional, Ultimate & Yield Stresses & Strains on water content, Lambda [mol H_2O/SO_3^-], of extruded Nafion 115 and recast TiO_2 composites at room temperature. Key is the same as previous figures.

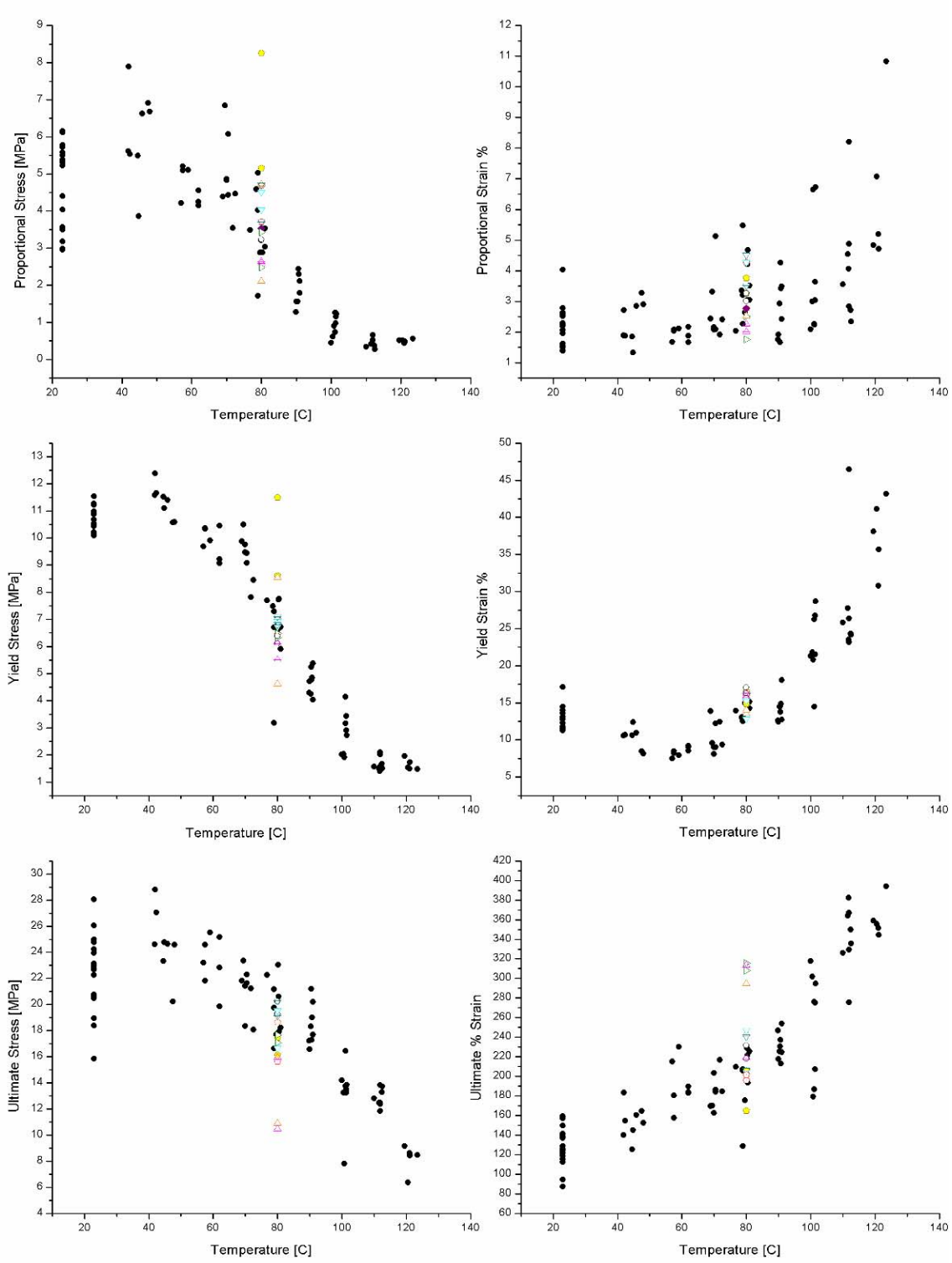

Figure 5.15: Dependence of Proportional, Ultimate & Yield Stresses & Strains on temperature, of extruded Nafion 115 and recast TiO_2. Key is the same as previous figures. Water contents are all below 4.5 [mol H_2O/SO_3^-].

Figure 5.16 through Figure 5.19 compare the temperature dependence of stress-relaxation behavior of the composites with extruded Nafion in fully humidified conditions at strains of 2%, 5%, 10% and 20% (Figure 15, 16, 17, & 18, respectively). In each figure the top graphs show stress-relaxation on a log-log plot, and the bottom graphs show time-temperature superposition master curves with insets plotting shift factor with temperature for each membrane.

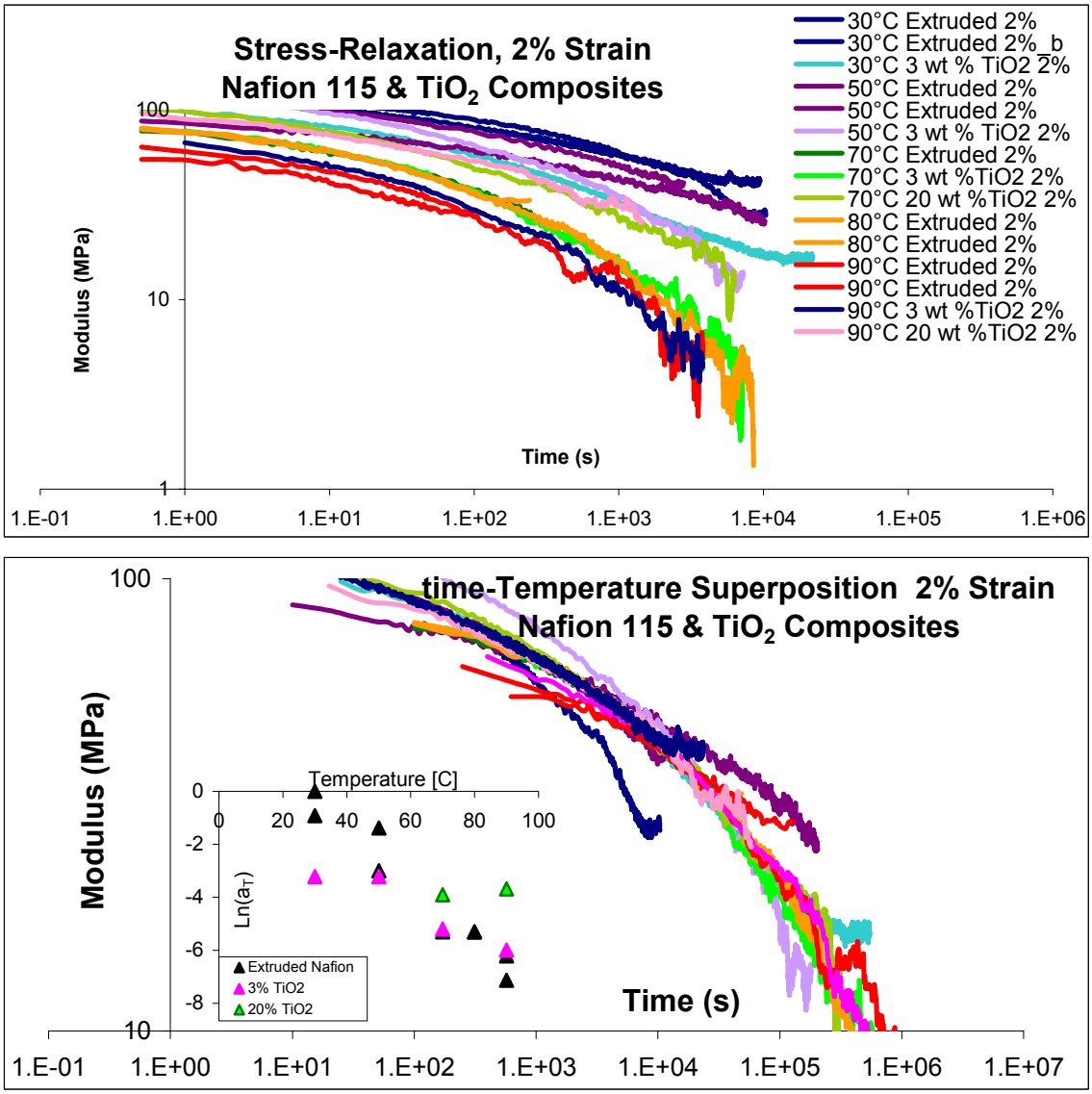

Figure 5.16: Stress-relaxation behavior (top) and time-temperature superposition (bottom) of Extruded Nafion & Nafion recast with 3 wt % & 20 wt % TiO_2. Strain is 2%, humidity is 100% & inset shows temperature shift factors.

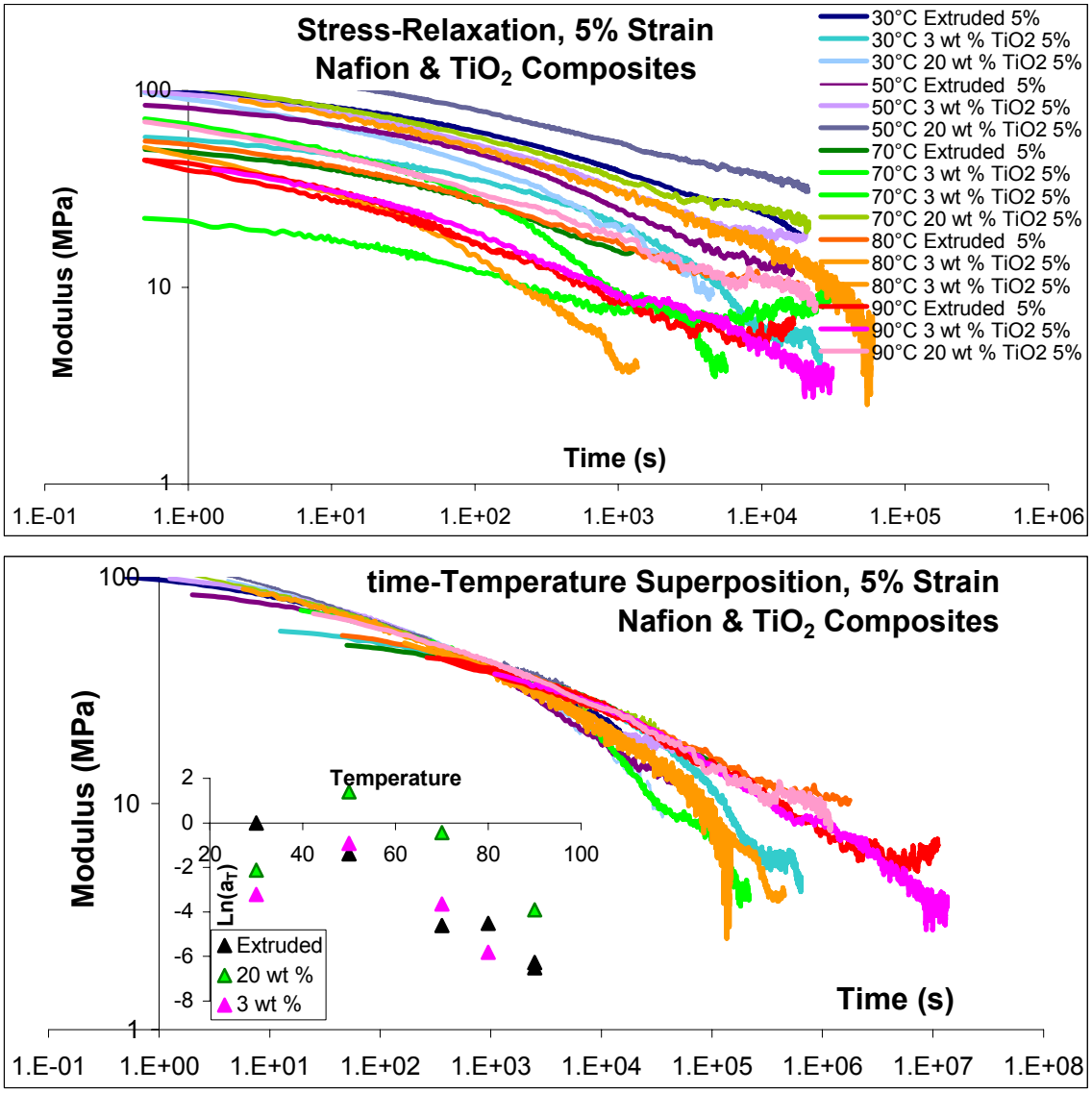

Figure 5.17: Stress-relaxation behavior (top) and time-temperature superposition (bottom) of Extruded Nafion & Nafion recast with 3 wt % & 20 wt % TiO_2. Strain is 5%, humidity is 100% & inset shows temperature shift factors.

At low strains (2% & 5%) the 20 wt % TiO_2 membrane are shifted further to the left (shorter times) to form a master curve with Nafion. The same trend was visible, but to a lesser degree for the 3 wt % TiO_2 composites. The shift factor is likely more due to a higher modulus than a slower relaxation rate. Values of viscosity determined from fitting with the generalized Maxwell model were somewhat higher for the composite membranes. However, the moduli that weight each viscous rate term increasingly

favored the lower viscosity terms at higher composite loading. Terms derived from KWW fits were similarly inconclusive.

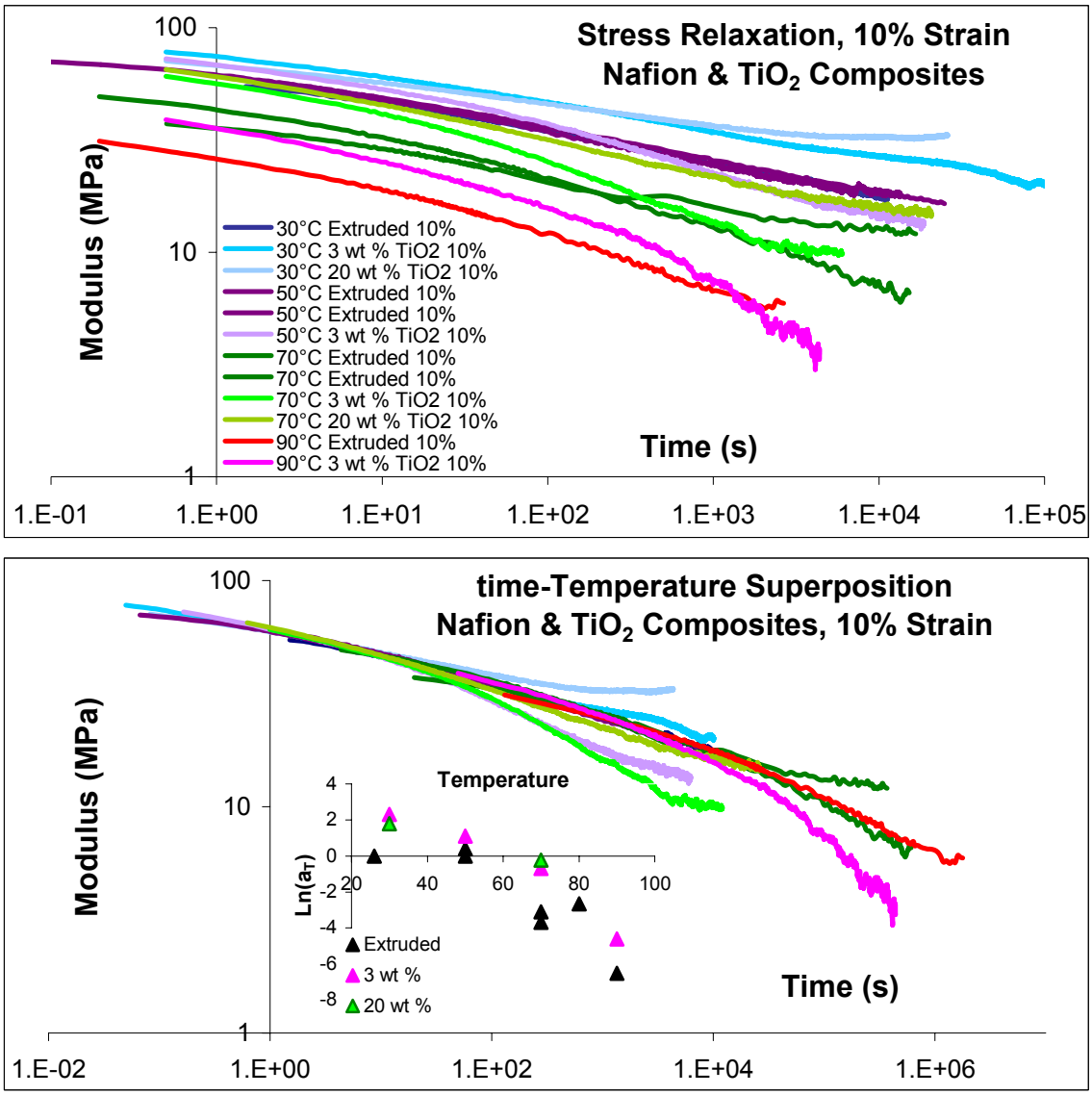

Figure 5.18: Stress-relaxation behavior (top) and time-temperature superposition (bottom) of Extruded Nafion & Nafion recast with 3 wt % & 20 wt % TiO_2. Strain is 10% & inset shows temperature shift factors.

At higher strains, particularly 20%, the difference in shift factor between extruded and composite Nafion becomes less pronounced, which is expected based on measured moduli at higher strains: the composites exhibited a lower plastic modulus.

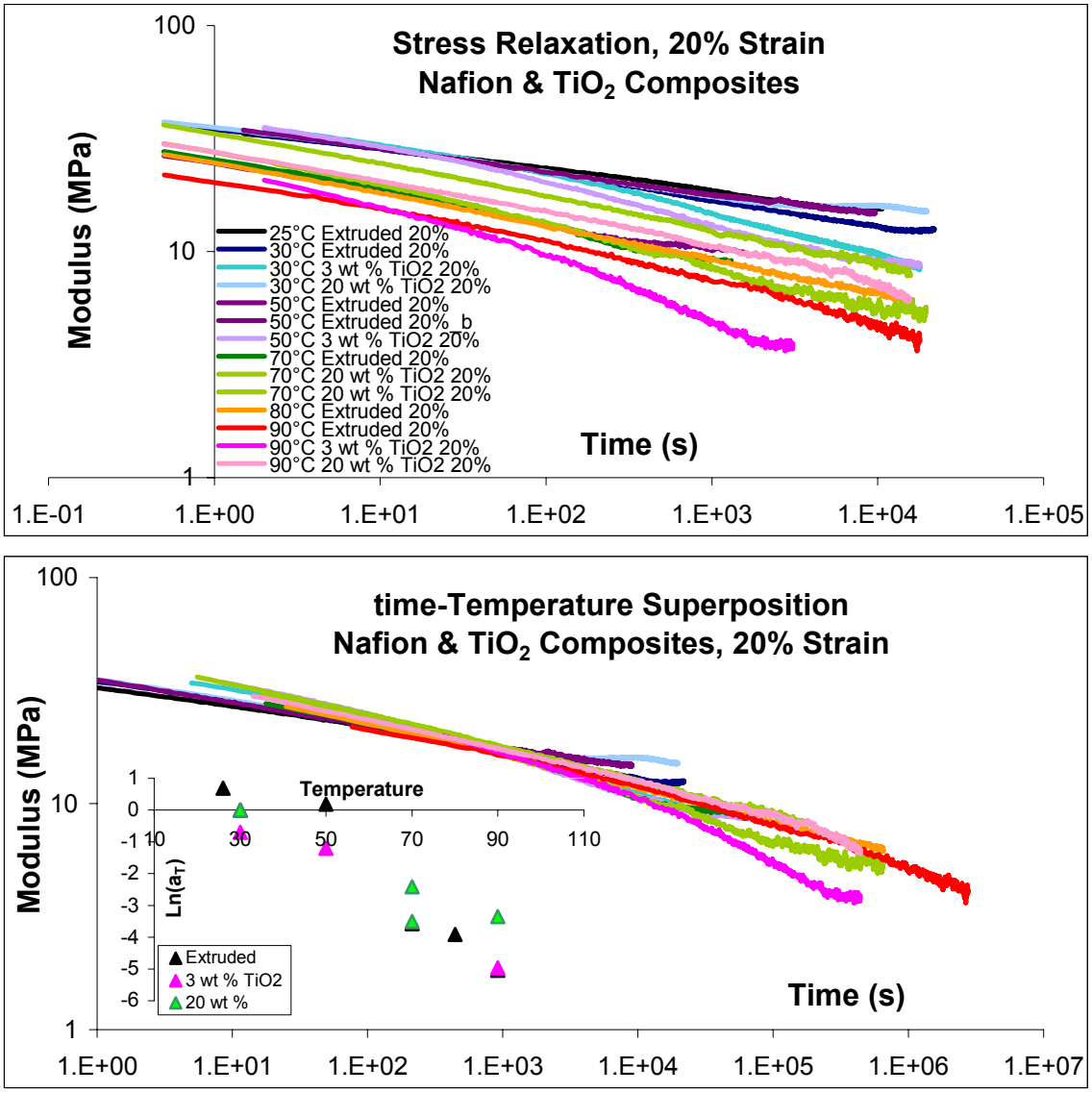

Figure 5.19: Stress-relaxation behavior (top) and time-temperature superposition (bottom) of Extruded Nafion & Nafion recast with 3 wt % & 20 wt % TiO_2. Strain is 10% & inset shows temperature shift factors.

Figure 5.20 though Figure 5.23 regroup the data presented above to compare the strain dependence of the stress-relaxation behavior of the composites with extruded Nafion at 30°C, 50°C, 70°C and 90°C. In each figure the top graphs show stress-relaxation on a log-log plot, and the bottom graphs show time-strain superposition master curves with insets that plot shift factors with strain for each membrane.

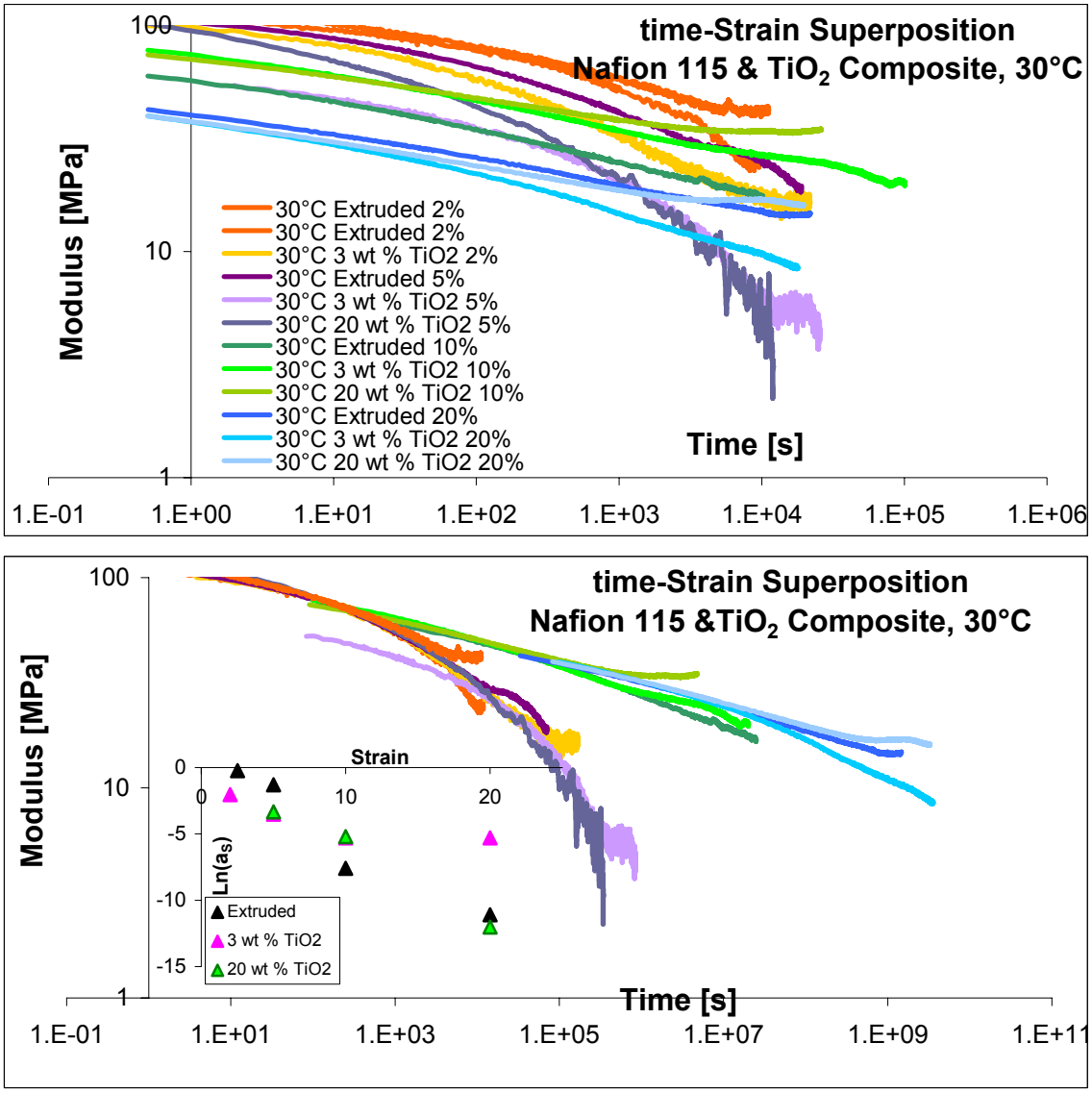

Figure 5.20: Stress-relaxation behavior (top) and time-strain superposition (bottom) of Extruded Nafion & Nafion recast with 3 wt % & 20 wt % TiO_2. Temperature is 30°C & inset shows strain shift factors.

As discussed in relation to extruded Nafion stress-relaxation, there is a striking difference between small (2%, 5%) and large (>10%) strain relaxation behavior, particularly at lower temperatures. The small strain relaxation curves begin at the same rate, but curve downwards on the log-log plot while large strain relaxation curves continue linearly. The effect is dampened for both plain and composite membranes at higher temperatures, as these are all humidified conditions.

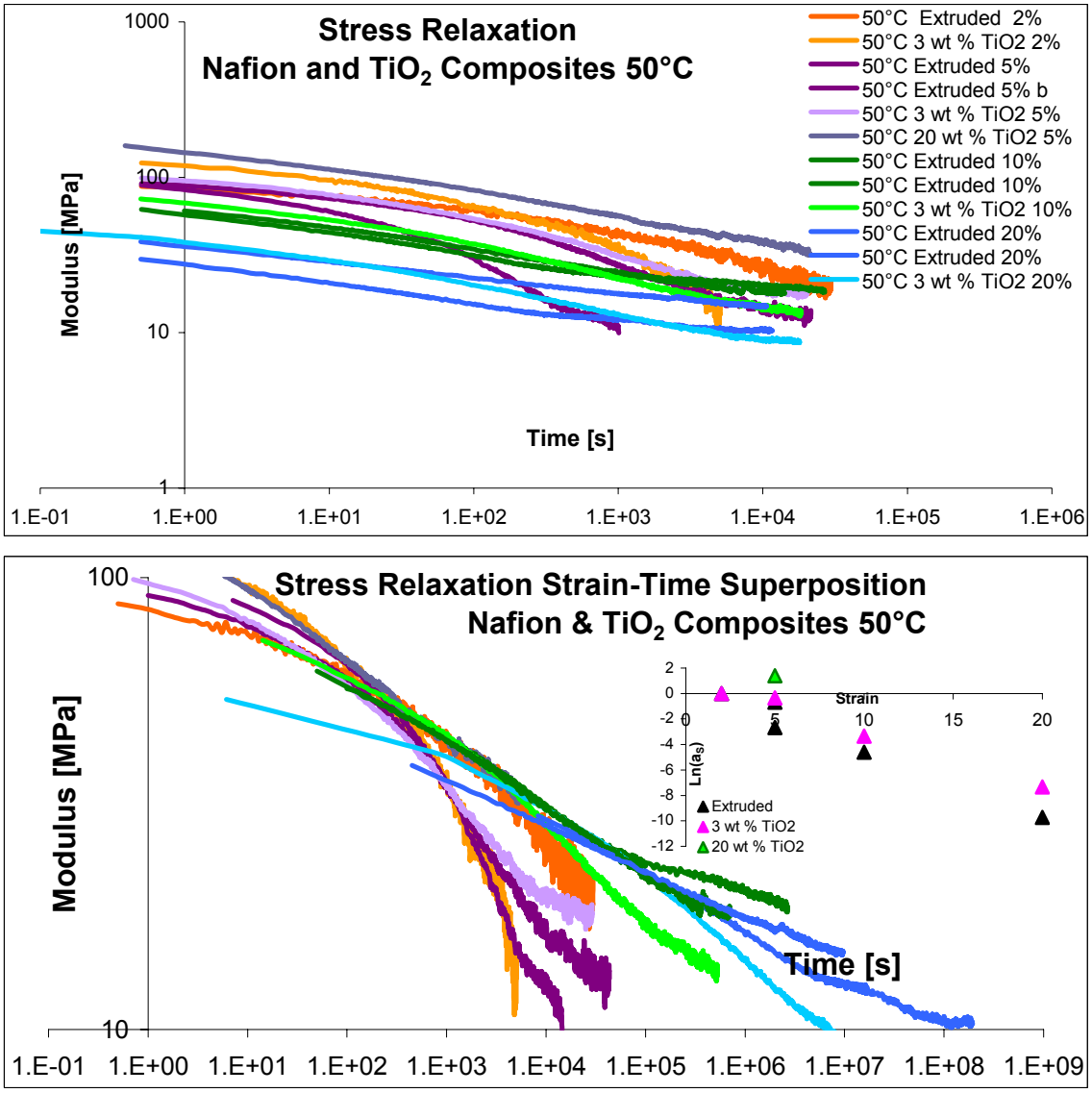

Figure 5.21: Stress-relaxation behavior (top) and time-strain superposition (bottom) of Extruded Nafion & Nafion recast with 3 wt % & 20 wt % TiO_2. Temperature is 50°C & inset shows strain shift factors.

At higher temperatures the addition of the TiO_2, particularly 20 wt % appears to increase the modulus and shift factor (shifted to shorter times) needed to produce a master curve with extruded Nafion. This effect is not visible at 30°C, where the offsets are actually lower.

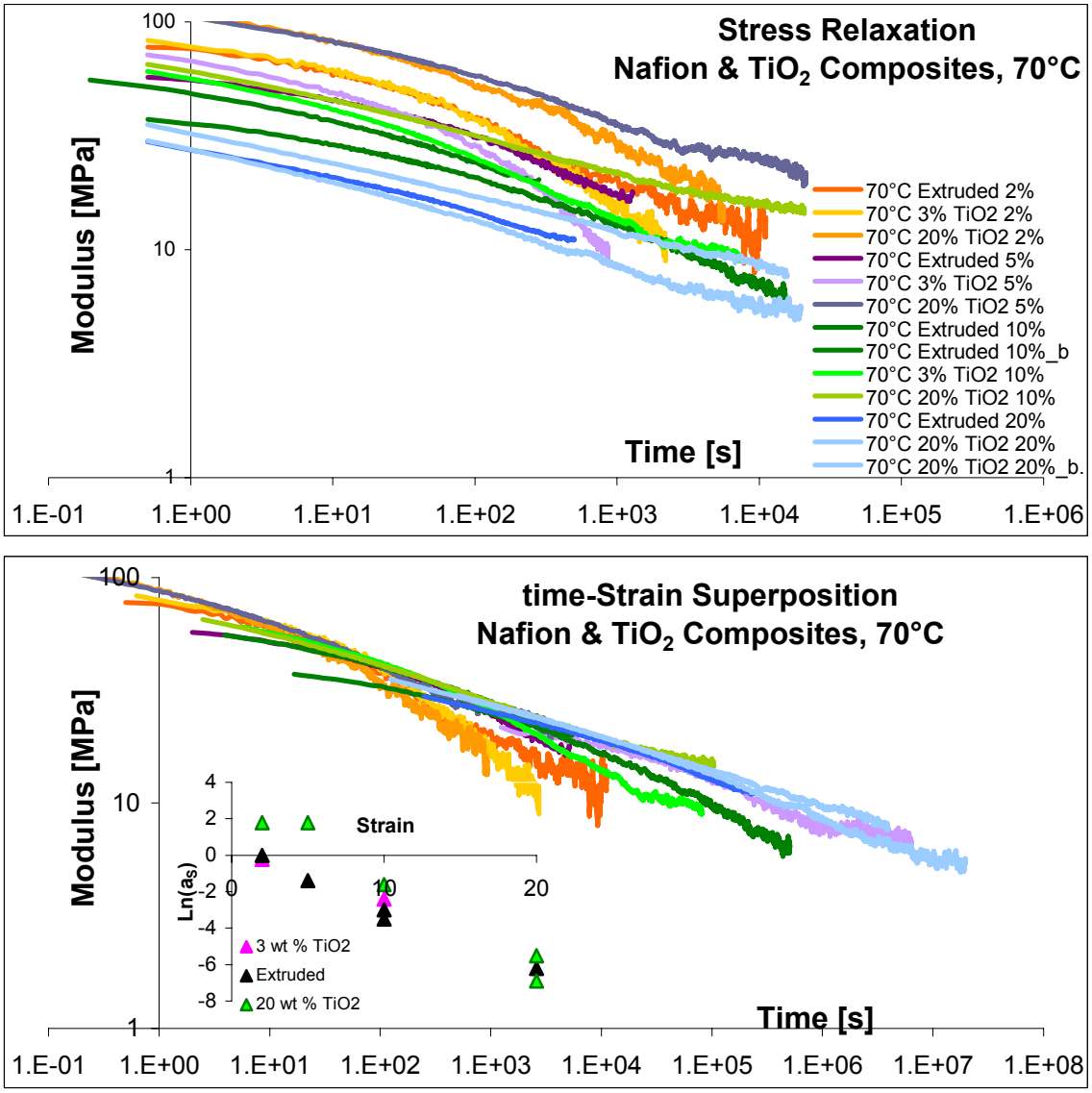

Figure 5.22: Stress-relaxation behavior (top) and time-strain superposition (bottom) of Extruded Nafion & Nafion recast with 3 wt % & 20 wt % TiO_2. Temperature is 70°C & inset shows strain shift factors.

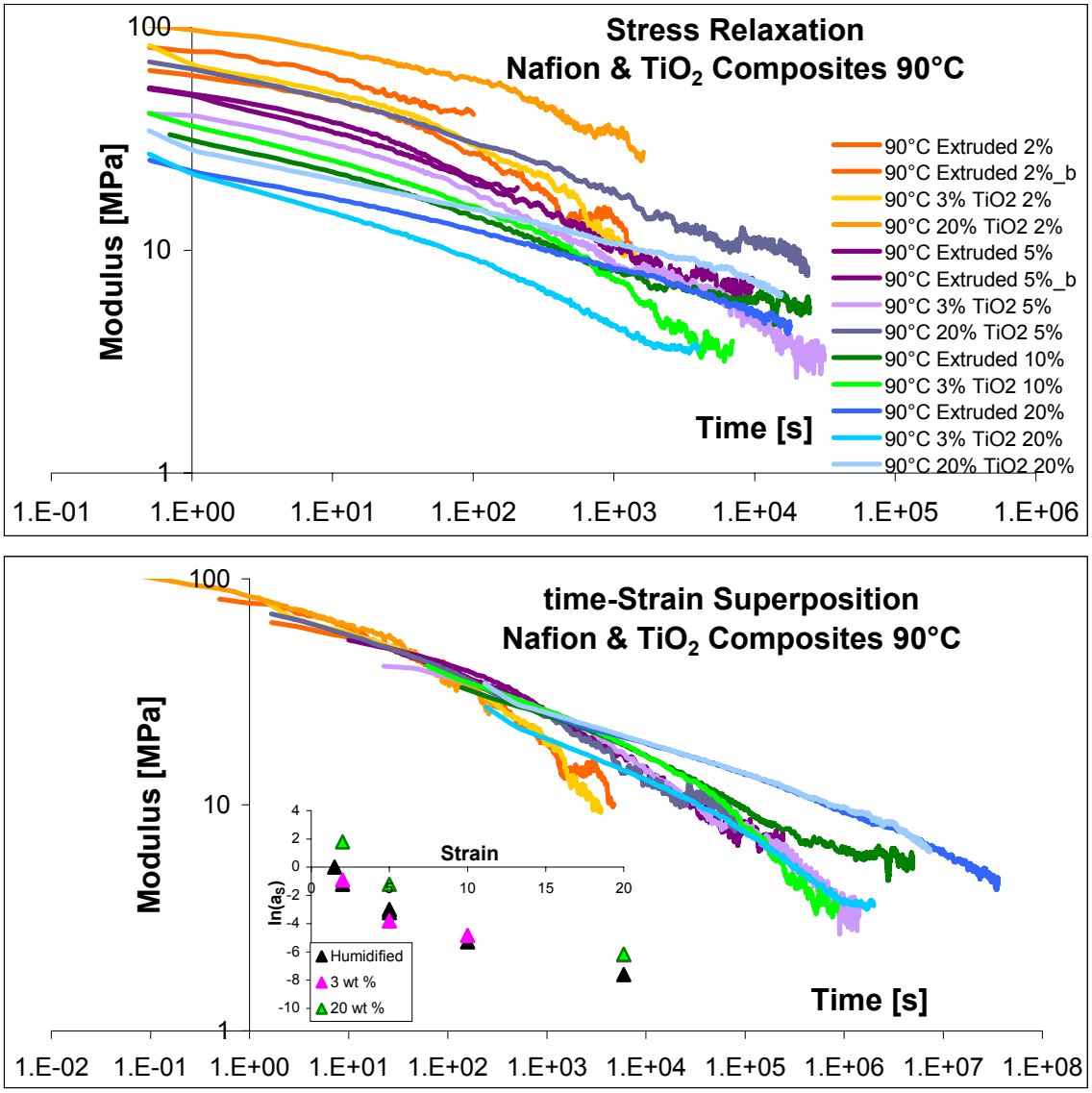

Figure 5.23: Stress-relaxation behavior (top) and time-strain superposition (bottom) of Extruded Nafion & Nafion recast with 3 wt % & 20 wt % TiO_2. Temperature is 70°C & inset shows strain shift factors.

Figure 5.24 through Figure 5.27 show the water sorption and desorption dynamics of extruded Nafion, recast membranes and composites recast with 3 wt % TiO_2 at 30°C, 50°C, 70°C and 90°C. Each line represents a different run, and the starting thickness of all membranes is 127 μm (0.005").

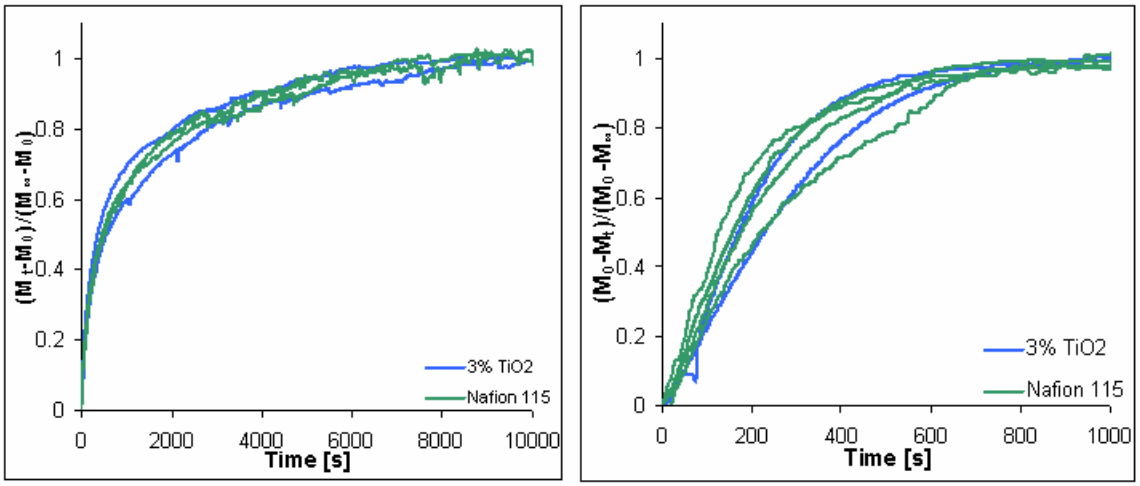

Figure 5.24: Water sorption (left) and desorption (right) dynamics of extruded Nafion (green) and Nafion recast with 3 wt % TiO_2 (blue). Temperature is 30°C.

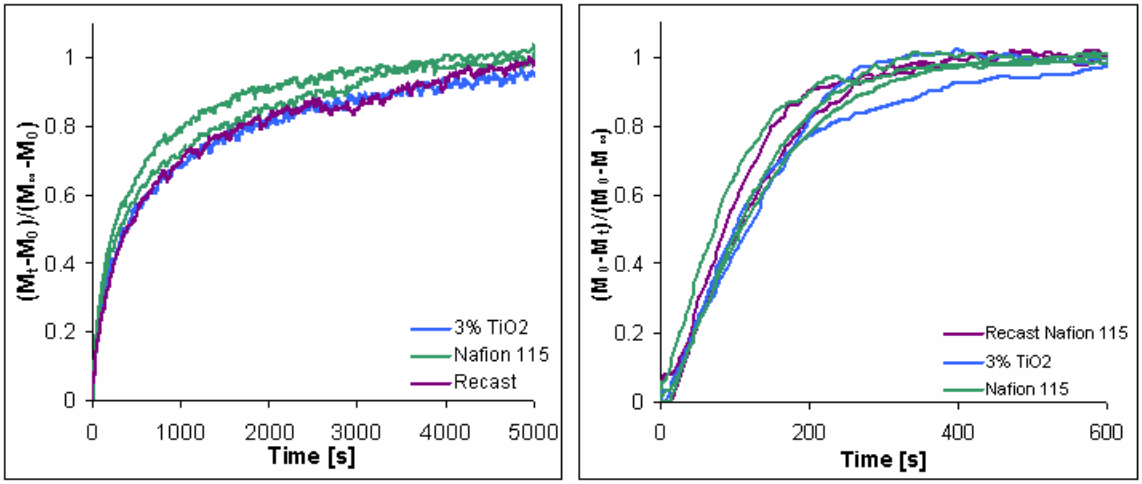

Figure 5.25: Water sorption (left) and desorption (right) dynamics of extruded Nafion (green), recast Nafion (purple) and Nafion recast with 3 wt % TiO_2 (blue). Temperature is 50°C.

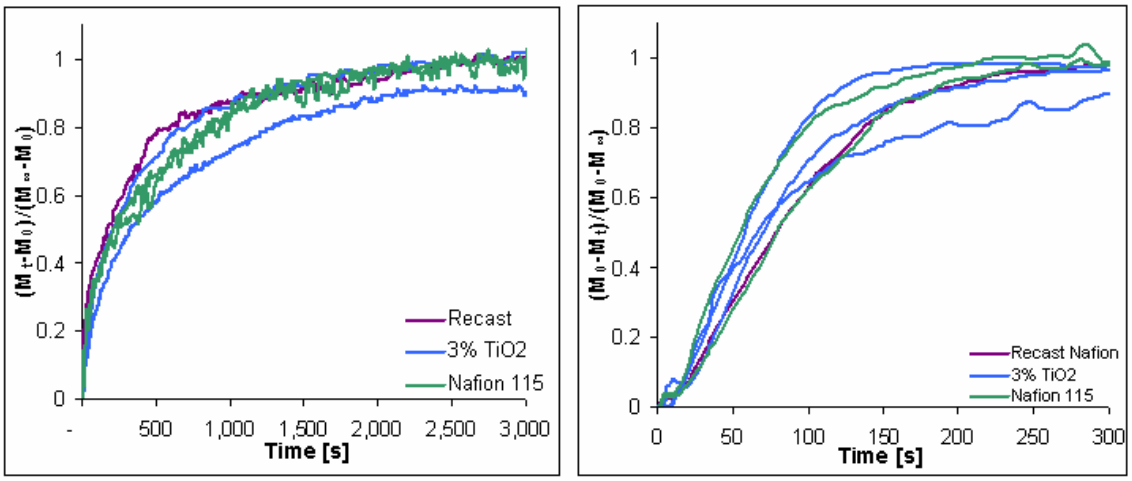

Figure 5.26: Water sorption (left) and desorption (right) dynamics of extruded Nafion (green), recast Nafion (purple) and Nafion recast with 3 wt % TiO_2 (blue). Temperature is 70°C.

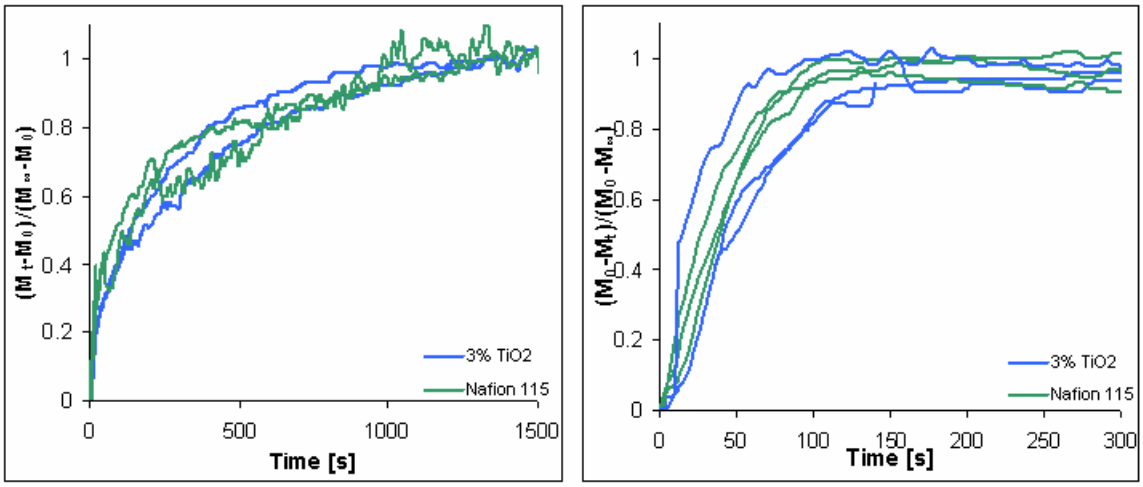

Figure 5.27: Water sorption (left) and desorption (right) dynamics of extruded Nafion (green) and Nafion recast with 3 wt % TiO_2 (blue). Temperature is 90°C.

The sorption dynamics between the composite membrane and extruded Nafion of similar thickness appear identical to within the normal run-to-run variation. Further, the interfacial mass-transport resistance measured through desorption is the same for extruded and composite membranes, as shown in Figure 5.28 and Figure 5.29.

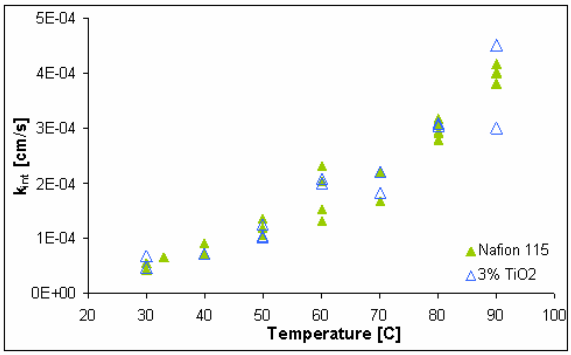

Figure 5.28: Interfacial mass transport resistance with temperature of extruded Nafion and 3 wt % TiO_2, both 127 µm thick.

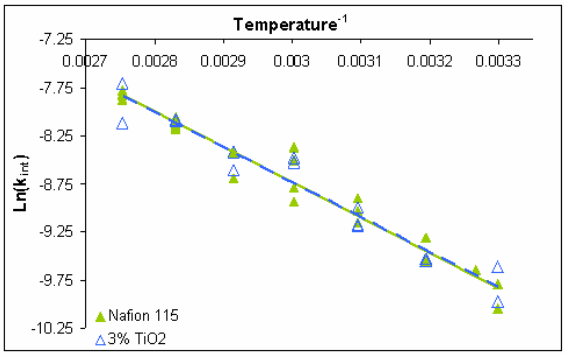

Figure 5.29: Arrhenius plot of interfacial mass transport resistance, extruded Nafion & 3 wt % TiO_2 composite, both 127 µm thick.

Though their approach to equilibrium occurred at the same rate, the composite membranes tended to gain 5%-10% more water than extruded Nafion during the sorption runs. This is almost within experimental uncertainty, as was reported by work done in this group by P. Majsztrik [7] but is consistent with findings by other researchers [3, 10, 19, 22].

The finding that sorption & desorption dynamics for extruded Nafion match those of the composites agrees well with Damay and Klein [11] and does not support the idea that these inorganic inclusions might block pathways for water transport. Further, it does not support the idea that the inorganic particles might prevent water loss by the membrane under adverse (drying) fuel cell conditions, as the extra water absorbed by the membranes during absorption is lost during desorption.

Figure 5.30 and Figure 5.31 show the results of two swelling response tests, one for extruded Nafion and the other for Nafion/TiO_2 composite. Both are at 70°C, with ~1 MPa of confining pressure. The composite membrane exhibited a greater pressure response against its constraints as the humidity in its environment increased.

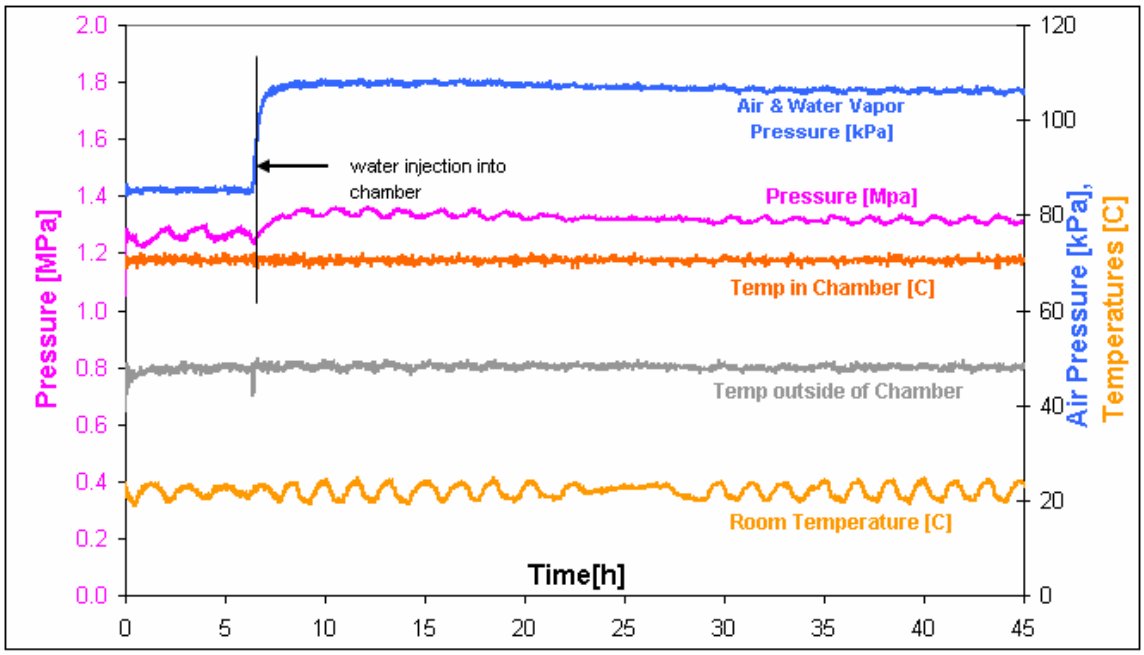

Figure 5.30: Pressure exerted by Nafion, normalized to 5 mil thick in response to step increase in humidity from 0% to 100% at time = 7 h. Test temperature = 70°C.

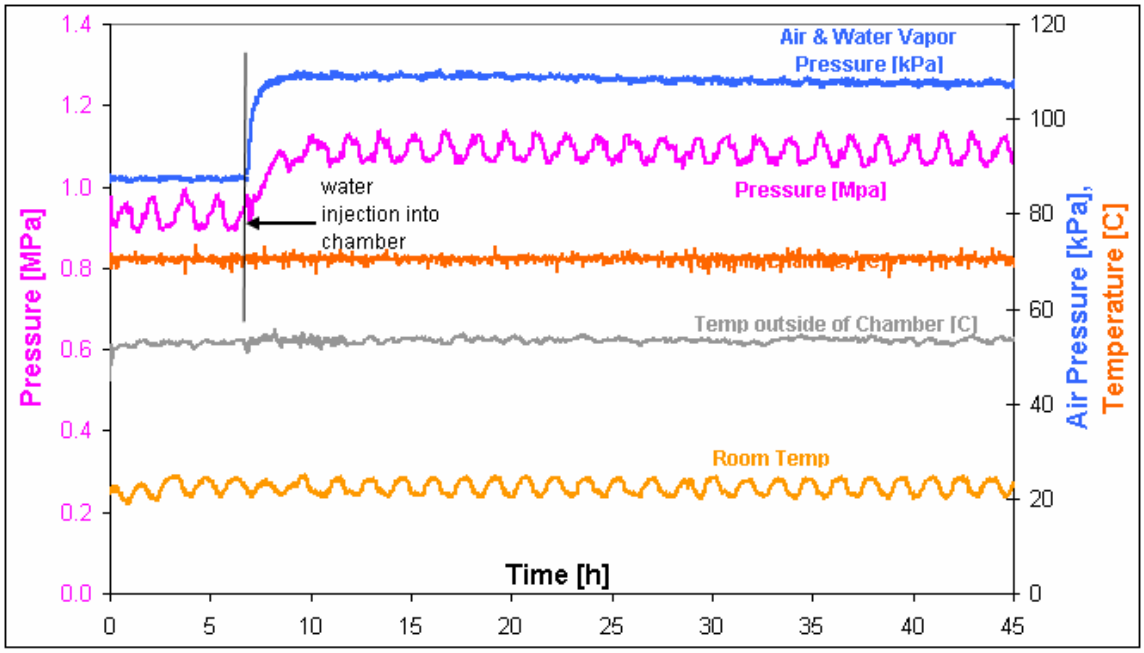

Figure 5.31: Pressure exerted by Nafion/3 wt % TiO_2, 5 mil thick in response to step increase in humidity from 0% to 100% at time = 7 h. Test temperature = 70°C.

This slight increase in pressure response is exhibited over the range of tests run, as shown in Figure 5.32.

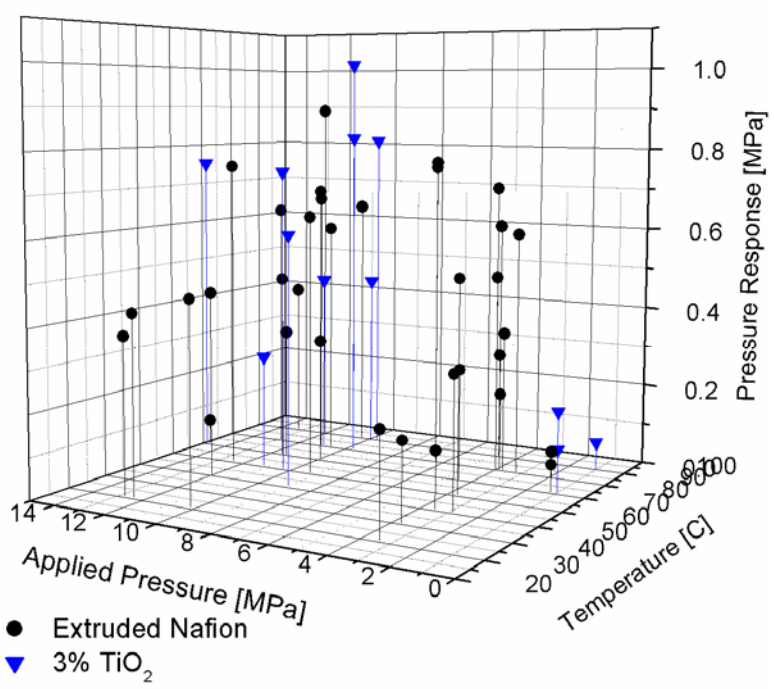

Figure 5.32: Pressure response of extruded Nafion & Nafion/TiO_2 (3 wt %) to step increase in relative humidity under different pressure constraints and temperatures.

5.5 Discussion

The results of this study indicate that recasting Nafion membranes with TiO_2 nanoparticles stiffens the membrane at low strains and extends the elastic region somewhat but weakens the membrane considerably at strains beyond its yield point. These results are consistent with the hypothesis [23] that the nanoparticles contribute to cross-linking between the sulfonic acid groups but do not interact with the hydrophobic polymer backbone. However, because the particles appear to agglomerate within the membrane, the stiffening effect observed here may not be due to any exceptional membrane-particle interaction, but rather the result of the simple addition of particles. The particles may even act to disrupt the backbone network, preventing strain-hardening and causing the observed decrease in plastic modulus at strains beyond the yield point.

The improvement in mechanical properties at short strains but not long strains is also seen in the results of the stress-relaxation tests: at strains of 2 and 5% the composite

membranes required a greater shift factor to match that of extruded Nafion, but the difference in shift factors decreased at high strains. It is suspected that the higher shift factor is mostly due to a higher modulus. The stress-relaxation rate may have been somewhat slower for the composite membranes as well, though viscosity and time-constant values obtained from fitting with the Kohlrausch-Williams-Watts and generalized Maxwell equations were inconclusive. A slower stress-relaxation rate would be consistent with work reported by P. Majsztrik [7] that the composite membranes creep less than the extruded Nafion under applied stresses similar to the initial stress recorded in these relaxation tests. However, a stress-relaxation rate that is unaffected by the addition of TiO_2 would be consistent with the understanding that the rates, particularly at large strains, are controlled by rearrangement of the polymer backbone rather than the ionic clusters [31], and that the particles interact more with the clusters than with the backbone.

A similarity in relaxation rates is also apparent in the comparison of the water sorption rates which, as discussed in Chapter 2, are strongly dependent on polymer rearrangement. Desorption rates are also unchanged by the addition of the nanoparticles, indicating that the interfacial mass-transport properties of the membranes are not changed.

The slight increase in pressure response upon water uptake may be due in part to the increased hygroscopic properties of the composite membranes, as was proposed by Yang et al.[5]. However, there was also a decrease in the amount of swelling into the pores, as seen in Figure 5.33. Though the opacity and gloss of the TiO_2 composite membrane may hide some of its surface roughness, it appears that the unmodified Nafion

was much more affected by the frit. As discussed in chapter 4, membrane swelling that occurs by extrusion into the frit's pores decreases the pressure response measured by the load cell, and the composite membrane did not appear to swell into the pores as much as the unmodified Nafion.

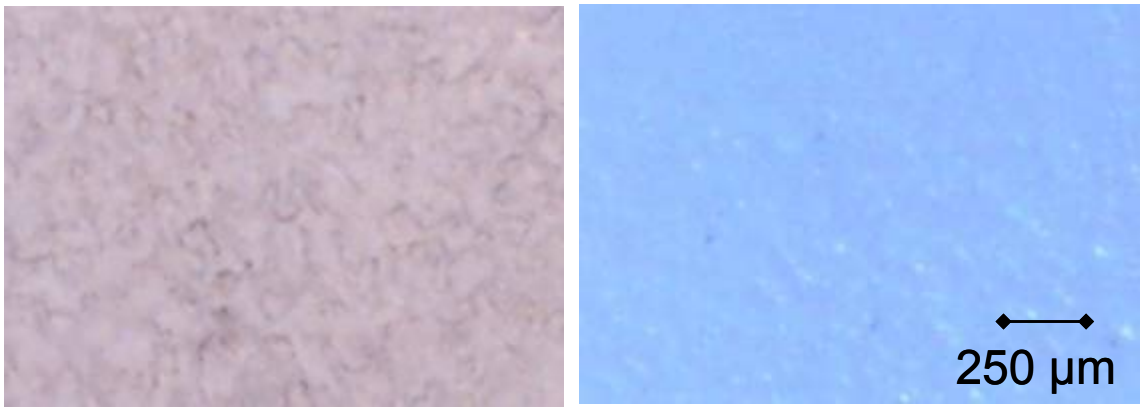

Figure 5.33: Microscope images of Nafion (left) and Nafion/3 wt % TiO_2 (right) after removal from compression test. Both membranes were tested at 80°C and constrained by about the same amount of pressure. Magnification is 60x.

The particles themselves may be preventing the composite Nafion from deforming into the frit. As seen in Figure 5.5, the particle size can reach up to ~500 nm, or 0.5 µm, which is approaching the size of the pores in the frit (5 µm). The decrease in deformation also supports the hypothesis put forth by Yang et al. [5] that the addition of nanoparticles creates a scaffolding effect within the membrane and contributes to dimensional stability. Though differences in tensile modulus measured here were not large, it may be that the improvement in mechanical properties noticed by so many researchers is manifest more in compressive indentation situations like this than in tensile tests. Further investigation of composite membrane's mechanical properties should explore testing geometries that have more applicability to fuel cell conditions, such as compression and indentation.

The effect that this sort of dimensional stability would have on the membrane's performance in a fuel cell is not entirely clear. Stresses due to microstructural changes during hydration and dehydration cycling are suspected of causing membrane embrittlement and degradation [32-36], and membranes with greater dimensional stability are expected to perform better in a fuel cell. However, this lab has measured the membrane after water uptake and loss and has not found drastic improvements in dimensional stability [7]. Further, the resistance to indentation seen here is not necessarily advantageous to membrane behavior in a fuel cell. It may improve the lifetime of the cell and help prevent the formation of pinholes at stress points, but it might also decrease the conductivity of the membrane-electrode assembly. Membrane deformation into the GDL improves the membrane/electrode contact and MEA conductivity, so it remains interesting that MEAs made with composite membranes so frequently exhibit improved conductivity within the fuel cell, particularly when ex-situ measurements do not predict that.

5.6 Conclusion

Stress-strain, stress-relaxation, water sorption and desorption rates and swelling pressures of Nafion and recast Nafion/TiO_2 composite membranes have been examined and compared. The composite membranes exhibit a slight increase in Young's modulus, proportional point and toughness, but a marked decrease in plastic modulus. The stress-relaxation rates of the composite membranes were comparable to those of extruded Nafion, though their higher modulus at low strains required that they be shifted to shorter times to form a master curve with extruded Nafion. The composite membranes exhibited

a slight increase in pressure exerted upon swelling, indicating that even at 3 wt % loading, the addition of nanoparticles may improve dimensional stability.

5.7 Acknowledgments

Many thanks to Paul Majsztrik for the steady supply of membranes to test and for the contribution of many supporting measurements and data, which are presented (along with much of this work) in [7]. Thanks also to Prof. George Scherer for thoughts on how the composite membrane particles may limit swelling into the pores of the compression frit.

5.8 References

1. Adjemian, K. T.; Srinivasan, S.; Benziger, J.; Bocarsly, A. B., Investigation of PEMFC operation above 100^{o}C employing perfluorosulfonic acid silicon oxide composite membranes. *Journal of Power Sources* **2002,** 109, (2), 356-364.
2. Cleghorn, S.; Kolde, J.; Liu, W., Catalyst Coated Composite Membranes. In *Handbook of Fuel Cells -- Fundamentals, Technology and Applications*, Vielstich, W.; Lamm, A.; Gasteiger, H. A., Eds. John Wiley & Sons, Ltd: Chichester, 2003; Vol. 3, pp 566-575.
3. Shao, Z. G.; Xu, H. F.; Li, M. Q.; Hsing, I. M., Hybrid Nafion-inorganic oxides membrane doped with heteropolyacids for high temperature operation of proton exchange membrane fuel cell. *Solid State Ionics* **2006,** 177, (7-8), 779-785.
4. Watanabe, M.; Uchida, H.; Seki, Y.; Emori, M.; Stonehart, P., Self-humidifying polymer electrolyte membranes for fuel cells. *Journal of the Electrochemical Society* **1996,** 143, (12), 3847-3852.
5. Yang, C.; Srinivasan, S.; Bocarsly, A. B.; Tulyani, S.; Benziger, J. B., A comparison of physical properties and fuel cell performance of Nafion and zirconium phosphate/Nafion composite membranes. *Journal of Membrane Science* **2004,** 237, (1-2), 145-161.
6. Chalkova, E.; Pague, M. B.; Fedkin, M. V.; Wesolowski, D. J.; Lvov, S. N., Nafion/TiO_2 proton conductive composite membranes for PEMFCs operating at elevated temperature and reduced relative humidity. *Journal of the Electrochemical Society* **2005,** 152, (6), A1035-A1040.
7. Satterfield, M. B.; Majsztrik, P. W.; Ota, H.; Benziger, J. B.; Bocarsly, A. B., Mechanical properties of Nafion and titania/Nafion composite membranes for PEM fuel cells. *Journal of Polymer Science B: Polymer Physics* **2006,** 44, (16), 2327-2345.
8. Jannasch, P., Recent developments in high-temperature proton conducting polymer electrolyte membranes. *Current Opinion in Colloid & Interface Science* **2003,** 8, (1), 96-102.
9. Chalkova, E.; Fedkin, M. V.; Wesolowski, D. J.; Lvov, S. N., Effect of TiO_2 surface properties on performance of Nafion-based composite membranes in high temperature and low relative humidity PEM fuel cells. *Journal of the Electrochemical Society* **2005,** 152, (9), A1742-A1747.
10. Sacca, A.; Carbone, A.; Passalacqua, E.; D'Epifanio, A.; Licoccia, S.; Traversa, E.; Sala, E.; Traini, F.; Ornelas, R., Nafion-TiO_2 hybrid membranes for medium temperature polymer electrolyte fuel cells (PEFCs). *Journal of Power Sources* **2005,** 152, (1), 16-21.
11. Damay, F.; Klein, L. C., Transport properties of Nafion$^{(TM)}$ composite membranes for proton-exchange membranes fuel cells. *Solid State Ionics* **2003,** 162, 261-267.
12. Wang, C.; Mao, Z. Q.; Xu, J. M.; Xie, X. F., Study of novel self-humidifying PEMFC with nano-TiO_2-based membrane. In *High-Performance Ceramics III, Pts 1 And 2*, Trans Tech Publications Ltd: Zurich-Uetikon, 2005; Vol. 280-283, pp 899-902.
13. Thampan, T. M.; Jalani, N. H.; Choi, P.; Datta, R., Systematic approach to design higher temperature composite PEMs. *Journal of the Electrochemical Society* **2005,** 152, (2), A316-A325.

14. Bauer, F.; Willert-Porada, M., Zirconium phosphate Nafion® composites - a microstructure-based explanation of mechanical and conductivity properties. *Solid State Ionics* **2006,** 177, (26-32), 2391-2396.
15. Kumar, B.; Fellner, J. P., Polymer-ceramic composite protonic conductors. *Journal of Power Sources* **2003,** 123, (2), 132-136.
16. Baglio, V.; Di Blasi, A.; Arico, A. S.; Antonucci, V.; Antonucci, P. L.; Trakanprapai, C.; Esposito, V.; Licoccia, S.; Traversa, E., Composite mesoporous titania nafion-based membranes for direct methanol fuel cell operation at high temperature. *Journal of the Electrochemical Society* **2005,** 152, (7), A1373-A1377.
17. Baglio, V.; Arico, A. S.; Di Blasi, A.; Antonucci, V.; Antonucci, P. L.; Licoccia, S.; Traversa, E.; Fiory, F. S., Nafion-TiO_2 composite DMFC membranes: physico-chemical properties of the filler versus electrochemical performance. *Electrochimica Acta* **2005,** 50, (5), 1241-1246.
18. Uchida, H.; Ueno, Y.; Hagihara, H.; Watanabe, M., Self-humidifying electrolyte membranes for fuel cells - Preparation of highly dispersed TiO_2 particles in Nafion 112. *Journal of the Electrochemical Society* **2003,** 150, (1), A57-A62.
19. Jalani, N. H.; Dunn, K.; Datta, R., Synthesis and characterization of Nafion®-MO_2 (M = Zr, Si, Ti) nanocomposite membranes for higher temperature PEM fuel cells. *Electrochimica Acta* **2005,** 51, (3), 553-560.
20. Alberti, G.; Casciola, M., Composite membranes for medium-temperature PEM fuel cells. *Annual Review of Materials Research* **2003,** 33, 129-154.
21. Li, Q. F.; He, R. H.; Jensen, J. O.; Bjerrum, N. J., Approaches and recent development of polymer electrolyte membranes for fuel cells operating above 100°C. *Chemistry of Materials* **2003,** 15, (26), 4896-4915.
22. Jalani, N. H.; Datta, R., The effect of equivalent weight, temperature, cationic forms, sorbates, and nanoinorganic additives on the sorption behavior of Nafion (R). *Journal of Membrane Science* **2005,** 264, (1-2), 167-175.
23. Adjemian, K. T.; Dominey, R.; Krishnan, L.; Ota, H.; Majsztrik, P.; Zhang, T.; Mann, J.; Kirby, B.; Gatto, L.; Velo-Simpson, M.; Leahy, J.; Srinivasan, S.; Benziger, J. B.; Bocarsly, A. B., Function and characterization of metal oxide-Nafion composite membranes for elevated-temperature H_2/O_2 PEM fuel cells. *Chemistry of Materials* **2006,** 18, (9), 2238-2248.
24. Shao, P. L.; Mauritz, K. A.; Moore, R. B., [Perfluorosulfonate Ionomer] [Mixed Inorganic Oxide] nanocomposites via polymer in-situ sol-gel chemistry. *Chemistry of Materials* **1995,** 7, (1), 192-200.
25. Shao, P. L.; Mauritz, K. A.; Moore, R. B., [Perfluorosulfonate ionomer] [SiO_2-TiO_2] nanocomposites via polymer-in situ sol-gel chemistry: Sequential alkoxide procedure. *Journal of Polymer Science Part B-Polymer Physics* **1996,** 34, (5), 873-882.
26. Rhee, C. H.; Kim, Y.; Lee, J. S.; Kim, H. K.; Chang, H., Nanocomposite membranes of surface-sulfonated titanate and Nafion(R) for direct methanol fuel cells. *Journal of Power Sources* **2006,** 159, (2), 1015-1024.
27. Kim, Y. M.; Choi, S. H.; Lee, H. C.; Hong, M. Z.; Kim, K.; Lee, H. I., Organic-inorganic composite membranes as addition of SiO_2 for high temperature-operation in polymer electrolyte membrane fuel cells (PEMFCs). *Electrochimica Acta* **2004,** 49, (26), 4787-4796.

28. Kwak, S. H.; Yang, T. H.; Kim, C. S.; Yoon, K. H., Nafion/mordenite hybrid membrane for high-temperature operation of polymer electrolyte membrane fuel cell. *Solid State Ionics* **2003,** 160, (3-4), 309-315.
29. Smitha, B.; Sridhar, S.; Khan, A. A., Proton conducting composite membranes from polysulfone and heteropolyacid for fuel cell applications. *Journal of Polymer Science Part B-Polymer Physics* **2005,** 43, (12), 1538-1547.
30. Liu, Y. H.; Yi, B. L.; Shao, Z. G.; Wang, L.; Xing, D. M.; Zhang, H. M., Pt/CNTs-Nafion reinforced and self-humidifying composite membrane for PEMFC applications. *Journal of Power Sources* **2007,** 163, (2), 807-813.
31. Kyu, T.; Eisenberg, A., Underwater stress-relaxation studies of Nafion (perfluorosulfonate) ionomer membranes. *Journal of Polymer Science-Polymer Symposia* **1984**, (71), 203-219.
32. Tang, Y. L.; Santare, M. H.; Karlsson, A. M.; Cleghorn, S.; Johnson, W. B., Stresses in proton exchange membranes due to hygro-thermal loading. *Journal of Fuel Cell Science and Technology* **2006,** 3, (2), 119-124.
33. Budinski, M.; Gittleman, C. S.; Lai, Y. H.; Litteer, B.; Miller, D., Characterization of perfluorosulfonic acid membranes for PEM fuel cell mechanical durability. In *AIChE Annual Meeting*, Austin, TX, 2004; p Presentation slides used at 2004 AIChE Annual Meeting.
34. Kusoglu, A.; Karlsson, A. M.; Santare, M. H.; Cleghorn, S.; Johnson, W. B., Mechanical response of fuel cell membranes subjected to a hygro-thermal cycle. *Journal of Power Sources* **2006,** 161, (2), 987-996.
35. Solasi, R.; Zou, Y.; Huang, X.; Reifsnider, K.; Condit, D., On mechanical behavior and in-plane modeling of constrained PEM fuel cell membranes subjected to hydration and temperature cycles. *Journal of Power Sources* **2007,** 167, (2), 366-377.
36. Huang, X. Y.; Solasi, R.; Zou, Y.; Feshler, M.; Reifsnider, K.; Condit, D.; Burlatsky, S.; Madden, T., Mechanical endurance of polymer electrolyte membrane and PEM fuel cell durability. *Journal of Polymer Science Part B-Polymer Physics* **2006,** 44, (16), 2346-2357.

6 Conclusion & Future Work

This work has explored the stress-strain and stress relaxation mechanical properties, water sorption and desorption dynamics and pressures exerted during constrained sorption of Nafion and Nafion/TiO_2 composite membranes for polymer electrolyte membrane fuel cells. Results indicate that while the addition of water plasticizes Nafion at room temperature, it acts to stiffen it and stabilize it against stress-relaxation at temperatures relevant to fuel cell operation: 40°C to 90°. Stress-relaxation rates and mechanical properties of Nafion play a significant role in its behavior in the cell. Membrane toughness and resistance to failure from stresses induced during hydration cycling affects cell longevity, and its ability to maintain contact with the porous catalyst electrode affects cell performance. It was found that the Nafion/TiO_2 composite membranes that perform better in fuel cells also exhibit somewhat different mechanical properties: slightly higher elastic modulus, drastically lower plastic modulus and higher pressure exerted while absorbing water, though similar sorption and stress-relaxation rates were observed.

These changes in mechanical properties do not appear to be significant enough to explain the improved fuel cell performance. However, the type of mechanical tests used here may not have probed the relevant properties of the membrane. In a fuel cell the membranes may experience tensile stress and strain (which was tested here), but are also compressed, sheared and indented. Thus, different testing geometries such as nano-indentation and bending experiments should be investigated before abandoning the idea that the composites have enhanced mechanical properties. These options were explored

to some degree at the outset of this work, but posed significant experimental difficulties and were abandoned for more readily-available tensile tests that had also not been explored.

Mechanical properties have also been investigated as they related to membrane water uptake, both the equilibrium (chapter 4) and the rate of water sorption (chapter 3). The pressures exerted by the membranes upon swelling to absorb water are significant and may have not been anticipated by those modeling and designing industrial-scale fuel cells. Also, the finding that water sorption rates follow nonFickian patterns and are governed by interfacial mass-transport and stress-relaxation rates was an unexpected result, and one that has not been reported for Nafion despite years of similar (though less thorough) studies [1-6]. Further work to investigate the water sorption behavior should work with different sample geometries, such as spherical beads, which would reveal whether the thickness dependence observed in flat-plate geometries is due to surface effects or to front propagation-style penetration of the solvent into the interior of the sample.

The stiffening effect of water was another unexpected result, but has also been observed in creep experiments performed by Paul Majsztrik [7], and contributes to our strengthening suspicion that the glass transition reported for dehydrated Nafion [8-12] is not actually a glass transition but some other phase change, and that this transition does not occur in hydrated Nafion.

There is also strong evidence from other researchers [10-12] that the presence of water at least pushes the phase transition to higher temperatures than 110°C, the value reported for dry Nafion. However, it is not clear whether the transition has simply been

pushed to higher temperatures (and—how much higher?) or erased, and one of the experimental limitations we and others have encountered is how to probe temperatures above 100°C while maintaining humid conditions. The systems designed here were not pressurized, and work to pressurize a mechanical testing system may involve some significant design hurdles. One possible experiment, suggested by Prof. George Scherer, which could investigate transitions in hydrated Nafion at higher temperatures are pressurized DSC (differential scanning calorimetry) pans.

Another question associated with the stiffening effect of water is at what hydration level the effect takes hold at different temperatures. From stress-strain plots of Nafion at room temperature in chapter 2, Figure 18, it appears that at hydration levels corresponding to humidity > 94% some sort of transition occurs, causing a distinct change in the shape of the stress-strain curves. Meanwhile, Yeo and Eisenberg[8] have reported that the glass transition of Nafion stays the same with the addition of 3 mol H_2O/SO_3^- and that stress relaxation rates are increased, while others[10-12] (discussed above) have found that the glass transition is decidedly changed in well-hydrated Nafion (>12 mol H_2O/SO_3^-), and this work has found that stress relaxation rates are decreased by the addition of water to ~13 mol H_2O/SO_3^-. This question could be probed with some degree of ease, using a plastic bag in an Instron machine that contains saturated salt solutions instead of water.

During the course of this work, evidence of the effect of thermal and water-content history on membrane properties was encountered, and has been reported on to some degree by other researchers[13-15]. For example, membranes dried at 130°C tended to absorb less water than those dried at lower temperatures, and membranes equilibrated

over water for two weeks were softer than those equilibrated over water for 1 day. Steps were taken to minimize these irregularities in order to concentrate on other effects: always drying the membranes at 70°C over drierite and trying to test membranes after a uniform amount of equilibration time. However, a full investigation of this could yield some interesting results that might help the understanding of how fuel cells respond to prolonged operation and cycling, as well as the effect of the hot-pressing step used to form the MEA.

6.1 References

1. Ge, S. H.; Li, X. G.; Yi, B. L.; Hsing, I. M., Absorption, desorption, and transport of water in polymer electrolyte membranes for fuel cells. *Journal of the Electrochemical Society* **2005,** 152, (6), A1149-A1157.
2. Rivin, D.; Kendrick, C. E.; Gibson, P. W.; Schneider, N. S., Solubility and transport behavior of water and alcohols in Nafion(TM). *Polymer* **2001,** 42, (2), 623-635.
3. Burnett, D. J.; Garcia, A. R.; Thielmann, F., Measuring moisture sorption and diffusion kinetics on proton exchange membranes using a gravimetric vapor sorption apparatus. *Journal of Power Sources* **2006,** 160, (1), 426-430.
4. Krtil, P.; Trojanek, A.; Samec, Z., Kinetics of water sorption in Nafion thin films -- Quartz crystal microbalance study. *Journal of Physical Chemistry B* **2001,** 105, 7979-7983.
5. Morris, D. R.; Sun, X., Water-sorption and transport properties of Nafion 117 H. *Journal of Applied Polymer Science* **1993,** 50, (8), 1445-1452.
6. Takamatsu, T.; Hashiyama, M.; Eisenberg, A., Sorption phenomena in Nafion membranes. *Journal of Applied Polymer Science* **1979,** 24, (11), 2199-2220.
7. Majsztrik, P. Thesis. forthcoming.
8. Yeo, S. C.; Eisenberg, A., Physical-properties and supermolecular structure of perfluorinated ion-containing (Nafion) polymers. *Journal of Applied Polymer Science* **1977,** 21, (4), 875-898.
9. Kyu, T.; Eisenberg, A., Mechanical relaxations in perfluorosulfonate-ionomer membranes. *ACS Symposium Series* **1982,** 180, 79-110.
10. Uan-Zo-li, J. T. Thesis: The Effects of Structure, Humidity and Aging on the Mechanical Properties of Polymeric Ionomers for Fuel Cell Applications. Master of Science, Virginia Polytechnic Institute and State University, Blacksburg, Virginia, 2001.
11. Bauer, F.; Denneler, S.; Willert-Porada, M., Influence of temperature and humidity on the mechanical properties of Nafion (R) 117 polymer electrolyte membrane. *Journal of Polymer Science Part B-Polymer Physics* **2005,** 43, (7), 786-795.
12. Budinski, M.; Gittleman, C. S.; Lai, Y. H.; Litteer, B.; Miller, D., Characterization of perfluorosulfonic acid membranes for PEM fuel cell mechanical durability. In *AIChE Annual Meeting*, Austin, TX, 2004; p Presentation slides used at 2004 AIChE Annual Meeting.
13. Jalani, N. H.; Choi, P.; Datta, R., TEOM: A novel technique for investigating sorption in proton-exchange membranes. *Journal of Membrane Science* **2005,** 254, (1-2), 31-38.
14. Zawodzinski, T. A.; Derouin, C.; Radzinski, S.; Sherman, R. J.; Smith, V. T.; Springer, T. E.; Gottesfeld, S., Water-uptake by and transport through Nafion(R) 117 membranes. *Journal of the Electrochemical Society* **1993,** 140, (4), 1041-1047.
15. Bunce, N. J.; Sondheimer, S. J.; Fyfe, C. A., Proton NMR method for the quantitative-determination of the water-content of the polymeric fluorosulfonic acid Nafion-H. *Macromolecules* **1986,** 19, (2), 333-339.